THE ASTROPHYSICAL JOURNAL

AN INTERNATIONAL REVIEW OF SPECTROSCOPY AND ASTRONOMICAL PHYSICS

VOLUME 105 MAY 1947 NUMBER 3

FINE STRUCTURE OF THE INFRARED ATMOSPHERIC OXYGEN BANDS

L. HERZBERG AND G. HERZBERG

Yerkes Observatory

Received February 1, 1947

ABSTRACT

Measurements of the 0–0 and 1–0 bands of the infrared atmospheric oxygen bands at 1.2683 μ and 1.0674 μ are presented. The structure of the bands is in complete agreement with the assumption that they represent a $^1\Delta_g - {}^3\Sigma_g^-$ transition. The vibrational and rotational constants of the $^1\Delta_g$ state of the O_2 molecule are evaluated (Table 3). A brief discussion is added of the problem of intensities within the system and relative to the ordinary atmospheric oxygen bands ($^1\Sigma_g^+ - {}^3\Sigma_g^-$) both for the gas and for the liquid.

A. INTRODUCTION

The existence of a low-lying $^1\Delta_g$ state of the O_2 molecule was first predicted by Mulliken.[1] The lowest electron configuration of O_2 is

$$(K)\,(K)\,(\sigma_g 2s)^2\,(\sigma_u 2s)^2\,(\sigma_g 2p)^2\,(\pi_u 2p)^4\,(\pi_g 2p)^2$$

which gives rise to the states $^3\Sigma_g^-$, $^1\Delta_g$, and $^1\Sigma_g^+$, in this order. The $^3\Sigma_g^-$ state is the ground state of the O_2 molecule, while $^1\Sigma_g^+$ is the upper state of the ordinary atmospheric oxygen bands.

The first definite evidence for the $^1\Delta_g$ state was obtained by Ellis and Kneser[2] in the infrared absorption spectrum of liquid oxygen, where it gives rise to a progression of prominent bands, starting at 1.261 μ and extending to shorter wave lengths. Ellis and Kneser[2,3] also found definite indications of the first band, at 1.268 μ in Abbot and Freeman's bolometer-curves of the solar spectrum.[4] Very shortly afterward, G. Herzberg[5] photographed this region of the solar spectrum under high dispersion and, from the

[1] R. S. Mulliken, *Phys. Rev.*, **32**, 186, 880, 1928.

[2] J. W. Ellis and H. O. Kneser, *Zs. f. Phys.*, **86**, 583, 1933.

[3] J. W. Ellis and H. O. Kneser, *Pub. A.S.P.*, **46**, 106, 1934.

[4] C. G. Abbot and H. B. Freeman, *Smithsonian Misc. Coll.*, Vol. **82**, No. 3026, 1929. The sharp maximum at 1.2678 μ superposed on the broad unresolved band with apparent center at 1.262 μ was interpreted by Ellis and Kneser as the *Na* I line at 1.2678. Actually, it is undoubtedly formed by the unresolved Q branches of the band (see the spectrogram, Fig. 1).

[5] *Nature*, **133**, 759, 1934.

structure of the band, definitely established that it represents a $^1\Delta - {}^3\Sigma$ transition of the O_2 molecule.

In the preliminary note by G. Herzberg, only provisional values for the constants of the $^1\Delta$ state were given. It is the object of this paper to present the detailed analysis and give considerably improved values for the molecular constants. In addition, a second band belonging to the $^1\Delta - {}^3\Sigma$ system has been found in the solar spectrum at 10674 A.

B. BAND ANALYSIS

The photographs that form the basis of the present analysis were taken with a Wood 10-foot grating in first order (dispersion 4.9 A/mm) on Agfa infrared plates (No. 1050), hypersensitized with ammonia. The integrated light of the sun was used. The exposure times ranged from 2 to 6 hours in the region above 12,000 A. The absorbing layer was therefore not quite constant during the exposure. In one of the exposures the solar spectrum was photographed to 13,300 A. In all other exposures the limit was at about 13,000 A.

In Figure 1 a spectrogram of the 0–0 band of the $^1\Delta_g - {}^3\Sigma_g^-$ system is reproduced. The fundamental difference of the band structure from that of the ordinary atmospheric oxygen bands ($^1\Sigma_g^+ - {}^3\Sigma_g^-$) is immediately seen. While the $^1\Sigma_g^+ - {}^3\Sigma_g^-$ bands have P and R form branches only, separated by a clear zero gap, the $^1\Delta_g - {}^3\Sigma_g^-$ band has no zero gap but, rather, two strong Q heads in its center and, in addition, an S and an O form branch, characterized by a spacing about twice as large as that in the P and R form branches.

A $^1\Delta_g - {}^3\Sigma_g^-$ transition, just as a $^1\Sigma_g^+ - {}^3\Sigma_g^-$ transition, is forbidden by the rigorous selection rules for dipole radiation and can appear only as magnetic dipole or quadrupole radiation.[6] Moreover, it is a singlet-triplet intercombination, a fact that further reduces its intensity. Since quadrupole radiation has only about one-thousandth of the intensity of magnetic dipole radiation, we can neglect it for our present purpose.

The selection rules for magnetic dipole radiation are

$$\Delta J = 0, \pm 1$$

and

$$+ \longleftrightarrow + \ , \quad - \longleftrightarrow - \ .$$

The transitions possible on the basis of these selection rules are indicated in the schematic diagram, Figure 2(*a*). For comparison, Figure 2(*b*) gives the corresponding diagram for the $^1\Sigma_g^+ - {}^3\Sigma_g^-$ transition. Since all three electronic states are even and the oxygen nuclei follow Bose statistics, only the positive rotational levels occur. The presence of the odd, as well as the even, rotational levels in the $^1\Delta_g$ state, unlike the $^1\Sigma_g^+$ state, causes the occurrence in the $^1\Delta_g - {}^3\Sigma_g^-$ bands of the Q, S, and O form branches (with $\Delta K = 0$ and ± 2) in addition to the P and R form branches (with $\Delta K = \pm 1$). The fact that all the predicted branches occur shows conclusively that the infrared bands represent such a $^1\Delta_g - {}^3\Sigma_g^-$ transition. It should be noted particularly that the line $P(1)$, which is a strong line in the ordinary atmospheric oxygen bands, does not occur in the infrared band in agreement with expectation, since the $^1\Delta$ state has no levels with $J = 0$ and 1.

Table 1 gives the wave numbers (*in vacuo*) of the observed band lines in the 0–0 and 1–0 bands. The relative accuracy of the wave numbers in the 0–0 band is about ± 0.03 cm^{-1} for unblended lines; in the 1–0 band, whose lines are all exceedingly weak, it is about ± 0.07 cm^{-1}. The absolute accuracy may be somewhat less.[6a]

[6] J. H. Van Vleck, *Ap. J.*, **80**, 161, 1934.

[6a] Note added in proof: Mr. H. D. Babcock kindly informs us that he has carried out new measurements of these O_2 bands which have undoubtedly a higher absolute accuracy. According to these, a constant 0.050 cm^{-1} should be subtracted from the above wave numbers of the 0–0 band, while 0.033 cm^{-1} should be subtracted from the wave numbers of the 1–0 band. The relative accuracy of Babcock's new

FIG. 1.—Spectrogram of the 0–0 band of the $^1\Delta_g - {}^3\Sigma_g^-$ system of O_2. The diffuse line at the right is the second line of the Paschen series of hydrogen at 12818 A.

The lines in Table 1 are numbered according to the K value in the lower state (K being the quantum number of the total angular momentum apart from electron spin). As usual, we designate the term values of the levels with $J = K + 1$, K, and $K - 1$ by $F_1(K)$, $F_2(K)$, and $F_3(K)$, respectively. It must be realized that only for the F_2 levels does a simple formula hold, namely,

$$F_2(K) = BK(K+1) - DK^2(K+1)^2,$$

and that both F_1 and F_3 lie below F_2. Formulae for the F_1 and F_3 levels have been given by Schlapp.[7]

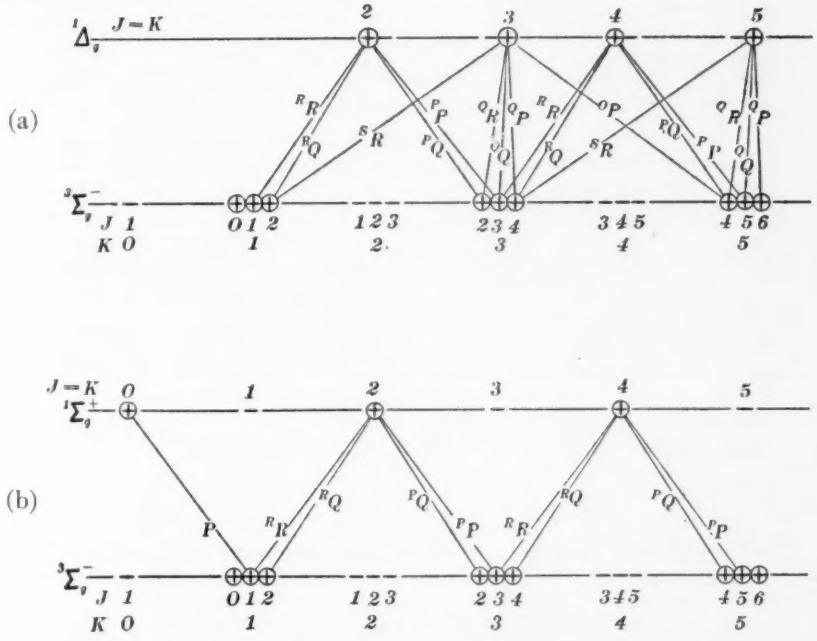

FIG. 2.—Origin of the branches: (*a*) in a $^1\Delta_g - {}^3\Sigma_g^-$ transition; (*b*) in a $^1\Sigma_g^+ - {}^3\Sigma_g^-$ transition. The levels that occur for the O_2 molecule are circled.

Only for the 0–0 band of the $^1\Delta_g - {}^3\Sigma_g^-$ system are the data sufficiently complete for the formation of the combination differences $^RR(K-1) - {}^PP(K+1) = \Delta_2F_2''(K)$. Excellent agreement with the corresponding differences of the $^1\Sigma_g^+ - {}^3\Sigma_g^-$ system is found. As in the case of the latter, the separations of ^RQ and ^RR and of ^PQ and ^PP for a given K give the triplet splittings, $F_2(K) - F_1(K)$ and $F_2(K) - F_3(K)$, respectively, of the lower state. In Table 2 these splittings, as obtained from the 0–0 band of the $^1\Delta_g - {}^3\Sigma_g^-$ system, are compared with the more accurate values obtained from Babcock's new unpublished measurements of the $^1\Sigma_g^+ - {}^3\Sigma_g^-$ system. It is seen that the agreement is very satisfactory, confirming the identity of the lower states of the two systems. The smallness of the separation of the F_1 and F_3 levels, as indicated

---

measurements is about the same as ours, so that the rotational constants in Table 3 are unchanged. The band origins and vibrational quantum listed in Table 3 have been changed in the proof to take account of the above small shifts given by Babcock.

[7] R. Schlapp, *Phys. Rev.*, **51**, 342, 1937.

TABLE 1

WAVE NUMBERS (ν_{vac}) OF BAND LINES IN THE $^1\Delta_g - {}^3\Sigma_g^-$ SYSTEM OF O_2

0–0 BAND

K''	^SR	^RR	^RQ	^QQ	^QP and ^QR	^PP	^PQ	^OP
1	7898.489 (3)*	7888.078 (3)	7889.963 (2)	.....	.....	.....	.....	.....
3	7909.739 (3)	93.538 (4)	95.489 (3)	.....	7884.235 (2)	7873.669 (2)	7875.724 (2)	.....
5	20.644 (4)†	98.879 (4)	7900.857 (3)	7881.941 (5)†	83.873 (3)	67.668 (2)	69.676 (3)	7858.315 (1)
7	31.488 (3)†	7903.965 (4)	06.018 (3)	81.380 (3)	83.347 (3)	61.476 (3)	63.439 (3)	46.411 (2)
9	42.206 (3)	08.965 (3)	11.022 (3)	80.692 (4)†	82.640 (3)	55.158 (3)	57.112 (3)	34.426 (2)
11	52.700 (3)	13.815 (3)	15.889 (3)	79.747 (3)†	81.941 (5)†	48.653 (3)	50.541 (3)	22.184 (1)
13	63.021 (2)	18.450 (2)	20.644 (4)†	78.814 (2)	80.692 (4)†	41.978 (2)	43.919 (3)	09.937 (0)
15	73.197 (2)	22.957 (2)	25.052 (2)	77.661 (2)	79.747 (3)†	35.211 (2)	37.032 (2)	
17	83.122 (1)	27.290 (1)	29.412 (1)	76.376 (1)	.....	28.185 (1)	30.162 (2)	
19	92.983 (1)	31.488 (3)†	33.540 (1)	74.883 (1)	76.752 (2)	21.133 (0)	22.983 (0)	
21	8002.568 (0)	35.392 (0)	37.493 (0)	73.127 (0)				
23	11.942 (00)	39.244 (00)	.....	71.402 (0)				

1–0 BAND

K''	^SR	^RR	^RQ	^QQ	^QP and ^QR
1	9381.687 (0)	9371.738 (1)	.....	.....	.....
3	92.650 (0.5)	76.827 (0)	.....	9365.570 (0)	9367.653 (0)
5	9403.189 (00)	81.687 (0)	9383.594 (00)	64.772 (0)	66.729 (2)†
7	.....	86.265 (0)	88.116 (0)	63.925 (0)	65.946 (0)
9	.....	90.568 (0)	92.650 (0.5)	62.610 (0)	64.772 (0)
11	.....	94.629 (00)	96.737 (00)	61.034 (0)	63.196 (00)
13	.....	98.263 (00)	9400.532 (00)	59.257 (0)	61.034 (0)
15	9451.751 (0)	9401.713 (00)	04.116 (00)	56.958 (0.5)	59.257 (0)
17	.....	04.944 (00)	06.863 (5)†	54.596 (00)	56.958 (0.5)
19	.....	.....	.....	52.254 (3)†	54.596 (00)

* The numbers in parentheses indicate estimated intensities.

† Indicates a blend.

TABLE 2

TRIPLET SPLITTINGS OF O_2 IN THE $^3\Sigma_g^-$ GROUND STATE WITH $v'' = 0$

K	$^RQ(K) - {}^RR(K) = F_2(K) - F_1(K)$		$^PQ(K) - {}^PP(K) = F_2(K) - F_3(K)$	
	From $^1\Delta_g - {}^3\Sigma_g^-$	From $^1\Sigma_g^+ - {}^3\Sigma_g^-$ (Babcock)	From $^1\Delta_g - {}^3\Sigma^-$	From $^1\Sigma_g^+ - {}^3\Sigma_g^-$ (Babcock)
1	1.885	1.873	.....	.....
3	1.951	1.951	2.055	2.085
5	1.978	1.986	2.008	2.012
7	2.053	2.017	1.963	1.975
9	2.057	2.041	1.954	1.949
11	2.074	2.063	1.888	1.919
13	2.194*	2.083	1.941	1.900
15	2.095	2.103	1.821	1.881
17	2.122	2.124	1.977	1.862
19	2.052*	2.150	1.850	1.844
21	2.101	.....	.....	.....
23	.....	2.180	.....	1.813

* Indicates differences involving blended lines.

by the smallness of the difference between $F_2 - F_1$ and $F_2 - F_3$, accounts for the fact that the branches ${}^{Q}P$ and ${}^{Q}R$ are not resolved in our measurements (see Table 1).

In order to check the correctness of the interpretation of the S and O form branches, one may use the relation

$$ {}^{S}R\,(K-2) - {}^{O}P\,(K+2) - [\,{}^{R}Q\,(K-2) - {}^{P}Q\,(K+2)\,] = {}^{R}R\,(K) - {}^{P}P\,(K)\ , $$

which may be read from Figure 2(a). When we substitute the wave numbers of Table 1, this combination relation is found to hold well within the accuracy of the measurements for all the K values for which the differences can be formed.

From the combination differences,

$$ \Delta_2 F'\,(K) = {}^{R}R\,(K) - {}^{P}P\,(K)\ , $$

a provisional value of the rotational constant B_0' was obtained in the usual manner. However, since a highly accurate value of B_0'' ($=1.43777_0\ \mathrm{cm}^{-1}$)[7a] is known from the ordinary atmospheric oxygen bands, a value of B_0' that is somewhat more accurate than that obtained from $\Delta_2 F'$ can be obtained by plotting ${}^{R}R(K) + {}^{P}P(K)$ against $K(K+1)$ and determining the slope of the line obtained.[8] The same plot also yields a precise value for the origin of the 0–0 band and an approximate value of the rotational constant D_0' (using D_0'' from the ${}^1\Sigma_g^+ - {}^3\Sigma_g^-$ bands).

Unlike the situation in the absorption spectrum of liquid oxygen,[2] where the 1–0 band is only slightly less intense than the 0–0 band, in the gas the 1–0 band is very faint and was identified only after several unsuccessful attempts among the weak lines in the solar spectrum in the 10,700 A region. A check on the correct identification of this band was obtained by calculating the differences of corresponding lines of the two bands. It is easily seen that these differences are given by

$$ \Delta G_{1/2}' + (B_1' - B_0')\,J'\,(J'+1)\ , $$

where a term, $-(D_1' - D_0')J'^2(J'+1)^2$, has been neglected. Consequently, when plotted against $J'(J'+1)$, the differences should form a straight line. Figure 3 shows that this is indeed the case. The deviations from a straight line are within the accuracy of the measurements, which is not as high as for the 0–0 band, on account of the faintness of the lines of the 1–0 band. The fact that no lines of the ${}^{P}P$, ${}^{P}Q$, and ${}^{O}P$ branches have been found in the 1–0 band is due to the presence of a number of strong and broad solar lines on the long-wave-length side of the band center.

The slope of the straight line in Figure 3 gives a fairly precise value for the rotational constant, α', and therefore of B_1', while the intercept on the ordinate axis gives a precise value for $\Delta G_{1/2}'$.

The various rotational and vibrational constants of the ${}^1\Delta_g$ state of the oxygen molecule, determined by the above methods, and a few constants derived from them are collected in Table 3. The origins of the two bands, ν_{00} and ν_{10}, are referred to the nonexistent state with $K = 0$ of the term series $F_2''(K)$.[6a]

The dissociation energy given in Table 3 was obtained from the known dissociation energy of the ground state under the assumption that the ${}^1\Delta_g$ state dissociates into normal atoms (which is in agreement with the correlation rules). The values of $\Delta G_{1/2}$, B_e, and α_e of the ${}^1\Delta_g$ state are very nearly halfway between the corresponding values for the ${}^3\Sigma_{g_i}^-$ and ${}^1\Sigma_g^+$ states (about 5 per cent more toward the ${}^3\Sigma_g^-$ state). This is as one would expect it from the fact that the three states have the same electron configuration and the same dissociation products. It is therefore very probable that the anharmonicity constant, $\omega_e x_e$, which cannot be determined directly, also has a value nearly halfway be-

[7a] From an analysis of Babcock's new measurements.

[8] G. Herzberg, *Molecular Spectra and Molecular Structure*, Vol. 1: *Diatomic Molecules*, p. 205.

tween those of the $^3\Sigma_g^-$ and $^1\Sigma_g^+$ states. With the $\omega_e x_e$ value thus obtained (see Table 3), ω_e can be determined from $\Delta G_{1/2}$. Its value, of course, is not as accurate as that of $\Delta G_{1/2}$.

One might question the correctness of the assumption made here that the two observed bands are 0–0 and 1–0, respectively, and not 1–0 and 2–0. If the latter were the case, the 0–0 band would be expected at 1.5687 μ. On account of the Franck-Condon principle and the above-determined B values, it should have a much larger intensity

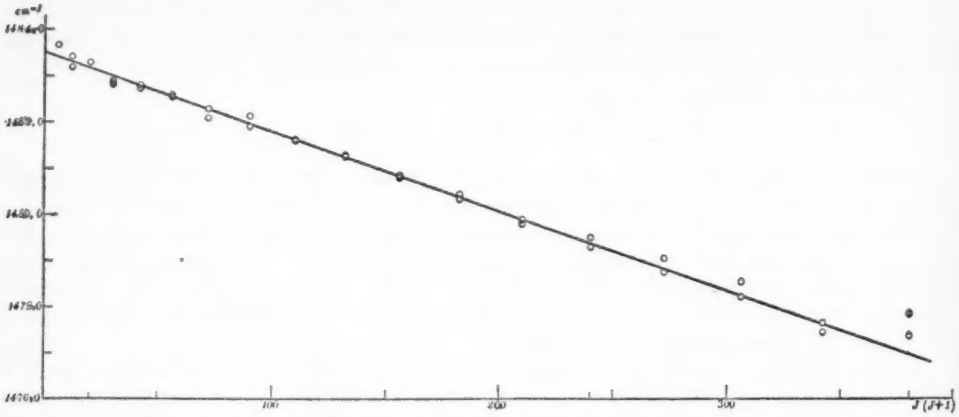

FIG. 3.—Differences of corresponding lines of the 1–0 and 0–0 bands plotted against $J'(J'+1)$.

TABLE 3

CONSTANTS OF THE $^1\Delta_g$ STATE OF O_2

Constant	Value
$A_0 = \nu_{00}$	7882.39 cm^{-1}
ν_{10}	9365.89 cm^{-1}
$\Delta G_{\frac{1}{2}}$	1483.5_0 cm^{-1}
ω_e	1509.$_3$ cm^{-1}
$\omega_e x_e$	12.$_9$ cm^{-1}
k_e	10.$73_2\times10^5$ dynes/cm
D_0 (diss. energy)	4.104 e.v.
B_0	1.4178_3 cm^{-1}
B_1	1.4007 cm^{-1}
B_e	1.4264 cm^{-1}
a_e	0.0171 cm^{-1}
I_e	19.620×10^{-40} gm cm^2
I_0	19.739×10^{-40} gm cm^2
r_e	1.2155×10^{-8} cm
r_0	1.2192×10^{-8} cm
D_0 (rot. const.)	4.86×10^{-6} cm^{-1}

than the band at 1.2683 μ (the intensity ratio of 0–0 and 1–0 band should be greater than for the ordinary atmospheric oxygen bands, for which it is about 20). No band of any strength is noticeable at 1.57 μ in Abbot's curves of the infrared solar spectrum, nor is any band near this position observed in liquid oxygen, proving that the band at 1.268 μ is indeed the 0–0 band.

In order to check the reliability of the rotational constants obtained, the individual band lines were calculated from these constants, assuming for the lower state very slightly revised constants derived from Babcock's new measurements. The agreement with the observed wave numbers was found to be within ±0.05 cm^{-1} for all unblended lines. No systematic deviations occur.

C. INTENSITY RELATIONS; COMPARISON WITH ABSORPTION SPECTRUM OF LIQUID OXYGEN

As is shown by the spectrogram (Fig. 1), the nine branches of the infrared atmospheric oxygen bands have intensities of the same order. This is in agreement with the theoretical results of Van Vleck,[6] who has given formulae for the intensity factors in $^1\Delta_g - {}^3\Sigma_g^-$ transitions, assuming negligible splitting in the $^3\Sigma_g^-$ state. In conformity with these formulae, the lines of the ^RR and ^PQ branches in Figure 1 are seen to be stronger than the corresponding (adjacent) lines of the ^RQ and ^PP branches, respectively (with the same J'). This behavior is opposite to the intensity ratios of the same branches in the $^1\Sigma_g^+ - {}^3\Sigma_g^-$ bands, which were investigated experimentally by Childs and Mecke[9] and theoretically by Schlapp.[10,7]

With the plates at our disposal no absolute intensity measurements were possible. It is, however, quite clear from these plates that the intensity of the $^1\Delta_g - {}^3\Sigma_g^-$ system for the same absorbing path is only a small fraction of that of the $^1\Sigma_g^+ - {}^3\Sigma_g^-$ system, probably less than one-twentieth. Both transitions, according to Van Vleck,[6] represent magnetic dipole radiation, and both are singlet-triplet intercombinations. However, the $^1\Delta - {}^3\Sigma$ system, in addition, violates the selection rule $\Delta\Lambda = 0, \pm 1$, which should hold for magnetic, as well as for electric, dipole radiation. This may explain the low intensity.

It is very striking that in liquid oxygen the $^1\Delta - {}^3\Sigma$ system is at least five times stronger than the $^1\Sigma - {}^3\Sigma$ system, as was found by Ellis and Kneser.[2] This reversal of the relative intensities as compared to the gas, is probably due to the fact that the quantum number Λ is no longer well defined in the liquid, particularly since most O_2 molecules have combined to $(O_2)_2$ complexes. It may also be mentioned that both transitions have a much greater absolute intensity in the liquid than in the gas.

A further anomaly in the absorption spectrum of liquid oxygen is the observation by Ellis and Kneser that the 1–0 band of the $^1\Delta - {}^3\Sigma$ system is almost as strong as the 0–0 band, whereas in the gas its intensity is very small as compared to that of the 0–0 band. The intensity ratio in the gas corresponds to expectation on the basis of the Franck-Condon principle; the ratio in the liquid does not. An analogous anomaly does not occur for the $^1\Sigma - {}^3\Sigma$ system in the liquid.

Both the 0–0 and the 1–0 band of the $^1\Delta - {}^3\Sigma$ system are shifted to shorter wave lengths in the liquid, as compared to the gas, the former by 48 cm^{-1}, the latter by 68 cm^{-1}. This shift indicates a firmer binding of the $(O_2)_2$ complex in the ground state than in the excited state. It may be mentioned that the vibrational frequency of the ground state is reduced by 5 cm^{-1} in the liquid, as compared to the gas.

We wish to thank Mr. H. D. Babcock for letting us use his new data for the ordinary atmospheric oxygen bands.

[9] W. H. J. Childs and R. Mecke, *Zs. f. Phys.*, **68**, 344, 1931.

[10] R. Schlapp, *Phys. Rev.*, **39**, 806, 1932.

ATOMIC LINES IN THE SPECTRUM OF R ANDROMEDAE*

PAUL W. MERRILL
Mount Wilson Observatory
Received February 3, 1947

ABSTRACT

The spectrum of the long-period variable R Andromedae, spectral type Se, was photographed from λ 3340 to λ 5000 with dispersion 10 A/mm. The observed portion of the light-cycle extended from 10 to 103 days after maximum. Because molecular bands do not interfere so seriously, this spectrum is better adapted than Me spectra to a general study of atomic lines. A few spectrograms were obtained of the region λλ 5000–6800, dispersion 20 A/mm.

Dark lines.—The identifications and displacements of more than thirteen hundred dark lines have been studied. A survey of the behavior of numerous multiplets includes the elements *Li* I, *Na* I, *Mg* I, *Al* I, *K* I, *Ca* I, *Ca* II, *Sc* I, *Sc* II, *Ti* I, *Ti* II, *V* I, *Cr* I, *Mn* I, *Fe* I, *Co* I, *Ni* I, *Ga* I, *Sr* I, *Sr* II, *Y* I, *Y* II, *Zr* I, *Zr* II, *Cb* I, *Ru* I, *Rh* I, *Ag* I, *In* I, *Ba* II, *Eu* I, *Eu* II, *Yb* I. A detailed study of the residuals from the mean radial velocity yielded by individual lines shows that the displacements of lines of neutral atoms (and of at least one ionized atom, *Y* II) increase algebraically with excitation potential. Lines of ionized atoms have positive displacements with respect to the lines of neutral atoms. The mean velocity exhibits little variation with phase.

Bright lines.—The behavior of bright lines of *H*, *Mg* I, *Fe* I, and *Fe* II was studied in considerable detail. Other lines measured include those of *Si* I, *Mn* I, *In* I, *Ca* II, *Ti* II, *Mn* II, *Sr* II. Speaking broadly, the behavior in the light-cycle resembles that in Me variables, but with some interesting differences. The velocities exhibit smaller variations with phase. Table 12 lists 60 unidentified bright lines; several, particularly λλ 3735.35, 4372.50, and 4455.31, are strong.

General.—Atoms of *Y* and *Zr* appear to be more abundant in R Andromedae than in Me variables. It is suggested that the trifurcation of the low-temperature end of the stellar sequence may have some connection with the nuclear stability of certain chemical elements.

R Andromedae, 001838, is a well-known red variable star, of period 407 days, magnitude range 5.6–14.7, the variability having been detected at Bonn in 1858. In the *Henry Draper Catalogue* the spectrum is described as very peculiar and in the continuous portion between $H\beta$ and $H\gamma$ is said to resemble the spectrum of the southern star π^1 Gruis. Bright hydrogen lines are conspicuous. The star was observed many years ago with slit spectrographs at Ann Arbor[1] and at Mount Wilson.[2,3] The spectrum is now considered a typical example of class Se.

The present investigation is based on a new series of spectrograms, dispersion 10.3 A/mm (20.6 A/mm in the visual region), similar to those recently used in my studies of several Me variables.[4,5,6] Dates of observation are in Table 1, and their relationship to the light-curve is shown in Figure 1. The photometric data were again supplied through the courtesy of Leon Campbell, of the Harvard Observatory.

ABSORPTION LINES

Because a considerably larger region of wave length is free from serious interference by molecular bands, the spectrum of R Andromedae, class Se, is better adapted to a

* *Contributions from the Mount Wilson Observatory, Carnegie Institution of Washington*, No. 730.

[1] P. W. Merrill, *Pub. Obs. U. Michigan*, **2**, 45, 1916.

[2] P. W. Merrill, *Mt. W. Contr.*, No. 252; *Ap. J.*, **56**, 457, 1922.

[3] P. W. Merrill, *Mt. W. Contr.*, No. 325; *Ap. J.*, **65**, 23, 1927.

[4] U Ori, R Ser, R Aql, R Cas, *Mt. W. Contr.*, No. 713; *Ap. J.*, **102**, 347, 1945.

[5] R Hya, *Mt. W. Contr.*, No. 717; *Ap. J.*, **103**, 6, 1946.

[6] R Leo, *Mt. W. Contr.*, No. 720; *Ap. J.*, **103**, 275, 1946.

general study of atomic lines than are the spectra of Me variables. The *ZrO* bands are much less extensive than the *TiO* bands of Me variables (see Figs. 2–5).

The continuous spectrum in the photographic region is well exposed on only four plates (at two epochs), Ce 3522, phase +9 days; Ce 3526, +10 days; Ce 3560, +44 days; and Ce 3564, +45 days. The rich dark-line spectrum with hundreds of measurable lines is very nearly the same at the two epochs. On the later plates, Ce 3611, phase

TABLE 1

JOURNAL OF OBSERVATIONS

Plate Ce	Date	JD 243	Mag.	Phase (Days)	Remarks
3078	1943 June 22	0898	7.0	+ 14	Sky spectrum superposed
3522	1944 Aug. 1	1304	6.9	+ 10	
3526	Aug. 2	1305	6.9	+ 11	
3560	Sept. 5	1339	7.3	+ 45	
3564	Sept. 6	1340	7.4	+ 46	
3565	Sept. 6	1340	7.4	+ 46	Bright lines only
3608	Oct. 6	1370	8.7	+ 76	Bright lines only
3611	Oct. 8	1372	8.8	+ 78	
3633	Nov. 2	1397	9.7	+103	
4003	1945 Sept. 28	1727	7.2	+ 27	Red region
4035	Oct. 24	1753	7.8	+ 53	Red region
4040	Oct. 25	1754	7.8	+ 54	Red region; three exposures

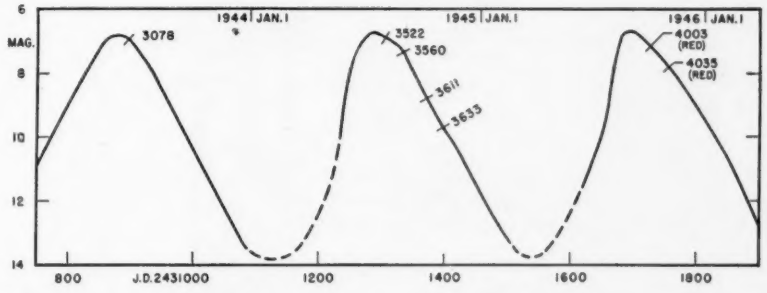

FIG. 1.—Light-curve of R Andromedae, showing dates of spectrograms (see Table 1)

+77 days, and Ce 3633, +102 days, the weak continuous spectrum allowed the measurement of 20–30 lines, enough to yield a fairly reliable radial velocity. All three red plates (Table 1) are measurable. The number of atomic lines, in absorption, measured on one or more plates is as shown in the accompanying tabulation.

λ	Dark Atomic Lines Measured
3340–4000	563
4000–4500	558
4500–5064	150
5800–6800	62
Total	1333

In the following condensed description of the behavior of the absorption lines of numerous chemical elements, the excitation potentials, E.P. (volts), are of the lower levels of the various multiplets. The multiplet references, Arabic numbers in parentheses, are to the Revised Multiplet Table.[7]

LINES OF *Li* I

E.P.

0.0 The ultimate line λ 6708, multiplet (1), is present in low intensity. The measurements (of relatively low weight) indicate that it is shifted shortward about 0.2 A. The observed shift is similar to that of the cores of the D lines of *Na* I.

LINES OF *Na* I

0.0 The D lines, multiplet (1), are strong and unsymmetrical, being shaded longward. In each line a narrow core, not well resolved from a broader component, is shifted shortward about 0.2 A with respect to the dark lines of most other elements.

LINES OF *Mg* I

0.0 Near maximum light the $^1S - {}^3P$ line λ 4571, (1), is of moderate intensity and in its normal position. As the cycle advances, the dark line is weakened and crowded longward by an emission fringe of increasing intensity. After phase +60 days the emission line dominates.

2.7 The lines of (3) are bright on all plates; on well-exposed plates taken near maximum, weak absorption lines were measured on the longward sides.

LINES OF *Al* I

0.0 Lines λ 3944 and λ 3961 of (1), although very strong, are not so outstanding as in R Leonis. On Ce 3526 the dark lines appear unsymmetrical, having a wing longward with a more abrupt boundary and possibly some emission on the shortward edge. On several of the later plates there is a trace of weak displaced emission like that exhibited so prominently by H and K of *Ca* II.

LINES OF *Si* I

1.9 The bright line λ 4103, (2), is notched by a dark line, but it is not certain that the absorption is due to atoms of *Si* I.

LINES OF *K* I

0.0 Lines λ 4044 and λ 4047 of (3), although weaker than in R Leonis, are easily identified. Their mean residual in radial velocity is small; as in several Me variables,[4] λ 4044 has a slight negative displacement with respect to λ 4047.

LINES OF *Ca* I

0.0 (1) moderate intensity; (2) λ 4226 extremely strong.
1.9 (3)–(6), (9) moderate intensity.
2.5 (23) and (25) probably present in low intensity.

LINES OF *Ca* II

0.0 The H and K lines, (1), are not extremely intense on these post-maximum plates. The profiles, especially that of the H line, are greatly distorted by the curious displaced emission within the shortward wings. This phenomenon, similar to that observed in several Me variables, will be described in the section on emission lines.

LINES OF *Sc* I

0.0 (1) doubtful; (2), (3) moderate intensity; (5), (6), (7), (8) strong.
1.4 (14) weak.
2.0 (20) weak.

[7] C. E. Moore, "A Multiplet Table of Astrophysical Interest," rev. ed., *Contributions from the Princeton Observatory*, No. 20, 1945.

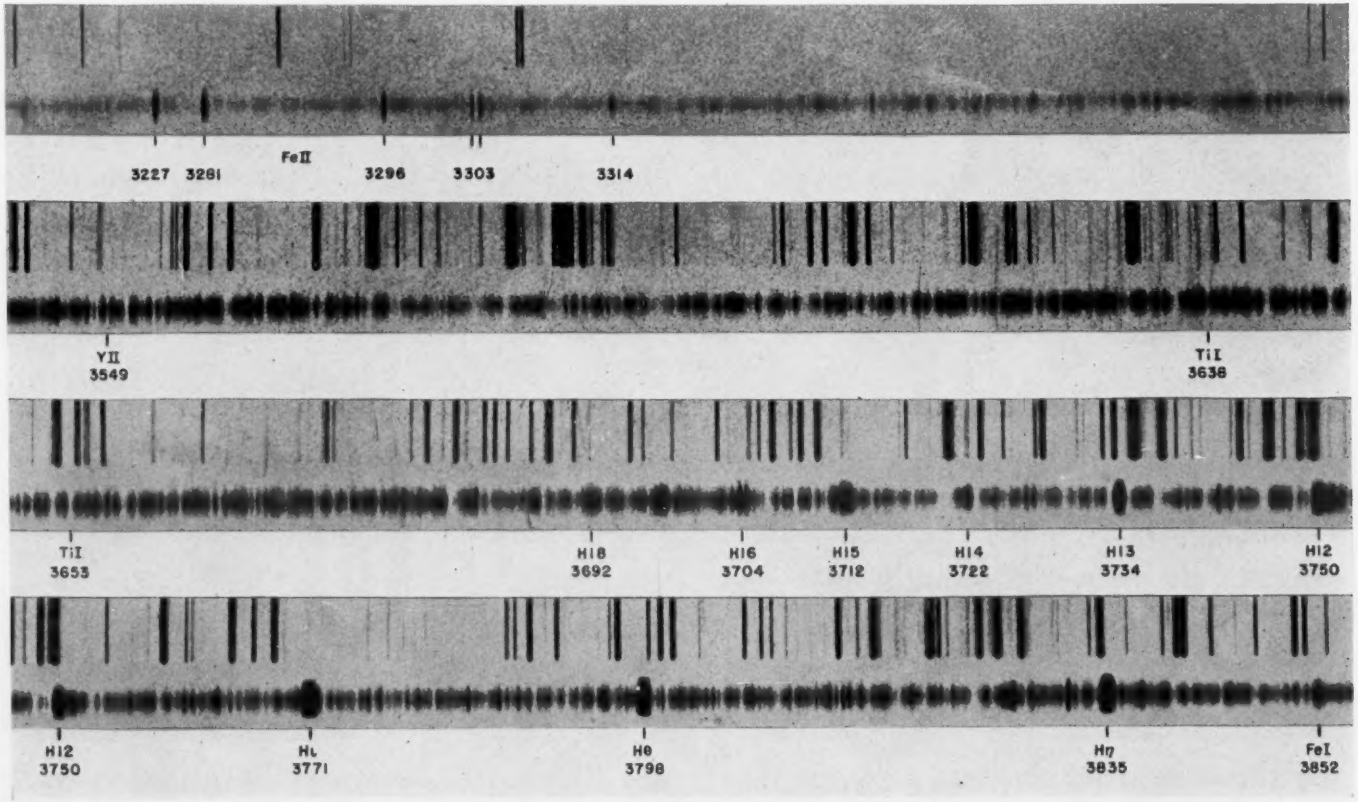

FIG. 2.—The spectrum of R Andromedae in the ultraviolet. Plate Ce 3526: August 2, 1944; magnitude 6.9; 11 days after maximum

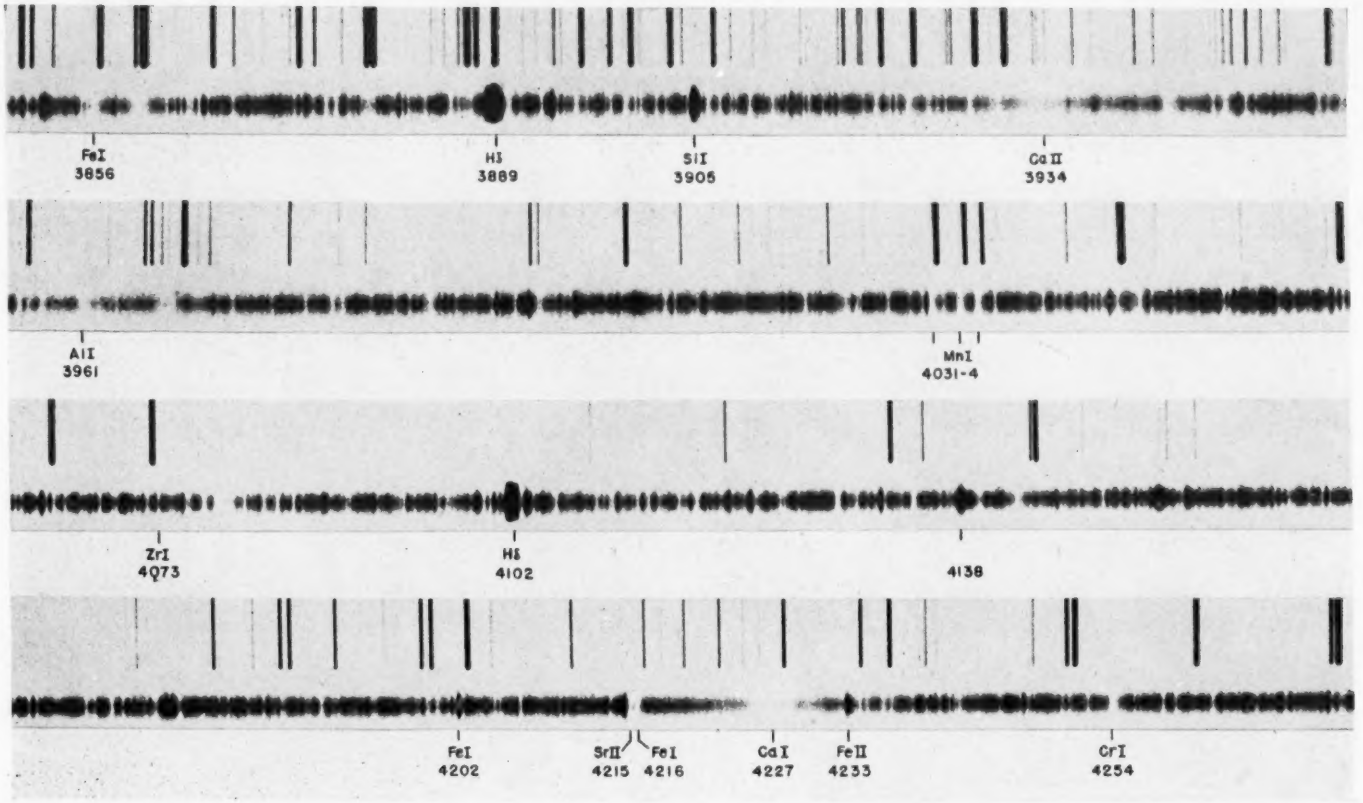

FIG. 3.—The spectrum of R Andromedae λλ 3850–4270. Plate Ce 3526: August 2, 1944; magnitude 6.9; 11 days after maximum

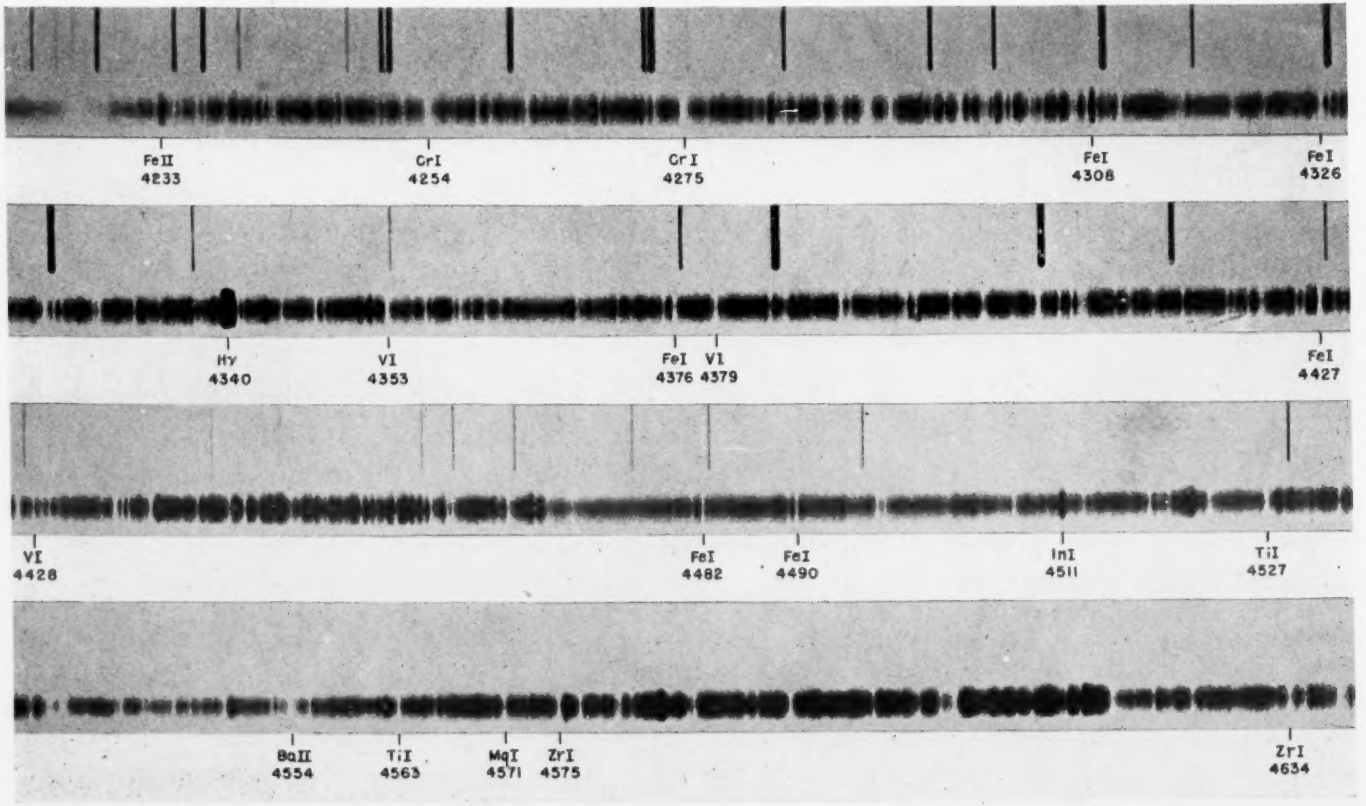

FIG. 4.—The spectrum of R Andromedae λλ 4220–4640. Plate Ce 3522: August 1, 1944; magnitude 6.9; 10 days after maximum

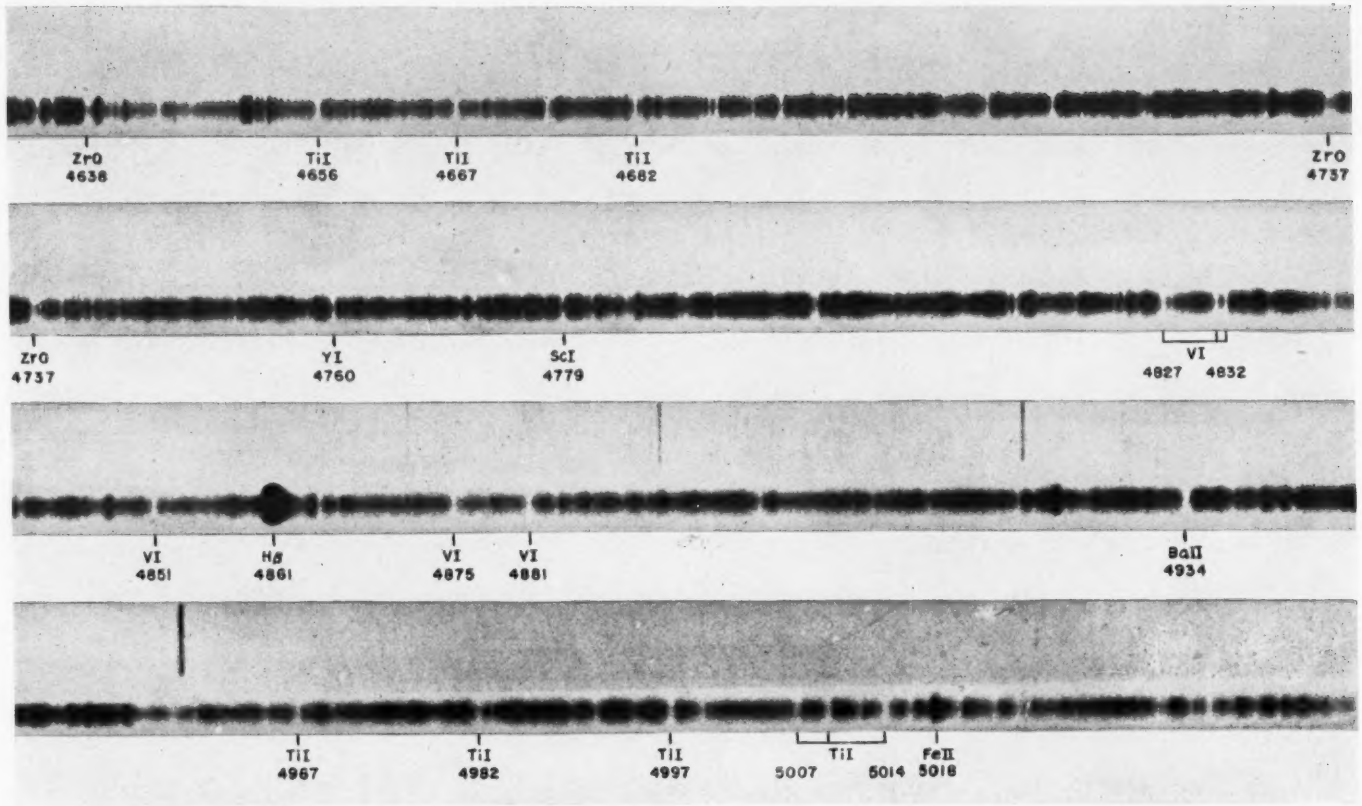

FIG. 5.—The spectrum of R Andromedae λλ 4630–5050. Plate Ce 3522: August 1, 1944; magnitude 6.9; 10 days after maximum

LINES OF *Sc* II

E.P.

0.0 (1) doubtful; (2), (3) strong.
0.3 (7), (11) strong; (8) weak; (10) probably present in low intensity.
0.6 (14), (15) probably present in low intensity.

LINES OF *Ti* I

0.0 (1) moderate intensity; (2) apparently present in low intensity; (6)–(21) strong, except (8), (16), which are weak and blended; (22) possibly present, observations inadequate.
0.8 (38), (41)–(44) strong; (39) doubtful.
1.0 (75), (80), (83) strong.
1.9 (160) moderate intensity; (157), (159), (161), (162), (163) probably present in low intensity.
2.1 (185) weak; (187), (188) little evidence.
2.2 (233) probably present in low intensity.

LINES OF *Ti* II

0.6 Near maximum light *Ti* II is represented by the three strongest lines of (13) and (14), λλ 3759, 3761, 3685. These dark lines are weak; the pair near λ 3760 have bright edges shortward, which strengthen somewhat as the light fades and which persist as weak emission lines throughout the observed interval.

LINES OF *V* I

0.0 (3)–(11) strong.
0.3 (19), (21), (22), (24), (25)?, (27), (28), (29) moderately strong; (20), (23), (26)? weak.
1.0 (34) moderate intensity.
1.1 (39), (40) not found; (41), (42) weak.

LINES OF *Cr* I

0.0 (1) very strong; (2), (3), (10) moderate intensity; (4) λλ 3579, 3593, 3605 extremely strong; (9), (11) apparently absent.
1.0 (21), (22), (23) moderate intensity; (24) weak.
2.5 A few strong lines of (38), (46), and (47) are probably present in low intensity.

LINES OF *Mn* I

0.0 The three lines of (2) near λ 4030 are very strong, with marked emission developing on the shortward edges during the post-maximum phase, as in Me variables.
2.1 (5) surprisingly strong; (6), (8) weak or absent.
2.3 (18) may be present in low intensity but blends interfere.

LINES OF *Fe* I

0.0 (2)–(5) strong; (6) present but not measured because of underexposure at the shortward end of the photographed spectrum.
0.9 (18)–(23) fairly strong; (24), (25) probably present but observations inadequate.
1.5 (41), (42), (43), (45) moderate intensity; (44), (46), (48) weak or absent.
2.2 (68) probably present in low intensity; (73), (78) possible; (71), (72), (74), (76) little evidence.
2.4 (152) apparently present in low intensity.
2.8 (354), (355) the strongest lines are probably present in low intensity.

LINES OF *Co* I

0.0 (1)–(6) fairly strong.
0.4 (16), (18), (19), (21), (22) fairly strong; (17), (20) weak or absent.
0.9 (28)–(35) except (32) moderate or low intensity; (32) weak or absent.
1.9 (58), (62) weak or absent.

LINES OF *Ni* I

E.P.

0.0 (1)–(4), (6) fairly strong.
0.1 (15), (16) fairly strong; (17), (18) present, observations inadequate.
0.4 (28), (30)–(33), (35), (36) fairly strong.

LINES OF *Ga* I

0.0 (1) seems to be represented by λ 4172, but the observation needs confirmation; λ 4030, if present, is blended with the strong line of *Mn* I.

LINES OF *Sr* I

0.0 (2) λ 4607 strong.

LINES OF *Sr* II

0.0 (1) λ 4077, λ 4215 strong. See description of emission edges in the section on emission lines.

LINES OF *Y* I

0.0 (1)–(8) fairly strong; blends interfere with some identifications.

LINES OF *Y* II

0.0 (1), (2) fairly strong.
0.1 (5)–(9) fairly strong.
0.4 (12) weak or absent; (13) fairly strong; (14), (15), (16) moderate or low intensity.
1.0 (22) may be represented by traces of the two leading lines, but the identification is doubtful because of blends.

LINES OF *Zr* I

0.0 (1), (2), (3), (5)–(16) fairly strong; (4) doubtful; (7), (11), (14) badly blended.
0.5 (29), (31), (32) moderate intensity; (28) not observed; (30), (33) doubtful because of blends.
0.6 (43), (45), (46) moderate intensity; (44) weak.
0.6 (48)–(52) moderate intensity.
1.0 (58) moderate intensity.
1.4 (61) weak.
1.5 (63), (64) no evidence.
1.8 (66) no evidence.

LINES OF *Zr* II

0.0 (1) fairly strong.
0.4 (2) moderate intensity, observations incomplete; (3) possible, observations incomplete; (7) little evidence; (8) doubtful; (9) strongest lines may be present in low intensity.

LINES OF *Cb* I

0.0 (1), (3) moderate intensity; (2), (4) doubtful.

LINES OF *Ru* I

0.0 (1), (2), (4) moderate intensity; (3) doubtful.

LINES OF *Rh* I

0.0 (1), (2), (3) strongest lines may be present in low intensity.

LINES OF *Ag* I

0.0 (1) λ 3382 moderate intensity. This may be the first observation of silver in the stars. Both lines of (1) are faintly present in the solar spectrum.

LINES OF *In* I

0.0 (1) λ 4101 may be present as a notch in bright *Hδ*. The other line of (1), λ 4511, is a strong emission line.

LINES OF *Ba* II

E.P.

0.0 (1) strong; the strength of λ 4554 and λ 4934 is characteristic of S-type spectra.
2.7 (3) probably absent; (4) probably present in low intensity.

LINES OF *Eu* I

0.0 (1) little evidence for or against.

LINES OF *Eu* II

0.0 (1) moderate intensity; (2) perhaps present in low intensity.
0.2 (4) no evidence for or against; (5) perhaps present in low intensity.

LINES OF *Yb* I

0.0 (2) moderate intensity.

TABLE 2

RADIAL VELOCITIES DERIVED FROM DARK LINES ON ONE-PRISM SPECTROGRAMS

Year	Phase (Days)	Rad. Vel. (Km/Sec)	No. Plates
1919	−12	− 8.2	2
1921	−16	(−14)	1
1928	+ 6	− 4	1

TABLE 3

RADIAL VELOCITIES FROM ABSORPTION LINES

Plate Ce	Date	Phase (Days)	Rad. Vel. (Km/Sec)
3522	1944 Aug. 1	+ 9	−10.7
3526	Aug. 2	+ 10	
3560	Sept. 5	+ 44	−12.1
3564	Sept. 6	+ 45	
3611	Oct. 8	+ 77	−11.0
3633	Nov. 2	+102	−13.5
4003	1945 Sept. 28	+ 27	− 9.5
4035	Oct. 24	+ 53	−11.4
4040	Oct. 25	+ 54	
Mean	.....	+ 57	−11.3

Radial velocities from dark lines.—The radial velocities previously derived[8, 9] from one-prism spectrograms, dispersion 35 A/mm, are listed in Table 2.

The values obtained from the present series of grating spectrograms are in Table 3. The observed interval extends only from 9 to 102 days after maximum. During this time there appears to be a slight decrease (algebraic) in velocity, but the change is small, scarcely exceeding errors of observation. With the possible exception of the observation in 1928, there is no evidence of differences between various maxima.

The measured relative displacements of numerous multiplets of various elements are recorded in Table 4, in which the tabulated residuals are the means from measurements

[8] P. W. Merrill, *Mt. W. Contr.*, No. 264; *Ap. J.*, **58**, 215, 1923.

[9] P. W. Merrill, *Mt. W. Contr.*, No. 649; *Ap. J.*, **94**, 171, 1941.

TABLE 4

DISPLACEMENTS OF MULTIPLETS (ABSORPTION LINES)

Element	E.P. (Volts)	Mult.	Resid. (Km/Sec)	Wt.
Mg I	0.0	1	(Var.)	2
	2.7	3	(+1.9)	1.5
Al I	0.0	1	(+2.6)	1
K I	0.0	3	−1.0	4
Ca I	0.0	2	(−2.1)	1
	1.9	4	−0.2	8
		5	0.0	6
		9	+0.3	2
	2.5	23	+0.7	1
		25	+5.5	1
Sc I	0.0	5	−0.6	6
		6	−1.8	4
		7	−0.4	4
		8	−0.7	4
	1.4	14	−0.1	2
	2.0	20	−1.9	1
Sc II	0.0	2	+2.8	4
		3	+2.4	4
	0.3	7	+2.0	2
		8	+4.2	1
		10	+2.3	0.5
		11	0.0	2
	0.6	14	+0.8	0.5
		15	+5.6	0.5
Ti I	0.0	5	−1.2	5
		6	−3.0	10
		7	−3.8	3
		8	−0.7	4
		9	−1.0	3
		10	+0.3	2
		11	+1.2	3
		12	−5.8	10
		13	−1.8	6
		14	−3.7	5
		15	−1.2	8
		17	−3.0	12
		18	−1.8	10
		19	−0.7	11
		20	−1.4	4
		21	−2.5	1
	0.8	38	+2.9	8
		41	−0.2	2
		42	+0.7	16
		43	+2.0	9
		44	−0.5	11
	1.0	75	+0.3	5
		80	−0.6	8
		83	−0.7	1
	1.9	157	−5.0	0.5
		159	+2.3	1
		160	−0.9	5
		161	+2.2	1
	2.1	185	+1.0	2
	2.2	233	−0.6	2
Ti II	0.6	13	+2.2	2
		14	+1.5	1

Element	E.P. Volts	Mult.	Resid. (Km/Sec)	Wt.
V I	0.0	3	−2.4	16
		4	−0.8	11
		5	+0.5	13
		6	+0.4	9
		7	−2.1	14
		8	−0.3	5
		9	−2.2	9
		10	−1.6	3
		11	−2.2	1
	0.3	21	+0.3	14
		22	+0.5	22
		23	+4.3	1
		24	+1.3	8
		25	+0.4	2
		27	+0.6	10
		28	+0.9	16
		29	+0.8	6
	1.1	41	−2.4	1
		42	0.0	3
Cr I	0.0	1	(−2.2)	4
		2	−2.2	4
		3	−0.8	1
		4	0.0	0.5
		10	+1.2	6
	1.0	21	+1.2	11
		22	+0.4	11
		23	+1.0	10
		24	0.0	2
	2.5	38	+2.9	2
		46	+0.5	1
Mn I	0.0	2	(−3.5)	5
	2.1	5	+2.6	4
Fe I	0.0	2	−1.2	19
		3	−1.7	9
		4	−0.5	15
	0.0	5	−1.2	7
	0.9	18	+3.5	2
		19	+0.9	5
		20	+0.4	12
		21	−0.5	16
		22	+1.3	3
		23	−0.6	13
		24	+1.0	3
		25	+3.7	1
	1.5	41	+1.2	6
		42	+1.0	10
		43	+1.8	9
		45	+0.5	6
	2.2	68	+2.7	3
		73	(+0.1)	1.5
		78	(+5.8)	0.5
	2.4	152	+3.6	6
	2.8	354	(−3.4)	2
		355	+1.4	1
Co I	0.0	1	+2.0	4
		2	−0.8	6
		3	−1.2	6
		4	+0.8	4
		5	0.0	1.5

TABLE 4—*Continued*

Element	E.P. (Volts)	Mult.	Resid. (Km/Sec)	Wt.	Element	E.P. (Volts)	Mult.	Resid. (Km/Sec)	Wt.
Co I—*Cont.*		6	−1.8	4	*Y* II—*Cont.*	0.4	13	+5.2	2
	0.4	16	+0.2	5			14	+4.3	1
		18	+0.6	4			15	−1.5	0.5
		19	+1.6	5			16	+3.0	0.5
		20	−0.8	0.5					
		21	+0.3	5	*Zr* I.....	0.0	5	−2.0	6
		22	−0.1	4			6	−1.3	8
		23	+1.6	1			8	−1.7	4
	0.9	28	+1.6	2			9	−0.6	1
		29	+3.1	1			10	−1.2	8
		30	+3.0	2			12	−1.8	4
		31	+2.5	1			13	−0.1	1
		33	+3.6	0.5			15	−1.1	3
		34	+2.1	1			16	+1.9	1
	1.9	62	+2.4	1		0.5	29	−4.0	2
							31	+3.3	6
Ni I.....	0.0	1	−2.6	2			32	+1.5	4
		2	+2.6	5		0.6	43	+0.1	12
		3	−2.7	2.5			44	+0.4	6
		4	+0.3	5			45	+0.3	17
		6	−1.7	2			46	−0.5	5
		9	+1.6	0.5		0.6	48	−4.0	1
	0.0	15	+0.2	7			49	−0.9	1
		16	−0.6	5			50	+3.4	2
		17	−2.2	1			51	+1.9	2
		18	−2.4	1			52	+1.7	2
	0.4	30	+1.6	1		1.0	58	−0.8	2
		31	+1.8	4			61	+1.9	2
		32	+1.4	1					
		33	+3.0	5	*Zr* II.....	0.0	1	+3.1	6
		35	+3.6	2			2	+4.3	2
		36	+3.9	1			3	+5.5	1
						0.4	8	(+3.6)	1
Ga I.....	0.0	1	(+1.2)	2			9	(+0.6)	1.5
Sr I.....	0.0	1	(−1.6)	2	*Cb* I.....	0.0	1	+0.4	13
							3	+0.2	6
Sr II.....	0.0	1	(−4.6)	4					
					Ru I.....	0.0	1	+0.9	1
Y I.....	0.0	4	−1.6	5			2	+2.1	7
		5	−2.9	6					
		6	−0.2	2	*Rh* I.....	0.0	2	+1.8	1
		7	−1.1	2					
		8	+1.7	1	*Ag* I.....	0.0	1	+1.3	1
Y II.....	0.0	1	−1.6	1	*Ba* II.....	0.0	1	(−2.8)	4
		2	0.0	2		2.7	4	+0.5	2
	0.1	5	+1.5	4					
		6	−0.2	2	*Eu* II.....	0.0	1	−0.8	5
		7	+0.4	4		0.2	5	+2.6	0.5
		8	−0.2	3					
		9	+0.3	9	*Yb* I.....	0.0	2	−1.8	2

of four plates with numerous lines, Ce 3522, 3526, 3560, 3564. The residuals in parentheses correspond to multiplets omitted in forming the velocities adopted for each plate. The weights in the last column depend largely on the number of lines measured. A well-defined line of suitable intensity for accurate settings measured on two plates was given

unit weight. Thus a multiplet with three good lines measured on all four plates would have weight 6.

The detailed results in Table 4 are summarized in Tables 5 and 6. Table 5 shows that residuals of lines of neutral atoms (and of at least one ionized atom, *V* II) increase

TABLE 5

DISPLACEMENTS OF ABSORPTION LINES AT VARIOUS EXCITATION POTENTIALS

Element	E.P. (Volts)	Resid. (Km/Sec)	Wt.	Element	E.P. (Volts)	Resid. (Km/Sec)	Wt.
Sc I	0.0	−0.9	18	*Fe* I	1.5	+1.2	31
	1.4	−0.1	2		2.2	+2.7	3
	2.0	−1.9	1		2.4	+3.6	6
					2.8	+1.4	1
Sc II	0.0	+2.6	8				
	0.3	+1.7	5.5	*Co* I	0.0	−0.3	25.5
	0.6	+3.2	1		0.4	+0.6	24.5
					0.9	+2.5	7.5
Ti I	0.0	−2.2	97		1.9	+2.4	1
	0.8	+1.0	46				
	1.0	−0.3	14	*Ni* I	0.0	−0.2	17
	1.9	−0.3	7.5		0.4	+2.6	14
	2.1	+1.0	2				
	2.2	−0.6	2	*V* II	0.0	−0.5	3
					0.1	+0.4	22
Ti II	0.6	+2.0	3		0.4	+3.9	4
V I	0.0	−1.2	81	*Zr* I	0.0	−1.4	36
	0.3	+0.7	79		0.5	+1.5	12
	1.1	−0.6	4		0.6*	+0.1	40
					0.6†	+1.1	8
Cr I	0.0	−0.2	11.5		1.0	−0.8	2
	1.0	+1.0	34		1.4	+1.9	2
	2.5	+2.1	3				
				Zr II	0.0	+3.7	9
Fe I	0.0	−1.0	50		0.4	(+1.8)	2.5
	0.9	+0.2	55				

* Lower term, a^5F. † Lower term, a^1D.

TABLE 6

DISPLACEMENTS OF LINES OF VARIOUS ELEMENTS

Element	Resid. (Km/Sec)	Wt.	Element	Resid. (Km/Sec)	Wt.
Al I	(+2.6)	1	*Sr* I	(−1.6)	2
K I	−1.0	4	*Sr* II	(−4.6)	2
Ca I	+0.3	18	*Y* I	−1.7	16
Sc I	−0.9	21	*Y* II	+0.8	29
Sc II	+2.4	14.5	*Zr* I	−0.2	100
Ti I	−1.0	168.5	*Zr* II	+3.7	9
Ti II	+2.0	3	*Cb* I	+0.3	19
V I	−0.3	164	*Ru* I	+1.9	8
Cr I	+0.8	48.5	*Rh* I	+1.8	1
Mn I*	+2.6	4	*Ag* I	+1.3	1
Fe I	+0.2	146	*Ba* II†	+0.5	2
Co I	+0.4	58.5	*Eu* II	−0.6	5.5
Ni I	+0.7	45	*Yb* I	−1.8	2
Ga I	(+1.2)	1			

* E.P. 2.1 volts. † E.P. 2.7 volts.

algebraically with excitation potential. A similar effect was previously found in the spectra of several Me variables.[10] The relative displacements in R Andromedae are equal to, or less than, those in the Me variables.

The results for various elements (Table 6) yield no evidence of differences in behavior between heavy metals and light ones. The lines of ionized atoms, however, have positive displacements with respect to those of neutral atoms. The most reliable displacements, shown in the accompanying tabulation, have a mean value, II *minus* I, of +3.2 km/sec.

Element	II−I	Element	II−I
Sc	+3.3 km/sec	*Y*	+2.5 km/sec
Ti	+3.0	*Zr*	+3.9

EMISSION LINES

Lines of hydrogen.—The bright lines of the Balmer series are outstanding on all plates, although at the faintest observed phase, +102 days, the intensities are somewhat decreased (see Figs. 2–7). Near maximum light the slightly widened *H* lines are badly

TABLE 7

RADIAL VELOCITIES FROM EMISSION LINES
(KM/SEC)

Element and Line or Multiplet	Phase (Days)				
	+10	+45	+76	+102	+58 (Mean)
H (several)	−26.0	−28.6	−28.3	−27.0	−27.5
Fe I (many)	33.8	31.7	29.8	28.5	30.7
Mg I λ 4571	.....	33.2	30.1	27.7	30.3
Mg I (3)	30.6	29.6	28.5	29.8	29.6
Si I (2), (3)	29.8	30.9	30.7	32.5	31.4
Mn I (2)	47.3	48.2	48.3	47.7	48.0
In I λ 4511	28.5	29.1	28.8	28.0	28.6
Ti II (13)	30.8	29.3	29.2	29.5	29.7
Fe II (many)	26.0	27.6	26.8	27.2	26.9
Sr II λ 4215	−42.0	−42.0	−40.0	−39.3	−40.8
	Absorption-Line Velocities				
Neutral metals	−10.7	−12.1	−11.0	−13.5	−11.3

mutilated by absorption lines of other elements; as the cycle advances, they tend to become narrower and to assume their normal (laboratory) relative intensities. At the later phases they are evidently subject to the absorption of the reversing layer to a far less degree than they are when near maximum. In this respect their behavior strongly resembles that in Me variables. A detailed study of the apparent structure of the bright lines before maximum when the mutilations are the greatest would be especially interesting. It might be possible to demonstrate that the hydrogen emission occurs at first not only below the reversing layer but even below the level of the normal photosphere.

Radial velocities, which depend chiefly on measurements of lines from *Hβ* to *H* 18, are listed in Table 7. The differences do not exceed errors of measurement. The mean velocity, −27.5 km/sec, agrees within errors with the value −29 km/sec, previously adopted,[9] which depends on one-prism spectrograms obtained during the years 1915–1939.

[10] *o* Ceti, W. S. Adams, *Mt. W. Contr.*, No. 638; *Ap. J.*, **93**, 11, 1941; U Ori, see n. 4; R Hya, see n. 5; R Leo, see n. 6.

Lines of Fe I.—The emission-line spectrum of *Fe* I is somewhat more fully developed in R Andromedae than in Me variables. The pattern of behavior with advancing phase in the light-cycle is similar to that in R Leonis, although not identical in all details. Some of the observed differences are probably due to the absence of *TiO* bands in R Andromedae.

The number of measurable bright lines increased from about 15 at phase +10 days to about 60 at +120 days (see Figs. 6 and 7). The three strongest lines are λλ 3852, 4202, and 4308. The lines λ 4202 and λ 4308 with the common upper level $z^3G_4^\circ$ have abnormally high intensities compared with other lines of multiplet (42) which appear faintly at the later phases. As in R Leonis,[11] the only observed lines of (24) are λ 3521 and λ 3565, which also have upper level $z^3G_4^\circ$. A comparison of the intensities of lines of multiplet (2) in R Andromedae and in R Leonis has previously been published.[12] The measured displacements of lines in 16 multiplets are included in Table 8. The mean displacements become slightly larger algebraically as the phase advances. This behavior, which differs from that of the hydrogen lines (Table 7), closely resembles that of *Fe* I λ 4202 in R Leonis.[6]

The negative residuals of (21) seem to be characteristic of this multiplet. The positive residuals in (41) at phases +10 and +45 depend on measurements of low weight, but they may be characteristic of the multiplet at these phases; at later phases the residuals, although smaller, are still positive. The positive residuals of (72) for phases +45, +76, and +102 days are the means of reasonably accordant values from three slightly diffuse lines and are probably characteristic of the multiplet. The behavior of λ 3852.57 is remarkably similar to its behavior in R Hydrae.[5] The shortward component yields the same displacements as those of other lines of multiplet (73). The close companion line longward, which gains in relative intensity as the phase advances, has a measured wave length of 3852.8. Since it occupies approximately the position corresponding to the displacement of the dark-line spectrum, it may possibly be a component of the iron line itself. On the whole, the measurements in the spectrum of R Andromedae tend to confirm the identification of this outstanding line with λ 3852.57, *Fe* I (73). Careful intercomparison of the behavior in the spectra of R Hydrae, R Leonis, R Andromedae, and χ Cygni of bright *Fe* I lines of various multiplets may assist in the detailed interpretation of their intensities and displacements.

Lines of Mg I.—The bright $^1S - {}^3P$ line λ 4571 multiplet (1) behaves much as it does in the spectra of Me variables, appearing a few weeks after maximum and becoming outstanding toward minimum. The apparent radial velocity increases algebraically by a few kilometers per second, as in R Hydrae and R Leonis. The bright lines of (3) are present in moderate intensity on all plates and increase only slightly with advancing phase. The radial velocity exhibits almost no change.

Lines of Si I.—Both of the lines λ 4102 (2) and λ 3905 (3) appear as close doubles, with a separation of about 0.32 A at phases +10 and +45 days, and about 0.23 A at phases +76 and +102 days. The shortward component yields the same velocities as other bright lines (Table 7). In λ 3905, the shortward component is much the stronger on all plates; in λ 4103, it is the stronger at phase +10 days, weaker at phases +45, +76, and +102 days, although the differences in intensity are not great. Both components appear somewhat narrower at phases +76 and +102 days than at +10 and +45 days, in conformity with the general tendency of bright lines to become narrower as the phase advances. The behavior of the components of these *Si* I lines resembles qualitatively that of λ 3852 *Fe* I. In all three lines the separation corresponds approximately to the general displacement between bright and dark lines; and in all three the longward components gain in relative intensity as the phase advances. These longward components,

[11] P. W. Merrill, *Mt. W. Contr.*, No. 720; *Ap. J.*, **103**, 275, Table 6, 1946.

[12] P. W. Merrill, *Pub. A.S.P.*, **58**, 304, 1946.

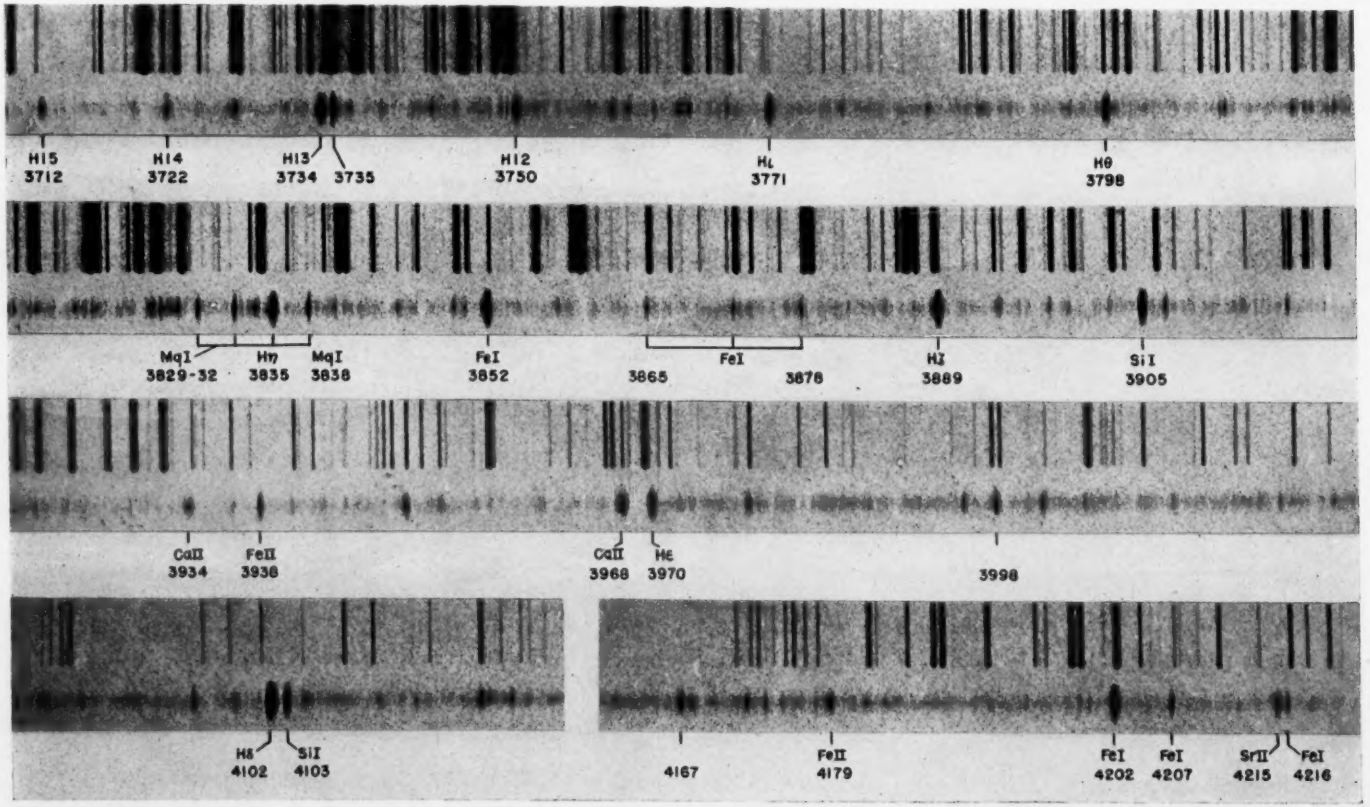

FIG. 6.—The spectrum of R Andromedae λλ 3700–4220. Plate Ce 3633: November 2, 1944; magnitude 9.7; 103 days after maximum

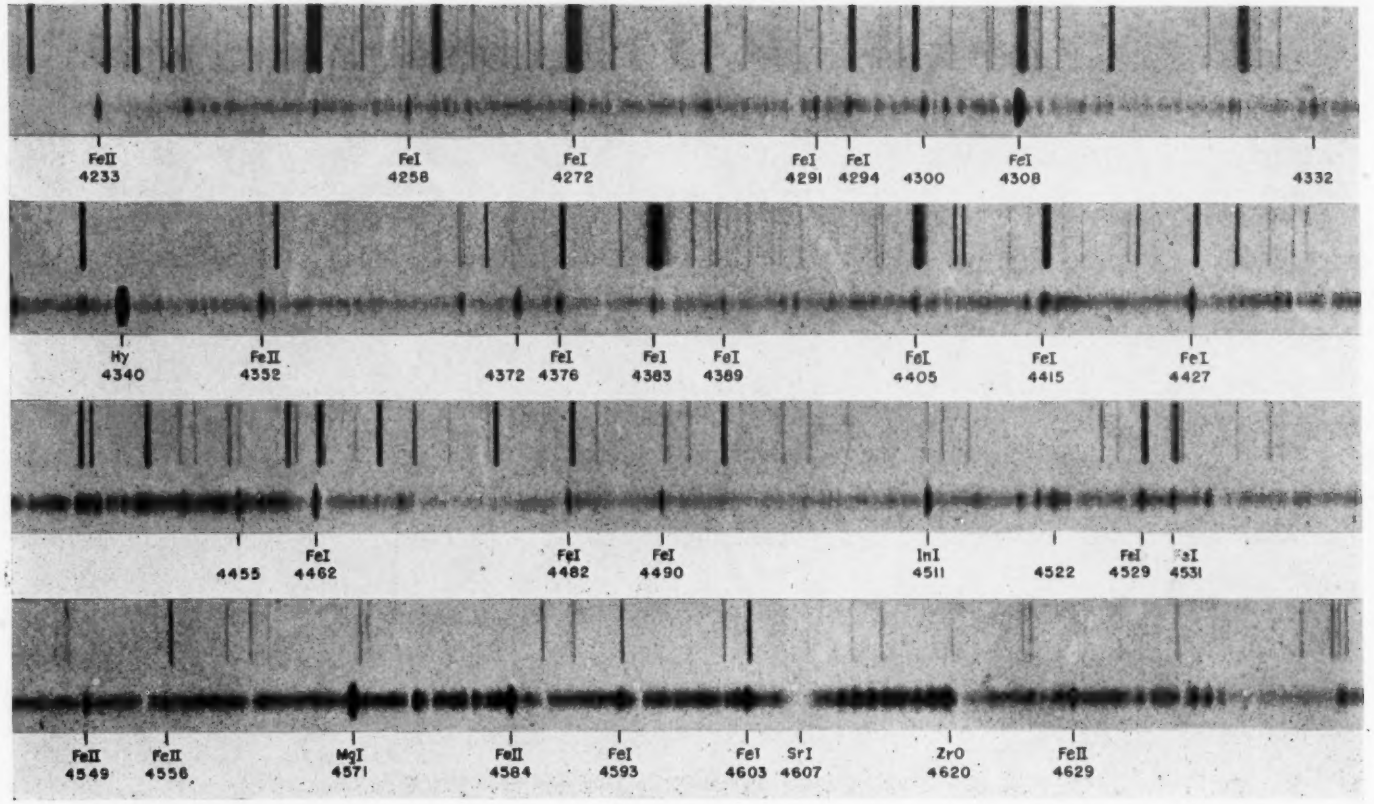

FIG. 7.—The spectrum of R Andromedae λλ 4230–4650. Plate Ce 3633: November 2, 1944; magnitude 9.7; 103 days after maximum

therefore, probably have the same atomic origins as the shortward components. Their positions suggest a relationship to the body of gas which produces the dark lines. Possibly the high-excitation potentials (about 2 volts for the lower levels) are responsible for the fact that the components appear in emission rather than in absorption. This slight clue to the enigmatic relationship between bright and dark lines in the spectra of long-period variables should be followed up in future investigations.

Lines of Mn I.—Emission in the well-known triplet of (2) near λ 4030 grows stronger as the cycle advances. At phase +10 days it consists only of a weak edge to the strong dark line λ 4030; later all three lines are bright, λ 4030 becoming outstanding. It is

TABLE 8

RADIAL VELOCITIES FROM EMISSION LINES OF *Fe* I
(KM/SEC)

Multiplet	Upper Level		Phase (Days)				
	Desig.	E.P. (Volts)	+10	+45	+76	+102	+58 (Mean)
2	$z^7F°$	2.8	−35.4 3*	−32.9 5*	−31.7 5*	−29.1 6*	−32.3
3	$z^7P°$	2.9	.....	31.2 1	32.8 2	28.0 4	30.7
20	$y^5D°$	4.1	35.6 1	32.8 2	27.4 6	27.3 7	30.8
21	$y^5F°$	4.2	40.1 1	40.2 2	33.7 4	31.6 6	36.4
22	$z^5P°$	4.2	30.9 1	28.7 2	24.5 2	29.1 2	28.3
23	$z^5G°$	4.3	36.5 1	37.1 2	29.8 3	29.6 3	33.2
24	$z^5G°$	4.4	.....	31.3 2	30.2 2	31.6 2	31.0
39	$y^5F°$	4.2	.....	.....	26.0 3	25.5 3	25.8
41	$z^5G°$	4.3	(21.2) 1	25.3 3	26.0 6	26.7 6	26.0
42	$z^3G°$	4.4	35.4 2	32.9 3	33.8 3	28.4 5	32.6
43	$y^3F°$	4.6	39.2 2	35.2 2	34.3 5	28.8 6	34.4
45	$y^3D°$	4.7	29.9 1	27.3 1	32.3 1	29.4 1	29.7
68	$x^5D°$	4.9	26.9 1	31.7 3	28.5 2	26.4 2	28.4
72	$x^5P°$	5.3	29.0 3	23.0 3	20.6 3	18.5 3	22.8
73	$w^5D°$	5.4	28.0 1	28.8 3	27.0 3	−28.4 2	28.0
74	$w^5F°$	5.4	−30.4 3	−28.4 2	−27.1 1	.....	−28.6
Mean All	.....	.....	−33.1 20	−31.0 36	−29.2 51	−28.0 58	−29.9 16†
Mean All except (72)	.....	.....	−33.8 17	−31.7 33	−29.8 48	−28.5 55	−30.4 15

* Number of lines. † Number of multiplets.

remarkable that the measured velocity does not change with phase; throughout the interval of observation it remains about 18 km/sec less than the velocity yielded by most other bright lines (Table 7).

The line λ 4511 (In I).—This bright line is moderately strong, 10 days after maximum, and becomes outstanding as the phase advances. The radial velocity is constant (Table 7).

Lines of Fe II.—About 25 bright lines of *Fe* II have been measured on one or more plates. Their intensities are greater during the interval from phase +45 to +102 days than at +10 days. Lines of multiplet (1) with wave lengths between λ 3200 and λ 3300 are remarkably strong, although little continuous spectrum is recorded in their region (Fig. 2). The line λ 3227.73 of (6) was measured on three plates; λ 3196.07 of (7) on one. Nearly all these lines have been observed by Swings and Struve[13] in bright-line stars of other types, and two or three of the strongest appeared on my spectrograms of R Leonis.[6]

[13] *Ap. J.*, **97**, 194, 1943.

The relative intensities of various lines of (1) estimated in BF Cygni and R Andromedae (Table 9) exhibit interesting departures from the laboratory values. The marked weakness of λ 3255 in R Andromedae suggests that this line may be partially suppressed by a dark line, but there is no direct evidence of this effect. Several lines in R Andromedae seem to change in relative intensity during the observed interval. In BF Cygni, λ 3281 and λ 3295 are relatively weak.

The line λ 3938.29 of (3), although rather weak 10 days after maximum, grew stronger during the observed interval. The companion line, λ 3914.48, was not observed. The strong dark line λ 3914.33 *Ti* I (15) may be responsible for its absence; the difference of wave length 0.15 A is only a few hundredths less than the observed difference between displacements of bright and dark lines.

TABLE 9

INTENSITIES OF EMISSION LINES OF *Fe* II MULTIPLET (1)

I.A.	J	Intensities			
		Lab.	BF Cygni*	R Andromedae	
				Ce 3526	Ce 3633
3277.35	3½–4½	9	6	6	6
3302.86	2½–3½	4	1	1.5	1
3312.71	1½–2½	(1)	.....	.....	.....
3314.00	½–1½	1	.....	0.5†	tr
3255.88	3½–3½	8	4	tr	0.5
3281.29	2½–2½	7	1–2	6†	4
3295.81	1½–1½	6	1	3†	1.5
3303.47	½– ½	4	1–0	2†	0.8
3234.92	3½–2½	0	.....	.....	.....
3264.76	2½–1½	P	.....	tr	tr
3285.42	1½– ½	(3)	1–0	.....	.....

* Swings and Struve, *Ap. J.*, **97**, 194, 1943.

† Slightly widened; the other lines are very narrow.

The velocities measured at various phases, tabulated by multiplets, are in Table 10. The velocities do not vary with phase during the observed interval; moreover, they agree with the velocity derived from the hydrogen lines. In these respects the *Fe* II lines differ in behavior from those in the Me spectra of R Hydrae[5] and R Leonis.[6]

Lines of Ti II.—Bright lines of a number of multiplets of *Ti* II were present on all the well-exposed spectrograms. The lines λ 3759 and λ 3761 of (13) are accurately measurable; their displacements remained constant throughout the observed interval (Table 7). Line λ 3685 of (14) was missing, probably because it is near the head of a narrow absorption band (of unknown origin). A few of the stronger lines of (11), (12), (19), (20), (34), and (41) were measured on two or more plates; the mean displacements for the four epochs were, respectively, −29.9, −27.8, −26.0, −26.3 km/sec.

Lines of Mn II.—Lines λ 3438 and λ 3460 of *Mn* II are probably present in emission in low intensity.

Displaced Lines of Ca II.—After maximum the broad displaced emission lines of *Ca* II behave much as in R Hydrae and R Leonis. The negative displacements (Table 11) are somewhat greater, however, especially at the latest observed phase +102 days.

Lines of Sr II.—Ten days after maximum light, λ 4215, (1), is a strong dark line with emission on the shortward edge; as the cycle advances, the emission grows stronger until

at the later phases it appears well marked on plates on which the near-by continuous spectrum is very weak. Despite the increase in intensity, the measured displacements change less than 3 km/sec (Table 7). The average velocity, however, is about 10 km/sec less (algebraically) than that of most other emission lines. In the companion line λ 4077 the emission is much weaker and apparently more greatly displaced shortward. Weak bright lines near the shortward edge of the dark line λ 4077 measured at phases +78 and

TABLE 10

RADIAL VELOCITIES FROM EMISSION LINES OF *Fe* II
(KM/SEC)

MULTIPLET	UPPER LEVEL		PHASE (DAYS)				
	Desig.	E.P.	+10	+45	+76	+102	+58 (Mean)
1	$z^6D°$	4.8	−28.4 4*	−28.2 5*	−27.4 5*	−28.8 7*	−28.2
3	$z^6D°$	4.8	25.3 1	25.4 1	25.1 1	24.7 1	(25.1
6	$z^4D°$	5.5	26 1	33 1	.....	29 1	(29)
7	$z^4F°$	5.5	26 1	.....	.....	.....	(26)
27	$z^4D°$	5.5	25.6 2	26.4 2	26.4 3	26.5 3	26.2
37	$z^4F°$	5.5	.....	25 1	20 1	25.3 3	(24)
38	$z^4D°$	5.5	23 2	27 3	29.1 3	−26.1 3	26.7
42	$z^6P°$	5.3	−23.6 2	−27.0 2	−26.4 1	.....	−25.7
Weighted mean	.....	.....	−26.0	−27.6	−26.8	−27.2	−26.9

* Number of lines.

TABLE 11

DISPLACEMENTS OF BROAD *Ca* II EMISSION LINES
WITH RESPECT TO DARK LINES

PHASE (DAYS)	*H*		*K*	
	Km/Sec	Int.	Km/Sec	Int.
+ 10	.....	.....	.....	.....
+ 44	−102	2	.....	tr
+ 76	− 94	3	−107	1
+102	− 79	5	− 97	2

+103 days, if properly identified with *Sr* II, yielded the values −62 and −59 km/sec, respectively. These negative displacements are larger than those for λ 4215. The behavior of the *Sr* II lines resembles qualitatively that of the analogous pair H and K of *Ca* II. This fact suggests that the anomalous reversal of intensities may have some relationship to atomic structure.

Unidentified lines.—Many bright lines, a few of them outstanding, remain unidentified; 60 are collected in Table 12. Their behavior during the post-maximum phase is indicated by the abbreviations "Inc." for increasing intensity, "Dec." for decreasing. In a complicated spectrum of this kind it is sometimes difficult to determine whether certain features are actually emission lines or only narrow spaces left in the continuous spectrum by closely packed absorption lines. Measured wave lengths believed to cor-

respond to spaces have been omitted from Table 12; others concerning which there is doubt are marked with an asterisk.

Although a few of the lines have been observed previously in the spectra of other long-period variables, many of them are new. It is hoped that additional information concerning these unidentified lines may be obtained from a study of the spectrum of χ Cygni.

TABLE 12

UNIDENTIFIED EMISSION LINES

I.A.	Change with Phase	Max. Obs.Int.	I.A.	Change with Phase	Max. Obs. Int.
3421.19*	Dec.	1	3952.82*	?	1
3535.54	Inc.	2	95.28	?	2
45.14*	Dec.	2	97.93	Inc.	4
56.58*	Dec.	1	4020.89*	Inc.	1
69.33*	Dec.	1	86.4	?	2
3677.56*	Dec.	1	95.48	Inc.	3
3735.35	Inc.!	6	98.9	Dec.	3
36.75	Inc.	1	4110.38	Dec.	2
42.30	Dec.	3	18.8	Inc.	2
58.0	Inc.	2	19.46	Dec.	2
60.6	?	2	21.30	?	2
63.32	?	3	38.43	?	6
64.2	?	1	49.34*	Dec.	1
75.51	Dec.	1	54.48	?	2
83.50	?	2	56.8	?	2
86.00	Dec.	2	66.61	Inc.!	4
87.57	Dec.	2	4172.00	Inc.	2
94.62*	Dec.	2	4240.33	?	2
3807.12	Inc.	1	40.70	Inc.	1
09.57*	Dec.	1	4300.15	Inc.	3
13.99*	?	1	31.72	Inc.	2
19.51	?	1	37.53*	?	1
22.86*	Dec.	1	71.30*	Dec.	1
27.80	Dec.	2	72.50	Inc.!	5
45.45	Inc.	1	4400.50	Inc.	1
58.26	Inc.	1	47.23	Inc.	1
65.42*	Dec.	1	55.31	Inc.!	6
81.30*	Dec.	1	4518.76	Inc.	1
93.91	?	4	21.60	?	5
3936.09	?	1	80.89	?	1

* Possibly a narrow space of continuous spectrum between dark lines.

REMARKS

Small differences in the structure and displacement of dark lines are apparently quite common in the spectra of giant red stars (e.g., α Orionis, g Herculis, long-period variables). These differences, showing well-marked relationships to excitation potential and to ionization, indicate that the reversing layers of these stars differ observably from homogeneous strata in thermodynamic equilibrium. Data on displacements may eventually, when the interpretation becomes clearer, be an effective means of increasing our knowledge of the atmospheric structure.

A cursory comparison of the dark-line spectrum of R Andromedae with that of R Leonis has yielded the following conclusions:

I. In the reversing layer of R Andromedae the concentration of atoms in their ground levels is less than in R Leonis.

II. In R Andromedae the ionization is greater (except for *Ca?*) than in R Leonis. I and II agree in indicating a higher temperature (and a lower density?) in R Andromedae.

III. The elements *Y* and *Zr* (atomic numbers 39 and 40) are relatively more abundant in R Andromedae. Otherwise it is difficult to explain the fact that neutral, ionized, and oxide lines (*Y* I, *Y* II, *YO*, *Zr* I, *Zr* II, *ZrO*) are all stronger in R Andromedae. (A comprehensive investigation will be required to rule out the possibility that this conclusion may be invalidated by lower general opacity in R Andromedae.) If, as now appears probable, the three types of red stars—M, S, and N—differ in the relative abundance of various atoms, then the trifurcation of the low-temperature end of the spectral sequence of giant stars may have some connection with the nuclear stability of chemical elements of the second, fourth, and fifth periods.

In the current series of *Contributions* devoted to the spectra of long-period variables, the emphasis is on identifications and displacements of atomic lines. For future consideration are studies of molecular lines, extensive measurements of line intensities, and detailed comparisons of several variables.

Note added in proof.—A study of the rich bright-line spectrum of χ Cygni, made after the present *Contribution* was written, shows the presence of numerous lines of cobalt and nickel. Comparison with the data for R Andromedae indicates that the following lines in Table 12 are probably due to these elements:

Co I		*Ni* I
3569.33	3997.93	3736.75
3845.45	4020.89	3775.51
3893.91	4086.4	3783.50
3936.09	4118.8	3807.12
3952.82	4121.30	3858.26
3995.28		4331.72

RELATIVE *gf*-VALUES FOR LINES OF *V* I*

ROBERT B. KING
Mount Wilson Observatory
Received January 16, 1947

ABSTRACT

The relative *gf*-values for 471 lines in 100 multiplets in the spectrum of *V* I have been measured in electric-furnace absorption spectra. The lines are in the region λλ 3043–6812, which includes most of the lines of astrophysical importance. A comparison of the results with theoretical multiplet and supermultiplet strengths for LS coupling shows that about 55 per cent of the multiplets exhibit normal line strengths but that in the supermultiplets the agreement with theory is relatively poor.

The relative *gf*-values for 471 lines in 100 multiplets in the spectrum of neutral vanadium (*V* I) have been measured. The measurements were made on lines produced in absorption by vaporizing pure vanadium metal in the graphite-tube electric furnace and passing the light of a tungsten filament or of a high-pressure mercury-vapor lamp through the heated vapor into the spectrograph to form a continuous spectrum, in which the vanadium lines appear in absorption. The general method of photography, photometry, and reduction of the measured total absorptions of lines to relative *gf*-values has been described in previous papers.[1,2,3]

The spectrum of *V* I has been very completely analyzed by Meggers and Russell.[4] From their list, lines of astrophysical importance have been selected by Charlotte E. Moore, arranged in multiplets, and published in the "Revised Multiplet Table of Astrophysical Interest."[5] Lines shortward from λ 2950 and many faint lines throughout the spectrum not likely to appear in astrophysical sources have been omitted from the RMT, with the result that less than one-third of the lines classified by Meggers and Russell are included there. In the present investigation, *gf*-values have been measured only for those lines appearing in the RMT (with a few additional) which are most readily obtained in furnace absorption spectra; these represent about 75 per cent of the lines listed in the RMT. The list could be greatly expanded if the labor involved were justified. A plate exposed in the region λλ 4100–4900 at a furnace temperature of 2800° C revealed practically all the lines classified by Meggers and Russell in this region. At 2500° C the strongest lines from the ground state of *V* II appear in absorption.

In the wave-length range covered by the measurements, substantially all lines in multiplets listed in the RMT arising from the four lowest terms, a^4F, a^6D, a^4D, and a^4P, are included. In multiplets from higher terms many of the fainter members have not been measured. However, measurements have been made on lines arising from all but four of the twenty-one low terms included in the RMT. These terms range in excitation potential from 0.00 to 2.36 volts. In addition, twenty-nine lines not listed in the RMT have been included. These lines, belonging to nine multiplets (three of which do not appear in the RMT), are faint members of multiplets from low-lying terms. Lines of this sort are particularly valuable in curve-of-growth investigations, and these are included

* *Contributions from the Mount Wilson Observatory, Carnegie Institution of Washington*, No. 731.

[1] R. B. and A. S. King, *Mt. W. Contr.*, No. 528; *Ap. J.*, **82**, 377, 1935.

[2] R. B. and A. S. King, *Mt. W. Contr.*, No. 581; *Ap. J.*, **87**, 24, 1938.

[3] R. B. King, *Mt. W. Contr.*, No. 648; *Ap. J.*, **94**, 27, 1941.

[4] *J. Research Nat. Bur. Standards*, **17**, 125, 1936.

[5] *Princeton U. Obs. Contr.*, No. 20, 1945.

because it is understood by the writer that some of them have been observed in late-type stellar spectra.

The furnace temperatures used in this investigation ranged from 1850° to 2750° C, although all spectral regions were not covered by this range in temperature. From λ 3000 to λ 4900 the measurements were made on Eastman IVO and Cramer Contrast plates obtained in the second order of the 15-foot concave-grating spectrograph (dispersion 1.86 A/mm). From λ 4900 to λ 6800 the measurements were made in the first order on Eastman IVF plates. Overlapping spectra were obtained in the second order from λ 4700 to λ 5600 on Eastman IVG plates. Single measurements of the total absorption of individual lines were made on from one to seventeen different exposures. The majority of the lines were measured on from six to ten exposures.

The results of the measurements are given in Table 1, where the arrangement of lines and multiplets follows the system adopted in the RMT. The first two columns of the table, headed "Mult. No." and "Designation" include, first, the multiplet number in parentheses assigned in the RMT; next, the over-all multiplet designation, followed by the inner quantum numbers, or *j*-values, of the individual lines in the multiplet. When the *gf*-values of all lines in the multiplet have not been measured, this fact is indicated by an asterisk (*) following the multiplet number. The three multiplets included here but not listed in the RMT have been inserted in their proper places in the table and have been assigned the numbers (0), (6*a*), and (6*b*).

The third column of the table gives the laboratory wave length of the lines corresponding to the transitions listed in the second column. Wave lengths are from the RMT or from Meggers and Russell[3] for lines not listed in the RMT. A dagger (†) before the wave length indicates that the line is a blend of two or more transitions in the vanadium spectrum. A coincidence with a line in the *V* II spectrum is indicated by the symbol § following the wave length; in these blends the effect of the *V* II line is insignificant in the laboratory data, but it cannot always be ignored at higher stellar temperatures.

The fourth column gives the estimated arc intensity of the line as given in the RMT. These data are qualitative and somewhat inhomogeneous. However, they give a good indication of the relative intensities of lines at a considerably higher excitation temperature than that used in the furnace in deriving *gf*-values. For this reason the arc intensities are often useful in forming judgment as to the behavior of blends of high- and low-level lines. Arc intensities followed by the letter "w" are widened by hyperfine structure in the arc. Most of these lines and some additional lines appear widened in the furnace absorption spectra.

The fifth column in the table lists the relative *gf*-values derived from the furnace absorption spectra. The *gf*-value is the product of the statistical weight (g) of the lower term involved in the transition and the oscillator strength (f) of the line. In previous papers[2,3] both the *gf*- and the *f*-values have been listed. But, since the *gf*-value is the factor usually employed by astrophysicists in applying the data to stellar material and since, if needed, the relative *f*-values may be readily derived by dividing the *gf*-values by the statistical weights ($g = 2j + 1$) of the lower term, the column of relative *f*-values has been omitted. The scale used for the relative *gf*-values is, of course, an arbitrary one. For blended lines, where it is improbable that this transition is the only one contributing to the measured intensity of the line under the furnace excitation conditions, the *gf*-value is placed in parentheses. For many blended lines, however, the *gf*-value is not in parentheses. For these lines the observed *gf*-value is considered to be entirely due to the transition with which it is listed, the contribution of other components of the blend being negligible at furnace temperatures.

The sixth column gives the weights assigned to the measurements. The letter "A" indicates that the *gf*-value is the result of concordant measurements on six or more spectra; "B" usually denotes three to five concordant measures, but sometimes more, only with poorer agreement than those assigned an "A"; "C" indicates that the line has been

TABLE 1

RELATIVE gf-VALUES FOR LINES OF V I

Mult. No.	Designation		λ	Arc Int.	gf	Wt.	Notes
(0)*.....	$a^4F-z^6G^0$	$4\frac{1}{2}-5\frac{1}{2}$	6109.176	(1)	0.31	B	
		$3\frac{1}{2}-4\frac{1}{2}$	6093.866	(3)	0.17	C	
		$2\frac{1}{2}-3\frac{1}{2}$	6082.789	(2)	0.16	C	
		$1\frac{1}{2}-2\frac{1}{2}$	6077.367	(2)	0.17	C	
		$2\frac{1}{2}-2\frac{1}{2}$	6128.543	(0)	0.14	B	
		$1\frac{1}{2}-1\frac{1}{2}$	6110.214	(3)	0.22	B	
		$2\frac{1}{2}-1\frac{1}{2}$	6161.913	(0)	0.17	C	
(1)*.....	$a^4F-z^6D^0$	$4\frac{1}{2}-3\frac{1}{2}$	5632.469	1	2.4	A	
		$3\frac{1}{2}-2\frac{1}{2}$	†5592.962	1	2.5	A	1
		$2\frac{1}{2}-1\frac{1}{2}$	5557.453	1	1.17	A	
		$1\frac{1}{2}-\frac{1}{2}$	5527.72	(1)	0.58	A	
		$3\frac{1}{2}-3\frac{1}{2}$	5560.548	(3)	1.15	A	
		$2\frac{1}{2}-2\frac{1}{2}$	5535.382	(1)	1.10	A	
		$1\frac{1}{2}-1\frac{1}{2}$	5515.371	(4)	0.56	A	
(2)*.....	$a^4F-z^6F^0$	$4\frac{1}{2}-5\frac{1}{2}$	5515.083	1	2.6	A	
		$3\frac{1}{2}-4\frac{1}{2}$	5496.020	(3)	0.98	A	
		$2\frac{1}{2}-3\frac{1}{2}$	5482.471	(1)	0.33	B	
		$1\frac{1}{2}-1\frac{1}{2}$	5500.816	(2)	0.30	B	
		$4\frac{1}{2}-3\frac{1}{2}$	†5610.20	1	0.51	B	2
		$3\frac{1}{2}-2\frac{1}{2}$	5573.992	1	0.82	A	
		$2\frac{1}{2}-1\frac{1}{2}$	5542.69	1	1.02	A	
		$1\frac{1}{2}-\frac{1}{2}$	5517.198	1	1.21	B	
(3).....	$a^4F-z^4D^0$	$4\frac{1}{2}-3\frac{1}{2}$	4881.554	50w	1340	B	
		$3\frac{1}{2}-2\frac{1}{2}$	4875.462	40w	1070	A	
		$2\frac{1}{2}-1\frac{1}{2}$	4864.741	40w	675	A	
		$1\frac{1}{2}-\frac{1}{2}$	4851.483	40w	417	A	
		$3\frac{1}{2}-3\frac{1}{2}$	4827.458	30	199	A	
		$2\frac{1}{2}-2\frac{1}{2}$	4831.642	35	230	A	
		$1\frac{1}{2}-1\frac{1}{2}$	4832.427	30	162	A	
		$2\frac{1}{2}-3\frac{1}{2}$	4784.480	5	10.6	A	
		$1\frac{1}{2}-2\frac{1}{2}$	4799.786	5	10.0	A	
(4).....	$a^4F-z^4G^0$	$4\frac{1}{2}-5\frac{1}{2}$	4594.103	60w	1530	B	
		$3\frac{1}{2}-4\frac{1}{2}$	4586.364	50w	946	B	
		$2\frac{1}{2}-3\frac{1}{2}$	4580.394	40w	633	B	
		$1\frac{1}{2}-2\frac{1}{2}$	4577.173	40w	534	B	
		$4\frac{1}{2}-4\frac{1}{2}$	4635.176	15	59	A	
		$3\frac{1}{2}-3\frac{1}{2}$	4619.771	25	70	A	
		$2\frac{1}{2}-2\frac{1}{2}$	4606.146	15	54	A	
		$4\frac{1}{2}-3\frac{1}{2}$	4669.273	(2)	1.80	A	
		$3\frac{1}{2}-2\frac{1}{2}$	4645.971	1	2.5	A	
(5).....	$a^4F-z^4F^0$	$4\frac{1}{2}-4\frac{1}{2}$	4352.872	50w	990	A	
		$3\frac{1}{2}-3\frac{1}{2}$	4341.013	40w	700	A	
		$2\frac{1}{2}-2\frac{1}{2}$	4332.823	30w	420	A	
		$1\frac{1}{2}-1\frac{1}{2}$	4330.024	30w	300	A	
		$4\frac{1}{2}-3\frac{1}{2}$	†4384.722	125r	(5300)	A	3
		$3\frac{1}{2}-2\frac{1}{2}$	4368.042	10	88	A	
		$2\frac{1}{2}-1\frac{1}{2}$	4355.943	10	59	B	
		$3\frac{1}{2}-4\frac{1}{2}$	4309.795	20	105	B	
		$2\frac{1}{2}-3\frac{1}{2}$	4306.214	15	142	B	
		$1\frac{1}{2}-2\frac{1}{2}$	4307.184	12	105	B	
(6).....	$a^4F-z^2D^0$	$3\frac{1}{2}-2\frac{1}{2}$	†4234.000	12	39	A	4
		$2\frac{1}{2}-1\frac{1}{2}$	4259.312	8	34	A	
		$2\frac{1}{2}-2\frac{1}{2}$	4200.89	1	6.2	A	
		$1\frac{1}{2}-1\frac{1}{2}$	†4234.524§	8	37	A	
		$1\frac{1}{2}-2\frac{1}{2}$	4176.793	(3)	3.6	B	

* The gf-values of all lines in multiplet have not been measured.

† Blend of two or more transitions in V I spectrum.

§ Coincident with a line in V II spectrum.

TABLE 1—*Continued*

Mult. No.	Designation		λ	Arc Int.	*gf*	Wt.	Notes
(6*a*)*.....	$a^4F-z^4P^0$	$3\frac{1}{2}-2\frac{1}{2}$	4029.90	2	7.0	B	
(6*b*)*.....	$a^4F-y^6F^0$	$4\frac{1}{2}-4\frac{1}{2}$	4070.78	4	12.0	B	
		$3\frac{1}{2}-3\frac{1}{2}$	4052.47	1	4.8	A	
		$4\frac{1}{2}-3\frac{1}{2}$	†4090.587	25	(79)	A	5
		$3\frac{1}{2}-2\frac{1}{2}$	4068.00	4	14.7	B	
		$2\frac{1}{2}-1\frac{1}{2}$	4048.619	4	12.8	B	
		$1\frac{1}{2}-\frac{1}{2}$	4032.85	2	7.0	B	
(7).....	$a^4F-y^4F^0$	$4\frac{1}{2}-4\frac{1}{2}$	3902.250	50r	2900	A	
		$3\frac{1}{2}-3\frac{1}{2}$	3875.075	35	1760	A	
		$2\frac{1}{2}-2\frac{1}{2}$	3864.862	35	1610	A	
		$1\frac{1}{2}-1\frac{1}{2}$	3855.370	30	1430	A	
		$4\frac{1}{2}-3\frac{1}{2}$	†3909.894	20	290	B	6
		$3\frac{1}{2}-2\frac{1}{2}$	3892.859	25	460	B	
		$2\frac{1}{2}-1\frac{1}{2}$	3875.902	20	340	A	
		$3\frac{1}{2}-4\frac{1}{2}$	3867.602	15	280	A	
		$2\frac{1}{2}-3\frac{1}{2}$	†3847.323§	20	380	B	
		$1\frac{1}{2}-2\frac{1}{2}$	3844.438	20	320	B	
(8).....	$a^4F-z^2G^0$	$4\frac{1}{2}-4\frac{1}{2}$	3876.086	20	930	A	
		$3\frac{1}{2}-3\frac{1}{2}$	†3890.184	25	550	B	7
		$4\frac{1}{2}-3\frac{1}{2}$	†3925.240	10	78	A	8
		$3\frac{1}{2}-4\frac{1}{2}$	3841.890	5	56	C	
		$2\frac{1}{2}-3\frac{1}{2}$	3862.223	12	91	C	
(9).....	$a^4F-y^4D^0$	$4\frac{1}{2}-3\frac{1}{2}$	3855.841	60r	4600	B	
		$3\frac{1}{2}-2\frac{1}{2}$	3840.752	60r	3500	B	
		$2\frac{1}{2}-1\frac{1}{2}$	3828.559	60r	2100	B	
		$1\frac{1}{2}-\frac{1}{2}$	†3818.244	60	1420	A	9
		$3\frac{1}{2}-3\frac{1}{2}$	3822.009	30	640	A	
		$2\frac{1}{2}-2\frac{1}{2}$	3813.492	60	700	A	10
		$1\frac{1}{2}-1\frac{1}{2}$	3808.521	40	560	A	
		$2\frac{1}{2}-3\frac{1}{2}$	†3794.964	50	(525)	A	11
		$1\frac{1}{2}-2\frac{1}{2}$	3793.614	8	49	A	
(10)*.....	$a^4F-y^6D^0$	$4\frac{1}{2}-4\frac{1}{2}$	3817.844	8	106	A	
		$3\frac{1}{2}-3\frac{1}{2}$	3803.902	6	33	A	
		$2\frac{1}{2}-2\frac{1}{2}$	3791.326	2	9.0	A	
		$3\frac{1}{2}-4\frac{1}{2}$	3784.676	2	11.8	A	
		$2\frac{1}{2}-3\frac{1}{2}$	3777.168	2	9.1	A	
(11)*.....	$a^4F-z^2F^0$	$4\frac{1}{2}-3\frac{1}{2}$	3713.957	5	23	A	
		$3\frac{1}{2}-2\frac{1}{2}$	3721.358	3	7.7	A	
(12).....	$a^4F-y^4G^0$	$4\frac{1}{2}-5\frac{1}{2}$	3298.139	15	195	A	
		$3\frac{1}{2}-4\frac{1}{2}$	3283.311	15	300	A	
		$2\frac{1}{2}-3\frac{1}{2}$	3271.637	12	310	A	
		$1\frac{1}{2}-2\frac{1}{2}$	3263.238	15	340	A	
		$4\frac{1}{2}-4\frac{1}{2}$	3308.246	3	15.0	A	
		$3\frac{1}{2}-3\frac{1}{2}$	3291.676	4	26	A	
		$2\frac{1}{2}-2\frac{1}{2}$	3277.939	5	33	A	
(13)*.....	$a^4F-x^4F^0$	$4\frac{1}{2}-4\frac{1}{2}$	3249.566	10	55	B	
		$3\frac{1}{2}-3\frac{1}{2}$	3230.646	6	39	B	
		$2\frac{1}{2}-2\frac{1}{2}$	3215.375	4	29	A	
		$1\frac{1}{2}-1\frac{1}{2}$	3204.196	3	20	A	
		$4\frac{1}{2}-3\frac{1}{2}$	†3254.773§	10	9.6	A	

TABLE 1—*Continued*

Mult. No.	Designation		λ	Arc Int.	*gf*	Wt.	Notes
(14).....	$a^4F-x^4G^0$	$4\frac{1}{2}-5\frac{1}{2}$	3185.396	200R	14900	B	
		$3\frac{1}{2}-4\frac{1}{2}$	3183.96	(125R)	11700	B	
		$2\frac{1}{2}-3\frac{1}{2}$	3183.406	150R	9000	B	
		$1\frac{1}{2}-2\frac{1}{2}$	3183.982	(150R)	9300	B	
		$4\frac{1}{2}-4\frac{1}{2}$	3207.410	20	1200	A	
		$3\frac{1}{2}-3\frac{1}{2}$	3202.381	25	1630	A	
		$2\frac{1}{2}-2\frac{1}{2}$	3198.012	20	1380	A	
		$4\frac{1}{2}-3\frac{1}{2}$	3226.106	4	34	B	
		$3\frac{1}{2}-2\frac{1}{2}$	†3217.121§	10	46	B	
(15)*.....	$a^4F-x^4D^0$	$4\frac{1}{2}-3\frac{1}{2}$	3091.437	20	79	A	
		$3\frac{1}{2}-2\frac{1}{2}$	3091.552	15	37	A	
		$2\frac{1}{2}-1\frac{1}{2}$	3093.24	6?	10.9	B	
		$3\frac{1}{2}-3\frac{1}{2}$	3069.645	30r	470	B	
		$2\frac{1}{2}-2\frac{1}{2}$	†3073.823	60r	(1040)	A	12
		$1\frac{1}{2}-1\frac{1}{2}$	3080.146	6	17.4	B	
		$2\frac{1}{2}-3\frac{1}{2}$	3052.194	20	133	B	
		$1\frac{1}{2}-2\frac{1}{2}$	3060.93	2	16.7	B	
(16)*.....	$a^4F-z^2P^0$	$2\frac{1}{2}-1\frac{1}{2}$	3063.734	12	106	A	
		$1\frac{1}{2}-1\frac{1}{2}$	3050.890	35r	520	A	
(17).....	$a^4F-w^4F^0$	$4\frac{1}{2}-4\frac{1}{2}$	3066.375	125R	9600	B	
		$3\frac{1}{2}-3\frac{1}{2}$	3060.460	125R	5000	B	
		$2\frac{1}{2}-2\frac{1}{2}$	3056.334	100R	3500	B	
		$1\frac{1}{2}-1\frac{1}{2}$	3053.65	80R	2900	B	
		$4\frac{1}{2}-3\frac{1}{2}$	3082.109	50r	1170	B	
		$3\frac{1}{2}-2\frac{1}{2}$	†3073.823	60r	(1190)	A	13
		$2\frac{1}{2}-1\frac{1}{2}$	3066.51	20	890	A	
		$3\frac{1}{2}-4\frac{1}{2}$	3044.936	50r	680	B	
		$2\frac{1}{2}-3\frac{1}{2}$	3043.124	50r	820	B	
		$1\frac{1}{2}-2\frac{1}{2}$	†3043.555§	50r	730	B	
(19)*.....	$a^6D-z^6D^0$	$4\frac{1}{2}-4\frac{1}{2}$	6243.11	30	490	B	
		$3\frac{1}{2}-3\frac{1}{2}$	6251.83	30	173	B	
		$2\frac{1}{2}-2\frac{1}{2}$	6256.906	8	32	A	
		$\frac{1}{2}-\frac{1}{2}$	6258.596	8	26	A	
		$4\frac{1}{2}-3\frac{1}{2}$	6296.518	15	78	A	
		$3\frac{1}{2}-2\frac{1}{2}$	6292.858	20	109	A	
		$2\frac{1}{2}-1\frac{1}{2}$	6285.185	20	102	A	
		$1\frac{1}{2}-\frac{1}{2}$	6274.670	15	72	A	
		$3\frac{1}{2}-4\frac{1}{2}$	6199.202	30	102	B	
		$2\frac{1}{2}-3\frac{1}{2}$	6216.368	30	156	B	
		$1\frac{1}{2}-2\frac{1}{2}$	6230.736	30	149	B	
		$\frac{1}{2}-1\frac{1}{2}$	6242.80	15	117	A	
(20)*.....	$a^6D-z^6F^0$	$4\frac{1}{2}-5\frac{1}{2}$	6150.132	15	83	A	
		$3\frac{1}{2}-4\frac{1}{2}$	6170.340	8	26	A	
		$2\frac{1}{2}-3\frac{1}{2}$	6189.350	3	5.4	A	
		$1\frac{1}{2}-2\frac{1}{2}$	6207.251	(5)	0.49	B	
		$4\frac{1}{2}-4\frac{1}{2}$	6213.874	15	45	A	
		$3\frac{1}{2}-3\frac{1}{2}$	6224.507	15	49	A	
		$2\frac{1}{2}-2\frac{1}{2}$	6233.187	12	43	B	
		$1\frac{1}{2}-1\frac{1}{2}$	6240.137	6	13.0	A	
		$\frac{1}{2}-\frac{1}{2}$	6245.214	2	3.5	A	
		$4\frac{1}{2}-3\frac{1}{2}$ $3\frac{1}{2}-2\frac{1}{2}$	†6268.841	8	{34} {33}	B	
		$2\frac{1}{2}-1\frac{1}{2}$	6266.32	7	26	A	
		$1\frac{1}{2}-\frac{1}{2}$	6261.236	5	13.1	B	

TABLE 1—*Continued*

Mult. No.	Designation		λ	Arc Int.	*gf*	Wt.	Notes
(21).....	$a^6D-z^6P^0$	$4\frac{1}{2}-3\frac{1}{2}$	4460.292	50	3550	A	
		$3\frac{1}{2}-2\frac{1}{2}$	4459.760	30	1570	A	
		$2\frac{1}{2}-1\frac{1}{2}$	4457.479	15	630	B	
		$3\frac{1}{2}-3\frac{1}{2}$	4437.837	20	910	A	
		$2\frac{1}{2}-2\frac{1}{2}$	4441.683	25	1080	A	
		$1\frac{1}{2}-1\frac{1}{2}$	4444.207	20	780	A	
		$2\frac{1}{2}-3\frac{1}{2}$	4419.935	12	133	A	
		$1\frac{1}{2}-2\frac{1}{2}$	4428.515	15	330	A	
		$\frac{1}{2}-1\frac{1}{2}$	4436.138	15	610	A	
(22).....	$a^6D-y^6F^0$	$4\frac{1}{2}-5\frac{1}{2}$	4379.238	150rw	26000	B	14
		$3\frac{1}{2}-4\frac{1}{2}$	†4384.722	125r	16100	B	15
		$2\frac{1}{2}-3\frac{1}{2}$	4389.974	100	10000	A	
		$1\frac{1}{2}-2\frac{1}{2}$	4395.228	80	4500	A	
		$\frac{1}{2}-1\frac{1}{2}$	4400.575	60	2150	A	
		$4\frac{1}{2}-4\frac{1}{2}$	4406.641	80	3200	A	
		$3\frac{1}{2}-3\frac{1}{2}$	4407.637	70	5100	A	
		$2\frac{1}{2}-2\frac{1}{2}$	4408.204	70	5200	A	
		$1\frac{1}{2}-1\frac{1}{2}$ $\frac{1}{2}-\frac{1}{2}$	†4408.511	90	{7200} {7000}	A	
		$4\frac{1}{2}-3\frac{1}{2}$	4429.796	15	300	B	
		$3\frac{1}{2}-2\frac{1}{2}$	4426.005	20	590	A	
		$2\frac{1}{2}-1\frac{1}{2}$	4421.573	20	660	A	
		$1\frac{1}{2}-\frac{1}{2}$	4416.474	20	590	B	
(23)*.....	$a^6D-z^4P^0$	$3\frac{1}{2}-2\frac{1}{2}$	†4381.04	1	2.9	C	16
		$2\frac{1}{2}-1\frac{1}{2}$	†4405.011	4	20	A	17
		$2\frac{1}{2}-2\frac{1}{2}$	4363.525	5	46	A	
		$1\frac{1}{2}-1\frac{1}{2}$	4392.074	5	55	A	
		$\frac{1}{2}-\frac{1}{2}$	4412.142	12	117	C	18
		$1\frac{1}{2}-2\frac{1}{2}$	4350.820	2	18.5	A	
		$\frac{1}{2}-1\frac{1}{2}$	4384.19	1	19.7	A	
(24)*.....	$a^6D-y^4F^0$	$4\frac{1}{2}-4\frac{1}{2}$	4209.857	20	250	A	
		$3\frac{1}{2}-3\frac{1}{2}$	4198.611	4	37	A	
		$4\frac{1}{2}-3\frac{1}{2}$	4218.710	4	37	A	
		$3\frac{1}{2}-2\frac{1}{2}$	4219.51	2	14	A	
		$3\frac{1}{2}-4\frac{1}{2}$	4189.841	12	164	A	
		$2\frac{1}{2}-3\frac{1}{2}$	4182.591	10	115	A	
		$1\frac{1}{2}-2\frac{1}{2}$	4191.558	10	50	A	19
(25)*.....	$a^6D-z^2G^0$	$4\frac{1}{2}-4\frac{1}{2}$	4179.419	15	230	A	
		$3\frac{1}{2}-4\frac{1}{2}$	4159.686	8	96	A	
		$2\frac{1}{2}-3\frac{1}{2}$	4200.190	4	30	A	
(26)*.....	$a^6D-y^4D^0$	$2\frac{1}{2}-1\frac{1}{2}$ $1\frac{1}{2}-\frac{1}{2}$	4160.40	1	{6.2} {5.8}	B	
		$3\frac{1}{2}-3\frac{1}{2}$	4136.386	3	29	A	
		$2\frac{1}{2}-2\frac{1}{2}$	4142.66	2	16.1	A	
		$1\frac{1}{2}-1\frac{1}{2}$	4148.859	2	17.3	A	
		$\frac{1}{2}-\frac{1}{2}$	4153.328	2	16.2	A	
		$1\frac{1}{2}-2\frac{1}{2}$	4131.20	1	11.0	A	
		$\frac{1}{2}-1\frac{1}{2}$	4141.85	2	7.2	A	
(27)*.....	$a^6D-y^6D^0$	$4\frac{1}{2}-4\frac{1}{2}$	†4111.785	100R	15300	A	20
		$3\frac{1}{2}-3\frac{1}{2}$	†4115.185	60	6400	A	21
		$2\frac{1}{2}-2\frac{1}{2}$	4116.470	50	1670	A	
		$1\frac{1}{2}-1\frac{1}{2}$	4116.703	4	85	A	
		$4\frac{1}{2}-3\frac{1}{2}$	4134.488	60	3100	A	
		$3\frac{1}{2}-2\frac{1}{2}$	4132.017	60	4900	A	
		$2\frac{1}{2}-1\frac{1}{2}$	4128.071	60	4400	A	
		$1\frac{1}{2}-\frac{1}{2}$	4123.566	60	2500	A	
		$3\frac{1}{2}-4\frac{1}{2}$	4092.694	50	3000	A	
		$2\frac{1}{2}-3\frac{1}{2}$	4099.796	60	4400	A	
		$1\frac{1}{2}-2\frac{1}{2}$	4105.167	60	3700	A	
		$\frac{1}{2}-1\frac{1}{2}$	4109.786	50	2700	A	22

TABLE 1—*Continued*

Mult. No.	Designation		λ	Arc Int.	*gf*	Wt.	Notes
(28)*.....	$a^6D-x^6D^0$	$4\frac{1}{2}-4\frac{1}{2}$	†3794.964	50	(2300)	A	23
		$3\frac{1}{2}-3\frac{1}{2}$	3803.474	25	1010	A	
		$2\frac{1}{2}-2\frac{1}{2}$	3809.597	15	310	A	
		$\frac{1}{2}-\frac{1}{2}$	3815.514	10	133	B	
		$4\frac{1}{2}-3\frac{1}{2}$	3819.963	15	460	B	
		$3\frac{1}{2}-2\frac{1}{2}$	3822.888	15	670	B	
		$2\frac{1}{2}-1\frac{1}{2}$	†3823.213	15	630	B	24
		$1\frac{1}{2}-\frac{1}{2}$	3821.487	15	460	B	
		$3\frac{1}{2}-4\frac{1}{2}$	3778.684	25	430	A	
		$2\frac{1}{2}-3\frac{1}{2}$	3790.324	20	680	A	
		$1\frac{1}{2}-2\frac{1}{2}$	3799.912	25	670	A	
		$\frac{1}{2}-1\frac{1}{2}$	3807.505	20	450	A	
(29).....	$a^6D-y^6P^0$	$4\frac{1}{2}-3\frac{1}{2}$	3703.584	100	7500	A	
		$3\frac{1}{2}-2\frac{1}{2}$	3704.699	60	4100	A	
		$2\frac{1}{2}-1\frac{1}{2}$	3705.035	30	1470	A	
		$3\frac{1}{2}-3\frac{1}{2}$	3688.069	50	2300	A	
		$2\frac{1}{2}-2\frac{1}{2}$	3692.225	50	2800	A	
		$1\frac{1}{2}-1\frac{1}{2}$	3695.865	40	2200	A	
		$2\frac{1}{2}-3\frac{1}{2}$	3675.700	20	350	A	
		$1\frac{1}{2}-2\frac{1}{2}$	3683.126	30	890	A	
		$\frac{1}{2}-1\frac{1}{2}$	3690.281	40	1540	A	
(31)*.....	$a^4D-z^4F^0$	$3\frac{1}{2}-4\frac{1}{2}$	6753.00	80w	110	B	25
		$2\frac{1}{2}-3\frac{1}{2}$	6766.49	60	70	B	26
		$1\frac{1}{2}-2\frac{1}{2}$	6784.98	40	36	B	
		$\frac{1}{2}-1\frac{1}{2}$	6812.40	20	23	B	
(33)*.....	$a^4D-y^6F^0$	$3\frac{1}{2}-4\frac{1}{2}$	6097.42	(1)	10.5	C	
		$2\frac{1}{2}-3\frac{1}{2}$	6090.54	P	12.6	C	
		$1\frac{1}{2}-2\frac{1}{2}$	6087.485	1	7.7	C	
		$1\frac{1}{2}-\frac{1}{2}$	6128.30	2	25	B	
(34).....	$a^4D-z^4P^0$	$3\frac{1}{2}-2\frac{1}{2}$	6090.184	50	2500	B	
		$2\frac{1}{2}-1\frac{1}{2}$	6119.505	40	1370	A	
		$1\frac{1}{2}-\frac{1}{2}$	6135.36	15	510	A	
		$2\frac{1}{2}-2\frac{1}{2}$	6039.690	25	640	A	
		$1\frac{1}{2}-1\frac{1}{2}$	6081.421	25	720	A	
		$\frac{1}{2}-\frac{1}{2}$	6111.622	25	570	A	
		$1\frac{1}{2}-2\frac{1}{2}$	6002.601	4	74	A	
		$\frac{1}{2}-1\frac{1}{2}$	6058.113	5	121	A	
(35).....	$a^4D-y^4F^0$	$3\frac{1}{2}-4\frac{1}{2}$	5727.024	60	5000	B	
		$2\frac{1}{2}-3\frac{1}{2}$	5698.509	60	6200	C	
		$1\frac{1}{2}-2\frac{1}{2}$	5703.562	40	3200	C	
		$\frac{1}{2}-1\frac{1}{2}$	5706.973	30	2200	C	
		$3\frac{1}{2}-3\frac{1}{2}$	5743.438	18	570	A	
		$2\frac{1}{2}-2\frac{1}{2}$	5737.040	25	920	B	
		$1\frac{1}{2}-1\frac{1}{2}$	5727.662	20	700	A	
		$3\frac{1}{2}-2\frac{1}{2}$	†5782.601	2	36	B	27
		$2\frac{1}{2}-1\frac{1}{2}$	5761.411	2	49	B	
(36).....	$a^4D-z^2G^0$	$3\frac{1}{2}-4\frac{1}{2}$	5670.827	30w	1900	B	28
		$2\frac{1}{2}-3\frac{1}{2}$	5731.257	30	870	B	28
		$3\frac{1}{2}-3\frac{1}{2}$	5776.670	4	145	A	28
(37).....	$a^4D-y^4D^0$	$3\frac{1}{2}-3\frac{1}{2}$	5627.628	30	2400	B	
		$2\frac{1}{2}-2\frac{1}{2}$	5624.605	20	1080	B	
		$1\frac{1}{2}-1\frac{1}{2}$	5624.895	10	460	B	
		$\frac{1}{2}-\frac{1}{2}$	5626.014	8	260	A	
		$3\frac{1}{2}-2\frac{1}{2}$	5668.369	12	390	A	
		$2\frac{1}{2}-1\frac{1}{2}$	5657.449	12	510	A	
		$1\frac{1}{2}-\frac{1}{2}$	5646.112	10	320	A	
		$2\frac{1}{2}-3\frac{1}{2}$	5584.490	10	200	B	
		$1\frac{1}{2}-2\frac{1}{2}$	5592.409	12	196	B	
		$\frac{1}{2}-1\frac{1}{2}$	5604.943	8	270	B	

TABLE 1—*Continued*

Mult. No.	Designation		λ	Arc Int.	gf	Wt.	Notes
(38)*.....	$a^4D-y^6D^0$	$3\frac{1}{2}-4\frac{1}{2}$	5547.080	8	240	B	
		$2\frac{1}{2}-3\frac{1}{2}$	5545.933	2	64	A	
		$1\frac{1}{2}-2\frac{1}{2}$	5544.865	(1)	19	C	
(39)*.....	$a^4D-y^4P^0$	$3\frac{1}{2}-2\frac{1}{2}$	4670.483	25w	1360	B	29
		$2\frac{1}{2}-1\frac{1}{2}$	4646.396	15w	640	B	30
		$1\frac{1}{2}-\frac{1}{2}$	4640.062	8	250	A	
		$2\frac{1}{2}-2\frac{1}{2}$	4640.735	7w	181	B	31
		$1\frac{1}{2}-1\frac{1}{2}$	†4624.404	8	300	A	32
		$\frac{1}{2}-\frac{1}{2}$	4626.480	7	290	A	33
(40)*.....	$a^4D-x^4F^0$	$3\frac{1}{2}-4\frac{1}{2}$	4423.212	8	580	B	34
		$2\frac{1}{2}-3\frac{1}{2}$	†4406.147	6	500	B	35
		$1\frac{1}{2}-2\frac{1}{2}$	4393.835	4	181	A	
		$\frac{1}{2}-1\frac{1}{2}$	4387.213	3	106	A	
(41)*.....	$a^4D-w^4F^0$	$3\frac{1}{2}-4\frac{1}{2}$	†4090.579	25	7900	A	36
		$2\frac{1}{2}-3\frac{1}{2}$	4095.486	25	4700	B	
		$1\frac{1}{2}-2\frac{1}{2}$	4102.159	20	2900	A	
		$3\frac{1}{2}-3\frac{1}{2}$	4118.643	8	1110	A	
		$2\frac{1}{2}-2\frac{1}{2}$	4119.457	8	1200	A	
		$1\frac{1}{2}-1\frac{1}{2}$	4120.538	8	830	A	
(42).....	$a^4D-w^4D^0$	$3\frac{1}{2}-3\frac{1}{2}$	3934.013	20	5800	C	
		$2\frac{1}{2}-2\frac{1}{2}$	3922.431	12	1780	A	
		$1\frac{1}{2}-1\frac{1}{2}$	3920.487	5	380	A	
		$\frac{1}{2}-\frac{1}{2}$	†3912.207	10	(1190)	A	37
		$3\frac{1}{2}-2\frac{1}{2}$	3943.664	12	540	A	
		$2\frac{1}{2}-1\frac{1}{2}$	3936.282	5	450	A	
		$1\frac{1}{2}-\frac{1}{2}$	3921.905	6	630	A	
		$2\frac{1}{2}-3\frac{1}{2}$	3912.886	4	300	A	
		$1\frac{1}{2}-2\frac{1}{2}$	†3906.748	6	(710)	A	38
		$\frac{1}{2}-1\frac{1}{2}$	3910.790	5	460	A	
(43)*.....	$a^4D-v^4F^0$	$3\frac{1}{2}-3\frac{1}{2}$	†3896.155§	6	510	A	
		$2\frac{1}{2}-2\frac{1}{2}$	†3906.748	6	(760)	A	39
		$1\frac{1}{2}-1\frac{1}{2}$	†3912.207	10	(1220)	A	40
(44)*.....	$a^4D-v^4D^0$	$2\frac{1}{2}-2\frac{1}{2}$	3839.002	10	1330	A	
		$1\frac{1}{2}-1\frac{1}{2}$	3836.054	5	510	A	
		$\frac{1}{2}-\frac{1}{2}$	3835.560	4	370	A	
		$3\frac{1}{2}-2\frac{1}{2}$	3859.341	6	590	A	
		$1\frac{1}{2}-2\frac{1}{2}$	3823.990	5	580	A	
		$\frac{1}{2}-1\frac{1}{2}$	3826.774	6	350	B	
(45)*.....	$a^4D-x^4P^0$	$3\frac{1}{2}-2\frac{1}{2}$	3583.704	8	320	B	
(46)*.....	$a^4D-t^4D^0$	$3\frac{1}{2}-3\frac{1}{2}$	3400.395	12	1740	B	
		$2\frac{1}{2}-2\frac{1}{2}$	3402.571	9	960	A	
		$1\frac{1}{2}-1\frac{1}{2}$	3405.160	6	470	A	
		$\frac{1}{2}-\frac{1}{2}$	3406.837	6	320	B	
		$2\frac{1}{2}-1\frac{1}{2}$	3417.069	5	470	B	
(48).....	$a^4P-z^4P^0$	$2\frac{1}{2}-2\frac{1}{2}$	6531.44	15	270	B	
		$1\frac{1}{2}-1\frac{1}{2}$	6543.51	5	64	B	
		$\frac{1}{2}-\frac{1}{2}$	6565.88	3	35	B	
		$2\frac{1}{2}-1\frac{1}{2}$	6624.86	7	124	B	
		$1\frac{1}{2}-\frac{1}{2}$	6605.98	10	105	B	
		$1\frac{1}{2}-2\frac{1}{2}$	6452.354	10	158	A	
		$\frac{1}{2}-1\frac{1}{2}$	6504.164	9	124	B	

TABLE 1—*Continued*

Mult. No.	Designation		λ	Arc Int.	*gf*	Wt.	Notes
(49)*.....	$a^4P-y^4D^0$	$2\frac{1}{2}-3\frac{1}{2}$	6002.273	2	60	A	
		$1\frac{1}{2}-2\frac{1}{2}$	5980.748	2	46	B	
		$\frac{1}{2}-1\frac{1}{2}$	5984.602	1	23	B	
		$1\frac{1}{2}-1\frac{1}{2}$	6017.90	tr	24	C	
		$\frac{1}{2}-\frac{1}{2}$	6008.648	tr	17	C	
(50)*.....	$a^4P-y^4P^0$	$2\frac{1}{2}-2\frac{1}{2}$	4925.657	10	800	A	41
		$1\frac{1}{2}-1\frac{1}{2}$	4886.821	2	127	A	
		$2\frac{1}{2}-1\frac{1}{2}$	4932.029	4	340	A	
		$1\frac{1}{2}-\frac{1}{2}$	4904.285	(8)	270	A	
		$1\frac{1}{2}-2\frac{1}{2}$	4880.560	8	350	A	42
		$\frac{1}{2}-1\frac{1}{2}$	4864.83	P	290	C	43
(52)*.....	$a^4P-w^4D^0$	$2\frac{1}{2}-3\frac{1}{2}$	4113.518	12	1730	A	
		$1\frac{1}{2}-2\frac{1}{2}$	4092.407	8	1080	A	44
		$2\frac{1}{2}-2\frac{1}{2}$	4124.072	5	470	B	
		$\frac{1}{2}-\frac{1}{2}$	4093.497	5	490	A	
(53)*.....	$a^4P-t^4D^0$	$2\frac{1}{2}-3\frac{1}{2}$	3533.676	10	3900	A	
		$1\frac{1}{2}-2\frac{1}{2}$	3529.735	10	2300	A	
		$\frac{1}{2}-1\frac{1}{2}$	3533.757	6	1380	A	
		$2\frac{1}{2}-2\frac{1}{2}$	3553.271	6	1250	B	
		$1\frac{1}{2}-1\frac{1}{2}$	3545.339	8	1400	A	
		$\frac{1}{2}-\frac{1}{2}$	3543.500	8	1250	A	
		$1\frac{1}{2}-\frac{1}{2}$	3555.142	3	490	B	
(54)*.....	$a^4P-w^4P^0$	$2\frac{1}{2}-2\frac{1}{2}$	3377.625	15	3100	A	
		$1\frac{1}{2}-1\frac{1}{2}$	3376.057	8	1100	A	
		$2\frac{1}{2}-1\frac{1}{2}$	3397.580	6	820	B	
		$1\frac{1}{2}-\frac{1}{2}$	3377.394	10	1550	A	
		$1\frac{1}{2}-2\frac{1}{2}$	3356.352	10	1580	A	
		$\frac{1}{2}-1\frac{1}{2}$	3365.553	10	1630	A	
(55).....	$a^4P-x^4S^0$	$2\frac{1}{2}-1\frac{1}{2}$	3329.855	12	2600	A	
		$1\frac{1}{2}-1\frac{1}{2}$	3309.176	8	1050	A	
		$\frac{1}{2}-1\frac{1}{2}$	3299.086	3	500	B	
(56)*.....	$a^4P-v^4P^0$	$1\frac{1}{2}-\frac{1}{2}$	3112.925	8	720	B	
		$1\frac{1}{2}-2\frac{1}{2}$	3088.114	30	2100	B	
		$\frac{1}{2}-1\frac{1}{2}$	3094.692	20	1230	A	
(57)*.....	$a^4P-r^4D^0$	$2\frac{1}{2}-3\frac{1}{2}$	3083.539	30	1410	B	
		$1\frac{1}{2}-2\frac{1}{2}$	3075.933	8	1190	B	
		$\frac{1}{2}-1\frac{1}{2}$	3080.333	12	760	B	
		$2\frac{1}{2}-2\frac{1}{2}$	3093.792	25	1790	B	
		$1\frac{1}{2}-1\frac{1}{2}$	3089.130	25	1500	B	
		$\frac{1}{2}-\frac{1}{2}$	3087.065	15	1310	B	
(60).....	$a^2G-z^2F^0$	$4\frac{1}{2}-3\frac{1}{2}$	6106.967	2	87	B	
		$3\frac{1}{2}-2\frac{1}{2}$	6135.07	2	81	B	
(62)*.....	$a^2G-y^2G^0$	$4\frac{1}{2}-4\frac{1}{2}$	4501.972	8	840	A	
		$3\frac{1}{2}-3\frac{1}{2}$	4449.573	5	450	A	
		$4\frac{1}{2}-3\frac{1}{2}$	4491.164	2	177	C	
(63)*.....	$a^2G-x^2G^0$	$4\frac{1}{2}-4\frac{1}{2}$	3930.023	10	3760	A	
		$3\frac{1}{2}-3\frac{1}{2}$	†3909.894	20	( )	.....	45
		$4\frac{1}{2}-3\frac{1}{2}$	3942.006	6	960	B	
(64)*.....	$a^2G-w^4G^0$	$4\frac{1}{2}-3\frac{1}{2}$	3886.587	6	1490	A	
		$3\frac{1}{2}-2\frac{1}{2}$	3864.300	(3)	1300	B	

TABLE 1—*Continued*

Mult. No.	Designation		λ	Arc. Int.	*gf*	Wt.	Notes
(66).....	$a^2G-x^2F^0$	$4\frac{1}{2}-3\frac{1}{2}$	3871.078	8	2500	A	
		$3\frac{1}{2}-2\frac{1}{2}$	†3863.866§	6	2100	A	
		$3\frac{1}{2}-3\frac{1}{2}$	3840.140	4	1850	A	
(68)*.....	$a^2G-v^2G^0$	$4\frac{1}{2}-4\frac{1}{2}$	3806.796	8	2700	A	
		$3\frac{1}{2}-3\frac{1}{2}$	3803.784	6	1250	A	
(69)*.....	$a^2G-w^2F^0$	$4\frac{1}{2}-3\frac{1}{2}$	3790.469	8	1970	A	
		$3\frac{1}{2}-2\frac{1}{2}$	3779.648	4	730	B	
(70)*.....	$a^2G-x^2H^0$	$4\frac{1}{2}-5\frac{1}{2}$	3686.262	8	2800	A	
		$3\frac{1}{2}-4\frac{1}{2}$	3671.205	10	2100	A	
(71)*.....	$a^2G-t^2G^0$	$4\frac{1}{2}-4\frac{1}{2}$	3284.360	6	2250	B	
		$3\frac{1}{2}-3\frac{1}{2}$	3273.027	7	1750	A	
(72)*.....	$a^2G-u^2F^0$	$4\frac{1}{2}-3\frac{1}{2}$	3233.190	6	2030	A	
		$3\frac{1}{2}-2\frac{1}{2}$	3218.869	5	1640	B	
(73)*.....	$a^2G-u^2H^0$	$4\frac{1}{2}-5\frac{1}{2}$	3212.434	15	12800	A	
		$3\frac{1}{2}-4\frac{1}{2}$	3205.582	15	10000	A	
(74)*.....	$a^2G-t^2F^0$	$4\frac{1}{2}-3\frac{1}{2}$	3050.400	25	2970	A	
(77).....	$a^2P-z^2S^0$	$1\frac{1}{2}-\frac{1}{2}$	5558.752	3	440	C	
		$\frac{1}{2}-\frac{1}{2}$	5561.670	2	290	C	
(82)*.....	$a^2D-y^2P^0$	$2\frac{1}{2}-1\frac{1}{2}$	4537.663	6	980	C	
(84)*.....	$a^4H-y^4G^0$	$6\frac{1}{2}-5\frac{1}{2}$	6326.845	6	780	B	
		$5\frac{1}{2}-4\frac{1}{2}$	6339.090	5	850	B	
		$4\frac{1}{2}-3\frac{1}{2}$	6349.477	5	640	B	
		$3\frac{1}{2}-2\frac{1}{2}$	6357.297	4	610	B	
(86)*.....	$a^4H-y^2H^0$	$4\frac{1}{2}-4\frac{1}{2}$	4496.864	5	1220	C	
		$4\frac{1}{2}-5\frac{1}{2}$	4490.815	5	2100	B	
		$3\frac{1}{2}-4\frac{1}{2}$	†4488.898	20	(10100)	A	46
(87)*.....	$a^4H-z^4I^0$	$6\frac{1}{2}-7\frac{1}{2}$	4452.008	20	21700	A	
		$5\frac{1}{2}-6\frac{1}{2}$	4462.363	20	15800	A	
		$4\frac{1}{2}-5\frac{1}{2}$	4469.710	15	11100	A	
		$3\frac{1}{2}-4\frac{1}{2}$	4468.010	8	3400	A	
(88)*.....	$a^4H-x^4H^0$	$6\frac{1}{2}-6\frac{1}{2}$	4268.643	20	22500	A	
		$5\frac{1}{2}-5\frac{1}{2}$	4271.554	12	15900	A	
		$4\frac{1}{2}-4\frac{1}{2}$	4276.958	12	12900	A	
		$3\frac{1}{2}-3\frac{1}{2}$	4284.055	15	13000	A	
(89)*.....	$a^4H-u^4G^0$	$6\frac{1}{2}-5\frac{1}{2}$	3998.730	15	15200	A	
		$5\frac{1}{2}-4\frac{1}{2}$	3992.801	12	14500	A	
		$4\frac{1}{2}-3\frac{1}{2}$ $3\frac{1}{2}-2\frac{1}{2}$	†3990.566	20	{16900} {16600}	A	
(92)*.....	$b^4P-x^4D^0$	$2\frac{1}{2}-3\frac{1}{2}$	5772.402	6	1360	B	
		$1\frac{1}{2}-2\frac{1}{2}$	†5748.860	4	700	B	47
		$2\frac{1}{2}-2\frac{1}{2}$	5850.286	2	610	B	
(94)*.....	$b^4P-x^4P^0$	$2\frac{1}{2}-2\frac{1}{2}$	4751.574	6	1120	C	
		$2\frac{1}{2}-1\frac{1}{2}$	4706.178	8	1630	C	
(99)*.....	$a^2H-v^2G^0$	$5\frac{1}{2}-4\frac{1}{2}$	4524.218	15	4550	A	
		$4\frac{1}{2}-3\frac{1}{2}$	4529.589	8	3000	A	

TABLE 1—*Continued*

Mult. No.	Designation		λ	Arc Int.	gf	Wt.	Notes
(100)*.....	$a^2H-z^4I^0$	$5\frac{1}{2}-4\frac{1}{2}$	4540.014	6	1310	C	
(101).....	$a^2H-z^2I^0$	$5\frac{1}{2}-6\frac{1}{2}$	†4474.714	12	(7300)	A	48
		$4\frac{1}{2}-5\frac{1}{2}$	4457.759	8	4900	A	
(102).....	$a^2H-w^2F^0$	$4\frac{1}{2}-3\frac{1}{2}$	4468.759	4	1290	B	
(103).....	$a^2H-x^2H^0$	$5\frac{1}{2}-5\frac{1}{2}$	4354.979	5	2200	B	
		$4\frac{1}{2}-4\frac{1}{2}$	4342.832	6	2040	C	
(104)*.....	$a^2H-u^2H^0$	$5\frac{1}{2}-5\frac{1}{2}$	3708.721	6	5500	B	
		$4\frac{1}{2}-4\frac{1}{2}$	3706.035	4	5400	B	
(109)*.....	$b^4F-v^4G^0$	$4\frac{1}{2}-5\frac{1}{2}$	4545.394	25	14100	A	
		$3\frac{1}{2}-4\frac{1}{2}$	4560.710	20	10900	A	
		$2\frac{1}{2}-3\frac{1}{2}$	4571.783	15	7500	A	
		$1\frac{1}{2}-2\frac{1}{2}$	4578.728	15	6400	A	
		$3\frac{1}{2}-3\frac{1}{2}$	4579.198	7	1850	B	
(110)*.....	$b^4F-t^4D^0$	$4\frac{1}{2}-3\frac{1}{2}$	4474.045	10	5600	B	
		$3\frac{1}{2}-2\frac{1}{2}$	4496.062	8	3600	B	
		$2\frac{1}{2}-1\frac{1}{2}$	4514.191	6	2050	B	
		$1\frac{1}{2}-\frac{1}{2}$	4525.168	5	1260	C	
		$2\frac{1}{2}-2\frac{1}{2}$	†4488.898	20	(14800)	A	49
(111)*.....	$b^4F-u^4F^0$	$4\frac{1}{2}-4\frac{1}{2}$	4232.460	15	13100	A	
		$3\frac{1}{2}-3\frac{1}{2}$	4232.952	12	8400	A	
		$2\frac{1}{2}-2\frac{1}{2}$	†4234.000	12	( )	.....	50
(112)*.....	$b^4F-s^4D^0$	$4\frac{1}{2}-3\frac{1}{2}$	4104.778	15	21500	A	
(113)*.....	$z^6G^0-e^6F$	$6\frac{1}{2}-5\frac{1}{2}$	4807.537	25	12100	A	
		$5\frac{1}{2}-4\frac{1}{2}$	4796.930	20	8300	A	
		$4\frac{1}{2}-3\frac{1}{2}$	4786.515	20	6500	A	
		$3\frac{1}{2}-2\frac{1}{2}$	4776.364	10	5200	A	
		$2\frac{1}{2}-1\frac{1}{2}$	4766.635	10	3800	A	
		$1\frac{1}{2}-\frac{1}{2}$	4757.50	8	2600	C	
		$4\frac{1}{2}-4\frac{1}{2}$	4753.957	7	2600	C	
		$3\frac{1}{2}-3\frac{1}{2}$	4750.990	8	2300	C	
		$2\frac{1}{2}-2\frac{1}{2}$	4748.525	7	1200	C	
		$1\frac{1}{2}-1\frac{1}{2}$	4746.638	5	1300	C	
(114)*.....	$z^6G^0-e^6H$	$6\frac{1}{2}-7\frac{1}{2}$	3695.335	30	47000	A	
		$5\frac{1}{2}-6\frac{1}{2}$	3687.473	12?	42000	C	
		$4\frac{1}{2}-5\frac{1}{2}$	3680.113	15	27000	A	
		$3\frac{1}{2}-4\frac{1}{2}$	3673.404	12	27000	A	
		$2\frac{1}{2}-3\frac{1}{2}$	3667.741	15	22000	A	
		$1\frac{1}{2}-2\frac{1}{2}$	3663.594	15	18800	A	
(115)*.....	$z^6G^0-f^6G$	$6\frac{1}{2}-6\frac{1}{2}$	3676.684	10	18600	A	
		$5\frac{1}{2}-5\frac{1}{2}$	3672.403	8	11200	B	
(118)*.....	$a^4G-y\,H^0$	$5\frac{1}{2}-6\frac{1}{2}$	4904.350	(9)	2500	A	
(119)*.....	$a^4G-x\,H^0$	$5\frac{1}{2}-6\frac{1}{2}$	4706.574	12	3900	C	
		$4\frac{1}{2}-5\frac{1}{2}$	4710.566	12	3800	C	
(120)*.....	$a^4G-w^4H^0$	$5\frac{1}{2}-6\frac{1}{2}$	4291.816	15	17000	A	
		$4\frac{1}{2}-5\frac{1}{2}$	4296.107	15	12900	A	
		$3\frac{1}{2}-4\frac{1}{2}$	4297.681	12	9700	B	
		$2\frac{1}{2}\ 3\frac{1}{2}$	4298.029	12	8800	B	

TABLE 1—*Continued*

Mult. No.	Designation		λ	Arc Int.	*gf*	Wt.	Notes
(121)*.....	$a^4G-t^4G^0$	$5\frac{1}{2}-5\frac{1}{2}$	†4051.352§	12	19800	B	
		$4\frac{1}{2}-4\frac{1}{2}$	†4050.963§	10	17300	B	
(125)*.....	$z^6F^0-e^6F$	$5\frac{1}{2}-5\frac{1}{2}$	5193.004	7	9800	B	
		$4\frac{1}{2}-4\frac{1}{2}$	†5194.824	10	(7600)	B	
		$3\frac{1}{2}-3\frac{1}{2}$	5195.394	5	3800	C	
		$2\frac{1}{2}-2\frac{1}{2}$	†5194.824	10	(6600)	B	
(127)*.....	$b^2P-y^2P^0$	$1\frac{1}{2}-\frac{1}{2}$	†5782.601	2	(7000)	B	51
(129).....	$b^2H-v^2G^0$	$5\frac{1}{2}-4\frac{1}{2}$	5487.915	10	6400	A	
		$4\frac{1}{2}-3\frac{1}{2}$	5507.753	8	6400	A	
(130)*.....	$b^2H-z^2I^0$	$5\frac{1}{2}-6\frac{1}{2}$	5415.277	10	9500	A	
		$4\frac{1}{2}-5\frac{1}{2}$	†5401.945	8	(7200)	A	52
(131)*.....	$b^2H-x^2H^0$	$5\frac{1}{2}-5\frac{1}{2}$	5240.878	9	10800	B	
		$4\frac{1}{2}-4\frac{1}{2}$	5234.088	8	9900	B	
(135)*.....	$a^2F-x^2G^0$	$3\frac{1}{2}-4\frac{1}{2}$	5725.633	6	5100	B	
(139)*.....	$b^2G-v^2F^0$	$3\frac{1}{2}-2\frac{1}{2}$	†5401.945	8	(29000)	A	53

NOTES TO TABLE 1

1. Blend with line in multiplet $b^2H-w^4G^o$ not listed in RMT. All (1) at low temperatures.
2. Blend with line in multiplet $a^2F-w^4G^o$ not listed in RMT. All (2) at low temperatures.
3. Blend with line in (22). All (22).
4. Blend with line in (111). All (6) at furnace temperatures.
5. Blend with line in (41). Probably all (41) at higher temperatures.
6. Blend with line in (63). Probably all (7) at furnace temperatures.
7. Blend with line in (126) not listed in RMT. All (8).
8. Blend with line in $a^2F-s^2G^o$ and line in (90) not listed in RMT. All (8) at furnace temperatures.
9. Blend with line in (10) not listed in RMT. All (9).
10. Masks predicted line λ 3813.45 in (28). All (9).
11. Blend with leading line in (28). Probably largely (28) even at furnace temperatures.
12. Blend with line in (17).
13. Blend with line in (15).
14. "Raie ultime" of *V* I.
15. Blend with line in (5). All (22).
16. Blend with lines in $a^4P-x^4D^o$ and $a^4G-u^4G^o$ not listed in RMT. Probably all (23).
17. Blend with line in $a^4H-v^4G^o$ not listed in RMT. Probably all (23).
18. Furnace intensity erratic. Behaves like blend with impurity.
19. Blend with line in $b^4P-w^4P^o$ not listed in RMT. Probably all (24) at furnace temperatures, but relative arc and furnace intensities of λ 4191 and λ 4182 indicate higher level line may contribute at high temperatures.
20. Blend with lines in six high-level multiplets. All (27).
21. Blend with line in $b^4F-u^4G^o$ not listed in RMT. All (27).
22. Masks predicted line 4109.81 in (41).
23. Blend with line in (9). All (28).
24. Blend with line in $a^2F-r^2G^o$ not listed in RMT. All (28).
25. Very much widened in furnace spectra.
26. Widened in furnace spectra.
27. Blend with line in (127). Probably all (35) at furnace temperatures.
28. All three lines of (36) are slightly widened in furnace spectra. Widening of λ 5731 and λ 5776 perhaps more marked than λ 5670.
29. Very much widened in furnace spectra.
30. Very much widened in furnace spectrum.
31. Much widened in furnace spectra.

(Notes to Table 1 continued on following page)

NOTES TO TABLE 1—*Continued*

32. Blend with line in $b^4F-w^2F^o$ not listed in RMT. All (33).
33. Widened in furnace spectra.
34. Widened in furnace spectra.
35. Blend with line in $b^4P-t^4D^o$ not listed in RMT. Probably all (40).
36. Blend with line in (6*b*). All (41).
37. Blend with line in (43).
38. Blend with line in (43).
39. Blend with line in (42).
40. Blend with line in (42).
41. Widened in furnace spectra.
42. Widened in furnace spectra.
43. In wing of 4864.741 (3).
44. Blend with line in $b^4P-s^4D^o$ not listed in RMT. All (52).
45. Blend with line in (7). All (7) at furnace temperatures. Appears at low furnace temperatures.
46. Blend with line in (110).
47. Blend with line in $a^2F-x^2D^o$ not listed in RMT. Probably all (92).
48. Blend with weak line in (87) not listed in RMT; (87) line may contribute at furnace temperatures.
49. Blend with line in (86).
50. Blend with line in (6). All (6) at furnace temperatures.
51. Blend with line in (35). Probably all (35) at furnace temperatures.
52. Blend with line in (139). Probably mostly (130).
53. Blend with line in (130). Probably mostly (130).

measured on fewer than three spectra, or that for other reasons the measurement is felt to be relatively uncertain. Measurements assigned weights "B" and "C" are not necessarily less accurate than those assigned "A" but are more open to question.

The numbers in the last column refer to notes at the end of the table, most of which deal with the behavior of blends. It is hoped that they may be of aid in applying the material.

The observational data are not complete enough to permit a detailed discussion of the comparative behavior of the observed *gf*-values and the theoretical strengths of lines in multiplets and of multiplets in supermultiplets and transition arrays and the application of the sum rule. However, a comparison of the observed *gf*-values with the theoretical relative strengths of lines in multiplets and of multiplets in supermultiplets, as compiled in tables derived from quantum mechanical formulae for unperturbed LS coupling, is of interest to show to what extent line strengths in the spectrum of *V* I conform to currently available theoretical data.

Of the 100 multiplets for which *gf*-values have been obtained, 82 are permitted by the selection rules for LS coupling, upon which the theoretical data are based; that is, the combining terms giving rise to these multiplets have the same multiplicity, and $\Delta L = 0$ or ± 1. Of the "permitted" multiplets, 68 contain two or more lines for which *gf*-values have been measured and which can be compared with theory. The comparison is far from definitive, however, because in the majority of these multiplets the intensity measurements are incomplete. A comparison of the relative *gf*-values with the theoretical relative strengths of lines within multiplets as given by H. N. Russell[6] shows that for 39 multiplets, or about 55 per cent of the "permitted" multiplets for which two or more lines have been measured, the relative strengths are in agreement with the theoretical values within estimated errors of measurement. Among these are five multiplets, (5), (21), (22), (27), and (29), whose arc intensities were measured by R. Frerich.[7] It is of interest to note that the percentage of multiplets of *V* I with normal intensities is about the same as that found by G. R. Harrison[8] in the spectrum of *Ti* I. Both *Ti* I[9] and *V* I

[6] *Mt. W. Contr.*, No. 537; *Ap. J.*, **83**, 129, 1936.

[7] *Ann. d. phys.*, **81**, 807, 1926.

[8] *J. Opt. Soc. Amer.*, **17**, 389, 1928.

[9] H. N. Russell, *Mt. W. Contr.*, No. 345; *Ap. J.*, **66**, 347, 1927.

are comparatively well-behaved complex spectra, in so far as their adherence to LS coupling is concerned

In 20 multiplets, disagreement between observed and theoretical strengths considered larger than errors of measurement occurs for one or more lines. In these cases, however, the divergences are not extreme, and some may not be real. In 11 multiplets the observed and theoretical strengths are widely divergent. Of the more completely observed multiplets with numerous lines, multiplets (12), (15), (20), and (57) are perhaps the worst offenders. In (15) $a^4F - x^4D^0$ and in (57) $a^4P - r^4D^0$, there is no relation between observed and theoretical line strengths. In (62) $a^2G - y^2G^0$, (63) $a^2G - x^2G^0$, and (66) $a^2G - x^2F^0$, the first satellite lines are far too strong with respect to lines on the main diagonal; and in (56) $a^4P - v^4P^0$ the satellite lines were the only ones strong enough to appear in the furnace spectra. In (20) $a^6D - z^6F^0$, line strengths along the main and satellite diagonals are correlated among themselves but fall off much too rapidly along the diagonals, while the leading satellite lines are too strong with respect to the leading line of the main diagonal. As might be expected, there is some tendency for abnormal multiplets to be associated with perturbed terms having abnormal intervals and Zeeman-effect *g*-values, as well as with terms that give rise to strong intersystem combinations. In particular, it may be noted that practically all the terms listed by Russell and Babcock[10] as having anomalous *g*-values due to *g*-sharing have multiplets with abnormal line strengths.

A comparison of observed *gf*-values of multiplets in supermultiplets and transition arrays with theoretical strengths given in tables computed by L. Goldberg[11] reveals a much wider divergence than is exhibited by lines within multiplets, although here the data are even less complete for a definitive analysis. The correlation between the *gf*-sums for multiplets and the theoretical strengths is better for the transition array $d^4s - d^4p$ than for the arrays $d^3s^2 - d^3sp$ and $d^4s - d^3sp$, which are, however, much less completely observed. But even in the array $d^4s - d^4p$ none of the supermultiplets exhibit perfectly normal relative strengths within themselves, and for the whole array the scatter is large.

Although the greatest number of strong multiplets are produced by transitions between the electron configurations d^4s and d^4p, it cannot be said that this transition array completely dominates the spectrum. Multiplets with comparable strengths, although fewer in number, occur also in the transitions $d^3s^2 - d^3sp$, $d^4s - d^3sp$, $d^3sp - d^3s \cdot s$, and the strongest multiplet measured, (114) $z^6G^0 - e^6H$ (including the strongest line, λ 3695.335), arises from the transition $d^3sp - d^3s \cdot d$.

In view of this it is not surprising that the empirical rule of Meggers and Scribner[12] concerning the selection of the "raie ultime" appears to be partially violated. This rule states that "a 'raie ultime' in any spectrum originates with a simple interchange of a single electron between s and p states, usually preferring configurations in which only one electron occurs in such states." W. F. Meggers[13] has selected λ 4379.238 in multiplet (22) $(d^4s)\ a^6D - (d^4p)y^6F^0$ as the raie ultime of *V* I. The present measurements indicate that, when frequency factors are taken into account, the line λ 3185.396 in (14) $(d^3s^2)\ a^4F - (d^3sp)x^4G^0$ should appear stronger than λ 4379 in emission spectra under moderate excitation. At extremely low excitation, such as exists in interstellar space, only lines from the lowest sublevel ($a^4F_{1½}$) of the ground term can be expected. Under these conditions the raie ultime should be λ 3183.982 (14).

[10] *Zeeman Verhandelingen* (The Hague: Nijhoff, 1935), p. 291.

[11] *Ap. J.*, **82**, 1, 1935.

[12] *J. Research Nat. Bur. Standards*, **13**, 657, 1934.

[13] *J. Opt. Soc. Amer.*, **31**, 39, 1941.

THE SPACE MOTIONS OF THE R STARS

NOAH W. MCLEOD
University of California, Berkeley, California
Received February 12, 1947

ABSTRACT

The space motions of the R stars were studied by means of radial-velocity data. A solution for 68 normal R stars gave a solar motion of 17.4 km/sec, with an apex at $\alpha = 19^h42^m$, $\delta = 62°$. The velocity ellipsoid gives a dispersion of 48.1 km/sec in the direction of the galactic center; 22.7 km/sec in the direction of the galactic pole; and 15.5 km/sec at right angles to these directions.

The R stars with strong g-bands and weak atomic lines form a very marked high-velocity group of stars, distinct from the other R stars, both physically and kinematically.

The R stars are rather peculiar, being strongly suspected of forming a high-velocity group. Study of the proper-motion data led to the conviction that the existing proper motions of the R stars were neither numerous, accurate, nor homogeneous enough. It was therefore decided to base the analysis on the radial-velocity data alone.

The radial velocities in Sanford's[1] list were used. Examination of the literature on the carbon stars convinced the writer that the R stars are a very heterogeneous group. All known Re stars were rejected from the solution as possible supergiants. All long-period variables and R Coronae stars were rejected as probably being physically abnormal. Eight stars with strong g-bands and weak atomic lines were placed in a group by themselves. This last group will be designated as the "peculiar R stars" throughout this paper.

The solution for the solar motion was made by Airy's method, which leads to the well-known equation of condition,

$$V = -X \cos \alpha \cos \delta - Y \sin \alpha \cos \delta - Z \sin \delta + K ,$$

in which V is the radial velocity; X is the solar-motion component in the direction of the vernal equinox; Y is the solar-motion component in the direction of 6 hours' right ascension and 0° declination; Z is the solar-motion component in the direction of the north celestial pole; K is the speed of contraction or expansion of the stars as a group relative to the sun; α is the right ascension; and δ is the declination.

A solution was made for the solar motion of the normal R stars by this method. Since the peculiar R stars were few in number and were confined, with one exception, to the northern hemisphere, two solutions were made for them, one with, and the other without, the K-term. The solar-motion solutions are given in Table 1. Of the two solutions for the peculiar R stars, the solution without the K-term is probably more accurate, in spite of its greater probable errors, because it is made with fewer unknowns in a case where the number of observations is comparable with the number of unknowns.

R. F. Sanford[2] found a solar motion of 21.9 km/sec toward $\alpha = 18^h$, $\delta = +28°$, from 62 radial velocities. He did not use Airy's method. R. E. Wilson[3] found a solar motion of 18.5 km/sec toward $\alpha = 18^h48^m$, $\delta = 44°$, from 37 radial velocities. In both cases high-velocity stars were rejected, but emission-line stars were retained.

The peculiar R stars are one of the most marked groups of high-velocity stars in the sky. They are separated from the normal R stars not only kinematically but spectro-

[1] *Mt. W. Contr.*, No. 689; *Ap. J.*, **99**, 145, 1944.

[2] *Mt. W. Contr.*, No. 689; *Ap. J.*, **99**, 145, 1944.

[3] *Mt. W. Contr.*, No. 631; *Ap. J.*, **90**, 492, 1939.

scopically and resemble the cluster variables in their solar motion. They have no galactic concentration but show a marked preference for the first quadrant of galactic longitude north of the celestial equator. Their distribution roughly resembles that of the globular clusters north of the celestial equator. It seems probable that these objects are the carbon stars characteristic of a stellar population of Baade's[4] type II. It might be worth while to conduct a search of the region of the galactic center, where the globular clusters are concentrated, in an attempt to find more of the peculiar R stars.

TABLE 1

THE SOLAR MOTION OF THE R STARS

	Normal R Stars	Peculiar R Stars (Solution with K-Term)	Peculiar R Stars (Solution without K-Term)
Number	68	8	8
X	+ 3.5±7.2 (p.e.) km/sec	+ 80.1± 46.8 (p.e.) km/sec	+124.1± 59.3 (p.e.) km/sec
Y	− 7.4±5.2 (p.e.) km/sec	−206.1±102.0 (p.e.) km/sec	−165.5±153.5 (p.e.) km/sec
Z	+15.5±7.5 (p.e.) km/sec	− 26.5± 71.5 (p.e.) km/sec	+249.0± 88.0 (p.e.) km/sec
K	− 1.8±3.7 (p.e.) km/sec	−185.8± 40.5 (p.e.) km/sec	.....
V	17.4 km/sec	222.5	325.2
Right ascension of apex	19^h42^m	19^h24^m	20^h28^m
Declination of apex	+62°	− 7°	+49°
Galactic longitude of apex	62°	359°	54°
Galactic latitude of apex	+18°	− 13°	+ 5°
Mean peculiar radial velocity	±28.8 km/sec	± 50.6 km/sec	±86.6 km/sec

TABLE 2

THE VELOCITY ELLIPSOID OF THE NORMAL R STARS

	Axis toward Galactic Center	Axis toward Galactic Pole	Third Axis
Dispersion	48.1 km/sec	22.7 km/sec	15.5 km/sec
Right ascension	17^h28^m	12^h40^m	20^h56^m
Declination	−30°	+28°	+46°
Galactic longitude	325°	0°	55°
Galactic latitude	0°	+90°	0°

The normal R stars show a slight galactic concentration and seem to have a preference for the first quadrant of galactic longitude and a tendency to avoid the third. This avoidance of the third quadrant may be purely apparent, however, and due to incompleteness of search of this quadrant, which is largely within the south circumpolar region.

The velocity ellipsoid of the normal R stars was computed by Charlier's[5] method. The six-moment method broke down, as it often does when less than a hundred stars are involved. A fixed-axis solution was then put through. The three axes were assumed as follows: the X-axis in the direction of the galactic center; the Y-axis in the galactic plane, 90° from the galactic center, in the direction of Cygnus; and the Z-axis in the direction of the

[4] *Mt. W. Contr.*, No. 696; *Ap. J.*, **100**, 137, 1944.

[5] *The Motion and the Distribution of the Stars* ("Memoirs of the University of California," No. 7 [1926]).

north galactic pole. The positions of the normal R stars with known radial velocities, 68 in number, were transformed to this system of galactic co-ordinates, three normal equations were formed, and the solution was made for the axes of the velocity ellipsoid (Table 2).

The dispersion is over twice as great in the direction of the galactic center as it is at right angles to it. The difference in length between the two shorter axes may not be real. The velocity ellipsoid of the R stars resembles that of the dwarf G stars.

The most striking characteristic of the space motions of the normal R stars is that they have reasonably large peculiar motions, yet the asymmetry is lacking in their motions.

The mystery of the R stars is still unsolved. The list is incomplete even for stars as bright as the tenth magnitude. A more intensive search should be made for R stars.

The proper-motion data for the R stars are still scanty and inaccurate. More proper motions should be determined, with a higher standard of accuracy than previously. Better proper motions might well lead to a revision of our values of the absolute magnitudes of these stars.

In closing I wish to thank Professor R. J. Trumpler and Dr. J. H. Moore, of the University of California, for much helpful advice on this research project

ON THE ORIGIN OF THE HEAVY ELEMENTS

G. B. VAN ALBADA
Warner and Swasey Observatory, Case Institute of Technology, Cleveland, Ohio
Received March 14, 1947

ABSTRACT

The present paper is an attempt to explain the formation of heavy elements and to trace the astronomical consequences of the results obtained from such a study. In Section I the problem is stated, and the general outline for a possible solution is indicated. Section II deals with the discussion of the expression for the energy content of atomic nuclei. The resulting formula represents the observational data as well as can be expected.

In Section III this formula is used to find what kind of nucleus is most stable under different conditions of density. It appears that, when the electron gas is degenerate, nuclei of large atomic weight may be formed. A small correction of the original formula, which is required by theory and which does not conflict with observational data, allows the formation of nuclei up to atomic weight 240 and higher.

In Section IV the astronomical consequences of the theory are discussed. It appears that the only favorable places for the formation of heavy nuclei are the interiors of massive stars, which cannot become regular white dwarfs on account of their relatively high masses. When these stars contract to very high densities, rotation begins to counterbalance gravity, and under certain conditions matter in their interiors will cool and become degenerate. This is the state at which the formation of heavy elements begins. The process results ultimately in an explosion, which distributes part of the heavy elements over the surrounding space and leaves one or more stellar remnants in the form of white dwarfs.

In Section V the problem of the formation of the light elements is touched. Since not every massive star can be expected to develop a degenerate core, the formation of the lighter elements may be explained as a result of thermonuclear reactions at temperatures of the order of 10^9 degrees.

Section VI deals with the possible observational evidence. Actual calculation of stellar models must be made in order to identify the different phenomena described with existing stars and thus provide observational checks.

I. INTRODUCTION

Many previous attempts to explain the existence of the heaviest elements begin with the assumption that they have been formed in a prestellar stage of the evolution of the universe, when all matter was compressed to extremely high densities and possessed correspondingly high temperatures. The reasons for this assumption are found in a consideration of the conditions of thermodynamic equilibrium between atomic nuclei.

When a uranium nucleus undergoes fission, energy of the order of 200 million electron volts (m.e.v.) is liberated. This energy, divided over the two fission products, corresponds to a temperature of approximately 5×10^{11} degrees. Building up of uranium from lighter elements seems to be possible only at temperatures of this order of magnitude. In addition, the density has to be very high, so that the neutron gas which is present at these high temperatures may approach the limit of degeneracy. In no other way is it possible to form nuclei consisting of approximately 240 particles protected from rapid decay.

The picture is somewhat altered if one takes into account possible degeneracy of the electron gas. If this gas is highly degenerate, its zero-point energy becomes of importance in nuclear equilibrium. This circumstance will favor the formation of nuclei of low specific charge at high density and low temperature. Consequently, there is a second range of physical conditions under which uranium may be formed.

Figure 1 shows the calculated abundance of uranium and some other nuclei under conditions of thermodynamic equilibrium if the partial degeneracy of the electron gas is taken into account. The density is assumed to be so high that the neutron gas is at the verge of becoming degenerate. In this case two maxima in the uranium abundance occur. The first maximum at a temperature of 25,000,000,000° and a density 10^{12} gm/cm^3 gives a concentration of only 6×10^{-25} by weight, while at higher temperatures the concentra-

tion drops to 2×10^{-96}. Consequently, it is of little help that at still higher temperatures the concentration rises again. The uranium formed at a temperature of 10^{13} degrees could never have persisted. But the first maximum is not sufficient to explain the present existence of uranium. The slightest decrease in temperature or density would cause a great drop in the uranium content; and, as a result of the large number of fast neutrons, this drop would occur almost instantly. In addition, the computed maximum concentration is certainly much too high, since in the calculation all elements between nickel and uranium have been neglected. If the presence of tin only is taken into account, the uranium concentration is still further reduced.

In all these computations one factor has been neglected. If it is not possible to form any appreciable quantity of uranium under the given conditions, it is quite possible to form other nuclei of similar mass but lower charge. At the given density these nuclei

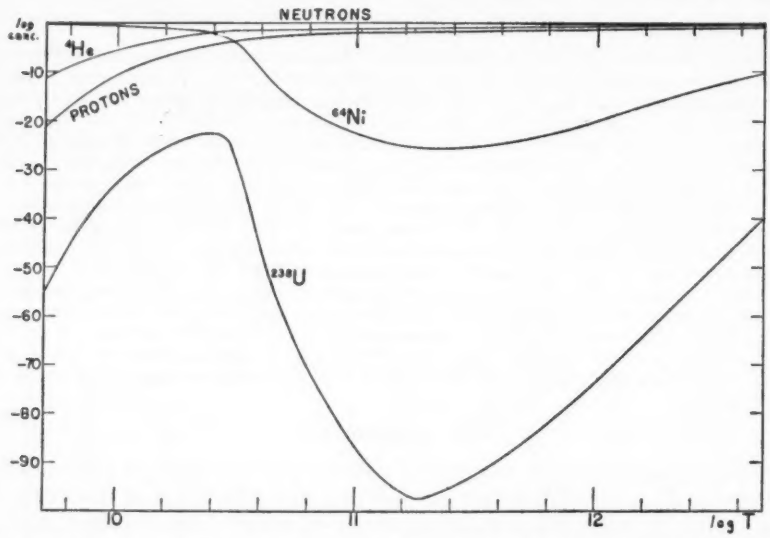

FIG. 1.—Calculated abundances of uranium and some other nuclei under conditions of thermodynamic equilibrium.

would not be beta-active as they are normally. The energy level corresponding to the emitted beta particle is already occupied by the particles in the degenerate electron gas. On the other hand, a nucleus of higher charge would necessarily absorb the fast electrons from the degenerate gas as long as this results in a reduction of the total energy. It has been shown in a previous paper[1] that in this way the formation of nuclei of mass $A = 150$ and reduced charge may be explained, even at a temperature of absolute zero. The reason for this is that these nuclei, having a low specific charge, are accompanied by only a relatively small number of electrons, so that the energy contribution of the degenerate electron gas is much lower than in the case of the ordinary more stable iron nuclei. A nucleus like the one just mentioned would go through a number of subsequent beta processes when the density is released and would increase its charge to 60.

In the earlier paper it was not possible to explain the formation of the very heavy nuclei. It appeared then that, when the density was increased beyond a certain limit, no heavier nuclei would be formed but that the added material would be transformed into neutrons. However, it was suspected that this failure might be due to the difficulty in the

[1] *B.A.N.*, **10**, 161, 1946.

calculation of the actual energy content of those nuclei with highly reduced charge. It will be shown in the present contribution that such calculations can be made and that on this basis the formation of the heaviest-known nuclei can be explained.

II. EXTENSION OF THE FORMULA FOR THE PACKING CONSTANT

For nuclei of equal mass, the packing constant is given by the equation

$$f = f_A + B_A (Z - Z_A)^2 , \tag{1}$$

where Z_A is the normal charge of the nucleus of mass A. This equation was extended by Bohr and Wheeler[2] in their consideration of the process of nuclear fission. Their formula is equivalent to

$$f = c_A + b_A (\tfrac{1}{2}A - Z)^2 + \frac{(M_n - M_p)(\tfrac{1}{2}A - Z)}{A} + kZ^2 A^{-4/3}, \tag{2}$$

where M_n and M_p are the masses of the neutron and the proton, respectively, and the final term is due to the Coulomb forces between the protons. The coefficient of this term may be expressed in the unit of nuclear radii as follows:

$$k = \tfrac{3}{5}\frac{e^2}{r_0} = 0.628 \text{ millimass unit} . \tag{3}$$

The term b_A is due to the interaction between the nuclear particles. Equation (2) is essentially a more detailed expression of equation (1); in both cases terms of higher than second order in $(\frac{1}{2}A - Z)$ have been neglected. As long as this approximation is used, we may suppose that this interaction depends on the number of particles per unit volume only, so that b_A will be proportional to $1/A^2$. This last assumption was not made by Bohr and Wheeler, but we shall show that it represents the actual nuclear parameters very accurately.

We suppose c_A to consist of a surface-tension term, as considered by Bohr and Wheeler, and of a constant which adjusts the zero value of f. If this is done, we may write, instead of equation (2),

$$f = \alpha \left(\frac{\frac{1}{2}A - Z}{A}\right)^2 + \beta \left(\frac{\frac{1}{2}A - Z}{A}\right) - \gamma + kZ^2 A^{-4/3} + sA^{-1/3} , \tag{4}$$

where

$$\beta = M_n - M_p = 0.81 \text{ millimass unit} . \tag{5}$$

The validity of this formula may be checked by considering actual nuclei.

Differentiating equation (4) with respect to Z and putting the derivative equal to zero, we obtain for the specific charge of the most stable nucleus of mass, A,

$$\frac{Z_A}{A} = \frac{\alpha + \beta}{2\alpha + 2kA^{2/3}} . \tag{6}$$

If this formula is sound, A/Z_A should be a linear function of $A^{2/3}$. Of course, the formula represents only smoothed values. The check is made with the following values for the coefficients:

$$\frac{2k}{\alpha + \beta} = 0.0152 , \tag{7}$$

and

$$\frac{2\alpha}{\alpha + \beta} = 1.984 . \tag{8}$$

[2] *Phys. Rev.*, **56**, 426, 1939.

The comparison of the computed values of A/Z_A with those given by Bohr and Wheeler in their table are shown in Table 1. The correspondence is as good as can be expected from any smooth curve. Even for nuclei of smaller atomic weight, equation (6) gives good average values (Fig. 2). Equation (6) is still trustworthy for values of $(\frac{1}{2}A - Z)/A$ as large as 0.10.

In principle it should be possible to determine both ratios k/α and α/β from equations (7) and (8). In practice, however, equation (8) does not permit an accurate determination. Instead we use equations (3) and (5) for the ratio k/β. Then it follows that

$$\alpha = 83 \text{ millimass units} . \tag{9}$$

With this value of α, the right-hand side of equation (8) becomes equal to 1.980.

TABLE 1

A	A/Z_A (Eq. [6])	A/Z_A (Bohr and Wheeler)	A	A/Z_A (Eq. [6])	A/Z_A (Bohr and Wheeler)
50	2.19	2.17	150	2.41	2.40
70	2.24	2.24	170	2.45	2.46
90	2.29	2.28	190	2.48	2.49
110	2.33	2.31	210	2.52	2.51
130	2.37	2.41	230	2.55	2.54

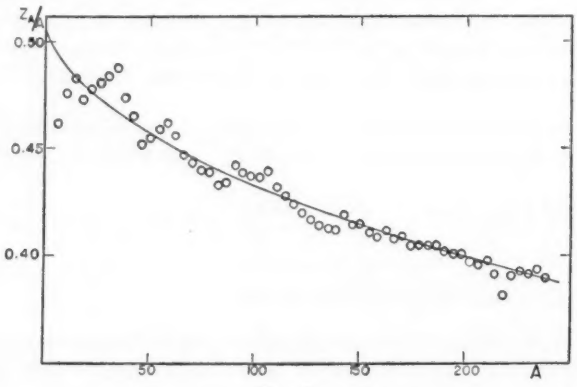

FIG. 2

Comparing equations (1), (4), and (6), we find

$$AZ_AB_A = \tfrac{1}{2}(\alpha + \beta) = 42 , \tag{10}$$

from which B_A may be calculated.

Finally, we have to check the terms $-\gamma + sA^{-1/3}$ in equation (4). To do this we calculate f_A, or the value of f resulting by placing $Z = Z_A$. Using equation (6) and the constants already known, we obtain

$$f_A = sA^{-1/3} + 21 - \gamma - \frac{42Z_A}{A} . \tag{11}$$

Bohr and Wheeler give the value of $s = 14$ m.e.v., corresponding to 15 millimass units. Using this, we calculate $f_A + \gamma$ and compare it with the values given by Mattauch and

Flügge.[3] These values were plotted and condensed in a number of standard points. The comparison is given in Table 2 and Figure 3.

The correspondence is good, even in the region of low nuclear weight. For the heaviest elements the calculated values of f_A seem to be a little too low, but the correspondence improves if in this region we use the measures obtained by Dempster, which are 0.05 unit lower. Since in the region of the heavy elements the theory of nuclear fission has given an additional check to the correctness of the surface-tension term, we feel justified in

TABLE 2

A	f_A (Mattauch and Flügge)	$f_A+\gamma$ (Eq. [11])	Difference	A	f_A (Mattauch and Flügge)	$f_A+\gamma$ (Eq. [11])	Difference
15.....	+0.20	+6.80	+6.60	100.....	−0.60	+6.03	+6.63
30.....	−0.55	6.09	6.64	140.....	−0.30	6.34	6.64
60.....	−0.80	+5.86	+6.66	220.....	+0.35	+6.90	+6.55

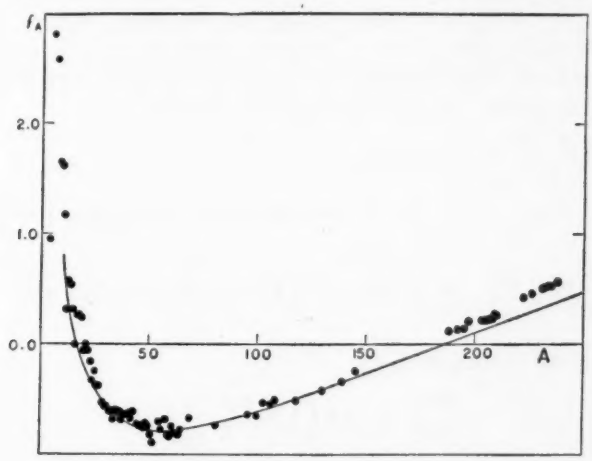

FIG. 3

assuming equation (11) and hence also equation (4) to be correct within the limits set by the accuracy of observation. For the numerical constants we adopt

$$s = 15 \text{ millimass units}, \qquad \gamma = 6.65 \text{ millimass units}. \tag{12}$$

Hence equation (4), given in a numerical form, becomes

$$f = \frac{83\,(\frac{1}{2}A - Z)^2}{A^2} + \frac{0.8\,(\frac{1}{2}A - Z)}{A} - 6.65 + 0.63\,Z^2 A^{-4/3} + 15\,A^{-1/3}. \tag{13}$$

III. FORMATION OF HEAVY NUCLEI AT HIGH DENSITY AND LOW TEMPERATURE

When matter is compressed to very high density while the temperature remains relatively low, two terms should be added to equation (4) in order to take into account the

[3] *Phys. Zeitschr.* **44**, 181, 1943.

electric attraction between the nucleus and surrounding electrons and the energy of the degenerate electron gas. Equation (5) is now replaced by[4]

$$F = a\left(\frac{\frac{1}{2}A - Z}{A}\right)^2 + \beta\left(\frac{\frac{1}{2}A - Z}{A}\right) - \gamma + kZ^2A^{-4/3} + sA^{-1/3} - p\rho^{1/3}Z^2A^{-4/3} + q\rho^{1/3}\left(\frac{Z}{A}\right)^{4/3}, \quad (14)$$

where

$$p = \frac{9}{10}\frac{10^3}{c^2}e^2\left(\frac{4\pi}{3}\right)^{1/3}m_H^{-4/3} = 1.91 \times 10^{-5} \quad (15)$$

and

$$q = \tfrac{3}{4}hc\frac{10^3}{c^2}\left(\frac{3}{8\pi}\right)^{1/3}m_H^{-4/3} = 4.15 \times 10^{-3}. \quad (16)$$

We write F instead of f, the latter symbol being reserved for the packing constant of the nucleus itself, without reference to the accompanying electrons. From equation (14) we may calculate the mass number and charge of the nucleus with the lowest specific energy.

Differentiating F with respect to Z, we obtain an equation which determines the most favorable charge for a nucleus of given mass number. When the density is low, the charge thus calculated will be equal to Z_A, but at higher density the charge is reduced. A second equation is found if in the differentiation we keep Z/A constant; the combination of both expressions gives the nucleus of lowest energy. We obtain

$$A\frac{\partial F}{\partial Z} = -2a\left(\frac{\frac{1}{2}A - Z}{A}\right) - \beta + 2kZA^{-1/3} - 2p\rho^{1/3}ZA^{-1/3} + \tfrac{4}{3}q\rho^{1/3}\left(\frac{Z}{A}\right)^{1/3} = 0 \quad (17)$$

and

$$Z\frac{\partial F}{\partial Z} + A\frac{\partial F}{\partial A} = \tfrac{2}{3}kZ^2A^{-4/3} - \tfrac{2}{3}p\rho^{1/3}Z^2A^{-4/3} - \tfrac{1}{3}sA^{-1/3} = 0. \quad (18)$$

Inserting numerical values, we find

$$\frac{A^2}{Z^2} = 0.084\left(1 - \frac{p\rho^{1/3}}{k}\right)A, \quad (19)$$

$$\frac{A}{Z} = 1.98 + 0.0152\left(1 - \frac{p\rho^{1/3}}{k}\right)A^{2/3} + 0.00697q\rho^{1/3}\left(1 - \frac{p\rho^{1/3}}{k}\right)^{1/3}A^{1/3}, \quad (20)$$

and

$$\frac{p}{k}\rho^{1/3} = 0.0073q\rho^{1/3}. \quad (21)$$

If we wish to know at what density a nucleus of mass A will be the most stable nucleus, we calculate A/Z from equation (19), neglecting p. Equation (20) then gives $q\rho^{1/3}$, and equation (210) yields $p\rho^{1/3}/k$. Inserting this value in equation (19), we obtain a second approximation. By a series of approximations the charge Z of the nucleus and the density at which it will be formed may be obtained.

The results of this calculation are given in Table 3. In this table the normal charge of the nucleus is shown in the second column. The third and fourth columns give its packing constant and the value of B_A, calculated from equation (10). The required density and the charge of the nucleus when formed are given in the next two columns. The seventh

[4] *B.A.N.*, **10**, 161, 1946.

column gives the packing constant of the nucleus formed, and the eighth column gives the energy of the electron gas per gram of matter (including the energy due to electric attraction and repulsion). The ninth column gives the total energy content of 1 gm of matter. The significance of the tenth, eleventh, and twelfth columns will be explained later.

We still have to consider the possibility of the formation of neutrons. We assume 1 gm of matter to consist of t gm of nuclei and $1-t$ gm of neutrons. If in equation (14) the energy contribution of the electron gas is called E, the energy content of 1 gm of mixture will be equal to

$$F = tf + t^{4/3}E + 8.94\,(1-t)\,. \tag{22}$$

TABLE 3

A	Z_A	f_A	B_A	log ρ	Z	f	E	F	$f+\frac{4}{3}E$	log ρ (Corr.)	A_{max}
60....	27.1	−0.79	0.0258	6.69	26.9	−0.79	0.23	−0.56	−0.48	6.69	84
80....	35.3	− .73	.0149	10.00	32.0	−0.57	2.50	+1.93	+2.76	9.98	112
100....	43.3	− .62	.00970	10.67	36.6	−0.19	3.74	+3.55	+4.80	10.63	140
120....	51.1	− .50	.00685	11.03	40.8	+0.23	4.40	+4.63	+6.10	10.91	168
140....	58.6	− .31	.00512	11.26	44.9	+0.65	4.88	+5.53	+7.16	11.07	196
160....	65.8	− .19	.00400	11.45	48.6	+0.99	5.20	+6.19	+7.92	11.20	224
180....	73.0	− .04	.00321	11.57	52.3	+1.34	5.38	+6.72	+8.51	11.28	252
200....	80.0	+ .11	.00262	11.68	55.8	+1.64	5.49	+7.13	+8.96	11.34	280
220....	86.8	+ .25	.00220	11.77	59.1	+1.94	5.63	+7.57	+9.45	11.37	308
240....	93.6	+0.39	0.00187	11.84	62.5	+2.20	5.65	+7.85	+9.73	11.39	336

Differentiation with respect to Z, A, and t gives

$$\frac{\partial F}{dZ} = t\,\frac{\partial f}{\partial Z} + t^{4/3}\,\frac{\partial E}{\partial Z} = 0\,, \tag{23}$$

$$\frac{\partial F}{\partial A} = t\,\frac{\partial f}{\partial A} + t^{4/3}\,\frac{\partial E}{\partial A} = 0\,, \tag{24}$$

and

$$\frac{\partial F}{\partial t} = f + \tfrac{4}{3}t^{1/3}E - 8.94 = 0\,. \tag{25}$$

As long as there are no neutrons, $t = 1$ and equation (25) need not be satisfied. The formation of neutrons begins when equation (25) is satisfied for $t = 1$. This gives $f + 4E/3 = 8.94$. From Table 3 we see that the formation of neutrons will start at a density of 5×10^{11} gm/cm^3.

For this critical density, equations (23) and (24) yield the solution $A = 200$ and $Z = 56$, as may be seen from Table 3. If higher densities are reached, all three equations, (23), (24), and (25), have to be satisfied simultaneously. In this case they will always give the same values for A, Z, and ρt. This means that at higher density every cubic centimeter will contain the same kind and the same amount of nuclei as at the critical density. The additional matter which is pressed into the space volume is completely transformed into neutrons without changing anything in the nuclei present. So the original nuclear constitution is not destroyed, but new nuclei are not formed. Still it is not possible to account for the formation of the heaviest nuclei.

The difficulty may be removed by a slight modification of our formula for the packing constant. That this formula cannot be accurate for nuclei of extremely low charge can be seen if in equation (13) we take $Z = 0$. With this value of Z we obtain $f > 14.5$, which is

impossible, since an aggregation of bound neutrons cannot have higher energy than the same number of free neutrons. The need of modification is also apparent from another consideration. If protons are transformed into neutrons, the new neutrons cannot move in the same quantum levels as the protons, since these levels were already occupied by other neutrons. Consequently, the volume of the nucleus has to increase, and we may anticipate that it will be approximately twice the normal volume if all protons are transformed into neutrons.

As a consequence of this increase in volume, the interaction term in equation (13) will diminish and eventually be halved. Without trying to give an accurate treatment of the problem, we may apply a correction by means of a term of the fourth degree in $(\frac{1}{2}A - Z)/A$, which will be symmetrical with respect to neutrons and protons, as is necessary. It seems proper to apply similar corrections to the Coulomb term and the surface-tension term, which terms contain the volume, respectively, in the $-\frac{1}{3}$ and in the $+\frac{2}{3}$ power.

Thus the total correction will be

$$\Delta f = -2\alpha\left(\frac{\frac{1}{2}A - Z}{A}\right)^4 - \tfrac{2}{3}k\,\frac{Z^2}{A^{4/3}}\left(\frac{\frac{1}{2}A - Z}{A}\right)^2 + \tfrac{4}{3}sA^{-1/3}\left(\frac{\frac{1}{2}A - Z}{A}\right)^2. \quad (26)$$

The coefficients are determined so as to correspond to double volume when all nuclear particles are of one kind.

The application of this correction to normal nuclei gives unimportant changes. For $A = 240$ we have $(\frac{1}{2}A - Z)/A = 0.110$, and the corrections obtained from equation (26) are small. The recalculated charge of the nucleus is 93.0 instead of 93.6, the packing constant changes from 0.39 to 0.38 millimass units. These changes are definitely below the limit of observational error. For nuclei of reduced charge the corrections become important. Since Δf increases with increasing charge, a positive term is added to equation (17), which requires a negative correction for q. This change is quite appreciable, whereas the influence on the calculated charge is small. For $A = 240$ the recalculated charge is 62.9 instead of 62.5, but the value of log ρ reduces from 11.84 to 11.39. We now find $f = 1.75$, $E = 4.04$, and, consequently, $f + 4E/3 = 7.14$. Formation of nuclei of mass 240 is now possible. The corrected values of log ρ are given in the eleventh column of Table 3.

It might be pointed out that for the formation of the heavy elements we depend not entirely on the validity of the correction just applied. Let us assume that the density of the degenerate gas is gradually increasing from 10^{10} to 10^{11} gm/cm^3. At the lower density, nuclei of mass number 80 will be numerous. At the higher density, nuclei of mass 120 should be expected. But there is no direct way for converting nuclei with $A = 80$ into nuclei with $A = 120$. The processes that are most likely to occur in the given circumstances are those of electron capture, but they will not increase the mass of the nuclei. Since the general tendency is toward a decrease in specific charge, neutron emission will be rare, and consequently it is not probable that a nucleus can increase its mass greatly by neutron capture. We may therefore expect that, at a density of 10^{11} gm/cm^3, part of the nuclei with mass 80 still persists. These nuclei will have a somewhat greater specific energy content than the nucleus $A = 120$. Consequently, the possibility that two such nuclei after a collision will form a nucleus of mass 160 is not excluded, if in this process energy is liberated.

The density of the electron gas is determined by the most frequent kind of nucleus, $A = 120$, $Z = 40.8$. If this mass and charge are denoted by A_0 and Z_0, the energy contribution of nucleus (A, Z) will be given by

$$\left.\begin{aligned} F = \alpha\left(\frac{\frac{1}{2}A - Z}{A}\right)^2 + \beta\left(\frac{\frac{1}{2}A - Z}{A}\right) - \gamma + kZ^2A^{-4/3} \\ + sA^{-1/3} - p\rho^{1/3}\frac{Z^2}{A}A_0^{-1/3} + \tfrac{4}{3}q\rho^{1/3}\frac{Z}{A}\left(\frac{Z_0}{A_0}\right)^{1/3}. \end{aligned}\right\} \quad (27)$$

In this formula we have taken into account the fact that the additional electrons which accompany this nucleus move in the upper energy levels of the degenerate electron gas.

The charge of the nucleus A is found by differentiating equation (27) with respect to Z. This gives

$$A\frac{\partial F}{\partial Z}=-2\alpha\left(\frac{\frac{1}{2}A-Z}{A}\right)-\beta+2kZA^{-1/3}-2p\rho^{1/3}ZA_0^{-1/3}+\tfrac{4}{3}q\rho^{1/3}\left(\frac{Z_0}{A_0}\right)^{1/3}=0. \quad (28)$$

For $A = A_0$, equation (28) is identical with equation (17). For other values of A, numerical calculations show that the calculated value of Z/A changes only very little, especially when the density is high. Neglecting the small variations, we may assume that Z/A is a function of the density only. The value of Z/A may be obtained from Table 3.

If in equation (27) we compare the F for a nucleus (A, Z) with the corresponding quantity for a nucleus $(2A, 2Z)$, we see that the two expressions differ only in the terms containing s, k, and p. The lighter nucleus will have the higher specific energy content if

$$\left.\begin{aligned} kZ^2A^{-4/3}+sA^{-1/3}-p\rho^{1/3}\frac{Z^2}{A}A_0^{-1/3} &> 2^{2/3}kZ^2A^{-4/3} \\ &\quad +2^{-1/3}sA^{-1/3}-2p\rho^{1/3}\frac{Z^2}{A}A_0^{-1/3}. \end{aligned}\right\} \quad (29)$$

We may expect the two nuclei (A, Z) to combine into one nucleus $(2A, 2Z)$ under liberation of energy if such inequality is satisfied.

We may simplify the above expression with the help of equation (18), making use of the equality of Z/A and Z_0/A_0. Since $p\rho^{1/3}/k$ is small, we find, as a good approximation,

$$A < 0.70A_0, \quad (30)$$

from which we see that nuclei of mass $A < 0.70\,A_0$ have the tendency to combine into nuclei of double mass. As a consequence, we may expect at any given density all nuclei with masses between $0.70\,A_0$ and $1.40\,A_0$ to be present. Since the energy liberated is small, it is quite possible that only part of the nuclei with $A < 0.70\,A_0$ will be eliminated in this way.

The twelfth column in Table 3 gives the values of $1.40\,A_0$. It will be seen that nuclei of mass number 240 may be formed at $\log \rho = 11.51$ or, if the correction Δf is applied, at $\log \rho = 11.24$. Even without the correction, there is no danger of the formation of neutrons at these densities.

The penetration of two nuclei of large mass will be hampered by the potential barrier. But we have to take into account the fact that the nuclei are already near each other at the given high density, so that only part of the barrier has to be penetrated. In addition, the presence of the negative electrons helps to reduce that barrier. The temperature required to make these encounters possible is not very high and does not endanger the degenerate state of the electron gas. The problem is analogous to that of the development of the proton-proton reaction in white dwarfs, which, according to Wildhack,[5] would go on even at absolute zero if any hydrogen were present.

IV. FORMATION OF HEAVY NUCLEI IN STARS

Nuclei of mass 240 will be formed in degenerate matter when the density is of the order of 2.5×10^{11} gm/cm^3. Assuming a value of 0.26 for Z/A, the value of x, used by Chandrasekhar[6] as a density parameter for degenerate matter, is equal to 100. The limiting temperature, above which matter cannot be degenerate, is then equal to 1.2×10^{11} degrees.

[5] *Phys. Rev.*, **59**, 539, 1941.

[6] S. Chandrasekhar, *An Introduction to the Study of Stellar Structure* (Chicago, 1939), p. 360.

According to the theory of white dwarfs, developed by Chandrasekhar, degenerate matter cannot occur in stars of mass exceeding a certain value M_3.[7] This fact excludes the explanation of the origin of the heavy elements in the "prestellar stage" of the universe. If the density parameter is to reach a value of 100 in the center of a star, the mass of this star should be equal to 0.9996 M_3. It is therefore extremely improbable that heavy elements could be formed in ordinary white dwarfs. For this reason we must look for another mechanism which will provide more freedom in the determination of mass.

If a star is rotating, centrifugal forces will, to a certain extent, counterbalance gravity. Consequently, the pressure in the interior will be diminished, and the star will be in equilibrium at a lower central temperature than without rotation. Eventually the core of the star might become degenerate, even when the mass is in excess of M_3. As Dr. Chandrasekhar has pointed out to me, the additional freedom which is gained in this manner is small for a star rotating uniformly throughout. For a polytrope $n = 3$, which in density distribution approaches the Roche model, rotational instability will develop at the equator long before an appreciable decrease of the central pressure is attained. For the Roche model, instability at the equator sets in when $\omega^2/2\pi G\rho$ reaches the value 0.36. Since for the polytrope $n = 3$ the density concentration $\rho_c/\bar{\rho} = 54$, $\omega^2/2\pi G\rho_c$ will then be equal to 0.0067. According to Chandrasekhar,[8] the mass of the rotating polytrope should then equal 1.04 M_3.

To overcome this difficulty we may assume that the rotation of the star is not uniform but increases toward the center. One may expect that, if the ratio of centrifugal force to gravity does not increase outward, rotational instability at the surface will not develop before an appreciable release in the central pressure occurs. This condition implies that the increase of ω^2 toward the center should be at least as rapid as the increase of the average density of the part of the star within the corresponding distance, r, from the center. It should be sufficient for a polytrope $n = 3$ if the central portions rotate at least seven times as fast as the outer regions. Since little is known about the rotation of stellar interiors, we do not know whether or not this condition can be fulfilled. For the present we shall accept it as a possible explanation.

If the increase of rotation toward the center is less pronounced, the contracting star will lose material from its surface by rotational instability, and eventually its mass will approach the critical mass, M_3. This is another way in which the stellar interior may become degenerate. Assuming that one or both processes occur, we shall investigate the further evolution of the star.

Before degeneracy develops, the core of the star will consist of helium and perhaps a certain amount of heavy elements with normal charge. The value of Z/A in the core in this case will be equal to one-half. As soon as the stage of degeneracy is reached at very high densities, electrons will be absorbed by the nuclei, and the value of Z/A will drop. For this reason the pressure in the central regions is no longer sufficient to withstand the weight of the outer layers, and the core will shrink. In accordance with this process, the core will increase its rotation, and it will pass through a number of subsequent stages in which rotational force and electron pressure together balance the gravitational pressure.

Since Z/A diminishes with increasing density, the pressure law of the core will not be identical with that of a polytrope $n = 3$, as would be the case for constant Z/A, but will correspond to a polytrope of higher index. Normally, this would render a star unstable. In this particular case, however, the star is protected by rotation.

An estimate of the amount of this protection may be made if we assume the equation of state, which applies at the center, to be valid throughout the star. In making this assumption, we certainly underestimate the stability of the star. The energy of the star under this condition will be given by

$$E = -A\frac{M^2}{R} + B\frac{M^{1+1/n}}{R^{3/n}} + C\frac{J^2}{MR^2}, \tag{31}$$

[7] *Ibid.*, p. 421.

[8] *M.N.*, **93**, 399, 1933.

where the first term gives the gravitational energy of the undisturbed polytrope and the second term the kinetic energy of the gas, while the third term indicates the energy due to rotation. It includes the additional energy resulting from small displacements of mass, as well as the kinetic energy of the rotation. The angular momentum of the star is denoted by J. The coefficients A, B, and C are positive functions of n. In addition, the value of C depends on the law of rotation. The equation may be written in this form only if $n < 5$.

In stable equilibrium, E should be a minimum. In particular, this should be true with respect to homologous contraction or expansion. Differentiating equation (31) with respect to R, we obtain

$$\frac{dE}{dR} = A\,\frac{M^2}{R^2} - \frac{3}{n}\,B\,\frac{M^{1+1/n}}{R^{1+3/n}} - 2C\,\frac{J^2}{MR^3} = 0 \tag{32}$$

and

$$\frac{d^2E}{dR^2} = -2A\,\frac{M^2}{R^3} + \frac{3}{n}\left(1+\frac{3}{n}\right)B\,\frac{M^{1+1/n}}{R^{2+3/n}} + 6C\,\frac{J^2}{MR^4} > 0\,, \tag{33}$$

as necessary conditions for stable equilibrium.

Equations (32) and (33) may be combined as follows:

$$\frac{3}{n}\left(\frac{3}{n}-1\right)B\,\frac{M^{1+1/n}}{R^{3/n}} + 2C\,\frac{J^2}{MR^2} > 0\,. \tag{34}$$

If the rotation has an appreciable effect on the central pressure, the three terms in equation (31) are comparable. In this case, n may become definitely larger than 3 before stability is endangered. In the limiting case, when the first and the second derivatives of E are equal to zero, we find that the third derivative is negative. In such a case we may expect explosion rather than collapse.

The foregoing representation, however, is a gross oversimplification. The equation of state in the outer layers will not be the same as in the center but will correspond to a lower value of the polytropic index. This circumstance gives an additional protection to the star, which may be quite considerable, as Ledoux[9] has shown.

Notwithstanding this protection, the formation of heavy elements in the core cannot surpass a certain limit. When the central region, where the heavy elements are formed, becomes too large, the star reaches instability. A slight increase in the external pressure will cause the nuclei to expel electrons, and, if the weight of the outer layers, where such phenomena do not occur, is not sufficient, the process will give rise to a violent explosion. In this way part of the heavy elements formed in the interior of the star will be distributed over space.

When the explosion occurs, the nuclei will expel electrons and thus regain their normal charges. In cases where a nucleus is left in an excited state, neutron decay may occur. Alpha decay or fission is much less probable as long as the charge is reduced. The energy liberated in this way, if any, would be exceedingly small, and the competing processes of beta or neutron decay are much more probable. Nuclei heavier than uranium will tend to undergo fission after they regain their normal charges. This process will be favored by the impact of neutrons, liberated by other nuclei.

V. FORMATION OF LIGHT ELEMENTS

The theory presented above gives a possible explanation for the formation of heavy elements. As is seen from Table 3, nuclei with masses smaller than 42 could hardly be expected to persist in degenerate cores of high density, since they would have a tendency to combine into nuclei with a double mass. Since the light elements have the higher abundance, there must exist some other mechanism, which produces them from hydrogen and helium in much greater quantities.

[9] *Ap. J.*, **104**, 333, 1946.

As Dr. Chandrasekhar has pointed out to me, the present theory about the formation of heavy elements does not preclude the current conception that the light elements have been formed under high-temperature conditions. Indeed, the phenomenon of fission, which makes the formation of heavy nuclei under nondegenerate conditions impossible, does not exist for lighter elements up to $A = 84$.

It is not possible to ascertain at present whether the light elements have been formed in a prestellar stage, when temperature and density might have been high throughout the universe, or that their origin is in stars. In this paper we shall discuss only the second possibility.

We observed in the preceding section that degeneracy in massive stars can be reached only under certain conditions. If these conditions are not fulfilled, the temperature in the interior of the star will remain too high for degeneracy. Nevertheless, the density will increase to very high values as long as the mass of the star is not reduced by instability, and in this case the lighter elements will be formed. Consequently, we should expect elements with mass below 84 to be formed in stars which do not develop degenerate cores. Elements with mass numbers 42 and higher should be formed in degenerate cores. Elements with mass numbers between 42 and 84 should be formed in both types of cores. It is possible that a nondegenerate core, where light elements are formed, becomes degenerate after the contraction develops further and rotation becomes important. In this case the light elements will constitute the basic material for the heavier elements, which are built in the later stage.

VI. POSSIBLE OBSERVATIONAL EVIDENCE

Many hypotheses have been made throughout this discussion which need careful checking by calculations as well as by observations. In particular, it will be of great interest to identify the different stages of evolution with the types of stars occurring in the universe. In order to do this, numerical integration of the corresponding stellar models must be made.

At this time we may give some broad aspects of what is to be expected. It is not difficult to identify the explosion of stars, when heavy elements have been formed with the supernova phenomenon and the remnants of the explosions with white dwarfs. For the evolution of this process itself there are two different possibilities. If the angular momentum of the core is not very small, rotational effects will become important before densities of the order of 10^{10} gm/cm^3 are reached. From Table 3 we see that the process of the formation of heavy elements will then go to about atomic weight 80 and no further. Likewise, the specific charge of the nuclei, which originally was one-half, will be reduced by only a small amount. If this causes instability, the resulting explosion cannot be very violent. The mass of the star will thus not be reduced to a very great extent, and the stellar remnant will have a mass almost equal to M_3.

If, on the other hand, the angular momentum of the core were very small, rotational effects would become important only at very high density. From Table 3 we see that the formation of very heavy elements and the reduction of nuclear charge sets in rather suddenly at densities in the neighborhood of 4×10^{10} gm/cm^3. Even if not all the material of the star is transformed into very heavy elements, the reduction of charge will occur for all nuclei, and all will contribute to the resulting instability. Probably an appreciable part of the stellar mass will be expelled.

The total amount of matter expelled by the white dwarfs should be equal to the total amount of heavy elements in interstellar space or in stars which have in their interiors heavy elements, as far as these have not been formed in the star itself. In order to make a quantitative comparison possible, it is necessary to know which part of their masses has been expelled by the white dwarfs and how much of the elements of the iron group is liberated along with heavier elements. This quantity might be considerable, since it is doubtful whether the star will have an opportunity to transform all the material in the

core into very heavy elements. In addition, elements of intermediate weight might occur as fission products of heavier nuclei.

From a numerical integration of a stellar model with a very dense and rapidly rotating degenerate core, consisting of heavy elements with reduced nuclear charge, it should be possible to find the appearance of a star in its pre-supernova stage.

An attempt might be made to identify stars with nondegenerate cores. Since elements like oxygen and heavier elements are built in the central regions of these stars, they should have a core of higher atomic weight and higher content of absorbing matter than the outer layers, where hydrogen is still predominant. If, then, the opacity follows the Kramers law, the star should appear as a red giant.[10]

If the chemical elements are really formed in stars, we may expect differences in chemical constitution between different parts of the galaxy or between different galactic systems. Perhaps we should find anomalies in stars where light or heavy elements are being built at present. Convection currents, caused by rotation or gravitational instability, might bring part of these elements toward the surface. In the case of red giants these elements would then be expelled into space, together with other material from the envelope. Before such an anomaly can be considered as evidence in favor of the theory, it is necessary for the theory to predict in which type of star the anomaly is to occur. Again this is possible only with the help of actual integration of stellar models.

VII. CONCLUSION

In the present paper an attempt has been made to explain the origin of the chemical elements from a building process in stellar interiors. Elements of moderate atomic weight are supposed to originate in stars with condensed but hot cores, which are tentatively identified as red giants. Heavy elements could be formed in degenerate cores of very high density, which might occur under special conditions. The building of heavy elements would render the star unstable after a while, giving rise to a supernova outburst, which leaves the stellar remnant as a white dwarf.

On account of the present theory the chemical composition of interstellar matter should go through an evolution. The more stars shed their material into space, the greater the heavy-element content of the interstellar matter becomes. Stars formed in later stages of the evolution of the galaxy would already contain a certain amount of heavy elements at their birth.

I wish to express my thanks to Dr. S. Chandrasekhar for his interest in the work and his valuable comments.

[10] *B.A.N.*, **10**, 63, 1945.

ATMOSPHERIC TEMPERATURES FROM INFRARED EMISSION SPECTRA OF THE MOON AND EARTH. I. THE OZONE LAYER

ARTHUR ADEL
McMath-Hulbert Observatory of the University of Michigan
Received March 21, 1947

ABSTRACT

A fundamental and independent method of determining the temperature of the ozone layer is applied to previously published infrared emission spectra of the moon, the earth, and the atmosphere. The method is a general one and is applicable as well to the atmospheric constituents H_2O, N_2O, and CO_2. The emissivity of atmospheric ozone in the band ν_2 at 9.6 μ is provided by the lunar spectrum. A gray-body comparison, in the spectral region occupied by the band, is then made between the radiation intensity of the earth's surface (thermocouple) to space and the return radiation intensity of the ozone layer. The method is a promising one, for, even preliminary, very low resolution spectra yield essentially correct temperatures. The temperature of the ozone layer is found to be $-44°$ and $-53°$ C for the evenings of September 5, 1941, and November 3, 1941, respectively.

In September and November, 1941, associated (in time) lunar and terrestrial infrared emission spectra were detected and recorded by the author at Flagstaff, Arizona. The *apparent* lunar spectrum was corrected by means of the terrestrial emission spectrum (radiation of the thermocouple to space) to obtain the true lunar emission spectrum, as modified only by atmospheric absorption.[1] It was pointed out that both the apparent lunar spectrum and the terrestrial spectrum were importantly affected by the characteristic radiations of the atmospheric constituents H_2O, O_3, and CO_2.[2] And it was emphasized in particular that the influence of a given characteristic emission of the atmosphere depends upon the temperature of the layer in question, as well as upon its emissivity.[1] Since the emissivity of an atmospheric layer, in a given band, can be supplied by the corresponding absorption band in the lunar spectrum[1] and since the terrestrial radiation intensity corresponds to a known temperature—room temperature of the thermocouple—the temperature of the gaseous layer in question can be obtained from the relative values of the terrestrial emission and the superimposed atmospheric emission.[1] The method will be detailed by application to the two sets of associated lunar-terrestrial spectra already published.[1]

A. SEPTEMBER 5, 1941

1. From Figure 5 in note 1, we find that between the edges of the ozone band, ν_2,[3] at 9.6 μ, approximately from 9 to 10 μ, the percentage absorption is 23.4.[4]

2. Hence, the emissivity of ozone, in ν_2, as impressed upon the curve of terrestrial emission (n. 1, Fig. 3), is also 23.4 per cent.

3. From Figure 3 in note 1, the ozone emission band, ν_2, between its edges, occupies an area which is 4.9 per cent that of the terrestrial emission in the same wave-length interval.

4. Therefore, 4.9 per cent of black-body radiation intensity at 300° K (the tempera-

[1] Arthur Adel, *Ap. J.*, **103**, 19, 1946.

[2] Resolution was insufficient to reveal the 7.78 μ band of N_2O.

[3] Arthur Adel and David M. Dennison, *Jour. Chem. Phys.*, **14**, 379, 1946.

[4] The disparity between this value and the much larger ones which have been determined from solar spectra (Arthur Adel and C. O. Lampland, *Ap. J.*, **91**, 481, 1940) is a consequence of reduced spectral purity in the lunar spectrum, a result of the comparatively low resolution.

ture of the thermocouple) is the equivalent of 23.4 per cent of black-body radiation intensity at T[ozone], the temperature of the ozone layer.

5. Now black-body radiation intensity in the interval 9–10 μ, at 300° K, is very nearly $10^4\ \pi$ erg/cm²/sec. Therefore, the radiation intensity of the ozone layer on the night of September 5, 1941, is given by 490 π erg/cm²/sec. And this is 23.4 per cent of the radiation intensity of a black body at the same temperature. That is, the black-body radiation intensity at T[ozone] $_{\text{September 5, 1941}}$ is 6600 erg/cm²/sec.

6. A black body at 220° K possesses a radiation intensity of 5010 erg/cm²/sec in the spectral interval 9–10 μ. At 230° K the intensity is increased to 6730 erg/cm²/sec.

7. Interpolation between the radiation intensities at 220° K and 230° K yields T[ozone] $_{\text{September 5, 1941}}$ = 229° K, or −44° C.[5]

The corresponding data and conclusion for November 3, 1941, taken from Figures 4 and 6 of note 1, are summarized briefly in section B, below.

B. November 3, 1941

1. 17.5 per cent.
2. 17.5 per cent.
3. 2.77 per cent.
4. 2.77 and 17.5 per cent.
5. 277 π erg/cm²/sec and 4970 erg/cm²/sec.
6. At 220° K, 5010 erg/cm²/sec; at 215° K, 4260 erg/cm²/sec.
7. T[ozone] $_{\text{November 3, 1941}}$ = 220° K, or −53° C.

It is clear that, despite the very low dispersion spectra of the moon and earth, surprisingly good values are found for the temperature of the ozone layer. With the increased resolution now possible, the method should be one of sensitivity and precision. The convenience of the method recommends it as an independent means of studying the ozone layer. It permits frequent observations with either sun or moon. The method is essentially one of measuring *relative* intensities at a *single* wave length with a *thermocouple*, and it possesses all the advantages inherent in such a technique. Furthermore, it is immaterial whether the thermocouple is black or gray, for the atmospheric radiation *to* the thermocouple is affected in the same degree as the terrestrial emission (radiation *from* the thermocouple). It is, of course, possible to apply the method to the H_2O, N_2O, and CO_2 layers of the atmosphere; and such studies are planned for the future.

[5] The absorptivity and emissivity of ozone on the night of September 5, 1941, appeared to be abnormally large. Whether a connection exists between this excessive activity of ozone and the comparatively high temperature T[ozone] = −44° C, is conjectural.

A SLOW CORPUSCULAR RADIATION FROM THE SUN

K. O. KIEPENHEUER
Fraunhofer Institute
Received March 8, 1947

ABSTRACT

It is shown that the solar filaments are sources of a slow corpuscular radiation; this radiation travels to the earth in 3–4 days after the filaments have passed the central meridian (Figs. 7 and 9). The mean velocity is therefore about 500 km/sec. Filaments in higher heliographic latitudes, up to 30°, contribute to this radiation, especially around the sunspot minimum.

Filaments near sunspots have no influence on the geomagnetic field. When the relative sunspot number, R, exceeds a critical value, the correlation between filaments and the intensity of the corpuscular radiation reaching the earth practically disappears (Figs. 3–6, 7, and 8). Coronal patches, bright in λ 5303, have an effect similar to that of sunspots but even more pronounced; this is shown by observations covering three years (Figs. 10 and 12).

Assuming that the filaments are supported by radiation pressure of $L\alpha$, we estimate the acceleration of an H-atom which has escaped by diffusion from the filament and is now exposed to the full $L\alpha$ flux. In calculating the acceleration, the $L\alpha$ profile and the gradually increasing Doppler shift are allowed for. The final velocity will depend on the lifetime of the atom, which is determined by the ionization probability and therefore by the intensity of the Lyman continuum. The latter may be estimated from the electron concentration in the terrestrial ionosphere. The resulting final velocity is about 500 km/sec, in agreement with observation.

The fact that sunspots destroy the correlation between the received corpuscular radiation and the filaments is explained by assuming that the magnetic field of the sunspots deflects the corpuscles. Simple calculations show that this assumption is justified. The behavior of bright coronal patches, being similar to that of the "magnetically effective areas" around sunspots, indicates that these two types of regions are probably identical; this conclusion is confirmed by Figure 13, which contains synoptic maps of the coronal intensities (λ 5303), the filaments, and the spots of different types.

1. *Introduction.*—In addition to "quiet days," which show the normal daily variation of the three components of the geomagnetic field, we may distinguish between "magnetic storms" with ΔH and $\Delta V \geq 150\gamma$ and the "moderate disturbances" with ΔH and $\Delta V \leq 150\gamma$ ($1\gamma = 10^{-5}$ Gauss). Magnetic storms and moderate disturbances differ not only in their amplitude but also in their general behavior, in their frequency, and especially in their relation to solar phenomena.

Some of the magnetic storms are produced by the radiation of particles which are ejected by very intense chromospheric eruptions and which reach the earth in about 26 hours, i.e., with a mean speed of ~1600 km/sec. In the case of very intense storms this interval seems to be a few hours shorter.[1]

In the case of the moderate disturbances, up to now no relation between individual disturbances of the earth's field and individual solar phenomena has been found. The so-called "M-regions," though, which cannot be traced in either chromospheric or photospheric features but which sometimes last longer than eight solar rotations, are persistent sources of corpuscular radiation.[2] It is this corpuscular radiation in particular with which this paper is concerned.

2. *Statistical relations between the corpuscular radiation and (1) the relative sunspot numbers, (2) the areas of the prominences, and (3) the projected areas of the filaments.*—As a measure of the intensity of the corpuscular radiation reaching the earth, we use the δP-values deduced by Bartels[3] from the daily variations of the earth's field. These values

[1] H. W. Newton, *M.N.*, **103**, 244, 1943.

[2] J. Bartels, *Terr. Magnet. Atm. El.*, **37**, 1, 1932.

[3] J. Bartels, *Abh. d. Preuss. Akad. d. Wissensch.*, 1941, *Mat. Naturw. Kl.*, No. 12, 1., 2. Mitt.

are now available in both monthly means and means taken over an eighth of a solar rotation for a long period of time. As is well known, the correlation between δP and the sunspot numbers, δR, is very small even in monthly and annual means; and between their daily values there is no correlation at all. In Figures 1 and 2, monthly means of δP and δR are plotted against each other for years of low and high sunspot activity, respectively. They demonstrate that there is no correlation between δP and δR in the second case.[4]

The correlation between the prominence areas[5] δF and the corresponding values of δP (Figs. 3 and 4), again separated into years of low and high solar activity, is found to be much closer, even for the smallest values of δP. It follows, further, that the observed correlation between prominences and corpuscular radiation disappears completely in months when many sunspots occur. This is shown by Figures 5 and 6 in which only values of δP and δF for $\delta R < -25$ and $\delta R > 40$, respectively, are plotted. Months having few spots give a relatively good correlation; those with many spots do not show any correlation. The circled dots in Figure 5, which fit poorly, having too low intensities, can be identified as those months which have small mean spot numbers but which fall between months having many spots. Thus sunspots seem to affect the correlation between prominences and corpuscular radiation not only during the time they are seen but also before their appearance and after their disappearance. Specifically, the spots appear to cause a decrease in the intensity of the corpuscular radiation. It should be noted that the correlation coefficient between the monthly means of the sunspot numbers and the prominence areas, that is, the relation between the two solar phenomena, is smaller than that between the prominence areas and the corpuscular radiation as measured by the variation of the geomagnetic field.

An attempt to discover a similar correlation between the daily values was unsuccessful because too much uncertainty is involved in estimating the values for the center of the disk from the prominence areas measured at the limb. Therefore, instead of prominence areas, I used the projected areas of the filaments observed near the central meridian; they were taken, for the years 1919–1937, from the "Cartes synoptiques de la chromosphère solaire" of the Paris-Meudon Observatory.[6]

For each day during this period I measured the projected areas of the filaments in a band one twenty-seventh of the solar circumference (about 14° in heliographic longitude) in width, extending symmetrically about the central meridian from pole to pole, using an arbitrary scale. Within this band the filaments in the equatorial and polar areas, separated by $\pm 30°$, were measured separately; those in the polar areas were roughly reduced to the apparent area shown to the terrestrial observer.

In studying the daily variation of these filamentary areas in the neighborhood of disturbed and quiet days, respectively, by the well-known superposition method, we find for years of low solar activity (1922–1924) the curves represented in Figure 7. The total of the filamentary areas in the entire band described above, and especially the total in the polar regions of the band, reach a pronounced maximum 4 days before a disturbed day. However, for magnetically quiet days, there is no particular variation of these areas. During a period of high solar activity (1926–1928) the correlation between filamentary area and corpuscular radiation again disappears (Fig. 8), just as it did in the case of the areas of the limb prominences. A smaller maximum is indicated, though, for the polar filaments 2 days before a disturbed day.

Here again the presence of spots appears to hinder the emission, or motion, of the corpuscular radiation from the sun to the earth. As a check I selected a number of days having large filamentary areas during the years of low activity (1922–1924). As expected,

[4] Bartels's publication is not available here, but it is assumed that the δ's refer to differences with respect to the mean for all years covered; e.g., $\bar{R} = R - \delta R$, with $\bar{R} = 31$ [EDITOR].

[5] W. Brunner, *Character Figures of Solar Phenomena*, 1 (Zürich, 1932), vii, Preface.

[6] L. d'Azambuja, "Cartes Synoptiques de la Chromosphère Solaire," *Ann. obs. Paris-Meudon.*

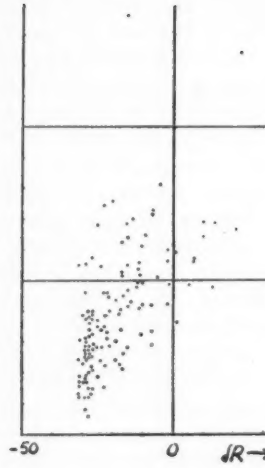

FIG. 1

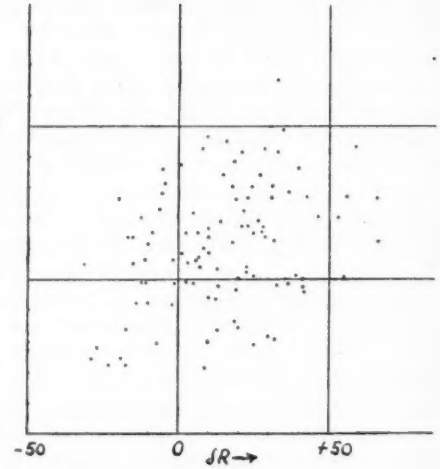

FIG. 2

FIG. 1.—Intensity of corpuscular radiation, δP, and relative sunspot numbers, δR, in monthly means for years of low solar activity, 1910–1914 and 1920–1925.

FIG. 2.—Intensity of corpuscular radiation, δP, and relative sunspot numbers, δR, in monthly means for years of high solar activity, 1916–1920 and 1924–1928.

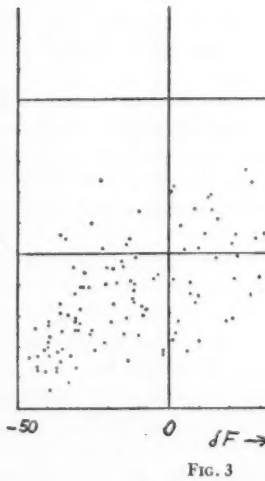

FIG. 3

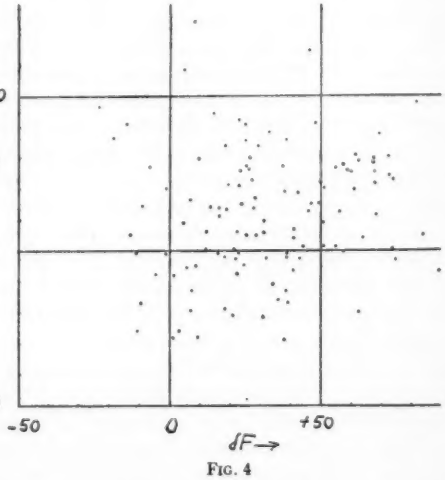

FIG. 4

FIG. 3.—Intensity of corpuscular radiation, δP, and prominence areas, δF, in monthly means for years of low solar activity, 1910–1914 and 1920–1925.

FIG. 4.—Intensity of corpuscular radiation, δP, and prominence areas, δF, in monthly means for years of high solar activity, 1916–1920 and 1924–1928.

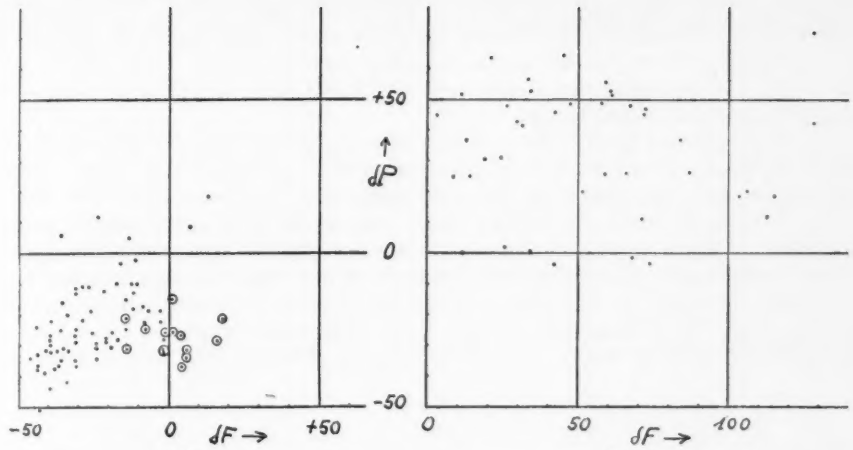

FIG. 5

FIG. 6

FIG. 5.—Intensity of corpuscular radiation, δP, and prominence areas, δF, for months with $\delta R < -25$. The encircled points refer to months whose neighbors have many spots.

FIG. 6.—Intensity of corpuscular radiation, δP, and prominence areas, δF, for months with $\delta R > 40$

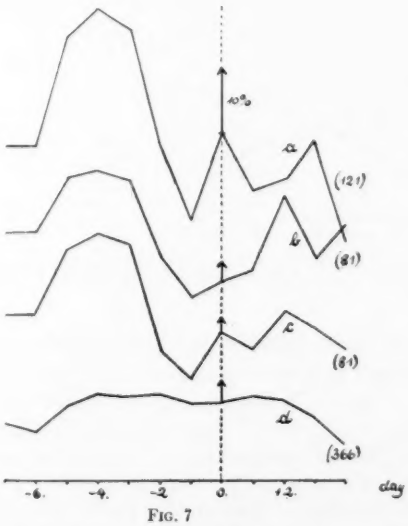

FIG. 7

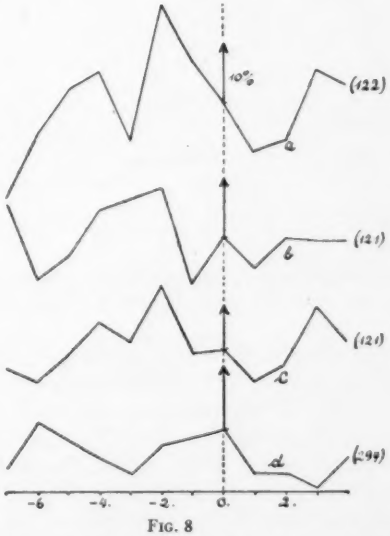

FIG. 8

FIG. 7—Variations of the daily filament areas in the neighborhood of both disturbed and quiet days in years of low solar activity (1922–1924). (*a*) Filaments in high latitudes for disturbed days; (*b*) filaments in low latitudes (up to $\pm 30°$) for disturbed days; (*c*) total filaments for disturbed days; (*d*) total filaments for quiet days.

FIG. 8.—Variation of the daily filament areas in the neighborhood of both disturbed and quiet days in years of high solar activity (1926–1928). (*a*) Filaments in high latitudes for disturbed days; (*b*) filaments in low latitudes for disturbed days; (*c*) total filaments for disturbed days; (*d*) total filaments for quiet days.

the magnetic-character figure, C, reaches a maximum about 4 days after the selected day, during all 3 years. It is not surprising that this maximum is highest in the year of lowest solar activity. The annual means of the spot numbers of the years 1922, 1923, and 1924 are 14.2, 5.8, and 16.7, respectively.

3. *Statistical relations between the corpuscular radiation and the intensity of the solar corona in λ 5303 A.*—Since the corona can be observed only at the sun's limb and since the corpuscular radiation reaching the earth originates in regions which are near the central meridian at the time of emission, the two cannot be directly correlated. Since the distribution of coronal intensities is rather stable for several days, sometimes even for weeks and months, an extrapolation can be made, which does not seem to affect the results seriously. We have at our disposal visual estimates of coronal intensities for the years 1943–1945. These observations were made with coronographs of the Lyot type[7] at the Wendelstein Observatory (Upper Bavaria) at 1840 meters, and in part at the

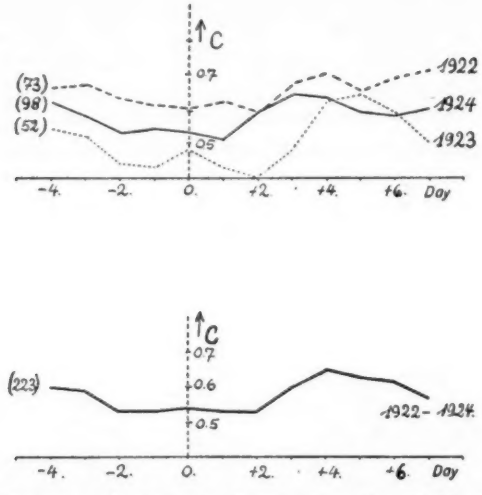

FIG. 9.—Variation of the magnetic-character figures, C, in the neighborhood of days with many filaments for years of low solar activity (1922–1924).

Zugspitze Observatory (Upper Bavaria) at 3000 meters.[8] Both coronographs had an aperture of 110 mm and a focal length of 1650 mm and were equipped with a prominence spectroscope. We use here only the results for the green line, λ 5303 A, whose intensity was measured at the eyepiece of the spectroscope at points 5° apart along the solar limb in an arbitrary scale of fifty steps. The intensities were estimated at points at a distance of about 40″ from the sun's limb. In addition, the intensity of the scattered light was measured in units of the intensity of the photospheric light at the limb. The coronal intensities were not reduced to constant intensities of scattered light, but those intensity estimates in which the uncertainty due to scattered light exceeded 30 per cent were rejected.

By adding all the measured intensities we obtained total intensities for the east and west limbs, respectively. These intensities were classified as "weak" (sum ≤ 30), "strong" (151–300), and "very strong" (301–600) cases. Since the weak cases were

[7] B. Lyot, *Zs. f. Ap.*, **5**, 73, 1932.

[8] Unpublished results of the Fraunhofer Institut. Most of the photometric results used here were obtained by Dr. Hans Haffner, the rest by Dr. Anton Brusek. A detailed publication of this material will follow elsewhere.

strongly affected by scattered light, they were rejected, and only the strong and very strong cases were considered. The years 1943–1945 yield the following good cases: 116 "strong" intensities, east limb; 113 "strong" intensities, west limb; 28 "very strong" intensities, east limb; and 19 "very strong" intensities, west limb. The superposition method was then applied to the days selected for their strong and very strong coronal intensities, and the relation between these intensities and the variation of the terrestrial magnetic field was sought. This method is suitable because it does not require a daily record of coronal intensities.

Considering, first, the "strong" cases, we see in Figure 10 the variation of the daily sum of the Potsdam *Kenziffern* for the fourth to the fifteenth day after the appearance of a strong corona at the east limb, and for the minus sixth to the plus fifth day from the appearance of a strong corona at the west limb. The number of cases used is noted in parentheses to the right of each curve. In 1943 we note a peculiar variation in the

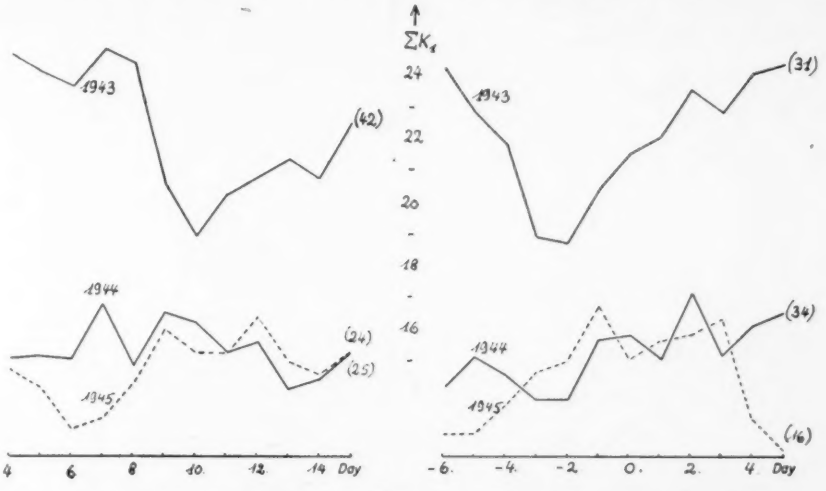

FIG. 10.—Variation of the daily sum of the 3-hour magnetic indices in the neighborhood of days with a "strong corona" at the east and west limbs, respectively, for the years 1943–1945.

intensities: there is a pronounced minimum in ΣK_1 about 10 days *after* the appearance of the corona in the east, and the same thing appears 2–3 days *before* the appearance of the corona in the west. This feature persists even when only a very few cases are superposed. Since the corona of the east limb reaches the central meridian in about 7 days, it may be inferred that the corpuscular radiation takes 3–4 days to reach the earth, just as in the case of the radiation from the filaments. However, in the present case, strong coronal intensities correspond to *weak* disturbances of the geomagnetic field. The same time interval is found for the coronal patches on the west limb: the reduced corpuscular radiation, leaving the sun when the coronal patches are near the central meridian, reaches the earth in 3–4 days, thus causing a minimum of terrestrial disturbance about 3 days before the appearance of the corona at the west limb.

This relationship disappears completely with the beginning of the new cycle at the end of 1943, as can be seen in Figure 10. There is no doubt that this sudden disappearance of the correlation is connected with the rather sudden variation of the distribution of coronal intensities over the heliographic latitudes. These distributions are represented in Figure 11 by the annual means for the years 1943–1945. It may be seen clearly that the equatorial maximum disappears and that, when the new cycle begins, new maxima appear at $\pm 30^\circ$ heliographic latitude.

Finally, selecting only the days with "very strong" coronas, we get quite a different picture (Fig. 12). The intensity is still at a minimum near the fourth day after the coronal patches cross the central meridian. However, during the transit of the corona through the central meridian, or shortly afterward, a new and fairly steep maximum occurs. The very strong patches of λ 5303 are therefore sources of a corpuscular radiation which, according to the above data, reaches the earth in 1 day or less. This speed is much faster than that of the slow corpuscular radiations emitted from the filaments. Evidently, the sources of this radiation are, in part, identical with the C-regions postulated by Waldmeier,[9] but they are certainly different from the M-regions. The fact that there are relatively frequent spots in the vicinity of these coronal patches indicates that the mechanism

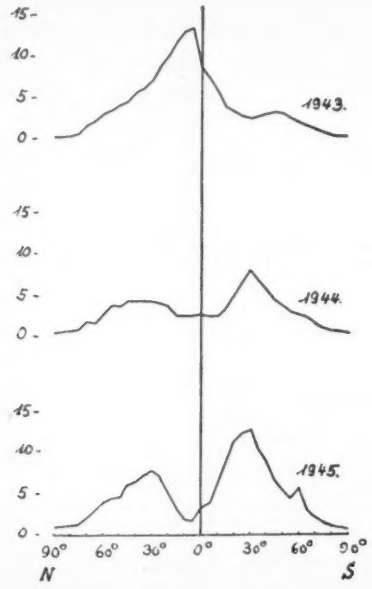

FIG. 11.—Annual means of the distribution of coronal intensities in λ 5303 A in heliographic latitude for the years 1943–1945, from observations of the Fraunhofer Institute.

of emission or propagation of this radiation must be different from that produced by the filaments. It may be assumed that intense chromospheric eruptions play an important part in the production of this fast corpuscular radiation.

It cannot be decided whether the minima of ΣK_1 on the eleventh to twelfth days (east limb) and on the minus sixth to minus second days (west limb) are identical with those produced by the "strong corona" or whether these minima are simply consequences of the preceding maxima. The latter explanation is supported by the fact that Bartels[10] was able to prove statistically that such a "gathering" effect in the terrestrial disturbances, i.e., in the corpuscular radiation, exists: after a strong magnetic disturbance the number of disturbed days is smaller, on the average, than could be expected statistically.

4. *Theory of the emission of slow corpuscular radiation.*—First, let us estimate the density of the corpuscular radiation. Let δH be the change in the magnetic field at the

[9] M. Waldmeier, *Zs. f. Ap.*, **21**, 275, 1942.

[10] Thanks to a communication from Dr. J. Bartels of Göttingen.

surface of the earth. Then the field energy, $E \approx H_0 \delta H a^3$ (where a is the earth's radius), must be supplied by the kinetic energy of the stream of particles in a period of time Δt (several hours). If n is the density, v the velocity, and m the mass of the heavy particles (the contribution of the electrons being negligible), we obtain

$$E \approx \tfrac{1}{2} F v n m v^2 \Delta t ,$$

where F is of the order of magnitude of the magnetic cross-section of the earth, $10^{18} \leq F \leq 10^{20}$ cm^2. Assuming $\delta H = 100\gamma$ and $v = 4 \times 10^7$ cm/sec, we find that n, the number of ions and electrons, must lie between 0.8 and 80 cm^{-3}. Further, one may conclude from the mean duration and behavior of the geomagnetic disturbances that the vertex angle of the cone of corpuscular radiation coming from the sun is very small and that the dilution of the corpuscular radiation on its way to the earth is due to thermal expansion entirely and not to the inverse-square law. The dilution factor is

$$\frac{n}{n_\odot} \approx \frac{d_\odot^2}{(2 v_t t)^2}$$

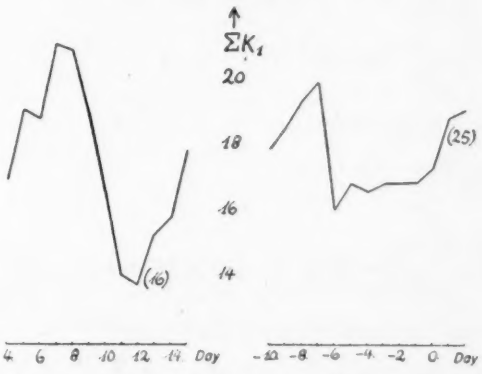

FIG. 12.—Variation of the daily sum of 3-hour magnetic indices in the neighborhood of days with a "very strong corona" on the east and west limbs, respectively, for the years 1943–1945.

in the case of a stream with a circular cross-section, and

$$\frac{n}{n_\odot} \approx \frac{d_\odot}{2 v_t t}$$

for a stream having a bandlike cross-section whose thickness, d, is much smaller than its width. In both formulae v_t is the thermal velocity of the heavy particles, and t is the time they need to reach the earth. Assuming $d = 10^9$–10^{10} cm, $v_t = 2 \times 10^6$ cm/sec (corresponding to a proton temperature of 10,000°), and $t = 3 \times 10^5$ sec (≈ 4 days), one obtains $7 \times 10^{-7} < n/n_\odot < 7 \times 10^{-5}$ for circular-shaped streams and $8 \times 10^{-4} < n/n_\odot < 8 \times 10^{-3}$ for band-shaped streams. Close to the sun we find, therefore, densities in the range $10^2 < n_\odot < 10^8$ cm^{-3}; if only band-shaped streams are considered, the density would be $> 10^5$ cm^{-3}. It might be possible, therefore, that the jets of corpuscular radiation are visible in the outer corona on account of the accompanying electrons.

The emission of slow corpuscular radiation takes place in the vicinity of the filaments. We may assume that these filaments are supported by the selective radiation pressure of the *La* emission of the subphotosphere and by the resonance line of helium (the contribution of the continuous radiation is negligible, as shown by Ten Bruggencate[11]).

[11] P. ten Bruggencate, *Veröff. d. Univ.-Sternw. Göttingen*, 1946.

Then the intensity of this line radiation is determined by the dimensions and density of the filaments supported by it. If *La* has a combined damping-Doppler contour, then, according to Unsöld,[12]

$$I_v = I_0 \left\{ e^{-v^2} - \frac{a}{\sqrt{\pi}} [1 - 2vF(v)] \right\},$$

where

$$F(v) = e^{-v^2} \int_0^v e^{z^2} dz; \qquad v = \frac{\Delta\lambda}{\Delta\lambda_D}; \qquad a = \frac{\Delta\lambda_N}{\Delta\lambda_D}.$$

Generally, a filament has a very great optical depth for *La*, so that only the very deepest parts of it can come in contact with radiation. Therefore, the upper layers must be supported by the lower layers. It may then happen that an atom leaves the body of the filaments and diffuses into the neighboring corona, where the density is much lower. Such an atom will be exposed to the intense *La* radiation and, consequently, will be accelerated. Let x be its velocity relative to the light-source, then $\Delta\lambda/\lambda = \dot{x}/c$, and $v = \lambda\dot{x}/(c\Delta\lambda_D) = a\dot{x}$. The line contour of the single atom is determined by radiation damping only: $\Delta\lambda_N \ll \Delta\lambda_D$. The atom absorbs, therefore,

$$E_\lambda = \int_0^\infty I_\lambda k_\lambda d\lambda = I_\lambda \int_0^\infty k_\lambda d\lambda = I_\lambda \frac{\pi e^2 \lambda^2}{m c^2} f.$$

Then the radiation pressure becomes

$$P = \frac{E_\lambda h\nu}{c} = \frac{I_\lambda \pi e^2 \lambda h f}{m c^2},$$

or

$$P = \frac{\pi e^2 h \lambda f}{m c^2} I_\lambda \left\{ e^{-v^2} - \frac{a}{\sqrt{\pi}} [1 - 2vF(v)] \right\}.$$

For large values of v this expression is transformed into[13]

$$P = \frac{\pi e^2 h \lambda f}{m c^2} I_\lambda \frac{a}{2\sqrt{\pi} v^2} \left(1 + \frac{3}{2}\frac{1}{v^2} + \dots\right).$$

The equation of motion of the H-atom then becomes

$$\ddot{x} = \frac{P}{m_H} - g_\odot = \frac{A}{\dot{x}^2} - g_\odot,$$

where

$$A = \frac{\sqrt{\pi} e^2 h \lambda f a I_\lambda}{m_H m c^2 2 a^2}$$

and $g_\odot$ is the acceleration of gravity on the sun's surface.

The acceleration goes on as long as the H-atom can absorb radiation, that is, until it loses its electron by photoelectric ionization. The mean life $\tau_{1\infty}$ of the H-atom, that is, the duration of the acceleration, depends essentially on the intensity of the Lyman continuum, which is radiated by the enveloping corona. If its intensity is I_c, then

$$\tau_{1\infty} = \frac{1}{I_c a_\nu}.$$

[12] A. Unsöld, *Physik der Sternatmosphären*, p. 161.

[13] A. Unsöld, *op. cit.*, p. 163.

By integrating the equation of motion, we obtain (neglecting gravitation) the final mean velocity of the H-atom at the moment of its ionization:

$$\dot{x}_\infty^3 = 3A\tau_{1\infty} = \frac{3\sqrt{\pi}e^2 h a \lambda f}{2a_\nu m m_H c^2 a^2}\frac{I_\lambda}{I_c}.$$

Considering that, by definition, the total emission of La is

$$I_{La} \approx 2I_0 \int_0^\infty e^{-v^2} d\lambda \approx I_0 \sqrt{\pi}\Delta\lambda_D ,$$

we obtain

$$\dot{x}_\infty^3 = \frac{3e^2 h \Delta\lambda_N f}{2mm_H a_\nu \lambda}\frac{I_{La}}{I_c} = 1.23\times 10^{16}\frac{T_{La}}{I_c}.$$

The intensity of the continuous ionizing radiation, which unquestionably differs greatly from the black-body radiation of the photosphere, can be estimated with some confidence from the electron density of the ionospheric layers[14] and is found to be

$$J_C \approx 10^{15}\frac{L_c \text{ quanta}}{\text{cm}^2 \text{ sec}}$$

on the sun's surface for a mean relative spot number of $R = 50$. This intensity changes a good deal during a cycle. The intensity of the La radiation follows from the equation of the mechanical balance of a normal filament,

$$Mg_\odot = I_{La}\frac{h\nu}{c},$$

where $M = 10^{-5}$ gm/cm^2, the mass of a filament in a column having a cross-section of 1 cm^2. This corresponds to a prominence density of 10^{10} H-atoms cm^{-3} and a prominence thickness of about 10^9 cm. We get $I_{La} \approx 10^{21}$ La Quanta/(cm^{2}sec) and a final velocity of

$$\dot{x} \approx 5\times 10^7 \frac{\text{cm}}{\text{sec}}.$$

The H-atoms will attain this velocity during a time equal to their mean life,

$$\tau_{1\infty} \approx 200 \text{ sec}$$

with $a_\nu \approx 5\times 10^{18}$ cm^2; and during this time they will have traveled a distance of

$$\Delta x \approx 2\left(\frac{3he^2\Delta\lambda_N f I_{La}}{2mm_H\lambda}\right)^{1/3}(\tau_{1\infty})^{3/2} \approx 5\times 10^9 \text{ cm}.$$

The final velocity is reached in the immediate vicinity of the filaments and compares very well with the value found from the correlation between filaments and geomagnetic disturbances. It should be noted, however, that the values found for $\dot{x}_\infty$, Δx, and $\tau_{1\infty}$ are only estimates of the order of magnitude. Moreover, these values show a variation during the sunspot cycle. The emission of the corpuscular radiation takes place along the entire border of the filament and takes the form of a band projecting the outline of the filament in radial direction. An upper limit of the density of the accelerated H-atoms[15]

[14] K. O. Kiepenheuer, *Ann. d'Ap.*, **8**, 210, 1945.

[15] The presence of small amounts of metals in the prominence matter has a negligible effect. The weak absorption in H and K (Ca^+) on magnetically disturbed days, observed at Mt. Wilson Observatory (see "Survey of the Year's Work at Mt. Wilson," *Pub. Astr. Soc. Pacific*, **56**, 213, 1944) probably concerns only the quick corpuscular radiation coming from the eruptions.

can be found by assuming that diffusion will cause the density distribution around the quiescent filament to merge exponentially into the density of the neighboring corona. The emission of the H-atoms begins at that distance where the free path of the atoms, as well as that of the $L\alpha$ quanta, is comparable to, or greater than, the acceleration path, Δx, i.e., where $n a_r \Delta x$ approaches 1, or the free path approaches Δx. In this way we find densities $10^4 < n_\odot < 10^6$ cm^{-3}, in accordance with the value estimated from the energy balance of a geomagnetic disturbance. Densities of this order should be visible in the outer parts of the corona in total light, and we have good reason to identify these corpuscular streamers coming from the filaments with the coronal streamers, most of which also come from the filaments, but which are very difficult to detect in the inner corona.

The bandlike shape of the jets of corpuscular radiation has one obvious consequence. If we were to try to explain the observed frequency of disturbances of short mean duration by corpuscular streamers with round cross-sections and vertex angles of a few degrees, there would have to be an enormous number of these streamers. This and other difficulties can be explained easily by band-shaped streamers. The probability that such a band will hit the earth is much greater than for round streamers, especially if the filament does not deviate too much from a north-south direction on the sun. A simple estimate shows that the mean number of magnetic disturbances in a year of minimum solar activity is much smaller than the number of large filaments which have passed the central meridian in the same interval.

Also the majority of the geomagnetically disturbed days are part of 27-day sequences, which often persist for more than ten rotations. According to our present knowledge of solar phenomena, this persistence is only matched by the filaments.

5. *Magnetic deviation of the slow corpuscular radiation.*—As is shown elsewhere,[16] the general magnetic field of the sun, which is measured at the base of the chromosphere, must be shielded almost entirely from the corona. The observed trajectories of prominences far from spots and the form of the coronal streamers show that the field strength is much less than 1 Gauss. Only the field of the spots can penetrate into the corona. The question is whether this field is capable of diverting the corpuscular streamers, which, though consisting of positive and negative charges, are macroscopically neutral. Since the density is extremely small and the free paths large in proportion to the dimensions of the stream, one would expect the forces acting upon an individual particle to be typical of the entire swarm of particles. But that is not true. Even if the density is extremely small (e.g., 0.1 proton and electron/cm^3), an electrical field $\boldsymbol{v} \times \boldsymbol{H}/c$ is set up, which eliminates every deviation inside the swarm (which may have a diameter of $\sim 10^9$ cm) even in a homogeneous magnetic field outside. Therefore, even for the smallest densities, it is necessary to calculate the force acting upon the induced current system as a whole and to consider the charged particles as members of a coherent mechanical system.

For the sake of simplicity, let us study the force acting upon a freely flying gas ball, having the estimated density of the corpuscular radiation, $n = 10^4$ protons and electrons/cm^3. If such a body, which represents a rather good electrical conductor, is moved in a nonhomogeneous magnetic field, currents will be induced. The force exerted by the outer magnetic field on a unit volume will be

$$K = \frac{1}{c} [i \times H] .$$

This force will be greater, the stronger the magnetic-field changes near the point where the gas ball is. It will be greatest when the motion of the conductor is in the direction of the field gradient, that is, perpendicular to the surfaces on which the absolute value of the magnetic-field strength is constant. Such a gas ball will therefore have a tendency to

[16] K. O. Kiepenheuer, *ibid.*, **9**, 57, 1946.

move along the surfaces where H^2 is constant, particularly if the gradient of H is sufficiently large.

The value of the guiding force, keeping the balls on the H^2 surfaces, can be estimated easily. A ball with radius R may be replaced by a ring with cross-section $\pi R^2/2$ and mean circumference $2\pi R$, so that we have by the induction law

$$\text{rot } E = -\frac{1}{c}\dot{H},$$

$$|E| = \frac{R\dot{H}}{4c},$$

$$i = K_\perp |E| = \frac{K_\perp R}{4c}\dot{H},$$

where $K_\perp$ is the electric conductivity perpendicular to the magnetic field. We substitute for the conductivity[17]

$$K_\perp \approx \frac{n^2 e^2 c^2}{K_i^0 H^2},$$

where

$$K_i^0 \approx \frac{(3kT)^{3/2}}{\pi e^2 \sqrt{m_H}} \approx 7.05 \times 10^6 T^{3/2}$$

is the ionic conductivity (protons) in the case of the absence of a magnetic field, and T is the temperature of the gas. The force on one unit of volume then is

$$|K| = \frac{iH}{c} = \frac{K_\perp R}{4c^2} H\dot{H} = \frac{n^2 e^2 R\dot{H}}{4K_i^0 H}.$$

Finally, we replace $\dot{H}$ by $(\dot{r}\cdot\text{grad } H)$ and express the magnetic force in units of the force of gravity, thus:

$$\mu = \frac{\text{Magnetic force}}{\text{Force of gravity}} = \frac{n e^2 \dot{r} |\text{grad } H| R}{4K_i^0 g_\odot m_H H}.$$

In case the field of a spot extends freely into the corona, at sufficiently large distances we may replace it by that of a magnetic dipole. Then we have grad $H/H \approx 3/r$, where r is the distance from the spot center. Since, in general, the field extends far beyond the diameter of the spot groups, this expression may be correct for distances $r > 10^{11}$ cm only.

For smaller distances, in particular during the development of the spots, a serious deformation of the field comes about as a result of the action of the current system induced in the inner corona. As shown elsewhere,[17] these currents produce a field gradient of the order of H/Z_0, where Z_0 has the significance of a penetration depth of a magnetic field. If the spot field is assumed to be a periodic function of time, having an oscillation period t_0, the value of Z_0 is

$$Z_0 = \sqrt{\frac{c^2}{4\pi K_\perp t_0}},$$

where $K_\perp$ is the electric conductivity of the coronal matter perpendicular to the magnetic field. It can be shown now that, for distances $r < 10^{11}$ cm, this critical length, Z_0,

[17] K. O. Kiepenheuer, *ibid.*, p. 42.

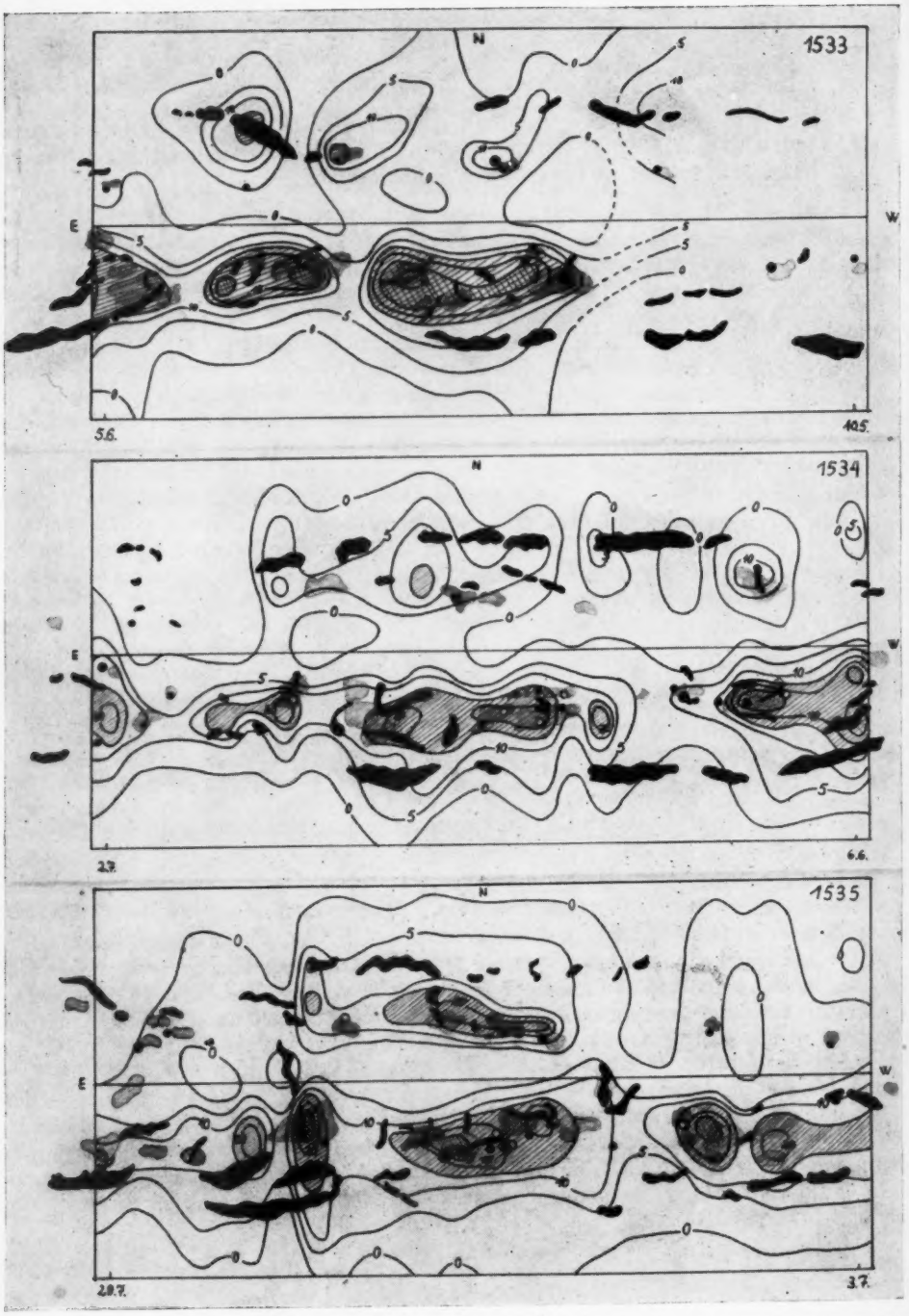

FIG. 13.—Isophotic maps of the solar corona in λ 5303 A for the rotations 1533–1537 (May 10–October 21, 1945). ▨ = regions with intensity >15; ▩ = regions with intensity >25. Days without observations are represented by dotted lines. The chromospheric faculae are gray, the filaments dark. The spot types are (Zürich classification): *A* and *B* = •; *C* and *D* = •; *E* and *F* = ●; *G* and *H* = ○; *J* = ○.

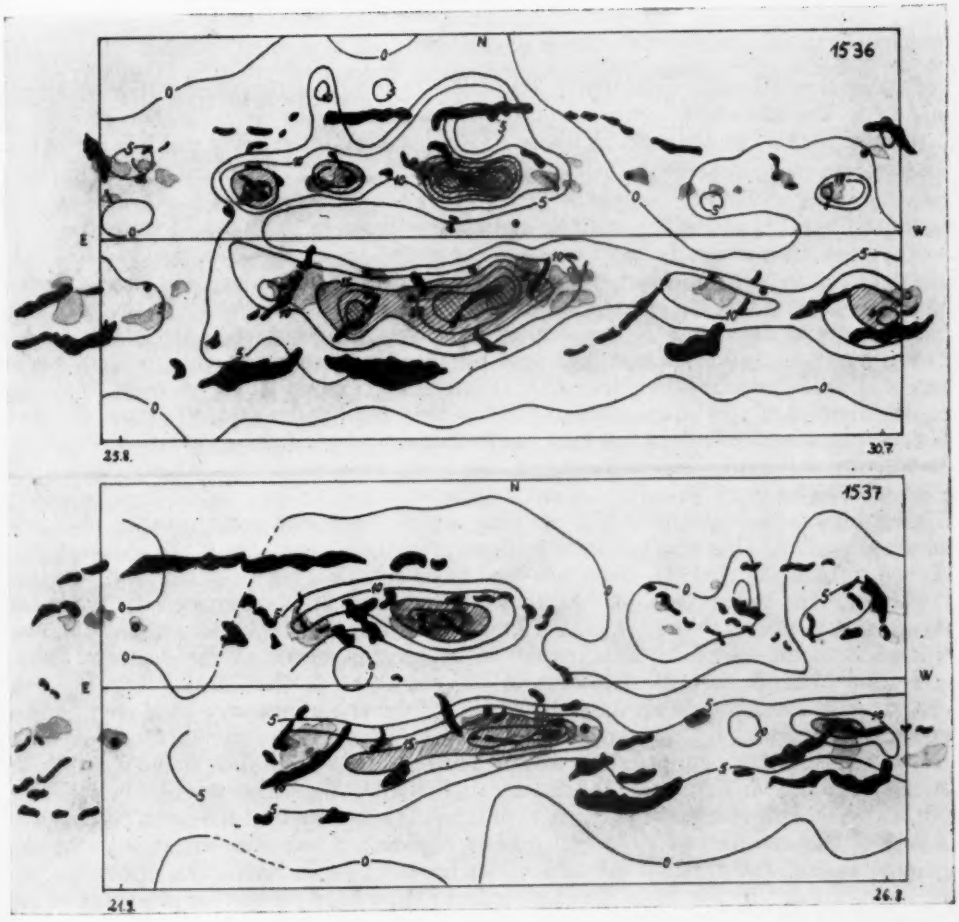

FIG. 13–*Continued*

will remain $<10^9$ cm in the case of field strengths smaller than a few hundred Gauss. Consequently, in a region around young sunspots extending far beyond the visible spot group, the effective field gradients are of the order of H/Z_0. For the relation between the magnetic and the gravitational forces on an element of the corpuscular radiation in this region we obtain, then,

$$\mu = \frac{3n\,e^2 R\,\dot{r}}{4K_i^0 g_\odot m_H Z_0}.$$

Setting $R = 10^9$ cm, $n = 10^5\,\mathrm{cm}^{-3}$, $T = 10{,}000°$, and $Z_0 < 10^9$ cm, we arrive at values of $\mu > 1$. The motion of a slow corpuscular streamer in the neighborhood of a spot is therefore guided by the surfaces where H^2 is a constant, if the initial distance is smaller than a few group diameters (heliographic latitude $\lesssim 30°$). In a first approximation these surfaces represent[16] concentric hemispheres over the spot group. All corpuscular streamers emitted inside the critical volume are therefore deflected back to the sun; in any case, they suffer a deviation from the radial trajectory. Practically all eclipse plates of the middle and outer parts of the corona show such concentric surfaces over sunspots; the coronal streamers appear to inclose these surfaces asymptotically. Here again we see an argument for the identity of coronal and corpuscular streamers.

We understand, now, why a high spot number has such a disturbing effect on the corpuscular radiation reaching the earth. It can be seen easily that the slightest deviation or deformation of the initial form of the invisible corpuscular streamer gives the terrestrial observer the impression that the radiation comes from an entirely different position on the sun's surface. Therefore, the association of single solar and terrestrial phenomena is no longer possible. Except for magnetic storms, the spots have a weakening effect on the corpuscular radiation reaching the earth, general opinion to the contrary notwithstanding. This result is in accordance with the findings of C. W. Allen,[18] who proved statistically that the M-regions tend to lie outside a region of radius 40° around the spot groups. Allen finds, further, that the frequency of M-regions on the border of these zones is greater than normal. We assume that this is a magnetic coupling effect or lens effect of the spot field, which seems to be very important in the electromagnetic formation of large coronal streamers. Allen's observation that 27-day sequences of geomagnetic disturbances are brought to an end by the appearance of a spot can be explained very well by the deviation of the corpuscular streamer in the spot field. Nevertheless, the sequence can be continued after the disappearance of the spot, which exists for a shorter time than the filament. This effect was also traced by Bartels.[19]

Finally, we consider the green coronal patches. It is known that the green coronal line is very often intensified over the spot regions, especially when there are strong chromospheric faculae. The nuclei of the coronal patches often lie on the outline of the faculae. This is illustrated by the maps of the corona in Figure 13, representing isophotes of the corona in λ 5303 A for five consecutive solar rotations. They have been constructed by extrapolating from the intensities measured on the east and west limbs. The photometric material again comes from the Wendelstein and Zugspitze observatories of the Fraunhofer Institut. The maps also show the faculae (gray patches) and the filaments (dark patches), taken from the "Cartes planisphère des tâches, des plages faculaire et des filaments principaux."[20] The different spot types are taken from observations at the observing stations Wendelstein, Zugspitze, Schauinsland, and Kanzelhöhe.

The regions in which λ 5303 is bright appear to coincide with the magnetically effective regions of spot groups for two reasons: first, they have the same intensity-weakening effect on the emission of corpuscular radiation, and, second, their geometric arrangement

[18] *M.N.*, **104**, 13, 1944.

[19] Private communication from Dr. Bartels.

[20] M. d'Azambuja, *L'Astronomie*, 1943–1945.

and extent is similar. It may be inferred that the green coronal regions are intimately related to the distribution of magnetic fields. In this connection we refer to a theory[17] which explains the excitation of certain coronal lines and the heating of chromospheric faculae by the impact of charged particles which have been accelerated in the variable magnetic field of the spot groups as a member of the current system induced in the chromosphere and corona. As a further consequence we may expect that the green coronal patches are indicators of magnetic anomalies outside the visible spot groups also.

The fact that the influence of the green corona on the corpuscular radiation is largest at the minimum of solar activity and disappears completely after the new cycle has begun is not so surprising in view of the results found. If one compares the mean configurations of spots and filaments belonging to the different phases of a solar cycle, it is seen that in the minimum epoch the mean distance in heliographic latitude between the spots and the main prominence zone is smallest. Therefore, the magnetic interaction must be greatest. The magnetic deviation of the corpuscular radiation will then be large, and the deflection will be toward the equator because the spot zone is always a little nearer the equator than the prominence zone. This effect corresponds to the typical form of the corona at the minimum epoch when the long equatorial streamers are present. Further, we understand now why the filaments of high latitudes contribute so much to the corpuscular radiation around the minimum, and only then. Finally, it is clear why just the effect of the weak corona of the minimum epoch can be traced so well in the behavior of the corpuscular radiation.

We may conclude that the distribution of the green corona—at least during the sunspot minimum—makes those regions appear from which the corpuscular radiation cannot reach the earth. It is hoped that by simultaneous photometry of the corona and measurement of the magnetic fields of the sun an explanation of these interesting relations will be found. Such measurements, which are rather laborious for both the corona and the magnetic fields, have already been started. Observations are also being made at wave lengths of a few meters.

SCHAUINSLAND, NEAR FREIBURG I. BR.
June 1, 1946

ON THE RADIATIVE EQUILIBRIUM OF A STELLAR ATMOSPHERE. XV

S. CHANDRASEKHAR
Yerkes Observatory
Received February 17, 1947

ABSTRACT

In this paper the general equations of transfer for an atmosphere scattering radiation in accordance with Rayleigh's law and allowing for a partial elliptic polarization of the radiation field are formulated. It is shown that, under these conditions, we must consider, in addition to the intensities I_l and I_r in two directions at right angles to each other in the plane of the electric and the magnetic vectors, the two further quantities

$$U = (I_l - I_r) \tan 2\chi \qquad \text{and} \qquad V = (I_l - I_r) \tan 2\beta \sec 2\chi ,$$

where χ denotes the inclination of the plane of polarization to the direction to which l refers and $-\pi/2 \leqslant \beta \leqslant +\pi/2$ is an angle, the tangent of which is equal to the ratio of axes of the ellipse characterizing the state of polarization. (The sign of β depends on whether the polarization is right handed or left handed.)

It is found that the equations of transfer for I_l, I_r, and U are of exactly the same forms as in cases in which only partial plane-polarization is contemplated and that the equation for V is independent of others. On Rayleigh's law, V is scattered in accordance with a phase function, $\frac{3}{4} \cos \Theta$.

The solution of the equation for V appropriate for the problem of diffuse reflection by a semi-infinite atmosphere is also given.

1. *Introduction.*—In earlier papers[1] of this series the general equations of transfer valid for an atmosphere scattering radiation in accordance with Rayleigh's law[2] and allowing for a partial plane-polarization of the radiation field have been formulated and solved for the case of an electron-scattering atmosphere and for the problem of diffuse reflection of a partially plane-polarized beam by a plane-parallel atmosphere. In this paper we shall extend this discussion to include the case of partial elliptic polarization of the radiation field.

2. *The parametric representation of partially elliptically polarized light and its resolution into two oppositely polarized streams. The composition of elliptically polarized streams with no mutual phase relationships.*—The most convenient characterization of an arbitrarily polarized light is due to Sir George Stokes,[3] and his representation with slight modifications will be used in this paper. However, in view of the general inaccessibility of Stokes's considerations, it may be useful to have them presented in a form suitable for our purposes.

Consider, first, an elliptically polarized beam with the plane of polarization[4] inclined at an angle χ to a certain fixed direction,[5] l (say). Let β denote the angle whose tangent is equal to the ratio of the axes of the ellipse traced by the end-point of the electric vector, the numerical value of β being supposed to lie between the limits 0 and $\pi/2$ and

[1] *Ap. J.*, **103**, 351, 1946; **104**, 110, 1946; and **105**, 151, 164, 1947. These papers will be referred to as "Papers X, XI, XIII, and XIV," respectively. We shall also have occasion to refer to Paper IX (*Ap. J.* **103**, 165, 1946).

[2] As in Papers XI, XIII, and XIV, we shall include under "Rayleigh's law" only that part of it which pertains to the state of polarization and the angular distribution of the scattered radiation.

[3] *Trans. Cambridge Phil. Soc.*, **9**, 399, 1852; or *Mathematical and Physical Papers of Sir George Stokes* (Cambridge, England, 1901), **3**, 233–51.

[4] We shall take this to coincide with the plane of vibration of the electric vector.

[5] These directions are referred in the plane containing the electric and the magnetic vectors.

the sign of β being positive or negative according to whether the polarization is right handed or left handed. Finally, let $\xi^{(0)}$ denote a quantity proportional to the mean amplitude of the electric vector, whose square is equal to the intensity of the beam:

$$I = [\xi^{(0)}]^2 . \tag{1}$$

Then, for the elliptically polarized beam with the specified characteristics, the *amplitudes* ξ_χ and $\xi_{\chi+\pi/2}$ in the directions χ and $\chi + \pi/2$ can be represented in the forms

$$\xi_\chi = \xi^{(0)} \cos\beta \sin\omega t \quad \text{and} \quad \xi_{\chi+\pi/2} = \xi^{(0)} \sin\beta \cos\omega t , \tag{2}$$

where ω denotes the circular frequency of the light considered.

From equations (2) it follows that the amplitudes ξ_l and ξ_r in the direction l and in the direction r at right angles to l are

$$\xi_l = \xi^{(0)} (\cos\beta \cos\chi \sin\omega t - \sin\beta \sin\chi \cos\omega t) \tag{3}$$

and

$$\xi_r = \xi^{(0)} (\cos\beta \sin\chi \sin\omega t + \sin\beta \cos\chi \cos\omega t) . \tag{4}$$

We can re-write the foregoing expressions for ξ_l and ξ_r in the forms

$$\xi_l = \xi_l^{(0)} \sin(\omega t - \epsilon_1) \quad \text{and} \quad \xi_r = \xi_r^{(0)} \sin(\omega t - \epsilon_2) , \tag{5}$$

where

$$\left.\begin{aligned} \xi_l^{(0)} &= \xi^{(0)} (\cos^2\beta \cos^2\chi + \sin^2\beta \sin^2\chi)^{1/2} , \\ \xi_r^{(0)} &= \xi^{(0)} (\cos^2\beta \sin^2\chi + \sin^2\beta \cos^2\chi)^{1/2} , \end{aligned}\right\} \tag{6}$$

and

$$\tan\epsilon_1 = \tan\chi \tan\beta ; \qquad \tan\epsilon_2 = -\cot\chi \tan\beta . \tag{7}$$

The intensities I_l and I_r in the directions l and r are therefore given by

$$I_l = [\xi_l^{(0)}]^2 = I (\cos^2\beta \cos^2\chi + \sin^2\beta \sin^2\chi) , \tag{8}$$

and

$$I_r = [\xi_r^{(0)}]^2 = I (\cos^2\beta \sin^2\chi + \sin^2\beta \cos^2\chi) . \tag{9}$$

Furthermore, from equations (6) and (7) it follows that

$$2\xi_l^{(0)} \xi_r^{(0)} \cos(\epsilon_1 - \epsilon_2) = I \cos 2\beta \sin 2\chi \tag{10}$$

and

$$2\xi_l^{(0)} \xi_r^{(0)} \sin(\epsilon_1 - \epsilon_2) = I \sin 2\beta . \tag{11}$$

Thus, whenever the amplitudes of an elliptically polarized beam in two directions at right angles to each other can be expressed in the form (5), we can at once write the relations

$$I = I_l + I_r = [\xi_l^{(0)}]^2 + [\xi_r^{(0)}]^2 , \tag{12}$$

$$Q = I_l - I_r = I \cos 2\beta \cos 2\chi = [\xi_l^{(0)}]^2 - [\xi_r^{(0)}]^2 , \tag{13}$$

$$U = (I_l - I_r) \tan 2\chi = I \cos 2\beta \sin 2\chi = 2\xi_l^{(0)} \xi_r^{(0)} \cos\delta , \tag{14}$$

and

$$V = (I_l - I_r) \tan 2\beta \sec 2\chi = I \sin 2\beta = 2\xi_l^{(0)} \xi_r^{(0)} \sin\delta , \tag{15}$$

where

$$\delta = \epsilon_1 - \epsilon_2 \tag{16}$$

denotes the difference in phase with which the components of the electric vector vibrate in the directions l and r.

It will be observed that, according to the definitions of the quantities Q, U, and V for an elliptically polarized beam,

$$I = (Q^2 + U^2 + V^2)^{1/2}. \tag{17}$$

Now Stokes has shown that any elliptically polarized beam (and therefore, as it will appear, *any* partially polarized beam) can be resolved into two other elliptically polarized beams of specified states of polarization. Thus, a beam of intensity I polarized in the direction χ and of an ellipticity corresponding to β can be expressed as the result of superposition of two beams polarized in the directions χ_1 and χ_2 and with ellipticities corresponding to β_1 and β_2, and of intensities

$$I_1 = \frac{\sin^2(\beta_2 - \beta)\cos^2(\chi_2 - \chi) + \cos^2(\beta_2 + \beta)\sin^2(\chi_2 - \chi)}{\sin^2(\beta_2 - \beta_1)\cos^2(\chi_2 - \chi_1) + \cos^2(\beta_2 + \beta_1)\sin^2(\chi_2 - \chi_1)} I \tag{18}$$

and

$$I_2 = \frac{\sin^2(\beta_1 - \beta)\cos^2(\chi_1 - \chi) + \cos^2(\beta_1 + \beta)\sin^2(\chi_1 - \chi)}{\sin^2(\beta_2 - \beta_1)\cos^2(\chi_2 - \chi_1) + \cos^2(\beta_2 + \beta_1)\sin^2(\chi_2 - \chi_1)} I, \tag{19}$$

respectively. Of these various modes of resolution, the one of greatest interest is the resolution into *oppositely polarized beams* when

$$\beta_2 = -\beta_1 \quad \text{and} \quad \chi_2 = \chi_1 + \frac{\pi}{2}, \tag{20}$$

i.e., when the ellipses described are similar, their major axes perpendicular to each other, and the direction of revolution of one contrary to that in the other. The importance of this concept of opposite polarization arises from the fact that *oppositely polarized beams cannot interfere with one another.*

For the case of resolution into oppositely polarized beams, equations (18) and (19) become

$$I_1 = I[\sin^2(\beta_1 + \beta)\sin^2(\chi_1 - \chi) + \cos^2(\beta_1 - \beta)\cos^2(\chi_1 - \chi)] \tag{21}$$

and

$$I_2 = I[\sin^2(\beta_1 - \beta)\cos^2(\chi_1 - \chi) + \cos^2(\beta_1 + \beta)\sin^2(\chi_1 - \chi)]. \tag{22}$$

When $\beta_1 = 0$, we have the resolution of the beam into plane-polarized components at right angles to each other, and equations (21) and (22) become equivalent to equations (8) and (9).

The expression (21) for I_1 can be expanded into the form

$$\left.\begin{aligned} I_1 = \tfrac{1}{2}[I + I\cos 2\beta\cos 2\chi\cos 2\beta_1\cos 2\chi_1 + I\cos 2\beta\sin 2\chi\cos 2\beta_1\sin 2\chi_1 \\ + I\sin 2\beta\sin 2\beta_1], \end{aligned}\right\} \tag{23}$$

or, in terms of the quantities Q, U, and V defined as in equations (13)–(15), we have

$$I_1 = \tfrac{1}{2}[I + Q\cos 2\beta_1\cos 2\chi_1 + U\cos 2\beta_1\sin 2\chi_1 + V\sin 2\beta_1). \tag{24}$$

The corresponding expression for I_2 can be obtained by simply changing the sign of β_1 and replacing χ_1 by $\chi_1 + \pi/2$. We have

$$I_2 = \tfrac{1}{2}[I - Q\cos 2\beta_1\cos 2\chi_1 - U\cos 2\beta_1\sin 2\chi_1 - V\sin 2\beta_1]. \tag{25}$$

Turning, next, to the consideration of the result of the superposition of a number of *independent* streams of elliptically polarized light, i.e., of polarized streams which have no phase relationships, we start with the following principle enunciated by Stokes: "When any number of polarized streams from different sources mix together, after having been variously modified by reflection, refraction, transmission through doubly refracting media, tourmalines, etc., the intensity of the mixture is equal to the sum of the intensities due to the separate streams."

From this principle it follows, in particular, that, if each of the separate streams is resolved into two states of opposite polarization, the resultant mixture will have intensities in the two states which are the sum of respective intensities of the separate streams. Thus, if $I^{(n)}$, $\chi^{(n)}$, and $\beta^{(n)}$ define the intensity, the plane of polarization, and the ellipticity of a typical stream and if $I_1^{(n)}$ and $I_2^{(n)}$ are its intensities in the states of polarization (β_1, χ_1) and $(-\beta_1, \chi_1 + \pi/2)$, respectively, then

$$I_1 = \Sigma I_1^{(n)} \qquad \text{and} \qquad I_2 = \Sigma I_2^{(n)} \tag{26}$$

where I_1 and I_2 refer to the mixture.

Using equation (24) to express the intensities of the various streams in the component (β_1, χ_1), we have

$$I_1 = \tfrac{1}{2}\left[\Sigma I^{(n)} + \Sigma Q^{(n)} \cos 2\beta_1 \cos 2\chi_1 + \Sigma U^{(n)} \cos 2\beta_1 \sin 2\chi_1 + \Sigma V^{(n)} \sin 2\beta_1\right]. \tag{27}$$

The intensity of the resultant mixture in the state of polarization (χ_1, β_1) can therefore be expressed in the form

$$I_1 = \tfrac{1}{2}\left[I + Q \cos 2\beta_1 \cos 2\chi_1 + U \cos 2\beta_1 \sin 2\chi_1 + V \sin 2\beta_1\right], \tag{28}$$

where

$$I = \Sigma I^{(n)}; \qquad Q = \Sigma Q^{(n)}; \qquad U = \Sigma U^{(n)}; \qquad V = \Sigma V^{(n)}. \tag{29}$$

We have, of course, a similar expression for I_2.

From equations (28) and (29) it follows that a beam resulting from the superposition of a number of independent streams of elliptically polarized light can again be characterized by a set of parameters, I, Q, U, and V, which are the sums of the respective parameters characterizing the individual streams. Moreover, any two polarized beams characterized by the same set of parameters, I, Q, U, and V, will be *optically equivalent* in the sense that "they will present exactly the same appearance on being viewed through a crystal followed by a Nicol's prism or other analyzer" (Stokes). On the other hand, it should be noted that, for a polarized beam obtained in this manner, the relation (17) (derived for an elliptically polarized beam) will not, in general, be valid, indicating the fact that the mixture of a number of independent streams of elliptically polarized light will, in general, lead to a beam which is only partially polarized. However, it is clear that, under the circumstances of partial polarization, we can regard the light as a mixture of an unpolarized beam of natural light, of intensity

$$I^{(u)} = I - (Q^2 + U^2 + V^2)^{1/2}, \tag{30}$$

and a polarized beam, of intensity

$$I^{(p)} = (Q^2 + U^2 + V^2)^{1/2}, \tag{31}$$

the plane of polarization and the ratio of the axes of the ellipse of this polarized part being given by

$$\tan 2\chi = \frac{U}{Q} \qquad \text{and} \qquad \sin 2\beta = \frac{V}{(Q^2 + U^2 + V^2)^{1/2}}. \tag{32}$$

An alternative way of regarding a partially polarized beam, defined in terms of the parameters I, Q, U, and V, is to express it as the resultant of two streams in the states of

opposite polarization (β, χ) and $(-\beta, \chi + \pi/2)$, where χ and β are given by equations (32). The intensities of the component streams in the two states can be readily written down when it is remembered that unpolarized, or natural, light is equivalent to any two independent oppositely polarized streams of half the intensity. The unpolarized part (30) of the beam is, therefore, equivalent to a mixture of two independent polarized beams, each of intensity $\frac{1}{2}I^{(u)}$, in the states of polarization (β, χ) and $(-\beta, \chi + \pi/2)$. Combining the former with the polarized part $I^{(p)}$ (eq. [31]) in the same state of polarization, we conclude that a beam characterized by the parameters I, Q, U, and V is equivalent to two independent beams of elliptically polarized light, of intensities

$$I^{(+)} = \tfrac{1}{2}\left[I + (Q^2 + U^2 + V^2)^{1/2}\right] \tag{33}$$

and

$$I^{(-)} = \tfrac{1}{2}\left[I - (Q^2 + U^2 + V^2)^{1/2}\right], \tag{34}$$

in the states of polarization

$$(\beta, \chi) \qquad \text{and} \qquad \left(-\beta, \chi + \frac{\pi}{2}\right), \tag{35}$$

respectively, where

$$\chi = \tfrac{1}{2}\tan^{-1}\frac{U}{Q} \qquad \text{and} \qquad \beta = \tfrac{1}{2}\sin^{-1}\frac{V}{(Q^2 + U^2 + V^2)^{1/2}}. \tag{36}$$

The particular importance of this resolution arises from the fact that we may regard the two streams $I^{(+)}$ and $I^{(-)}$ as *independent*.

3. *The source functions* $\mathfrak{J}_l$, $\mathfrak{J}_r$, $\mathfrak{J}_U$, *and* $\mathfrak{J}_V$.—From the discussion of Stokes's representation of partially polarized light in the preceding section, it follows that, for the purposes of formulating the equation of transfer, we may uniquely characterize the radiation field at any given point by the four intensities $I_l(\vartheta, \varphi)$, $I_r(\vartheta, \varphi)$, $U(\vartheta, \varphi)$, and $V(\vartheta, \varphi)$, where ϑ and φ are the polar angles, referred to an appropriately chosen co-ordinate system through the point under consideration (see Fig. 1 in Paper X), and l and r refer to the directions in the meridian plane and at right angles to it, respectively.

To evaluate the source functions, $\mathfrak{J}_l(\vartheta, \varphi)$, $\mathfrak{J}_r(\vartheta, \varphi)$, $\mathfrak{J}_U(\vartheta, \varphi)$, and $\mathfrak{J}_V(\vartheta, \varphi)$, appropriate to any point in the atmosphere, we shall first consider the contributions to these source functions arising from the scattering of the radiation in the direction (ϑ', φ').

The radiation in the direction (ϑ', φ') will be characterized by the intensities $I_l(\vartheta', \varphi)'$, $I_r(\vartheta', \varphi')$, $U(\vartheta', \varphi')$, and $V(\vartheta', \varphi')$. Equivalently, we may also characterize it by the intensities

$$I^{(+)}(\vartheta', \varphi') = \tfrac{1}{2}\left\{I_l + I_r + \left[(I_l - I_r)^2 + U^2 + V^2\right]^{1/2}\right\}_{\vartheta', \varphi'} \tag{37}$$

and

$$I^{(-)}(\vartheta', \varphi') = \tfrac{1}{2}\left\{I_l + I_r - \left[(I_l - I_r)^2 + U^2 + V^2\right]^{1/2}\right\}_{\vartheta', \varphi'}, \tag{38}$$

in the states of opposite polarization,

$$(\beta, \chi) \qquad \text{and} \qquad \left(-\beta, \chi + \frac{\pi}{2}\right), \tag{39}$$

respectively, where

$$\left.\begin{aligned} \tan 2\chi &= \frac{U(\vartheta', \varphi')}{I_l(\vartheta', \varphi') - I_r(\vartheta', \varphi')} \\ \text{and} \qquad \sin 2\beta &= \frac{V(\vartheta', \varphi')}{\sqrt{\left[I_l(\vartheta', \varphi') - I_r(\vartheta', \varphi')\right]^2 + U^2(\vartheta', \varphi') + V^2(\vartheta', \varphi')}}. \end{aligned}\right\} \tag{40}$$

And, as we have already explained in § 2, in this type of resolution the polarized components $I^{(+)}(\vartheta', \varphi')$ and $I^{(-)}(\vartheta', \varphi')$ may be regarded as uncorrelated in their phases.

We may accordingly consider the scattering of the radiation in the direction (ϑ', φ') as the result of scattering of the two independent, oppositely polarized components, $I^{(+)}(\vartheta', \varphi')$ and $I^{(-)}(\vartheta', \varphi')$. Each of these polarized components will give rise to polarized scattered beams, which will again have no correlation in phases. In other words, the radiation scattered in the direction (ϑ, φ) from other directions can be considered as a mixture of a very large number of independent, elliptically polarized streams and can, therefore, be combined according to the additive law of composition of the parameters I_l, I_r, U, and V.

Consider, then, the scattering of the elliptically polarized component $I^{(+)}(\vartheta', \varphi')$ in the direction (ϑ', φ') and confined to an element of solid angle, $d\omega'$, into the direction (ϑ, φ). Introducing the qualities, ξ's, as in § 2, we may express the amplitudes $\xi_\chi^{(+)}$ and $\xi_{\chi+\pi/2}^{(+)}$ in the forms

$$\xi_\chi^{(+)} = \xi^{(+,\,0)} \cos\beta \sin\omega t \quad \text{and} \quad \xi_{\chi+\pi/2}^{(+)} = \xi^{(+,\,0)} \sin\beta \cos\omega t\,, \tag{41}$$

where $\xi^{(+,\,0)}$ is so defined that (cf. eq. [1])

$$I^{(+)}(\vartheta', \varphi') = [\xi^{(+,\,0)}]^2\,. \tag{42}$$

The amplitude, $\xi_\chi^{(+)}$, when scattered in the direction (ϑ, φ) will lead to amplitudes in the meridian plane through (ϑ, φ) and at right angles to it which are proportional, respectively, to (cf. Paper XI, eqs. [31] and [32])

$$\xi_\chi^{(+)}\,[\,(l, l)\cos\chi + (r, l)\sin\chi] \tag{43}$$

and

$$\xi_\chi^{(+)}\,[\,(l, r)\cos\chi + (r, r)\sin\chi]\,, \tag{44}$$

where (cf. Paper XI, eq. [33]),

$$\left.\begin{aligned}
(l, l) &= \sin\vartheta \sin\vartheta' + \cos\vartheta \cos\vartheta' \cos(\varphi' - \varphi)\,,\\
(r, l) &= +\cos\vartheta \sin(\varphi' - \varphi)\,,\\
(l, r) &= -\cos\vartheta' \sin(\varphi' - \varphi)\,,\\
(r, r) &= \cos(\varphi' - \varphi)\,.
\end{aligned}\right\} \tag{45}$$

Similarly, the amplitude $\xi_{\chi+\pi/2}^{(+)}$ will lead to scattered amplitudes in the directions, parallel, respectively, perpendicular to the meridian plane through (ϑ, φ) of amounts proportional to

$$\xi_{\chi+\pi/2}^{(+)}[-(l, l)\sin\chi + (r, l)\cos\chi] \tag{46}$$

and

$$\xi_{\chi+\pi/2}^{(+)}\,[-(l, r)\sin\chi + (r, r)\cos\chi]\,. \tag{47}$$

The phase relationship between $\xi_\chi^{(+)}$ and $\xi_{\chi+\pi/2}^{(+)}$ will be maintained in these scattered amplitudes and must, therefore, be added as amplitudes with the correct phase differences. Therefore, the elliptically polarized component, $I^{(+)}(\vartheta', \varphi')$, of the radiation in the direction (ϑ', φ'), when scattered in the direction (ϑ, φ), will give rise to an elliptically polarized beam, the amplitudes of which in the meridian plane and at right angles to it will be proportional, respectively, to

$$\xi_l^{(s)} = \xi^{(+,\,0)}\,(A_\chi \cos\beta \sin\omega t + A_{\chi+\pi/2} \sin\beta \cos\omega t) \tag{48}$$

and

$$\xi_r^{(s)} = \xi^{(+,\,0)}\,(B_\chi \cos\beta \sin\omega t + B_{\chi+\pi/2} \sin\beta \cos\omega t)\,, \tag{49}$$

where, for the sake of brevity, we have written

$$\left.\begin{aligned} A_\chi &= +\,(l,\,l)\cos\chi\,+\,(r,\,l)\sin\chi\,,\\ B_\chi &= +\,(l,\,r)\cos\chi+\,(r,\,r)\sin\chi\,,\\ A_{\chi+\pi/2} &= -\,(l,\,l)\sin\chi\,+\,(r,\,l)\cos\chi\,,\\ B_{\chi+\pi/2} &= -\,(l,\,r)\sin\chi+\,(r,\,r)\cos\chi\,. \end{aligned}\right\} \tag{50}$$

We can now re-write equations (48) and (49) in the standard form (cf. eq. [5]),

$$\left.\begin{aligned} \xi_l^{(s)} &= \xi_l^{(s,\,0)}\sin(\omega t-\epsilon_1)\,,\\ \xi_r^{(s)} &= \xi_r^{(s,\,0)}\sin(\omega t-\epsilon_2)\,, \end{aligned}\right\} \tag{51}$$

where

$$\left.\begin{aligned} \xi_l^{(s,\,0)} &= \xi^{(+,\,0)}\,(A_\chi^2\cos^2\beta+A_{\chi+\pi/2}^2\sin^2\beta)^{1/2}\,,\\ \xi_r^{(s,\,0)} &= \xi^{(+,\,0)}\,(B_\chi^2\cos^2\beta+B_{\chi+\pi/2}^2\sin^2\beta)^{1/2}\,, \end{aligned}\right\} \tag{52}$$

and

$$\tan\epsilon_1=-\frac{A_{\chi+\pi/2}}{A_\chi}\tan\beta\,;\qquad \tan\epsilon_2=-\frac{B_{\chi+\pi/2}}{B_\chi}\tan\beta\,. \tag{53}$$

With the amplitudes of the scattered radiation expressed in the form (51), we can write down the contributions, $d\mathfrak{I}_l^{(+)}(\vartheta,\varphi;\vartheta',\varphi')$, $d\mathfrak{I}_r^{(+)}(\vartheta,\varphi;\vartheta'\,\varphi')$, $d\mathfrak{I}_U^{(+)}(\vartheta,\varphi;\vartheta'\,\varphi')$, and $d\mathfrak{I}_V^{(+)}(\vartheta,\varphi;\vartheta',\varphi')$, to the source functions, $\mathfrak{I}_l(\vartheta,\varphi)$, $\mathfrak{I}_r(\vartheta,\varphi)$, $\mathfrak{I}_U(\vartheta,\varphi)$, and $\mathfrak{I}_V(\vartheta,\varphi)$, arising from the scattering of the elliptically polarized component, $I^{(+)}(\vartheta',\varphi')$, of the radiation in the direction (ϑ',φ') and confined to an element of solid angle, $d\omega'$, in the following forms (cf. eqs. [8]–[15]):

$$\left.\begin{aligned} d\mathfrak{I}_l^{(+)}(\vartheta,\varphi;\vartheta',\varphi') &= \frac{3}{8\pi}\,[\xi_l^{(s,\,0)}]^2\,d\omega'\,,\\ d\mathfrak{I}_r^{(+)}(\vartheta,\varphi;\vartheta',\varphi') &= \frac{3}{8\pi}\,[\xi_r^{(s,\,0)}]^2\,d\omega'\,,\\ d\mathfrak{I}_U^{(+)}(\vartheta,\varphi;\vartheta',\varphi') &= \frac{3}{8\pi}\,[2\,\xi_l^{(s,\,0)}\xi_r^{(s,\,0)}\cos(\epsilon_1-\epsilon_2)\,]\,d\omega'\,,\\ d\mathfrak{I}_V^{(+)}(\vartheta,\varphi;\vartheta',\varphi') &= \frac{3}{8\pi}\,[2\,\xi_l^{(s,\,0)}\xi_r^{(s,\,0)}\sin(\epsilon_1-\epsilon_2)\,]\,d\omega'\,. \end{aligned}\right\} \tag{54}$$

The various quantities which occur on the right-hand sides of the foregoing expressions can be evaluated according to equations (50)–(53). Thus

$$\left.\begin{aligned} [\xi_l^{(s,\,0)}]^2 &= [\xi^{(+,\,0)}]^2\,(A_\chi^2\cos^2\beta+A_{\chi+\pi/2}^2\sin^2\beta)\\ &= I^{(+)}(\vartheta',\varphi')\,\{\,(l,\,l)^2\,[\cos^2\chi\cos^2\beta+\sin^2\chi\sin^2\beta]\\ &\quad+\,(r,\,l)^2\,[\sin^2\chi\cos^2\beta+\cos^2\chi\sin^2\beta]\,+\,(l,\,l)\,(r,\,l)\sin 2\chi\cos 2\beta\,\}\,; \end{aligned}\right\} \tag{55}$$

or, using equations (8), (9), and (14), we have

$$[\xi_l^{(s,\,0)}]^2=(l,\,l)^2I_l^{(+)}(\vartheta',\varphi')+(r,\,l)^2I_r^{(+)}(\vartheta',\varphi')+(l,\,l)\,(r,\,l)\,U^{(+)}(\vartheta',\varphi')\,. \tag{56}$$

Similarly,

$$[\xi_r^{(s,\,0)}]^2=(l,\,r)^2I_l^{(+)}(\vartheta',\varphi')+(r,\,r)^2I_r^{(+)}(\vartheta',\varphi')+(l,\,r)\,(r,\,r)\,U^{(+)}(\vartheta',\varphi')\,. \tag{57}$$

Again, according to equations (50), (52), and (53),

$$\left.\begin{aligned} 2\xi_l^{(s,\,0)}\xi_r^{(s,\,0)}\cos(\epsilon_1-\epsilon_2) &= 2I^{(+)}(\vartheta',\varphi')\,(A_\chi B_\chi\cos^2\beta + A_{\chi+\pi/2}B_{\chi+\pi/2}\sin^2\beta)\\ &= 2I^{(+)}(\vartheta',\varphi')\,\{(l,l)(l,r)[\cos^2\chi\cos^2\beta+\sin^2\chi\sin^2\beta]\\ &\quad+(r,l)(r,r)[\sin^2\chi\cos^2\beta+\cos^2\chi\sin^2\beta]\\ &\quad+[(l,l)(r,r)+(r,l)(l,r)]\cos\chi\sin\chi\cos 2\beta\}\end{aligned}\right\}\quad(58)$$

or

$$\left.\begin{aligned} 2\xi_l^{(s,\,0)}\xi_r^{(s,\,0)}\cos(\epsilon_1-\epsilon_2) &= 2(l,l)(l,r)\,I_l^{(+)}(\vartheta',\varphi')+2(r,l)(r,r)\,I_r^{(+)}(\vartheta',\varphi')\\ &\quad+[(l,l)(r,r)+(r,l)(l,r)]\,U^{(+)}(\vartheta',\varphi').\end{aligned}\right\}\quad(59)$$

And, finally,

$$\left.\begin{aligned} 2\xi_l^{(s,\,0)}\xi_r^{(s,\,0)}\sin(\epsilon_1-\epsilon_2) &= I^{(+)}(\vartheta',\varphi')\,(A_\chi B_{\chi+\pi/2}-B_\chi A_{\chi+\pi/2})\sin 2\beta\\ &= I^{(+)}(\vartheta',\varphi')\,[(l,l)(r,r)-(r,l)(l,r)]\sin 2\beta,\end{aligned}\right\}\quad(60)$$

or

$$2\xi_l^{(s,\,0)}\xi_r^{(s,\,0)}\sin(\epsilon_1-\epsilon_2) = V^{(+)}(\vartheta',\varphi')\,[(l,l)(r,r)-(r,l)(l,r)]. \quad(61)$$

Equations (54) now become

$$\left.\begin{aligned} d\Im_l^{(+)}(\vartheta,\varphi;\vartheta',\varphi') &= \frac{3}{8\pi}\{(l,l)^2 I_l^{(+)}(\vartheta',\varphi')+(r,l)^2 I_r^{(+)}(\vartheta',\varphi')\\ &\quad+(l,l)(r,l)\,U^{(+)}(\vartheta',\varphi')\}\,d\omega',\end{aligned}\right\}\quad(62)$$

$$\left.\begin{aligned} d\Im_r^{(+)}(\vartheta,\varphi;\vartheta',\varphi') &= \frac{3}{8\pi}\{(l,r)^2 I_l^{(+)}(\vartheta',\varphi')+(r,r)^2 I_r^{(+)}(\vartheta',\varphi')\\ &\quad+(l,r)(r,r)\,U^{(+)}(\vartheta',\varphi')\}\,d\omega',\end{aligned}\right\}\quad(63)$$

$$\left.\begin{aligned} d\Im_U^{(+)}(\vartheta,\varphi;\vartheta',\varphi') &= \frac{3}{8\pi}\{2(l,l)(l,r)\,I_l^{(+)}(\vartheta',\varphi')+2(r,l)(r,r)\,I_r^{(+)}(\vartheta',\varphi')\\ &\quad+[(l,l)(r,r)+(r,l)(l,r)]\,U^{(+)}(\vartheta',\varphi')\}\,d\omega',\end{aligned}\right\}\quad(64)$$

and

$$d\Im_V^{(+)}(\vartheta,\varphi;\vartheta',\varphi') = \frac{3}{8\pi}[(l,l)(r,r)-(r,l)(l,r)]\,V^{(+)}(\vartheta',\varphi')\,d\omega'. \quad(65)$$

The corresponding contributions to the various source functions arising from the scattering of the other polarized component, $I^{(-)}(\vartheta',\varphi')$, in the opposite state of polarization, $(-\beta,\,\chi+\pi/2)$, can be obtained by simply writing $(-)$ in place of $(+)$ in the foregoing equations. And, since the intensities I_l, I_r, U, and V are simply additive when streams of polarized light with no correlation in their phases are mixed, it is clear that the contributions to the various source functions arising from the scattering of the radiation $[I_l(\vartheta',\varphi'),\ I_r(\vartheta',\varphi'),\ U(\vartheta',\varphi'),\ V(\vartheta',\varphi')]$ in the direction (ϑ',φ') and confined to an element of solid angle, $d\omega'$, are

$$\left.\begin{aligned} d\Im_l(\vartheta,\varphi;\vartheta',\varphi') &= \frac{3}{8\pi}\{(l,l)^2 I_l(\vartheta',\varphi')+(r,l)^2 I_r(\vartheta',\vartheta')\\ &\quad+(l,l)(r,l)\,U(\vartheta',\varphi')\}\,d\omega',\end{aligned}\right\}\quad(66)$$

$$\left.\begin{aligned} d\Im_r(\vartheta,\varphi;\vartheta',\varphi') &= \frac{3}{8\pi}\{(l,r)^2 I_l(\vartheta',\varphi')+(r,r)^2 I_r(\vartheta',\varphi')\\ &\quad+(l,r)(r,r)\,U(\vartheta',\varphi')\}\,d\omega',\end{aligned}\right\}\quad(67)$$

$$\left.\begin{aligned} d\Im_U(\vartheta,\varphi;\vartheta',\varphi') &= \frac{3}{8\pi}\{2(l,l)(l,r)\,I_l(\vartheta',\varphi')+2(r,l)(r,r)\,I_r(\vartheta',\varphi')\\ &\quad+[(l,l)(r,r)+(r,l)(l,r)]\,U(\vartheta',\varphi')\}\,d\omega',\end{aligned}\right\}\quad(68)$$

and

$$d\mathfrak{I}_V(\vartheta, \varphi; \vartheta', \varphi') = \frac{3}{8\pi}[(l, l)(r, r) - (r, l)(l, r)]\, V(\vartheta', \varphi')\, d\omega'. \quad (69)$$

Integrating these equations over the unit sphere, we obtain the required source functions. We have

$$\left.\begin{aligned}\mathfrak{I}_l(\mu, \varphi) = \frac{3}{8\pi}\int_{-1}^{+1}\int_0^{2\pi} \{ &(l, l)^2 I_l(\mu', \varphi') + (r, l)^2 I_r(\mu', \varphi') \\ &+ (l, l)(r, l)\, U(\mu', \varphi') \}\, d\mu' d\varphi',\end{aligned}\right\} \quad (70)$$

$$\left.\begin{aligned}\mathfrak{I}_r(\mu, \varphi) = \frac{3}{8\pi}\int_{-1}^{+1}\int_0^{2\pi} \{ &(l, r)^2 I_l(\mu', \varphi') + (r, r)^2 I_r(\mu', \varphi') \\ &+ (l, r)(r, r)\, U(\mu', \varphi') \}\, d\mu' d\varphi',\end{aligned}\right\} \quad (71)$$

$$\left.\begin{aligned}\mathfrak{I}_U(\mu, \varphi) = \frac{3}{8\pi}\int_{-1}^{+1}\int_0^{2\pi} \{ &2(l, l)(l, r) I_l(\mu', \varphi') + 2(r, l)(r, r) I_r(\mu', \varphi') \\ &+ [(l, l)(r, r) + (r, l)(l, r)]\, U(\mu', \varphi') \}\, d\mu' d\varphi',\end{aligned}\right\} \quad (72)$$

and

$$\mathfrak{I}_V(\mu, \varphi) = \frac{3}{8\pi}\int_{-1}^{+1}\int_0^{2\pi} [(l, l)(r, r) - (r, l)(l, r)]\, V(\mu', \varphi')\, d\mu' d\varphi', \quad (73)$$

where the direction cosines, μ and μ', have been used in place of $\cos\vartheta$ and $\cos\vartheta'$.

Comparing equations (70)–(72) with the corresponding equations obtained in Paper XI (eqs. [49]–[51]) for a partially plane-polarized radiation field, we observe that they are of identical forms. The intensities I_l, I_r, and U, therefore, satisfy the same equations of transfer as in cases in which only partial plane-polarization is contemplated. The equations of transfer for I_l, I_r, and U can therefore be expressed quite generally in vector form as in Paper XIV, § 2. However, when elliptic polarization is contemplated,[6] an additional equation for V must be considered. This equation is, however, independent of the others and is given by (cf. eq. [73])

$$\left.\begin{aligned}\frac{dV(s, \mu, \varphi)}{\rho\sigma ds} = -V(s, \mu, \varphi) + \frac{3}{8\pi}\int_{-1}^{+1}\int_0^{2\pi} &[(l, l)(r, r) - (r, l)(l, r)] \\ &\times V(s, \mu', \varphi')\, d\mu' d\varphi',\end{aligned}\right\} \quad (74)$$

where s measures the linear distance in the direction (ϑ, φ) and σ denotes the mass-scattering coefficient.

Finally, we may notice that, according to equations (45),

$$(l, l)(r, r) - (r, l)(l, r) = \mu\mu' + (1 - \mu^2)^{1/2}(1 - \mu'^2)^{1/2}\cos(\varphi - \varphi'). \quad (75)$$

The intensity V *is therefore scattered in accordance with a phase function* $\frac{3}{2}\cos\Theta$.

4. *The solution of the equation of transfer for* V *for the problem of diffuse reflection by a semi-infinite plane-parallel atmosphere.*—In the problem of diffuse reflection we distinguish, as usual, between the part of the incident radiation which penetrates to various depths and the diffuse scattered radiation. Similarly, we also distinguish between the contributions to the source function arising from the scattering of the reduced incident radiation prevailing at any level and from the scattering of the diffuse radiation.

If πV_0 denotes the flux in V incident as a parallel beam on a plane-parallel atmosphere

[6] It is, of course, evident—and it is, indeed, required by the equations of transfer—that, on Rayleigh scattering, partial elliptic polarization in the radiation field can be induced only by the direct incidence of such radiation.

at an angle $\cos^{-1}\mu_0$ normal to the boundary, the equation of transfer (74) can be rewritten in the following form:

$$\left.\begin{aligned}\mu\frac{dV(\tau,\mu,\varphi)}{d\tau} &= V(\tau,\mu,\varphi)\\ -\frac{3}{8\pi}\int_{-1}^{+1}\int_{0}^{2\pi}&[\mu\mu'+(1-\mu^2)^{1/2}(1-\mu'^2)^{1/2}\cos(\varphi-\varphi')]\,V(\mu',\varphi')\,d\mu'd\varphi'\\ &-\tfrac{3}{8}V_0[-\mu\mu_0+(1-\mu^2)^{1/2}(1-\mu_0^2)^{1/2}\cos\varphi]\,e^{-\tau/\mu_0}.\end{aligned}\right\}\quad(76)$$

From equation (76) it follows that the solution $V(\tau,\mu,\varphi)$ must be expressible in the form

$$V(\tau,\mu,\varphi) = V^{(0)}(\tau,\mu) + V^{(1)}(\tau,\mu)\cos\varphi\,,\qquad(77)$$

where, as the notation implies, $V^{(0)}$ and $V^{(1)}$ are functions of τ and μ only. Equation (76) now breaks up into the following two equations:

$$\mu\frac{dV^{(0)}}{d\tau} = V^{(0)} - \tfrac{3}{4}\mu\int_{-1}^{+1}V(\tau,\mu')\,\mu'd\mu' + \tfrac{3}{8}V_0\mu\mu_0e^{-\tau/\mu_0}\qquad(78)$$

and

$$\left.\begin{aligned}\mu\frac{dV^{(1)}}{d\tau} &= V^{(1)} - \tfrac{3}{8}(1-\mu^2)^{1/2}\int_{-1}^{+1}V^{(1)}(\tau,\mu')(1-\mu'^2)^{1/2}d\mu'\\ &\quad-\tfrac{3}{8}V_0(1-\mu^2)^{1/2}(1-\mu'^2)^{1/2}e^{-\tau/\mu_0}.\end{aligned}\right\}\quad(79)$$

Equations (78) and (79) are of the standard form considered in Paper IX, § 4. We can therefore write down at once the angular distribution of the radiation reflected from a semi-infinite atmosphere. We have

$$V^{(0)}(0,\mu) = -\tfrac{3}{8}V_0\mu\mu_0H_\nu(\mu)\,H_\nu(\mu_0)\,\frac{\mu_0}{\mu+\mu_0}\qquad(80)$$

and

$$V^{(1)}(0,\mu) = \tfrac{3}{8}V_0(1-\mu^2)^{1/2}(1-\mu'^2)^{1/2}H_\nu^{(1)}(\mu)\,H_\nu^{(1)}(\mu_0)\,\frac{\mu_0}{\mu+\mu_0},\qquad(81)$$

where, in the nth approximation of the method of solution of the earlier papers, H_ν and $H_\nu^{(1)}$ are H-functions (cf. Paper XIV) defined in terms of the roots of the characteristic equations,

$$1 = \frac{3}{2}\sum_{j=1}^{n}\frac{a_j\mu_j^2}{1-k^2\mu_j^2}\qquad(82)$$

and

$$1 = \frac{3}{4}\sum_{j=1}^{n}\frac{a_j(1-\mu_j^2)}{1-k^2\mu_j^2},\qquad(83)$$

respectively.

It will be noticed that the characteristic equation defining $H_\nu^{(1)}$ is the same as the one defining $H_r(\mu)$ in Papers X and XI. Hence $H_\nu^{(1)}(\mu)$ is identical with $H_r(\mu)$.

Combining solutions (80) and (81) in accordance with equation (77), we have the law of reflection:

$$\left.\begin{aligned}V(\mu,\varphi;\mu_0,\varphi_0) &= \tfrac{3}{8}V_0[-\mu\mu_0H_\nu(\mu)\,H_\nu(\mu_0)\\ &\quad+(1-\mu^2)^{1/2}(1-\mu_0^2)^{1/2}H_r(\mu)\,H_r(\mu_0)\cos(\varphi-\varphi_0)]\,\frac{\mu_0}{\mu+\mu_0}.\end{aligned}\right\}\quad(84)$$

A table of the function $H_r(\mu)$ in the third approximation will be found in Paper XI (Table 3). A similar tabulation of the function H_v is now provided (Table 1).

TABLE 1

THE FUNCTION $H_v(\mu)$ IN THE THIRD APPROXIMATION

μ	$H_v(\mu)$	μ	$H_v(\mu)$	μ	$H_v(\mu)$
0	1.000	0.35	1.107	0.70	1.168
0.05	1.021	.40	1.118	0.75	1.175
.10	1 039	45	1.128	0.80	1.182
.15	1.055	.50	1.137	0.85	1.188
.20	1.070	.55	1.146	0.90	1.193
.25	1.084	.60	1.154	0.95	1.199
0.30	1.096	0.65	1.161	1.00	1.204

$k_1 = 0.8540755;$ $k_2 = 1.3690329;$ $k_3 = 4.1105114.$

Finally, we may remark that, according to the ideas developed in Paper XIV, the exact solution for $V(\mu, \varphi; \mu_0, \varphi_0)$ can be obtained by simply redefining the functions H_v and H_r, which occur in equation (84) as solutions of the functional equations,

$$H_v(\mu) = 1 + \tfrac{3}{4}\mu H_v(\mu) \int_0^1 \frac{H_v(\mu')}{\mu + \mu'} \mu'^2 d\mu' \tag{85}$$

and

$$H_r(\mu) = 1 + \tfrac{3}{8}\mu H_r(\mu) \int_0^1 \frac{H_r(\mu')}{\mu + \mu'} (1 - \mu'^2)\, d\mu'. \tag{86}$$

Tables of solutions of these and other functional equations will be found in Paper XVI.

ON THE RADIATIVE EQUILIBRIUM OF A STELLAR ATMOSPHERE. XVI

S. CHANDRASEKHAR AND FRANCES H. BREEN
Yerkes Observatory
Received February 17, 1947

ABSTRACT

In this paper we tabulate the various H-functions which occur in the solutions of transfer problems involving Rayleigh's phase function and Rayleigh scattering (including the state of polarization of the scattered radiation). The H-functions have been determined numerically as the solutions of the exact functional equations which they satisfy.

The exact laws of darkening in the two states of polarization of the emergent radiation from an electron-scattering atmosphere are also tabulated in this paper.

1. *Introduction.*—In Paper XIV[1] of this series, it was shown how exact solutions for a large class of problems in the theory of radiative transfer can be obtained by simply letting the H-functions (defined in terms of the Gaussian division and characteristic roots), which appear in their solutions (in the nth approximation), become solutions of associated functional equations of a certain standard form, namely,

$$H(\mu) = 1 + \mu H(\mu) \int_0^1 \frac{H(\mu)\,\Psi(\mu')}{\mu + \mu'}\, d\mu', \tag{1}$$

where the *characteristic function* $\Psi(\mu)$ is an even polynomial in μ, satisfying the condition

$$\int_0^1 \Psi(\mu)\, d\mu \leqslant \tfrac{1}{2}. \tag{2}$$

The practical importance of this result arises from the fact that, starting with a solution for $H(\mu)$ in the third approximation (for example), we can obtain by a process of iteration the exact H-functions which characterize the problem. And, as we have further seen in Paper XIV, once the exact H-functions have been determined in this (or similar fashion), such other constants as the solutions may involve can be evaluated directly in terms of the moments of these functions.

We have now completed the numerical solution of the various H-functions which occur in the problems considered in Papers III, IX (Part II), X, XI, XIII, and XV; and these solutions are tabulated in this paper. Reference may be made here to the exact laws of darkening and to the degree of polarization of the emergent radiation from an electron-scattering atmosphere, which are also tabulated (see Table 6).

I. TRANSFER PROBLEMS INVOLVING RAYLEIGH'S PHASE FUNCTION

The problem of a semi-infinite plane-parallel atmosphere with a constant net flux πF. *The law of darkening.*—

$$I(\mu) = \tfrac{3}{4} qF H^{(0)}(\mu).$$

The law of diffuse reflection from a semi-infinite plane-parallel atmosphere.—

$$\begin{aligned} I(\mu, \varphi; \mu_0, \varphi_0) = \tfrac{3}{32} F \{ & H^{(0)}(\mu)\, H^{(0)}(\mu_0) [3 - c(\mu + \mu_0) + \mu\mu_0] \\ & - 4\mu\mu_0 (1-\mu^2)^{\frac{1}{2}} (1-\mu_0^2)^{\frac{1}{2}} H^{(1)}(\mu)\, H^{(1)}(\mu_0) \cos(\varphi - \varphi_0) \\ & + (1-\mu^2)(1-\mu_0^2)\, H^{(2)}(\mu)\, H^{(2)}(\mu_0) \cos 2(\varphi - \varphi_0) \} \frac{\mu_0}{\mu + \mu_0}. \end{aligned}$$

[1] *Ap. J.*, **105**, 164, 1947.

The characteristic functions in terms of which $H^{(0)}(\mu)$, $H^{(1)}(\mu)$, and $H^{(2)}(\mu)$ are defined are, respectively,

$$\Psi^{(0)}(\mu) = \tfrac{3}{16}(3-\mu^2),$$

$$\Psi^{(1)}(\mu) = \tfrac{3}{8}\mu^2(1-\mu^2),$$

and

$$\Psi^{(2)}(\mu) = \tfrac{3}{32}(1-\mu^2)^2.$$

The constants q and c are given by

$$q = \frac{2}{3a_1} \quad \text{and} \quad c = \frac{a_2}{a_1},$$

where a_1 and a_2 are the moments of order 1 and 2 of $H^{(0)}(\mu)$. Further, q and c are related according to

$$8q^2 = 3 - c^2.$$

TABLE 1

THE FUNCTIONS $H^{(0)}(\mu)$, $H^{(1)}(\mu)$, AND $H^{(2)}(\mu)$, OBTAINED AS SOLUTIONS OF THE EXACT FUNCTIONAL EQUATIONS

μ	$H^{(0)}(\mu)$	$H^{(1)}(\mu)$	$H^{(2)}(\mu)$	μ	$H^{(0)}(\mu)$	$H^{(1)}(\mu)$	$H^{(2)}(\mu)$
0	1.00000	1.00000	1.00000	0.55	2.17098	1.02539	1.03586
0.05	1.14691	1.00430	1.01145	0.60	2.26650	1.02652	1.03679
0.10	1.26470	1.00786	1.01724	0.65	2.36162	1.02757	1.03761
0.15	1.37457	1.01089	1.02134	0.70	2.45639	1.02854	1.03836
0.20	1.48009	1.01352	1.02448	0.75	2.55085	1.02944	1.03904
0.25	1.58281	1.01582	1.02700	0.80	2.64503	1.03028	1.03966
0.30	1.68355	1.01785	1.02909	0.85	2.73899	1.03106	1.04024
0.35	1.78287	1.01968	1.03085	0.90	2.83274	1.03179	1.04076
0.40	1.88105	1.02132	1.03236	0.95	2.92631	1.03247	1.04125
0.45	1.97836	1.02280	1.03368	1.00	3.01973	1.03312	1.04170
0.50	2.07496	1.02415	1.03483				

TABLE 2

THE CONSTANTS DERIVED FROM THE EXACT FUNCTION, $H^{(0)}(\mu)$

$a_0 = 2.06088$	$q = 0.55835$
$a_1 = 1.19400$	$c = 0.71139$
$a_2 = 0.84940$	

TABLE 3

THE EXACT LAW OF DARKENING FOR AN ATMOSPHERE WITH A CONSTANT NET FLUX AND SCATTERING RADIATION IN ACCORDANCE WITH RAYLEIGH'S PHASE FUNCTION

μ	$I(0,\mu)/F$	$I(0,\mu)/I(0,1)$	μ	$I(0,\mu)/F$	$I(0,\mu)/I(0,1)$
0	0.41876	0.33116	0.55	0.90912	0.71893
0.05	.48028	.37981	0.60	0.94912	0.75056
.10	.52961	.41881	0.65	0.98896	0.78206
.15	.57562	.45520	0.70	1.02864	0.81345
.20	.61981	.49014	0.75	1.06820	0.84473
.25	.66282	.52416	0.80	1.10764	0.87592
.30	.70501	.55752	0.85	1.14698	0.90703
.35	.74660	.59041	0.90	1.18624	0.93808
.40	.78771	.62292	0.95	1.22543	0.96906
.45	.82846	.65514	1.00	1.26455	1.00000
0.50	0.86891	0.68791			

II. TRANSFER PROBLEMS WHICH INVOLVE RAYLEIGH SCATTERING AND IN WHICH THE POLARIZATION OF THE SCATTERED RADIATION IS ACCURATELY ALLOWED FOR

The problem of a semi-infinite plane-parallel atmosphere with a constant net flux πF. *The law of darkening in the two states of polarization.—*

$$I_l(0, \mu) = \tfrac{3}{8}F\frac{q}{\sqrt{2}}H_l(\mu)$$

and

$$I_r(0, \mu) = \tfrac{3}{8}F\frac{1}{\sqrt{2}}H_r(\mu)(\mu + c).$$

The law of diffuse reflection of a parallel beam of partially elliptically polarized light from a semi-infinite plane-parallel atmosphere.—

$$I(\mu, \varphi; \mu_0, \varphi_0) = \frac{3}{16\mu}Q\,[\boldsymbol{S}^{(0)}(\mu, \mu_0) + (1-\mu^2)^{\frac{1}{2}}(1-\mu_0^2)^{\frac{1}{2}}\boldsymbol{S}^{(1)}(\mu, \varphi; \mu_0, \varphi_0) + \boldsymbol{S}^{(2)}(\mu, \varphi; \mu_0, \varphi_0)]\,\boldsymbol{F}$$

and

$$V(\mu, \varphi; \mu_0, \varphi_0) = \tfrac{3}{8}V_0\,[-\mu\mu_0 H_v(\mu)H_v(\mu_0) + (1-\mu^2)^{\frac{1}{2}}(1-\mu_0^2)^{\frac{1}{2}}H_r(\mu)H_r(\mu_0)\cos(\varphi-\varphi_0)]\frac{\mu_0}{\mu+\mu_0},$$

where

$$\left(\frac{1}{\mu}+\frac{1}{\mu_0}\right)\boldsymbol{S}^{(0)}(\mu, \mu_0) =$$

$$\begin{pmatrix} 2H_l(\mu)H_l(\mu_0)[1-c(\mu+\mu_0)+\mu\mu_0] & qH_l(\mu)H_r(\mu_0)(\mu+\mu_0) & 0 \\ qH_r(\mu)H_l(\mu_0)(\mu+\mu_0) & H_r(\mu)H_r(\mu_0)[1+c(\mu+\mu_0)+\mu\mu_0] & 0 \\ 0 & 0 & 0 \end{pmatrix}$$

$$\left(\frac{1}{\mu}+\frac{1}{\mu_0}\right)\boldsymbol{S}^{(1)}(\mu, \varphi; \mu_0, \varphi_0) = H^{(1)}(\mu)H^{(1)}(\mu_0) \times \begin{pmatrix} -4\mu\mu_0\cos(\varphi-\varphi_0) & 0 & -2\mu\sin(\varphi-\varphi_0) \\ 0 & 0 & 0 \\ -2\mu_0\sin(\varphi-\varphi_0) & 0 & \cos(\varphi-\varphi_0) \end{pmatrix}$$

and

$$\left(\frac{1}{\mu}+\frac{1}{\mu_0}\right)\boldsymbol{S}^{(2)}(\mu, \varphi; \mu_0, \varphi_0) = H^{(2)}(\mu)H^{(2)}(\mu_0) \times \begin{pmatrix} \mu^2\mu_0^2\cos 2(\varphi-\varphi_0) & -\mu^2\cos 2(\varphi-\varphi_0) & \mu^2\mu_0\sin 2(\varphi-\varphi_0) \\ -\mu_0^2\cos 2(\varphi-\varphi_0) & \cos 2(\varphi-\varphi_0) & -\mu_0\sin 2(\varphi-\varphi_0) \\ \mu\mu_0^2\sin 2(\varphi-\varphi_0) & -\mu\sin 2(\varphi-\varphi_0) & -\mu\mu_0\cos 2(\varphi-\varphi_0) \end{pmatrix}.$$

The characteristic functions in terms of which $H_l(\mu)$, $H_r(\mu)$, $H_v(\mu)$, $H^{(1)}(\mu)$, and $H^{(2)}(\mu)$ are defined, are, respectively,

$$\Psi_l(\mu) = \tfrac{3}{4}(1-\mu^2) \qquad \Psi_r(\mu) = \tfrac{3}{8}(1-\mu^2); \qquad \Psi_v(\mu) = \tfrac{3}{4}\mu^2$$

and

$$\Psi^{(1)}(\mu) = \tfrac{3}{8}(1-\mu^2)(1+2\mu^2); \qquad \Psi^{(2)}(\mu) = \tfrac{3}{16}(1+\mu^2)^2.$$

The constants q and c are given by

$$q = 2\,\frac{4\,(A_1 + 2a_1) - 3\,(A_0 a_1 + A_1 a_0)}{3\,(A_1^2 + 2a_1^2)}$$

and

$$c = \frac{8\,(A_1 - a_1) + 3\,(2a_1 a_0 - A_1 A_0)}{3\,(A_1^2 + 2a_1^2)}\,,$$

where a_0, A_0, and a_1, A_1, are the moments of order 0 and 1 of $H_l(\mu)$ and $H_r(\mu)$, respectively. Further, the constants q and c are related according to

$$q^2 = 2\,(1 - c^2)\,.$$

TABLE 4

THE FUNCTIONS $H_l(\mu)$, $H_r(\mu)$, $H_v(\mu)$, $H^{(1)}(\mu)$, AND $H^{(2)}(\mu)$ OBTAINED AS SOLUTIONS OF THE EXACT FUNCTIONAL EQUATIONS

μ	$H_l(\mu)$	$H_r(\mu)$	$H_v(\mu)$	$H^{(1)}(\mu)$	$H^{(2)}(\mu)$
0	1.0000	1.00000	1.000000	1.00000	1.00000
0.05	1.1814	1.05737	1.020307	1.07301	1.04967
0.10	1.3255	1.09113	1.038341	1.12164	1.08621
0.15	1.4596	1.11703	1.054580	1.16151	1.11762
0.20	1.5884	1.13816	1.069338	1.19571	1.14552
0.25	1.7137	1.15594	1.082844	1.22577	1.17075
0.30	1.8367	1.17128	1.095250	1.25256	1.19383
0.35	1.9579	1.18468	1.106714	1.27674	1.21508
0.40	2.0778	1.19654	1.117346	1.29872	1.23476
0.45	2.1966	1.20713	1.127237	1.31882	1.25308
0.50	2.3146	1.21668	1.136467	1.33733	1.27019
0.55	2.4319	1.22532	1.145102	1.35444	1.28624
0.60	2.5486	1.23320	1.153203	1.37030	1.30132
0.65	2.6649	1.24042	1.160816	1.38507	1.31554
0.70	2.7807	1.24705	1.167989	1.39886	1.32895
0.75	2.8962	1.25318	1.174758	1.41179	1.34166
0.80	3.0113	1.25886	1.181158	1.42392	1.35371
0.85	3.1262	1.26414	1.187217	1.43533	1.36515
0.90	3.2408	1.26906	1.192967	1.44608	1.37601
0.95	3.3552	1.27366	1.198427	1.45625	1.38638
1.00	3.4695	1.27797	1.203620	1.46586	1.39625

TABLE 5

THE CONSTANTS DERIVED FROM THE EXACT FUNCTIONS, $H_l(\mu)$ AND $H_r(\mu)$

$a_0 = 2.29767$	$A_1 = 0.61733$
$A_0 = 1.19736$	$q = 0.68989$
$a_1 = 1.34864$	$c = 0.87294$

2. *Remarks on the computation of the* H*-functions; the accuracy of the tabulated solutions.*—We shall briefly indicate the procedure which was adopted in the solution of the various functional equations satisfied by $H(\mu)$.

First, we may observe that, as a general rule, the functional equation in the form (Paper XIV, eq. [171])

$$\frac{1}{H(\mu)} = \left\{\left[1 - 2\int_0^1 \Psi(\mu)\,d\mu\right]^{\frac{1}{2}} + \int_0^1 \frac{H(\mu')\,\Psi(\mu')}{\mu + \mu'}\,\mu'\,d\mu'\right\} \tag{3}$$

was found more suitable for purposes of iteration than the equation in its original form.

The solution was generally started with the third approximation for $H(\mu)$ in terms of the Gaussian division and characteristic roots. (In conservative cases [cf. Paper XIV, p. 190] the fourth approximation was available.) The first iteration was performed with this approximate solution for $H(\mu)$ in accordance with equation (3), evaluating the integral on the right-hand side for various values of μ. It was found that in most cases the first iterate had to be obtained for steps of 0.05 over the entire interval $0 \leqslant \mu \leqslant 1$. However, in the second and the following iterations, it was sufficient to evaluate the iterate for fewer and fewer values of the argument, since for the intermediate values the

TABLE 6

THE EXACT LAWS OF DARKENING IN THE TWO STATES OF POLARIZATION FOR AN ELECTRON-SCATTERING ATMOSPHERE; DEGREE OF POLARIZATION OF THE EMERGENT RADIATION

μ	I_l/F	I_r/F	I/F	LAW OF DARKENING IN STATE OF POLARIZATION		DEGREE OF POLARIZATION
				l	r	
0	0.18294	0.23147	0.41441	0.28823	0.36470	0.11713
0.05	.21613	.25877	0.47490	0.34053	0.40771	.08979
0.10	.24247	.28150	0.52397	0.38203	0.44352	.07448
0.15	.26702	.30299	0.57001	0.42070	0.47739	.06311
0.20	.29057	.32381	0.61439	0.45782	0.51019	.05410
0.25	.31350	.34420	0.65770	0.49394	0.54231	.04667
0.30	.33599	.36429	0.70029	0.52939	0.57397	.04041
0.35	.35817	.38417	0.74234	0.56432	0.60529	.03502
0.40	.38010	.40388	0.78398	0.59888	0.63634	.03033
0.45	.40184	.42346	0.82530	0.63313	0.66719	.02619
0.50	.42343	.44294	0.86637	0.66714	0.69788	.02252
0.55	.44489	.46233	0.90722	0.70095	0.72844	.01923
0.60	.46624	.48165	0.94789	0.73459	0.75888	.01627
0.65	.48750	.50092	0.98842	0.76809	0.78924	.01358
0.70	.50869	.52013	1.02882	0.80147	0.81950	.011123
0.75	.52981	.53930	1.06911	0.83475	0.84971	.008880
0.80	.55087	.55844	1.10931	0.86794	0.87986	.006818
0.85	.57189	.57754	1.14943	0.90105	0.90996	.004919
0.90	.59286	.59661	1.18947	0.93409	0.94001	.003155
0.95	.61379	.61566	1.22945	0.96707	0.97002	0.001522
1.00	0.63469	0.63469	1.26938	1.00000	1.00000	0

function could be predicted with accuracy by interpolating among the differences between the successive iterates. The process of iteration was continued until the function did not change within the limits of the accuracy of the calculations.

The numerical computations were carried out in all stages with at least six-figure accuracy. It is believed that in the tabulated solutions errors exceeding two (and in rare cases three) units in the last place retained are unlikely.

It may be further stated that, as a check on the accuracy attained at each stage of the iteration, the integral

$$\int_0^1 H(\mu)\Psi(\mu)\,d\mu) \tag{4}$$

was evaluated numerically and compared with its exact value (Paper XIV, eq. [165]),

$$1-\left[1-2\int_0^1 \Psi(\mu)\,d\mu\right]^{\frac{1}{2}}. \tag{5}$$

In conservative cases the further integral (Paper XIV, eq. [177]),

$$\int_0^1 H(\mu)\Psi(\mu)\,\mu d\mu = \left[2\int_0^1 \Psi(\mu)\,\mu^2 d\mu\right]^{\frac{1}{2}}, \tag{6}$$

was also used. In Table 7 we exhibit this comparision between the various integrals evaluated with the aid of the tabulated functions and their exact values. It is seen that the agreement between the two sets of values confirms our estimate of the accuracy of the tabulated solutions.

TABLE 7

COMPARISON OF THE VALUES OF CERTAIN INTEGRALS EVALUATED WITH THE AID OF THE TABULATED FUNCTIONS WITH THEIR EXACT VALUES

Case	Integral	Exact Value	Value Found Numerically
I.....	$\frac{3}{16}\int_0^1 H^{(0)}(\mu)(3-\mu^2)\,d\mu$	1.00000	0.99998
	$\frac{3}{16}\int_0^1 H^{(0)}(\mu)(3-\mu^2)\,\mu d\mu$	$\sqrt{0.3} = 0.5477226$	0.547735
	$\frac{3}{8}\int_0^1 H^{(1)}(\mu)\,\mu^2(1-\mu^2)\,d\mu$	$1-\sqrt{0.9} = 0.05131670$	0.051317
	$\frac{3}{32}\int_0^1 H^{(2)}(\mu)(1-\mu^2)^2 d\mu$	$1-\sqrt{0.9} = 0.05131670$	0.051316
II...	$\int_0^1 H_l(\mu)(1-\mu^2)\,d\mu$	$\frac{4}{3} = 1.333333$	1.3332
	$\int_0^1 H_l(\mu)(1-\mu^2)\,\mu d\mu$	$\frac{4}{3}\sqrt{0.2} = 0.5962848$	0.59628
	$\frac{3}{8}\int_0^1 H_r(\mu)(1-\mu^2)\,d\mu$	$1-\frac{1}{\sqrt{2}} = 0.2928932$	0.29288
	$\frac{3}{4}\int_0^1 H_v(\mu)\,\mu^2 d\mu$	$1-\frac{1}{\sqrt{2}} = 0.2928932$	0.292893
	$\frac{3}{8}\int_0^1 H^{(1)}(\mu)(1-\mu^2)(1+2\mu^2)\,d\mu$	$1-\sqrt{0.3} = 0.45227744$	0.45226
	$\frac{3}{16}\int_0^1 H^{(2)}(\mu)(1+\mu^2)^2 d\mu$	$1-\sqrt{0.3} = 0.45227744$	0.45227

ON THE RADIATIVE EQUILIBRIUM OF A STELLAR ATMOSPHERE XVII

S. CHANDRASEKHAR
Yerkes Observatory
Received February 25, 1947

ABSTRACT

In this paper a systematic study is made of the various functional equations which characterize the transfer problems in plane-parallel atmospheres.

First, a functional equation relating the angular distribution of the emergent radiation from a semi-infinite atmosphere and the law of diffuse reflection by the same atmosphere is derived. This equation arises in consequence of the invariance of the emergent radiation from a semi-infinite atmosphere to the addition (or removal) of layers of arbitrary optical thickness to (or from) the atmosphere. Next, four functional equations governing the problem of transmission and diffuse reflection by an atmosphere of finite optical thickness are formulated. These equations have been derived under very general conditions; and they have been further reduced to a basic system of functional equations for the case in which scattering takes place in accordance with a phase function expressible as a series in Legendre polynomials. And, finally, further functional equations are formulated which determine the radiation field in the interior in terms of the scattering and transmission functions of atmospheres of finite optical thicknesses.

1. *Introduction.*—In the study of the transfer of radiation in stellar atmospheres the two basic problems are, first, the radiative equilibrium of a semi-infinite atmosphere with a constant net flux and, second, the law of diffuse reflection by the same atmosphere. It is, of course, apparent that the first of these problems is significant only in conservative cases; for in all other cases the equation of transfer will not admit the integral which insures the constancy of the net flux through the atmosphere.

In the problem of a semi-infinite atmosphere with a constant net flux, the radiation field will be axially symmetrical at each point about the direction normal to the plane of stratification, and greatest interest is attached to the *law of darkening*,

$$I(0, \mu) \qquad (0 \leqslant \mu \leqslant 1), \quad (1)$$

which expresses the angular distribution of the emergent radiation. On the other hand, in the problem of diffuse reflection, our principal interest is in the intensity,

$$I(\mu, \varphi; \mu_0, \varphi_0), \quad (2)$$

diffusely reflected in the direction (μ, φ) when a parallel beam of radiation of net flux πF per unit area normal to itself is incident on the atmosphere in the direction $(-\mu_0, \varphi_0)$. This *reflected intensity* is generally expressed in terms of a *scattering function* $S(\mu, \varphi; \mu_0, \varphi_0)$ in the form

$$I(\mu, \varphi; \mu_0, \varphi_0) = \frac{1}{4\mu} S(\mu, \varphi; \mu_0, \varphi_0) F. \quad (3)$$

When the polarization of the scattered radiation has also to be allowed for, then, in the problem with a constant net flux, we must distinguish between the intensities I_l and I_r in the two states of polarization in which the electric vector vibrates in the meridian plane and at right angles to it, respectively. Correspondingly, in the problem of diffuse reflection we must consider a *scattering matrix*, $\mathbf{S}(\mu, \varphi; \mu_0, \varphi_0)$, defined suitably (cf. Papers XIII and XIV[1]).

Explicit solutions for the two basic problems have been found under a variety of con-

[1] *Ap. J.*, **105**, 151 (eq. [63]), and 164 (eq. [19]), 1947.

ditions in the earlier papers of this series.[2] And an examination of these solutions reveals certain remarkable relationships between the angular distribution of the emergent radiation in the problem with a constant net flux and the law of diffuse reflection. The relationship is naturally the simplest in the case of isotropic scattering, when[3]

$$I(0, \mu) = \frac{\sqrt{3}}{4} FH(\mu) \tag{4}$$

and

$$\left(\frac{1}{\mu}+\frac{1}{\mu_0}\right) S(\mu, \mu_0) = H(\mu) H(\mu_0), \tag{5}$$

where $H(\mu)$ satisfies the functional equation,

$$H(\mu) = 1 + \tfrac{1}{2}\mu H(\mu) \int_0^1 \frac{H(\mu')}{\mu+\mu'} d\mu'. \tag{6}$$

In the other cases the relationship is of a much more complex nature and has to be sought between the darkening function and the *azimuth independent* term,

$$S^{(0)}(\mu, \mu_0) = \frac{1}{2\pi} \int_0^{2\pi} S(\mu, \varphi; \mu_0, \varphi_0)\, d\varphi, \tag{7}$$

in the law of diffuse reflection.[4] The question now arises as to the origin and meaning of this relationship. While it should, in principle, be possible to go back to the original equations of transfer and derive the relationships in question as integrals of the problem, it would seem, in view of the complex nature of the relationships to be established, that such a procedure would not disclose the *physical* origin of the relationships. However, in this paper we shall show that there is an alternative way of looking at the problem which enables us to obtain in a simple way a functional equation relating $I(0, \mu)$ and $S^{(0)}(\mu, \mu_0)$. As we shall see, this functional equation arises essentially from the invariance of $I(0, \mu)$ to the addition (or removal) of layers of arbitrary thickness to (or from) the atmosphere. And it is to this invariance that we should attribute the relationship between the two basic problems.

The ideas leading to the establishment of the functional equation that we have just mentioned enable us to formulate further functional equations, which together appear to characterize the problems of radiative transfer in plane-parallel atmospheres (both finite and semi-infinite) in their entirety. In §§ 5–8 of this paper these other functional equations of the problem are derived.

I. THE FUNCTIONAL EQUATION RELATING THE LAW OF DARKENING AND THE SCATTERING FUNCTION FOR SEMI-INFINITE PLANE-PARALLEL ATMOSPHERES

2. *The functional equation relating* $I(0, \mu)$ *and* $S^{(0)}(\mu, \mu_0)$.—Considering, first, the case in which the scattering of radiation is described simply in terms of a phase function $p(\cos\Theta)$, we shall suppose that

$$p(\cos\Theta) = \Sigma \varpi_l P_l(\cos\Theta), \tag{8}$$

where ϖ_l's are constants and

$$\varpi_0 = 1, \tag{9}$$

[2] See esp. Paper XVI (*Ap. J.*, **105**, 435, 1947), where the solutions for the important cases of Rayleigh phase function and Rayleigh scattering are tabulated.

[3] Cf. Papers VIII (*Ap. J.*, **101**, 348, 1945) and XIV (*ibid.*, **105**, 164, eqs. [178]–[183]).

[4] When polarization is taken into account, we must consider the corresponding matrix, $\mathbf{S}^{(0)}(\mu, \mu_0)$ (see eq. [51], below).

to insure the constancy of the net flux through the atmosphere. For this case the equation of transfer for the problem with a constant net flux (and no incident radiation) can be expressed in the form

$$\mu \frac{dI(\tau, \mu)}{d\tau} = I(\tau, \mu) - \frac{1}{2}\int_{-1}^{+1} j(\mu, \mu') I(\tau, \mu')\, d\mu', \tag{10}$$

where

$$j(\mu, \mu') = \Sigma \varpi_l P_l(\mu) P_l(\mu') \tag{11}$$

is a symmetrical function in the variables μ and μ'.

We shall find it convenient to re-write equation (10) in the form

$$\mu \frac{dI(\tau, \mu)}{d\tau} = I(\tau, \mu) - B(\tau, \mu), \tag{12}$$

where the source function

$$B(\tau, \mu) = \frac{1}{2}\int_{-1}^{+1} j(\mu, \mu') I(\tau, \mu')\, d\mu'. \tag{13}$$

Now consider the radiation at a depth $d\tau$ below the boundary of the atmosphere at $\tau = 0$. The radiation field at this level, which is directed *inward*, can be inferred from the equation of transfer (12); for, since at $\tau = 0$ there is no incident intensity, at the level $d\tau$ we must have an inward intensity,

$$I(d\tau, -\mu') = \frac{1}{\mu'} B(0, -\mu')\, d\tau, \tag{14}$$

in the direction $-\mu'$. This inward-directed radiation will be reflected by the atmosphere below $d\tau$ by the law of diffuse reflection of a semi-infinite plane-parallel atmosphere. If this law is expressed in the form (3), the reflection of the radiation (14) will contribute to the *outward* intensity at the level $d\tau$, the amount

$$\frac{d\tau}{4\pi\mu}\int_0^1\int_0^{2\pi} S(\mu, \varphi; \mu', \varphi') B(0, -\mu') \frac{d\mu'}{\mu'}\, d\varphi', \tag{15}$$

or, in view of the axial symmetry of $B(0, -\mu')$,

$$\frac{d\tau}{2\mu}\int_0^1 S^{(0)}(\mu, \mu') B(0, -\mu') \frac{d\mu'}{\mu'}, \tag{16}$$

where $S^{(0)}(\mu, \mu')$ is defined as in equation (7).

Now *the outward intensity* $I(d\tau, \mu)$ *at the level* $d\tau$ *can differ from* $I(0, \mu)$ *only by the amount* (*16*); for the intensity and the angular distribution of the emergent radiation from a semi-infinite plane-parallel atmosphere cannot be altered by the removal (or addition) of layers of arbitrary optical thickness from (or to) the atmosphere. Consequently, the removal of the layers above the level $d\tau$ must restore $I(d\tau, \mu)$ to $I(0, \mu)$. We must therefore have

$$I(d\tau, \mu) = I(0, \mu) + \frac{d\tau}{2\mu}\int_0^1 S^{(0)}(\mu, \mu') B(0, -\mu') \frac{d\mu'}{\mu'}. \tag{17}$$

On the other hand, from the equation of transfer (12), we can directly conclude that

$$\left.\begin{aligned} I(d\tau, \mu) &= I(0, \mu) + d\tau \left(\frac{dI}{d\tau}\right)_{\tau=0} \\ &= I(0, \mu) + \frac{d\tau}{\mu}[I(0, \mu) - B(0, \mu)]. \end{aligned}\right\} \tag{18}$$

Combining equations (17) and (18) and passing to the limit $d\tau = 0$, we obtain

$$I(0, \mu) = B(0, \mu) + \frac{1}{2}\int_0^1 S^{(0)}(\mu, \mu') B(0, -\mu') \frac{d\mu'}{\mu'}. \tag{19}$$

But, according to equation (13),

$$B(0, \mu) = \frac{1}{2}\int_0^1 j(\mu, \mu'') I(0, \mu'') d\mu''. \tag{20}$$

Using this expression for $B(0, \mu)$ in equation (19), we have

$$\left.\begin{aligned} I(0, \mu) = {} & \frac{1}{2}\int_0^1 j(\mu, \mu'') I(0, \mu'') d\mu'' \\ & + \frac{1}{4}\int_0^1\int_0^1 S^{(0)}(\mu, \mu') j(-\mu', \mu'') I(0, \mu'') \frac{d\mu'}{\mu'} d\mu''. \end{aligned}\right\} \tag{21}$$

Finally, substituting for $j(\mu, \mu')$ according to equation (11), we find

$$\left.\begin{aligned} I(0, \mu) = {} & \frac{1}{2}\sum_l \varpi_l \left[\int_0^1 P_l(\mu') I(0, \mu') d\mu'\right] \\ & \times \left[P_l(\mu) + (-1)^l \frac{1}{2}\int_0^1 S^{(0)}(\mu, \mu') P_l(\mu') \frac{d\mu'}{\mu'}\right]. \end{aligned}\right\} \tag{22}$$

Equation (22) is a functional equation relating $I(0, \mu)$ and $S^{(0)}(\mu, \mu')$; and it is apparent how this equation will determine $I(0, \mu)$ uniquely in terms of $S^{(0)}(\mu, \mu')$, and conversely

3. *Illustrations of the functional equation (22).*—We shall illustrate equation (22) by considering, first, the case of isotropic scattering. In this case

$$\varpi_0 = 1, \quad \text{and} \quad \varpi_l = 0 \quad (l \neq 0), \tag{23}$$

and (cf. eq. [5])

$$\left(\frac{1}{\mu} + \frac{1}{\mu'}\right) S^{(0)}(\mu, \mu') = H(\mu) H(\mu'), \tag{24}$$

and equation (22) reduces to

$$I(0, \mu) = \left[\frac{1}{2}\int_0^1 I(0, \mu') d\mu'\right]\left[1 + \tfrac{1}{2}\mu H(\mu)\int_0^1 \frac{H(\mu')}{\mu + \mu'} d\mu'\right]. \tag{25}$$

Using equation (6), satisfied by $H(\mu)$, we find the foregoing equation to be

$$I(0, \mu) = \left[\frac{1}{2}\int_0^1 I(0, \mu') d\mu'\right] H(\mu). \tag{26}$$

It is seen that equation (26) is consistent with itself, since, according to Paper XIV, equation (180),

$$\int_0^1 H(\mu) d\mu = 2. \tag{27}$$

We may therefore write

$$I(0, \mu) = \text{constant } H(\mu) \tag{28}$$

and determine the constant of proportionality from the condition

$$2\int_0^1 I(0, \mu)\, \mu d\mu = F. \tag{29}$$

We find in this manner that (cf. Paper XIV, eqs. [182]–[183])

$$I(0, \mu) = \frac{\sqrt{3}}{4} FH(\mu), \tag{30}$$

in agreement with equation (4).

As a second illustration of equation (22), we shall consider the case of scattering in accordance with Rayleigh's phase function. In this case

$$\varpi_0 = 1, \quad \varpi_2 = \tfrac{1}{2}, \quad \text{and} \quad \varpi_l = 0 \qquad (l \neq 0, 2), \tag{31}$$

and equation (22) reduces to

$$\left.\begin{aligned} I(0, \mu) = {} & \frac{1}{2}\Big[\int_0^1 I(0, \mu')\, d\mu'\Big]\Big[1 + \frac{1}{2}\int_0^1 S^{(0)}(\mu, \mu')\frac{d\mu'}{\mu'}\Big] \\ & + \frac{1}{16}\Big[\int_0^1 I(0, \mu')(3\mu'^2 - 1)\, d\mu'\Big] \\ & \times \Big[3\mu^2 - 1 + \frac{1}{2}\int_0^1 S^{(0)}(\mu, \mu')(3\mu'^2 - 1)\frac{d\mu'}{\mu'}\Big]. \end{aligned}\right\} \tag{32}$$

Also, for this case (Paper XIV, eqs. [231] and [246] or Paper XVI, Sec. II),

$$\left(\frac{1}{\mu} + \frac{1}{\mu'}\right) S^{(0)}(\mu, \mu') = \tfrac{3}{8} H^{(0)}(\mu) H^{(0)}(\mu')[3 - c(\mu + \mu') + \mu\mu'], \tag{33}$$

where $H^{(0)}(\mu)$ is defined in terms of the functional equation (cf. Paper XIV, eq. [253]),

$$H^{(0)}(\mu) = 1 + \tfrac{3}{16}\mu H^{(0)}(\mu)\int_0^1 \frac{H^{(0)}(\mu')}{\mu + \mu'}(3 - \mu'^2)\, d\mu', \tag{34}$$

and

$$c = \frac{a_2}{a_1}, \tag{35}$$ [5]

a_2 and a_1 being the moments of order 1 and 2 of $H^{(0)}(\mu)$.

Inserting the reflection function (33) in equation (32), we find, after some reductions in which repeated use is made of Paper XIV, equations (254)–(256), that

$$\left.\begin{aligned} I(0, \mu) = {} & \tfrac{3}{16}(3A_0 - A_2) H^{(0)}(\mu) \\ & + \tfrac{3}{32}[-2A_0a_2 + 3A_2a_1^2 + 3A_2a_2(2 - a_0)]\frac{1}{a_1}\mu H^{(0)}(\mu), \end{aligned}\right\} \tag{36}$$

where A_0 and A_2 are the (unknown!) moments of order 0 and 2 of $I(0, \mu)$.

The constants A_0 and A_2 in equation (36) can be determined by taking the zero and second moments of this equation. We find that

$$A_0 = \tfrac{3}{16}(3A_0 - A_2)a_0 + \tfrac{3}{32}[-2A_0a_2 + 3A_2a_1^2 + 3A_2a_2(2 - a_0)] \tag{37}$$

and

$$A_2 = \tfrac{3}{16}(3A_0 - A_2)a_2 + \tfrac{3}{32}[-2A_0a_2 + 3A_2a_1^2 + 3A_2a_2(2 - a_0)]\frac{a_3}{a_1}. \tag{38}$$

[5] In Paper XIV the constant c was defined somewhat differently (cf. eq. [264]). But, since the discriminant of eq. (262) vanishes, we could equally well have written

$$c = \frac{9a_0 - 16}{3a_1}.$$

Using the relation $9a_0 - 3a_2 = 16$ (Paper XIV, eq. [254]) in this equation for c, we obtain formula (35).

These equations determine A_0 and A_2. However, a simple inspection shows that

$$\frac{A_0}{a_0} = \frac{A_2}{a_2} = \text{constant} \tag{39}$$

satisfies equations (37) and (38); for (cf. Paper XIV, eqs. [254] and [255])

$$3a_0 - a_2 = \tfrac{16}{3}\,, \tag{40}$$

and

$$\left.\begin{aligned} -2a_0a_2 + 3a_2a_1^2 + 3a_2^2(2-a_0) &= a_2[-2a_0 + 3a_1^2 + (9a_0 - 16)(2-a_0)] \\ &= a_2[3a_1^2 - 9a_0^2 + 32(a_0 - 1)] = 0\,. \end{aligned}\right\} \tag{41}$$

Hence,

$$I(0, \mu) = \text{constant } H^{(0)}(\mu)\,; \tag{42}$$

and the constant of proportionality can again be determined from the flux condition (29). In this manner we find that

$$I(0, \mu) = \frac{1}{2a_1} FH^{(0)}(\mu)\,, \tag{43}$$

in agreement with Paper XIV, equation (274).

4. *The functional equations relating the laws of darkening and diffuse reflection in cases in which the polarization of the scattered radiation is taken into account.*—As sufficiently illustrative of the general problem, we shall consider the case of Rayleigh scattering for which the general equations of transfer have already been formulated in earlier papers.[6] However, in our present context we require the equations of transfer for the case of axial symmetry when it is sufficient to distinguish only between the intensities I_l and I_r in the two states of polarization in which the electric vector vibrates in the meridian plane and at right angles to it, respectively.[7] And the equations of transfer relevant to this problem have been derived in Paper X (eqs. [37] and [38]). For our present purposes it is convenient to combine these equations into a single vector equation, considering $I_l(\tau, \mu)$ and $I_r(\tau, \mu)$ as the components of a *two*-dimensional vector,

$$\boldsymbol{I} = (I_l, I_r)\,. \tag{44}$$

The equation of transfer (Paper X, eqs. [37] and [38]) for I_l and I_r can then be expressed in the form (cf. Paper XIV, eqs. [10] and [15])

$$\mu \frac{d\boldsymbol{I}}{d\tau} = \boldsymbol{I}(\tau, \mu) - \frac{3}{8}\int_{-1}^{+1} \boldsymbol{J}(\mu, \mu')\boldsymbol{I}(\tau, \mu')\, d\mu'\,, \tag{45}$$

where $\boldsymbol{J}(\mu, \mu')$ denotes the matrix,

$$\boldsymbol{J}(\mu, \mu') = \begin{pmatrix} 2(1-\mu^2)(1-\mu'^2) + \mu^2\mu'^2 & \mu^2 \\ \mu'^2 & 1 \end{pmatrix}. \tag{46}$$

Introducing the source function,

$$\boldsymbol{B}(\tau, \mu) = \frac{3}{8}\int_{-1}^{+1} \boldsymbol{J}(\mu, \mu')\boldsymbol{I}(\tau, \mu')\, d\mu'\,, \tag{47}$$

[6] Papers X (*Ap. J.*, **103**, 351, 1946), XI (*ibid.*, **104**, 110, 1946), XIII (*ibid.*, **105**, 151, 1947), XIV (*ibid.*, p. 164), and XV (*ibid.*, p. 424).

[7] The other Stokes parameters, $U = (I_l - I_r)\tan 2\chi$ and $V = (I_l - I_r)\sec 2\chi \tan 2\beta$ are identically zero for the problem with a constant net flux.

we can re-write equation (45) in the form

$$\mu \frac{d\boldsymbol{I}}{d\tau} = \boldsymbol{I}(\tau, \mu) - \boldsymbol{B}(\tau, \mu). \tag{48}$$

To derive the functional equation for $\boldsymbol{I}(0, \mu)$, we proceed exactly as in § 2 by considering the radiation field at a level $d\tau$ below the boundary of the atmosphere at $\tau = 0$. At this level there will be an inward intensity, of amount

$$\frac{d\tau}{\mu'} \boldsymbol{B}(0, \mu'), \tag{49}$$

in the direction $-\mu'$. On account of the axial symmetry of this field and the consequent vanishing of the component U, the radiation (49) will be reflected by the atmosphere below $d\tau$ in accordance with the two-dimensional scattering matrix (cf. Paper XVI, § 3),

$$\frac{3}{16\mu} \boldsymbol{S}^{(0)}(\mu, \mu'), \tag{50}$$

where

$$\left(\frac{1}{\mu}+\frac{1}{\mu'}\right) \boldsymbol{S}^{(0)}(\mu, \mu') = \begin{pmatrix} 2H_l(\mu) H_l(\mu') [1 - c(\mu+\mu') + \mu\mu'] & qH_l(\mu) H_r(\mu') (\mu+\mu') \\ qH_r(\mu) H_l(\mu') (\mu+\mu') & H_r(\mu) H_r(\mu') [1 + c(\mu+\mu') + \mu\mu'] \end{pmatrix}. \tag{51}$$

(The definitions of the various quantities occurring on the right-hand side of the foregoing equation will be found in Paper XIV, Part II).

The reflection of the radiation (49) by the atmosphere below $d\tau$ will, accordingly, contribute to the outward intensity, $\boldsymbol{I}(d\tau, \mu)$, at the level $d\tau$, the amount

$$\frac{3}{8\mu} d\tau \int_0^1 \boldsymbol{S}^{(0)}(\mu, \mu') \boldsymbol{B}(0, -\mu') \frac{d\mu'}{\mu'}. \tag{52}$$

Again, from the invariance of $\boldsymbol{I}(0, \mu)$ to the removal (or addition) of layers of arbitrary thickness from (or to) the atmosphere, we conclude that $\boldsymbol{I}(d\tau, \mu)$ can differ from $\boldsymbol{I}(0, \mu)$ only by the amount (52). Hence,

$$\boldsymbol{I}(d\tau, \mu) = \boldsymbol{I}(0, \mu) + \frac{3}{8\mu} d\tau \int_0^1 \boldsymbol{S}^{(0)}(\mu, \mu') \boldsymbol{B}(0, -\mu') \frac{d\mu'}{\mu'}. \tag{53}$$

On the other hand, from the equation of transfer we directly find that

$$\boldsymbol{I}(d\tau, \mu) = \boldsymbol{I}(0, \mu) + \frac{d\tau}{\mu} [\boldsymbol{I}(0, \mu) - \boldsymbol{B}(0, \mu)]. \tag{54}$$

Combining equations (53) and (54) and passing to the limit $d\tau = 0$, we obtain

$$\boldsymbol{I}(0, \mu) = \boldsymbol{B}(0, \mu) + \frac{3}{8} \int_0^1 \boldsymbol{S}^{(0)}(\mu, \mu') \boldsymbol{B}(0, -\mu') \frac{d\mu'}{\mu'}. \tag{55}$$

Finally, substituting for $\boldsymbol{B}(0, \mu)$ according to equation (47) in equation (55), we have

$$\left.\begin{aligned} \boldsymbol{I}(0, \mu) = \frac{3}{8}\Big[& \int_0^1 J(\mu, \mu') \boldsymbol{I}(0, \mu') \, d\mu' \\ & + \frac{3}{8} \int_0^1 \int_0^1 \boldsymbol{S}^{(0)}(\mu, \mu') J(-\mu', \mu'') \boldsymbol{I}(0, \mu'') \frac{d\mu'}{\mu'} \, d\mu'' \Big]. \end{aligned}\right\} \tag{56}$$

This is the required functional equation relating $\boldsymbol{I}(0, \mu)$ and $\boldsymbol{S}^{(0)}(\mu, \mu')$.

It should, of course, be possible to deduce the solution for $I(0, \mu)$ from the known form of $S^{(0)}(\mu, \mu')$. The necessary calculations are likely to be somewhat tedious, since it is not too easy even to verify that the solution (Paper XIV, eqs. [119] and [120])

$$I(0, \mu) = \frac{3}{8\sqrt{2}} F \begin{pmatrix} qH_l(\mu) \\ H_r(\mu)(\mu + c) \end{pmatrix} \tag{57}$$

actually satisfies equation (56). Thus, for $I(0, \mu)$ given by equation (57),

$$B(0, \mu) = \frac{3}{8\sqrt{2}} F \begin{pmatrix} q(1 - \mu^2) + c\mu^2 \\ c \end{pmatrix}, \tag{58}$$

and the validity of equation (56) requires that the equation

$$\begin{pmatrix} qH_l(\mu) \\ H_r(\mu)(\mu + c) \end{pmatrix} = \begin{pmatrix} q(1 - \mu^2) + c\mu^2 \\ c \end{pmatrix} + \tfrac{3}{8}\mu \int_0^1 \frac{d\mu'}{\mu + \mu'} \times \begin{pmatrix} 2H_l(\mu) H_l(\mu')[1 - c(\mu + \mu') + \mu\mu'] & qH_l(\mu) H_r(\mu')(\mu + \mu') \\ qH_r(\mu) H_l(\mu')(\mu + \mu') & H_r(\mu) H_r(\mu')[1 - c(\mu + \mu') + \mu\mu'] \end{pmatrix} \times \begin{pmatrix} q(1 - \mu'^2) + c\mu'^2 \\ c \end{pmatrix} \tag{5}$$

be true. By a series of reductions, in which the various integral properties[8] of the functions $H_l(\mu)$ and $H_r(\mu)$ are used repeatedly it can be shown that this is indeed the case. But we shall not go into the details of these reductions here.

II. FUNCTIONAL EQUATIONS FOR TRANSFER PROBLEMS IN PLANE-PARALLEL ATMOSPHERES

5. *Functional equations for the problem of transmission and diffuse reflection by a plane-parallel atmosphere of finite optical thickness.*—In Paper XIV we formulated the functional equation satisfied by the scattering matrix in the problem of diffuse reflection, on Rayleigh's law, by a semi-infinite plane-parallel atmosphere. The corresponding functional equation for the case of scattering according to a general phase function (but not allowing for the polarization of the scattered radiation) had been derived earlier by V. A. Ambarzumian.[9] The principle underlying the derivation of these functional equations is the invariance, first pointed out byAmbarzumian, of the intensity and the angular distribution of the reflected light to the addition (or removal) of layers of arbitrary optical thickness to (or from) the atmosphere. It is apparent that similar functional equations must govern the problem of transmission and reflection by a plane-parallel atmosphere of finite optical thickness, τ_1 (say). This possibility has, indeed, been envisaged by Ambarzumian,[10] who stated that the required functional equations can be obtained from the invariance of the reflected and the transmitted light to the addition of a layer of a certain optical thickness to the atmosphere above $\tau = 0$ and the *simultaneous* removal of a layer of equal optical thickness from the atmosphere, below, at $\tau = \tau_1$. This invariance will lead to two functional equations governing the intensities and the angular distributions of the reflected and the transmitted radiations. Ambarzumian has, in fact, written down these two equations for the case of isotropic scattering.[11] However, on consideration it

[8] Cf. Paper XIV, §§ 7 and 8.

[9] *J. Phys. Acad. Sc. U.S.S.R.*, **8**, 64, 1944.

[10] *C.R.* (Doklady) *Acad. d. Sc. U.R.S.S.*, **38**, 229, 1943.

[11] *Ibid.*, eqs. (8) and (9). The derivation of these equations is not given in this short note. However, from the details of the treatment of the semi-infinite case, which are given, it is not difficult to reconstruct the proof that the author probably had in mind. The present writer has been unable to trace any later publication in which Ambarzumian has returned to these matters.

appears that the two functional equations which can be derived from the invariance referred to by Ambarzumian are not sufficient to characterize the problem completely. Actually, it would seem that four equations are necessary to make the problem determinate, and we shall show how these four equations arise by considering in detail the case of scattering according to a general phase function. The modifications required to include the polarization of the scattered radiation will be indicated later.

The equation of transfer for the problem of diffuse reflection by a plane-parallel atmosphere can be written in the form[12]

$$\mu \frac{dI(\tau, \mu, \varphi)}{d\tau} = I(\tau, \mu, \varphi) - B(\tau, \mu, \varphi), \tag{60}$$

where the source function $B(\tau, \mu, \varphi)$ is given by

$$\left.\begin{aligned} B(\tau, \mu, \varphi) = \frac{1}{4\pi} \int_{-1}^{+1} \int_{0}^{2\pi} p(\mu, \varphi; \mu', \varphi') I(\tau, \mu', \varphi') \, d\mu' d\varphi' \\ + \tfrac{1}{4} F e^{-\tau/\mu_0} p(\mu, \varphi; -\mu_0, \varphi_0), \end{aligned}\right\} \tag{61}$$

when a parallel beam of radiation of flux πF per unit area normal to itself is incident on the atmosphere in the direction $(-\mu_0, \varphi_0)$. In equation (61), $p(\mu, \varphi; \mu', \varphi')$ is the phase function governing the probability that the radiation in the direction (μ', φ') will be scattered in the direction (μ, φ).

We shall suppose that the optical thickness of the atmosphere is τ_1. We shall then be interested not only in the intensity $I(0, \mu, \varphi)$, $(0 \leqslant \mu \leqslant 1)$, reflected by the atmosphere in the direction (μ, φ), but also in the intensity $I(\tau_1, \mu, \varphi)$ transmitted in the direction $(-\mu, \varphi)$.[13] We shall express these intensities in the forms

$$I(0, \mu, \varphi) = \frac{1}{4\mu} FS(\tau_1; \mu, \varphi; \mu_0, \varphi_0) \tag{62}$$

and

$$I(\tau_1, \mu, \varphi) = \frac{1}{4\mu} FT(\tau_1; \mu, \varphi; \mu_0, \varphi_0), \tag{63}$$

to emphasize the fact that we are considering the reflection and transmission by an atmosphere of optical thickness τ_1.

Now consider the radiation field present at a depth $d\tau$ below the boundary of the atmosphere at $\tau = 0$. At this level there will be the incident flux, reduced to the amount

$$\pi F \left(1 - \frac{d\tau}{\mu_0}\right), \tag{64}$$

and a diffuse radiation field. The intensity in this latter diffuse field, which is directed inward, can be inferred from the equation of transfer: for, since at $\tau = 0$ there is no inward intensity, at the level $d\tau$ we must have the intensity

$$\frac{d\tau}{\mu'} B(0, -\mu', \varphi') \tag{65}$$

in the direction $(-\mu', \varphi')$. Both the radiation fields (64) and (65) will be reflected by the atmosphere of optical thickness $\tau_1 - d\tau$ below $d\tau$ and will contribute

$$\left.\begin{aligned} \frac{F}{4\mu}\left(1 - \frac{d\tau}{\mu_0}\right) S(\tau_1 - d\tau; \mu, \varphi; \mu_0, \varphi_0) \\ + \frac{d\tau}{4\pi\mu} \int_0^1 \int_0^{2\pi} S(\tau_1 - d\tau; \mu, \varphi; \mu', \varphi') B(0, -\mu', \varphi') \frac{d\mu'}{\mu'} d\varphi' \end{aligned}\right\} \tag{66}$$

[12] Cf. Paper XII (*Ap. J.*, **104**, 191, 1946), eqs. (1)–(3).

[13] Note the minus sign here.

to the intensity in the outward direction (μ, φ) at $d\tau$. Hence

$$\left.\begin{aligned} I(d\tau, \mu, \varphi) = \frac{F}{4\mu}\left[\left(1-\frac{d\tau}{\mu_0}\right) S(\tau_1; \mu, \varphi; \mu_0, \varphi_0) - \frac{\partial S(\tau_1; \mu, \varphi; \mu_0, \varphi_0)}{\partial \tau_1}\, d\tau\right] \\ + \frac{d\tau}{4\pi\mu}\int_0^1\int_0^{2\pi} S(\tau_1; \mu, \varphi; \mu', \varphi') B(0, -\mu', \varphi')\frac{d\mu'}{\mu'}\, d\varphi', \end{aligned}\right\} \quad (67)$$

where we have neglected all quantities of order higher than the first in $d\tau$. On the other hand, from the equation of transfer it directly follows that

$$I(d\tau, \mu, \varphi) = \frac{F}{4\mu}\left(1+\frac{d\tau}{\mu}\right) S(\tau_1; \mu, \varphi; \mu_0, \varphi_0) - \frac{d\tau}{\mu} B(0, \mu, \varphi). \quad (68)$$

Combining equations (67) and (68), we have

$$\left.\begin{aligned} \tfrac{1}{4}F\left[\left(\frac{1}{\mu}+\frac{1}{\mu_0}\right) S(\tau_1; \mu, \varphi; \mu_0, \varphi_0) + \frac{\partial S(\tau_1; \mu, \varphi; \mu_0, \varphi_0)}{\partial \tau_1}\right] \\ = B(0, \mu, \varphi) + \frac{1}{4\pi}\int_0^1\int_0^{2\pi} S(\tau_1; \mu, \varphi; \mu', \varphi') B(0, -\mu', \varphi')\frac{d\mu'}{\mu'}\, d\varphi'. \end{aligned}\right\} \quad (69)$$

In addition to equation (69), there is a further relation which can be derived from considerations relating to the radiation field present at the depth $d\tau$. The relation arises from the fact that the transmission of the flux πF incident on $\tau = 0$ by the entire atmosphere of optical thickness τ_1 must be the same as the transmission of the radiations (64) and (65) by the atmosphere of optical thickness $\tau_1 - d\tau$ below the level $d\tau$. Of the flux (64), the amount transmitted in the direction $(-\mu, \varphi)$ by the atmosphere below $d\tau$ is given by

$$\frac{F}{4\mu}\left(1-\frac{d\tau}{\mu_0}\right) T(\tau_1 - d\tau; \mu, \varphi; \mu_0, \varphi_0), \quad (70)$$

or, to the first order in $d\tau$,

$$\frac{F}{4\mu}\left[\left(1-\frac{d\tau}{\mu_0}\right) T(\tau_1; \mu, \varphi; \mu_0, \varphi_0) - \frac{\partial T(\tau_1; \mu, \varphi; \mu_0, \varphi_0)}{\partial \tau_1}\, d\tau\right]. \quad (71)$$

On the other hand, the transmission of the diffuse field (65) will contribute to the radiation in the direction $(-\mu, \varphi)$ the additional intensity

$$\left.\begin{aligned} \frac{d\tau}{4\pi\mu}\int_0^1\int_0^{2\pi} T(\tau_1; \mu, \varphi; \mu', \varphi') B(0, -\mu', \varphi')\frac{d\mu'}{\mu'}\, d\varphi' \\ + \frac{d\tau}{\mu} B(0, -\mu, \varphi)\, e^{-\tau_1/\mu}, \end{aligned}\right\} \quad (72)$$

where the second term arises from the intensity in the *diffuse* field (65), which is already in the direction $(-\mu, \varphi)$.

Adding contributions (71) and (72) and remembering that this must equal

$$\frac{F}{4\mu} T(\tau_1; \mu, \varphi; \mu_0, \varphi_0), \quad (73)$$

we obtain

$$\left.\begin{aligned} \tfrac{1}{4}F\left[\frac{1}{\mu_0} T(\tau_1; \mu, \varphi; \mu_0, \varphi_0) + \frac{\partial T(\tau_1; \mu, \varphi; \mu_0, \varphi_0)}{\partial \tau_1}\right] \\ = B(0, -\mu, \varphi)\, e^{-\tau_1/\mu} + \frac{1}{4\pi}\int_0^1\int_0^{2\pi} T(\tau_1; \mu, \varphi; \mu', \varphi') B(0, -\mu', \varphi')\frac{d\mu'}{\mu'}\, d\varphi'. \end{aligned}\right\} \quad (74)$$

Consider, next, the radiation field present at the level $\tau_1 - d\tau$. Since there is no outward intensity at $\tau = \tau_1$, at the level $\tau_1 - d\tau$ there must be the intensity

$$\frac{d\tau}{\mu'} B(\tau_1, \mu', \varphi'), \tag{75}$$

in the direction $(+\mu', \varphi')$. The reflection of this radiation by the atmosphere *above* $\tau_1 - d\tau$ will contribute to the intensity in the direction $(-\mu, \varphi)$ the amount

$$\frac{d\tau}{4\pi\mu} \int_0^1 \int_0^{2\pi} S(\tau_1; \mu, \varphi; \mu', \varphi') B(\tau_1, \mu', \varphi') \frac{d\mu'}{\mu'} d\varphi'. \tag{76}$$

In addition, there will be the radiation directly transmitted in the direction $(-\mu, \varphi)$ by the atmosphere above the level $\tau_1 - d\tau$. The intensity arising from this account is given by

$$\frac{F}{4\mu}\left[T(\tau_1; \mu, \varphi; \mu_0, \varphi_0) - \frac{\partial T(\tau_1; \mu, \varphi; \mu_0, \varphi_0)}{\partial \tau_1} d\tau\right]. \tag{77}$$

Hence

$$\left.\begin{aligned} I(\tau_1 - d\tau, -\mu, \varphi) = {} & \frac{F}{4\mu}\left[T(\tau_1; \mu, \varphi; \mu_0, \varphi_0) - \frac{\partial T(\tau_1; \mu, \varphi; \mu_0, \varphi_0)}{\partial \tau_1} d\tau\right] \\ & + \frac{d\tau}{4\pi\mu} \int_0^1 \int_0^{2\pi} S(\tau_1; \mu, \varphi; \mu', \varphi') B(\tau_1, \mu', \varphi') \frac{d\mu'}{\mu'} d\varphi'. \end{aligned}\right\} \tag{78}$$

But this must equal

$$I(\tau_1 - d\tau, -\mu, \varphi) = \frac{F}{4\mu}\left(1 + \frac{d\tau}{\mu}\right) T(\tau_1; \mu, \varphi; \mu_0, \varphi_0) - \frac{d\tau}{\mu} B(\tau_1, -\mu, \varphi), \tag{79}$$

which follows from the equation of transfer. From equations (78) and (79) we now obtain

$$\left.\begin{aligned} & \tfrac{1}{4}F\left[\frac{1}{\mu} T(\tau_1; \mu, \varphi; \mu_0, \varphi_0) + \frac{\partial T(\tau_1; \mu, \varphi; \mu_0, \varphi_0)}{\partial \tau_1}\right] \\ & \quad = B(\tau_1, -\mu, \varphi) + \frac{1}{4\pi} \int_0^1 \int_0^{2\pi} S(\tau_1; \mu, \varphi; \mu', \varphi') B(\tau_1, \mu', \varphi') \frac{d\mu'}{\mu'} d\varphi'. \end{aligned}\right\} \tag{80}$$

Again, in addition to equation (80), there is a further relation which can be derived from considerations relating to the field present at the level $\tau_1 - d\tau$. The relation arises from the fact that the reflection of the flux πF incident on $\tau = 0$ by the entire atmosphere of optical thickness τ_1 must be the same as the reflection of the same flux by the atmosphere of optical thickness $\tau_1 - d\tau$ and the transmission of the radiation (75) incident on the level $\tau_1 - d\tau$ from below, by the atmosphere above it. In other words, we must have

$$\left.\begin{aligned} \frac{F}{4\mu} S(\tau_1, \mu, \varphi; \mu_0, \varphi_0) = {} & \frac{F}{4\mu}\left[S(\tau_1, \mu, \varphi; \mu_0, \varphi_0) - \frac{\partial S(\tau_1; \mu, \varphi; \mu_0, \varphi_0)}{\partial \tau_1} d\tau\right] \\ & + \frac{d\tau}{4\pi\mu} \int_0^1 \int_0^{2\pi} T(\tau_1; \mu, \varphi; \mu', \varphi') B(\tau_1, \mu', \varphi') \frac{d\mu'}{\mu'} d\varphi' \\ & + \frac{d\tau}{\mu} B(\tau_1, \mu, \varphi)\, e^{-\tau_1/\mu}, \end{aligned}\right\} \tag{81}$$

where the three terms on the right-hand side arise, respectively, from the reflection of the flux πF by the atmosphere of optical thickness $\tau_1 - d\tau$, from the *diffuse* transmis-

sion of the radiation (75) incident on the level $\tau_1 - d\tau$, and, finally, from the intensity in the field (75) already in the direction (μ, φ). From equation (81) it now follows that

$$\left.\begin{aligned} \tfrac{1}{4}F\frac{\partial S(\tau_1;\,\mu,\,\varphi;\,\mu_0,\,\varphi_0)}{\partial\tau_1} &= B(\tau_1,\,\mu,\,\varphi)\,e^{-\tau_1/\mu} \\ &\quad + \frac{1}{4\pi}\int_0^1\int_0^{2\pi} T(\tau_1;\,\mu,\,\varphi;\,\mu',\,\varphi')\,B(\tau_1,\,\mu',\,\varphi')\,\frac{d\mu'}{\mu'}\,d\varphi'\,. \end{aligned}\right\} \tag{82}$$

Now, according to equations (61)–(63)

$$\left.\begin{aligned} B(0,\,\mu,\,\varphi) &= \tfrac{1}{4}F\Big[p(\mu,\,\varphi;\,-\mu_0,\,\varphi_0) \\ &\quad + \frac{1}{4\pi}\int_0^1\int_0^{2\pi} p(\mu,\,\varphi;\,\mu'',\,\varphi'')\,S(\tau_1;\,\mu'',\,\varphi'';\,\mu_0,\,\varphi_0)\,\frac{d\mu''}{\mu''}\,d\varphi''\Big], \end{aligned}\right\} \tag{83}$$

and

$$\left.\begin{aligned} B(\tau_1,\,\mu,\,\varphi) &= \tfrac{1}{4}F\Big[p(\mu,\,\varphi;\,-\mu_0,\,\varphi_0)\,e^{-\tau_1/\mu_0} \\ &\quad + \frac{1}{4\pi}\int_0^1\int_0^{2\pi} p(\mu,\,\varphi;\,-\mu'',\,\varphi'')\,T(\tau_1;\,\mu'',\,\varphi'';\,\mu_0,\,\varphi_0)\,\frac{d\mu''}{\mu''}\,d\varphi''\Big]. \end{aligned}\right\} \tag{84}$$

Using equations (83) and (84) in equations (69), (74), (80), and (82), we obtain

$$\left(\frac{1}{\mu}+\frac{1}{\mu_0}\right)S(\tau_1;\ \mu,\ \varphi;\ \mu_0,\ \varphi_0)+\frac{\partial S(\tau_1;\ \mu,\ \varphi;\ \mu_0,\ \varphi_0)}{\partial\tau_1}=p(\mu,\ \varphi;-\mu_0,\ \varphi_0)$$
$$+\frac{1}{4\pi}\int_0^1\int_0^{2\pi}p(\mu,\ \varphi;\ \mu'',\ \varphi'')\,S(\tau_1;\ \mu'',\ \varphi'';\ \mu_0,\ \varphi_0)\frac{d\mu''}{\mu''}\,d\varphi''$$
$$+\frac{1}{4\pi}\int_0^1\int_0^{2\pi}S(\tau_1;\ \mu,\ \varphi;\ \mu',\ \varphi')\,p(\mu',\ \varphi';\ \mu_0,\ \varphi_0)\frac{d\mu'}{\mu'}\,d\varphi'$$
$$+\frac{1}{16\pi^2}\int_0^1\int_0^{2\pi}\int_0^1\int_0^{2\pi}S(\tau_1;\ \mu,\ \varphi;\ \mu',\ \varphi')\,p(-\mu'\ \varphi';\ \mu'',\ \varphi'')\,S(\tau_1;\ \mu'',\ \varphi'';\ \mu_0,\ \varphi_0)\frac{d\mu'}{\mu'}\,d\varphi'\frac{d\mu''}{\mu''}\,d\varphi'',\tag{85}$$

$$\frac{\partial S(\tau_1;\ \mu,\ \varphi;\ \mu_0,\ \varphi_0)}{\partial\tau_1}=p(\mu,\ \varphi;-\mu_0,\ \varphi_0)\exp\left\{-\tau_1\left(\frac{1}{\mu}+\frac{1}{\mu_0}\right)\right\}$$
$$+\frac{e^{-\tau_1/\mu}}{4\pi}\int_0^1\int_0^{2\pi}p(\mu,\ \varphi;-\mu'',\ \varphi'')\,T(\tau_1;\ \mu'',\ \varphi'';\ \mu_0,\ \varphi_0)\frac{d\mu''}{\mu''}\,d\varphi''$$
$$+\frac{e^{-\tau_1/\mu_0}}{4\pi}\int_0^1\int_0^{2\pi}T(\tau_1;\ \mu,\ \varphi;\ \mu',\ \varphi')\,p(\mu',\ \varphi';-\mu_0,\ \varphi_0)\frac{d\mu'}{\mu'}\,d\varphi'$$
$$+\frac{1}{16\pi^2}\int_0^1\int_0^{2\pi}\int_0^1\int_0^{2\pi}T(\tau_1;\ \mu,\ \varphi;\ \mu',\ \varphi')\,p(\mu',\ \varphi';-\mu'',\ \varphi'')\,T(\tau_1;\ \mu'',\ \varphi'';\ \mu_0,\ \varphi_0)\frac{d\mu'}{\mu'}\,d\varphi'\frac{d\mu''}{\mu''}\,d\varphi'',\tag{86}$$

$$\left.\begin{aligned}\frac{1}{\mu_0}T(\tau_1;\,\mu,\varphi;\,\mu_0,\varphi_0)+\frac{\partial T(\tau_1;\,\mu,\varphi;\,\mu_0,\varphi_0)}{\partial\tau_1}&=e^{-\tau_1/\mu}p(\mu,\varphi;\,\mu_0,\varphi_0)\\&+\frac{e^{-\tau_1/\mu}}{4\pi}\int_0^1\int_0^{2\pi}p(-\mu,\varphi;\,\mu'',\varphi'')\,S(\tau_1;\,\mu'',\varphi'';\,\mu_0,\varphi_0)\frac{d\mu''}{\mu''}\,d\varphi''\\&+\frac{1}{4\pi}\int_0^1\int_0^{2\pi}T(\tau_1;\,\mu,\varphi;\,\mu',\varphi')\,p(\mu',\varphi';\,\mu_0,\varphi_0)\frac{d\mu'}{\mu'}\,d\varphi'\\+\frac{1}{16\pi^2}\int_0^1\int_0^{2\pi}\int_0^1\int_0^{2\pi}&T(\tau_1;\,\mu,\varphi;\,\mu',\varphi')\,p(-\mu',\varphi';\,\mu'',\varphi'')\,S(\tau_1;\,\mu'',\varphi'';\,\mu_0,\varphi_0)\frac{d\mu'}{\mu'}\,d\varphi'\,\frac{d\mu''}{\mu''}\,d\varphi'',\end{aligned}\right\}\tag{87}$$

and

$$\left.\begin{aligned}\frac{1}{\mu}T(\tau_1;\,\mu,\varphi;\,\mu_0,\varphi_0)+\frac{\partial T(\tau_1;\,\mu,\varphi;\,\mu_0,\varphi_0)}{\partial\tau_1}&=e^{-\tau_1/\mu_0}p(\mu,\varphi;\,\mu_0,\varphi_0)\\&+\frac{1}{4\pi}\int_0^1\int_0^{2\pi}p(\mu,\varphi;\,\mu'',\varphi'')\,T(\tau_1;\,\mu'',\varphi'';\,\mu_0,\varphi_0)\frac{d\mu''}{\mu''}\,d\varphi''\\&+\frac{e^{-\tau_1/\mu_0}}{4\pi}\int_0^1\int_0^{2\pi}S(\tau_1;\,\mu,\varphi;\,\mu',\varphi')\,p(\mu',\varphi';-\mu_0,\varphi_0)\frac{d\mu'}{\mu'}\,d\varphi'\\+\frac{1}{16\pi^2}\int_0^1\int_0^{2\pi}\int_0^1\int_0^{2\pi}&S(\tau_1;\,\mu,\varphi;\,\mu',\varphi')\,p(\mu',\varphi';-\mu'',\varphi'')\,T(\tau_1;\,\mu'',\varphi'';\,\mu_0,\varphi_0)\frac{d\mu'}{\mu'}\,d\varphi'\,\frac{d\mu''}{\mu''}\,d\varphi''.\end{aligned}\right\}\tag{88}$$

Equations (85)–(88) represent the four functional equations governing the problem of transmission and reflection by a plane-parallel atmosphere of finite optical thickness. A simple inspection of these equations shows that

$$S(\tau_1; \mu, \varphi; \mu_0, \varphi_0) = S(\tau_1; \mu_0, \varphi_0; \mu, \varphi) \tag{89}$$

and

$$T(\tau_1; \mu, \varphi; \mu_0, \varphi_0) = T(\tau_1; \mu_0, \varphi_0; \mu, \varphi)\,. \tag{90}$$

Equations (89) and (90) are the expression of the reciprocity principle for the problem on hand.

Finally, we may remark that, when we allow for the polarization of the scattered radiation, we must consider a scattering matrix, $\boldsymbol{S}(\tau_1; \mu, \varphi; \mu_0, \varphi_0)$, and a *transmission matrix*, $\boldsymbol{T}(\tau_1; \mu, \varphi; \mu_0, \varphi_0)$, in place of the functions $S(\tau_1; \mu, \varphi; \mu_0, \varphi_0)$ and $T(\tau_1; \mu, \varphi; \mu_0, \varphi_0)$. It is, however, clear that the functional equations satisfied by $\boldsymbol{S}(\tau_1; \mu, \varphi; \mu_0, \varphi_0)$ and $\boldsymbol{T}(\tau_1; \mu, \varphi; \mu_0, \varphi_0)$ will be of the same forms as equations (85)–(88), only they will be matrix equations in which a *phase matrix* $\boldsymbol{P}(\mu, \varphi; \mu', \varphi')$ will play the same role as the phase function $p(\mu, \varphi; \mu', \varphi')$. Thus, in the case of Rayleigh scattering, the matrix $-\frac{3}{4}\boldsymbol{Q}\,\boldsymbol{J}(\mu, \varphi; -\mu', \varphi')$, defined as in Paper XIV, equations (10) and (17), will replace $p(\mu, \varphi; \mu', \varphi')$.

6. *The reduction of the functional equations (85)–(88) for the case in which the phase function is expressible as a series in Legendre polynomials.*—For the case in which the phase function $p(\cos\Theta)$ is expressible as a series in Legendre polynomials in the form

$$p(\cos\Theta) = \sum_l \varpi_l P_l(\cos\Theta)\,, \tag{91}$$[14]

the functional equations (85)–(88) can be reduced in the following manner:

First, we may observe that, for a phase function of the form (91),

$$\left.\begin{aligned} p(\mu, \varphi; \mu', \varphi') = \sum_l \varpi_l \Big[& P_l(\mu) P_l(\mu') \\ & + 2\sum_{m=1}^{l} \frac{(l-m)!}{(l+m)!} P_l^m(\mu) P_l^m(\mu') \cos m(\varphi - \varphi') \Big]. \end{aligned}\right\} \tag{92}$$

Rearranging the series on the right-hand side of this equation, we can write

$$p(\mu, \varphi; \mu', \varphi') = \sum_m \Big[\sum_{l=m} \varpi_l^m P_l^m(\mu) P_l^m(\mu') \Big] \cos m(\varphi - \varphi')\,, \tag{93}$$

where

$$\varpi_l^m = (2 - \delta_{0,m})\,\varpi_l \frac{(l-m)!}{(l+m)!} \qquad (l = m, m+1, \ldots.) \tag{94}$$

and

$$\left.\begin{aligned} \delta_{0,m} &= 1 \quad \text{if} \quad m = 0 \\ &= 0 \quad \text{otherwise}\,. \end{aligned}\right\} \tag{95}$$

From the expansion (93) for the phase function, it follows that the scattering and the transmission functions, $S(\tau_1; \mu, \varphi; \mu_0, \varphi_0)$ and $T(\tau_1; \mu, \varphi; \mu_0, \varphi_0)$, must be expressible in the forms

$$S(\tau_1; \mu, \varphi; \mu_0, \varphi_0) = \sum_m S^{(m)}(\tau_1; \mu, \mu_0) \cos m(\varphi - \varphi_0) \tag{96}$$

[14] In all practical cases the series on the right-hand side will be a terminating one; but it is not necessary to make this restriction at this point.

and

$$T(\tau_1;\ \mu,\ \varphi;\ \mu_0,\ \varphi_0) = \sum_m T^{(m)}(\tau_1;\ \mu,\ \mu_0)\cos m(\varphi - \varphi_0), \tag{97}$$

where, as the notation implies, $S^{(m)}$ and $T^{(m)}$ are functions of τ_1, μ, and μ_0 only.

Substituting the forms (96) and (97) for S and T in equations (85)–(88), we find that the equations for the various Fourier components separate and that they can be further reduced to the following forms:

$$\left.\begin{aligned}&\left(\frac{1}{\mu}+\frac{1}{\mu_0}\right)S^{(m)}(\tau_1;\ \mu,\ \mu_0) + \frac{\partial S^{(m)}(\tau_1;\ \mu,\ \mu_0)}{\partial \tau_1}\\ &= \sum_{l=m}\varpi_l^m\,(-1)^{m+l}\left[P_l^m(\mu) + \frac{(-1)^{m+l}}{2\,(2-\delta_{0,\,m})}\int_0^1 S^{(m)}(\tau_1;\ \mu,\ \mu')P_l^m(\mu')\frac{d\mu'}{\mu'}\right]\\ &\qquad\times\left[P_l^{(m)}(\mu_0) + \frac{(-1)^{m+l}}{2\,(2-\delta_{0,\,m})}\int_0^1 P_l^m(\mu'')\,S^{(m)}(\tau_1;\ \mu'',\ \mu_0)\frac{d\mu''}{\mu''}\right],\end{aligned}\right\} \tag{98}$$

$$\left.\begin{aligned}&\frac{\partial S^{(m)}(\tau_1;\ \mu,\ \mu_0)}{\partial \tau_1} = \sum_{l=m}\varpi_l^m\,(-1)^{m+l}\\ &\qquad\times\left[e^{-\tau_1/\mu}P_l^m(\mu) + \frac{1}{2\,(2-\delta_{0,\,m})}\int_0^1 T^{(m)}(\tau_1;\ \mu,\ \mu')\,P_l^m(\mu')\frac{d\mu'}{\mu'}\right]\\ &\qquad\times\left[e^{-\tau_1/\mu_0}P_l^m(\mu_0) + \frac{1}{2\,(2-\delta_{0,\,m})}\int_0^1 P_l^m(\mu'')\,T^{(m)}(\tau_1;\ \mu'',\ \mu_0)\frac{d\mu''}{\mu''}\right],\end{aligned}\right\} \tag{99}$$

$$\left.\begin{aligned}&\frac{1}{\mu_0}T^{(m)}(\tau_1;\ \mu,\ \mu_0) + \frac{\partial T^{(m)}(\tau_1;\ \mu,\ \mu_0)}{\partial \tau_1}\\ &\quad= \sum_{l=m}\varpi_l^m\left[P_l^m(\mu_0) + \frac{(-1)^{m+l}}{2\,(2-\delta_{0,\,m})}\int_0^1 P_l^m(\mu'')\,S^{(m)}(\tau_1;\ \mu'',\ \mu_0)\frac{d\mu''}{\mu''}\right]\\ &\qquad\times\left[e^{-\tau_1/\mu}P_l^m(\mu) + \frac{1}{2\,(2-\delta_{0,\,m})}\int_0^1 T^{(m)}(\tau_1;\ \mu,\ \mu')\,P_l^m(\mu')\frac{d\mu'}{\mu'}\right],\end{aligned}\right\} \tag{100}$$

and

$$\left.\begin{aligned}&\frac{1}{\mu}T^{(m)}(\tau_1;\ \mu,\ \mu_0) + \frac{\partial T^{(m)}(\tau_1;\ \mu,\ \mu_0)}{\partial \tau_1}\\ &\quad= \sum_{l=m}\varpi_l^m\left[P_l^m(\mu) + \frac{(-1)^{m+l}}{2\,(2-\delta_{0,\,m})}\int_0^1 S^{(m)}(\tau_1;\ \mu,\ \mu')\,P_l^m(\mu')\frac{d\mu'}{\mu'}\right]\\ &\qquad\times\left[e^{-\tau_1/\mu_0}P_l^m(\mu_0) + \frac{1}{2\,(2-\delta_{0,\,m})}\int_0^1 P_l^m(\mu'')\,T^{(m)}(\tau_1;\ \mu'',\ \mu_0)\frac{d\mu''}{\mu''}\right].\end{aligned}\right\} \tag{101}$$

If we now let

$$\psi_l^m(\tau_1,\ \mu) = P_l^m(\mu) + \frac{(-1)^{m+l}}{2\,(2-\delta_{0,\,m})}\int_0^1 S^{(m)}(\tau_1;\ \mu,\ \mu')\,P_l^m(\mu')\frac{d\mu'}{\mu'} \tag{102}$$

and

$$\phi_l^m(\tau_1,\ \mu) = e^{-\tau_1/\mu}P_l^m(\mu) + \frac{1}{2\,(2-\delta_{0,\,m})}\int_0^1 T^{(m)}(\tau_1;\ \mu,\ \mu')\,P_l^m(\mu')\frac{d\mu'}{\mu'}, \tag{103}$$

then, in view of equations (89) and (90), we can re-write equations (98)–(101) in the forms

$$\left.\begin{aligned}\left(\frac{1}{\mu}+\frac{1}{\mu_0}\right) S^{(m)}(\tau_1;\,\mu,\,\mu_0) \\ +\frac{\partial S^{(m)}(\tau_1;\,\mu,\,\mu_0)}{\partial \tau_1} = \sum_{l=m} \varpi_l^m (-1)^{m+l} \psi_l^m(\tau_1,\,\mu)\,\psi_l^m(\tau_1,\,\mu_0)\,,\end{aligned}\right\} \tag{104}$$

$$\frac{\partial S^{(m)}(\tau_1;\,\mu,\,\mu_0)}{\partial \tau_1} = \sum_{l=m} \varpi_l^m (-1)^{m+l} \phi_l^m(\tau_1,\,\mu)\,\phi_l^m(\tau_1,\,\mu_0)\,, \tag{105}$$

$$\frac{1}{\mu} T^{(m)}(\tau_1;\,\mu,\,\mu_0) + \frac{\partial T^{(m)}(\tau_1;\,\mu,\,\mu_0)}{\partial \tau_1} = \sum_{l=m} \varpi_l^m \psi_l^m(\tau_1,\,\mu)\,\phi_l^m(\tau_1,\,\mu_0) \tag{106}$$

and

$$\frac{1}{\mu_0} T^{(m)}(\tau_1;\,\mu,\,\mu_0) + \frac{\partial T^{(m)}(\tau_1;\,\mu,\,\mu_0)}{\partial \tau_1} = \sum_{l=m} \varpi_l^m \psi_l^m(\tau_1,\,\mu_0)\,\phi_l^m(\tau_1,\,\mu)\,. \tag{107}$$

Alternative forms of the foregoing equations are

$$\left.\begin{aligned}\left(\frac{1}{\mu}+\frac{1}{\mu_0}\right) S^{(m)}(\tau_1;\,\mu,\,\mu_0) \\ = \sum_{l=m} \varpi_l^m (-1)^{m+l} \left[\psi_l^m(\tau_1,\,\mu)\,\psi_l^m(\tau_1,\,\mu_0) - \phi_l^m(\tau_1,\,\mu)\,\phi_l^m(\tau_1,\,\mu_0)\right],\end{aligned}\right\} \tag{108}$$

$$\left.\begin{aligned}\left(\frac{1}{\mu}-\frac{1}{\mu_0}\right) T^{(m)}(\tau_1;\,\mu,\,\mu_0) \\ = \sum_{l=m} \varpi_l^m \left[\psi_l^m(\tau_1,\,\mu)\,\phi_l^m(\tau_1,\,\mu_0) - \psi_l^m(\tau_1,\,\mu_0)\,\phi_l^m(\tau_1,\,\mu)\right],\end{aligned}\right\} \tag{109}$$

$$\frac{\partial S^{(m)}(\tau_1;\,\mu,\,\mu_0)}{\partial \tau_1} = \sum_{l=m} \varpi_l^m (-1)^{m+l} \phi_l^m(\tau_1,\,\mu)\,\phi_l^m(\tau_1,\,\mu_0)\,, \tag{110}$$

and

$$\left.\begin{aligned}\left(\frac{1}{\mu}-\frac{1}{\mu_0}\right) \frac{\partial T^{(m)}(\tau_1;\,\mu,\,\mu_0)}{\partial \tau_1} \\ = \sum_{l=m} \varpi_l^m \left[\frac{1}{\mu}\psi_l^m(\tau_1,\,\mu_0)\,\phi_l^m(\tau_1,\,\mu) - \frac{1}{\mu_0}\psi_l^m(\tau_1,\,\mu)\,\phi_l^m(\tau_1,\,\mu_0)\right].\end{aligned}\right\} \tag{111}$$

Finally, substituting for $S^{(m)}(\tau_1;\,\mu,\,\mu')$ and $T^{(m)}(\tau_1;\,\mu,\,\mu')$ from equations (108) and (109) in equations (102) and (103), we obtain

$$\left.\begin{aligned}\psi_l^m(\tau_1,\,\mu) = P_l^m(\mu) + \frac{1}{2}\sum_{k=m} (-1)^{k+l} \varpi_k \frac{(k-m)!}{(k+m)!}\,\mu \\ \times \int_0^1 \frac{d\mu'}{\mu+\mu'} \left[\psi_k^m(\tau_1,\,\mu)\,\psi_k^m(\tau_1,\,\mu') - \phi_k^m(\tau_1,\,\mu)\,\phi_k^m(\tau_1,\,\mu')\right] P_l^m(\mu')\end{aligned}\right\} \tag{112}$$

and

$$\left.\begin{aligned}\phi_l^m(\tau_1,\mu) &= P_l^m(\mu)\, e^{-\tau_1/\mu} + \frac{1}{2}\sum_{k=m}\varpi_k \frac{(k-m)!}{(k+m)!}\,\mu \\ &\times \int_0^1 \frac{d\mu'}{\mu-\mu'}\left[\psi_k^m(\tau_1,\mu')\,\phi_k^m(\tau_1,\mu) - \psi_k^m(\tau_1,\mu)\,\phi_k^m(\tau_1,\mu')\right] P_l^m(\mu'),\end{aligned}\right\} \quad (113)$$

where we have further substituted for ϖ_k^m in accordance with equation (94).

7. *The functional equations for the case of isotropic scattering.*—In the case of isotropic scattering,

$$\varpi_l = 0 \qquad (l \neq 0), \quad (114)$$

and equations (108)–(113) reduce to

$$\left(\frac{1}{\mu}+\frac{1}{\mu_0}\right) S(\tau_1;\mu,\mu_0) = \varpi_0\left[\psi(\tau_1,\mu)\,\psi(\tau_1,\mu_0) - \phi(\tau_1,\mu)\,\phi(\tau_1,\mu_0)\right], \quad (115)$$

$$\left(\frac{1}{\mu}-\frac{1}{\mu_0}\right) T(\tau_1;\mu,\mu_0) = \varpi_0\left[\psi(\tau_1,\mu)\,\phi(\tau_1,\mu_0) - \psi(\tau_1,\mu_0)\,\phi(\tau_1,\mu)\right], \quad (116)$$

$$\frac{\partial S(\tau_1;\mu,\mu_0)}{\partial \tau_1} = \varpi_0 \phi(\tau_1,\mu)\,\phi(\tau_1,\mu_0), \quad (117)$$

$$\left(\frac{1}{\mu}-\frac{1}{\mu_0}\right)\frac{\partial T(\tau_1;\mu,\mu_0)}{\partial \tau_1} = \varpi_0\left[\frac{1}{\mu}\psi(\tau_1,\mu_0)\,\phi(\tau_1,\mu) - \frac{1}{\mu_0}\psi(\tau_1,\mu)\,\phi(\tau_1,\mu_0)\right], \quad (118)$$

$$\psi(\tau_1,\mu) = 1 + \tfrac{1}{2}\varpi_0\mu\int_0^1 \frac{d\mu'}{\mu+\mu'}\left[\psi(\tau_1,\mu)\,\psi(\tau_1,\mu') - \phi(\tau_1,\mu)\,\phi(\tau_1,\mu')\right], \quad (119)$$

and

$$\phi(\tau_1,\mu) = e^{-\tau_1/\mu} + \tfrac{1}{2}\varpi_0\mu\int_0^1 \frac{d\mu'}{\mu-\mu'}\left[\psi(\tau_1,\mu')\,\phi(\tau_1,\mu) - \psi(\tau_1,\mu)\,\phi(\tau_1,\mu')\right]. \quad (120)$$

Equations (115), (116), (119), and (120) agree with the equations given by Ambarzumian.[10] But equations (117) and (118) are new.

The question now arises as to whether the solution of the system of equations (115)–(120) can be obtained in closed forms when the integrals on the right-hand sides of equations (119) and (120) are replaced by Gauss sums in the nth approximation. This question is related to the elimination of the constants in the method of solution of the earlier papers of this series (Paper XII, for example) and to the still larger question of whether the systems of functional equations to which we were led in § 6 can be reduced to single (or, more possibly, a pair of) functional equations of standard forms. All these questions, as they arise in connection with transfer problems in semi-infinite atmospheres, were essentially answered in Paper XIV; but they remain to be investigated in the present more general context. (See note added at end of paper.)

8. *Functional equations governing the radiation field in the interior of plane-parallel atmospheres.*—We have concerned ourselves, so far, with only the radiations emerging from the boundaries of plane-parallel atmospheres. But it is clear that the ideas, particularly those leading to the functional equations derived in §§ 2, 4, and 5, can be applied equally to formulate functional equations for the radiation field in the interior. In this section we shall give some examples of such functional equations.

We shall consider, first, the radiation field in an atmosphere of optical thickness τ_1, on which is incident a parallel beam of radiation of flux πF, in the direction $(-\mu_0, \varphi_0)$. At a depth τ in this atmosphere, there will be the incident flux reduced to the amount

$$\pi F\, e^{-\tau/\mu_0}, \quad (121)$$

as well as a diffuse radiation field characterized by the intensity $I(\tau, \mu, \varphi)$. To distinguish between the radiation in the outward $(0 \leqslant \mu \leqslant 1)$ and the inward $(0 > \mu \geqslant -1)$ directions, we shall write

$$I(\tau, +\mu, \varphi) \qquad (0 \leqslant \mu \leqslant 1) \tag{122}$$

and

$$I(\tau, -\mu, \varphi) \qquad (0 < \mu \leqslant 1). \tag{123}$$

Now the atmosphere below τ will reflect the radiations (121) and (123) according to the reflective power of an atmosphere of optical thickness $(\tau_1 - \tau)$ and will contribute to an outward intensity in the direction $(+\mu, \varphi)$ which must equal $I(\tau, +\mu, \varphi)$. In other words,

$$\left.\begin{aligned} I(\tau, +\mu, \varphi) &= \frac{1}{4\mu} F e^{-\tau/\mu_0} S(\tau_1 - \tau;\ \mu, \varphi;\ \mu_0, \varphi_0) \\ &\quad + \frac{1}{4\pi\mu} \int_0^1 \int_0^{2\pi} S(\tau_1 - \tau;\ \mu, \varphi;\ \mu', \varphi')\, I(\tau; -\mu', \varphi')\, d\mu' d\varphi' . \end{aligned}\right\} \tag{124}$$

Similarly, we must have

$$\left.\begin{aligned} I(\tau, -\mu, \varphi) &= \frac{1}{4\mu} FT(\tau;\ \mu, \varphi;\ \mu_0, \varphi_0) \\ &\quad + \frac{1}{4\pi\mu} \int_0^1 \int_0^{2\pi} S(\tau;\ \mu, \varphi;\ \mu', \varphi')\, I(\tau, +\mu', \varphi')\, d\mu' d\varphi' , \end{aligned}\right\} \tag{125}$$

expressing the fact that the intensity in the direction $(-\mu, \varphi)$ may be regarded as resulting from the transmission of the incident flux by the part of the atmosphere above τ and the reflection of the radiation (122) incident on τ, from below.

Functional equations of a different sort arise from considerations of the type which led to the functional equations (74) and (82) in § 5. Thus, from the equivalence of the transmission by the atmosphere of optical thickness τ_1 and the transmission of the radiations (121) and (123) by the atmosphere of optical thickness $(\tau_1 - \tau)$ below the level τ, we conclude that

$$\left.\begin{aligned} &\frac{1}{4\mu} FT(\tau_1;\ \mu, \varphi;\ \mu_0, \varphi_0) = \\ &\frac{1}{4\mu} F e^{-\tau/\mu_0} T(\tau_1 - \tau;\ \mu, \varphi;\ \mu_0, \varphi_0) + I(\tau, -\mu, \varphi)\, e^{-(\tau_1 - \tau)/\mu} \\ &\qquad + \frac{1}{4\pi\mu} \int_0^1 \int_0^{2\pi} T(\tau_1 - \tau;\ \mu, \varphi;\ \mu', \varphi')\, I(\tau; -\mu', \varphi')\, d\mu' d\varphi' . \end{aligned}\right\} \tag{126}$$

The three terms on the right-hand side of equation (126) represent, respectively, the contributions from the transmission of the flux (121) by the atmosphere below τ, the intensity in the diffuse field (123) already in the direction $(-\mu, \varphi)$ and the diffuse transmission of the field (123) by the atmosphere of optical thickness $(\tau_1 - \tau)$.

Similarly, we must have

$$\left.\begin{aligned} \frac{1}{4\mu} FS(\tau_1;\ \mu, \varphi;\ \mu_0, \varphi_0) &= \frac{1}{4\mu} FS(\tau;\ \mu, \varphi;\ \mu_0, \varphi_0) + I(\tau, +\mu, \varphi)\, e^{-\tau/\mu} \\ &\quad + \frac{1}{4\pi\mu} \int_0^1 \int_0^{2\pi} T(\tau;\ \mu, \varphi;\ \mu', \varphi')\, I(\tau, +\mu', \varphi')\, d\mu' d\varphi' , \end{aligned}\right\} \tag{127}$$

which expresses the equivalence of the reflection by the atmosphere of optical thickness τ_1 and the reflection by the part of the atmosphere above τ and the transmission of the radiation (122) incident on τ from below.

Equations (126) and (127) can be re-written in the forms

$$\left.\begin{aligned} I(\tau, +\mu, \varphi)\, e^{-\tau/\mu} = {} & \frac{F}{4\mu}\left[S(\tau_1; \mu, \varphi; \mu_0, \varphi_0) - S(\tau; \mu, \varphi; \mu_0, \varphi_0)\right] \\ & - \frac{1}{4\pi\mu}\int_0^1\int_0^{2\pi} T(\tau; \mu, \varphi; \mu' \varphi')\, I(\tau, +\mu', \varphi')\, d\mu' d\varphi' \end{aligned}\right\} \quad (128)$$

and

$$\left.\begin{aligned} & I(\tau, -\mu, \varphi)\, e^{-(\tau_1-\tau)/\mu} = \\ & \frac{F}{4\mu}\left[T(\tau_1; \mu, \varphi; \mu_0, \varphi_0) - e^{-\tau/\mu_0} T(\tau_1 - \tau; \mu, \varphi; \mu_0, \varphi_0)\right] \\ & \qquad - \frac{1}{4\pi\mu}\int_0^1\int_0^{2\pi} T(\tau_1 - \tau; \mu, \varphi; \mu', \varphi')\, I(\tau, -\mu', \varphi')\, d\mu' d\varphi'. \end{aligned}\right\} \quad (129)$$

It is clear that equations (124) and (125) or (128) and (129) will suffice to determine the radiation field in the interior uniquely, in terms of the scattering and transmission functions of atmospheres of finite optical thicknesses.

The functional equations analogous to equations (124)–(129) for the axially symmetric radiation field in the interior of a semi-infinite atmosphere with a constant net flux are

$$I(\tau, +\mu) = I(0, +\mu) + \frac{1}{2\mu}\int_0^1 S^{(0)}(\infty; \mu, \mu')\, I(\tau, -\mu')\, d\mu', \quad (130)$$

$$I(0, +\mu) = I(\tau, +\mu)\, e^{-\tau/\mu} + \frac{1}{2\mu}\int_0^1 T^{(0)}(\tau; \mu, \mu')\, I(\tau, +\mu')\, d\mu', \quad (131)$$

and

$$I(\tau, -\mu) = \frac{1}{2\mu}\int_0^1 S^{(0)}(\tau; \mu, \mu')\, I(\tau, +\mu')\, d\mu', \quad (132)$$

where $S^{(0)}$ and $T^{(0)}$ are the azimuth independent terms in the scattering and the transmission functions defined as in equation (7). Equations (130), (131), and (132) express, respectively, the invariance of the emergent intensity to the removal of layers of arbitrary optical thickness from the atmosphere, the consideration that the emergent intensity may be regarded as the transmission of the radiation $I(\tau, +\mu)$ by the atmosphere above the level τ, and the fact that the inward intensity prevailing at any level arises in consequence of the reflection of the outward radiation field by the atmosphere above τ.

It is evident that the functional equations (124)–(132), together with the equations (85)–(88), satisfied by the scattering and the transmission functions, are entirely equivalent to the transfer problems formulated in terms of the equations of transfer and boundary conditions.

In a later paper we propose to undertake a detailed study of the various functional equations which we have formulated in this paper; but it is of interest to recall, meantime, that the basic ideas underlying the formulation of these functional equations resemble those which were introduced by Sir George Stokes and Lord Rayleigh in their treatment of the reflection and transmission of light by piles of plates.[15]

Note added April 15.—The questions raised at the end of § 7 have now been answered. In particular, solutions in closed forms for equations (119) and (120) have been found when the integrals on the right-hand sides are replaced by the corresponding Gauss sums. It is hoped to publish the results of these investigations in the near future.

[15] *Mathematical and Physical Papers of Sir George Stokes*, IV (Cambridge, England, 1904), 145; and *Scientific Papers of Lord Rayleigh*, VI (Cambridge, England, 1920), 492. I am indebted to Sir K. S. Krishnan for drawing my attention to these early investigations.

ON THE RADIATIVE EQUILIBRIUM OF A STELLAR ATMOSPHERE. XVIII

S. CHANDRASEKHAR AND FRANCES H. BREEN
Yerkes Observatory
Received February 26, 1947

ABSTRACT

In this paper we provide tables of certain integrals and functions which are necessary for the reduction of observations relating to the continuous spectrum of the stars on the basis of the theory developed in Paper VII.

1. *The integrals determining the law of darkening and the intensity distribution in the continuous spectrum of the stars.*—In Paper VII[1] it was shown that in a stellar atmosphere in local thermodynamic equilibrium the temperature distribution will be given, approximately, by a formula of the standard type,

$$T^4 = \tfrac{3}{4}T_e^4\,(\tau + q\,[\tau]) \qquad \left(q\,(0) = \frac{1}{\sqrt{3}}\right), \tag{1}$$

where T_e denotes the effective temperature and $q(\tau)$ a certain monotonic increasing function of the optical depth τ, provided that the mean absorption coefficient, $\bar{\kappa}$, in terms of which τ is measured, is defined as a straight average of the monochromatic absorption coefficient κ_ν, weighted according to the flux $F_\nu^{(1)}$ of the radiation of frequency ν in a gray atmosphere, and provided also that $\kappa_\nu/\bar{\kappa}$ is independent of depth. On this approximation the emergent intensity, $I_\nu(\vartheta)$ in the frequency ν and in the direction inclined at an angle ϑ to the normal, will be given by

$$I_\nu\,(\vartheta) = \int_0^\infty B_\nu\,(T_\tau)\,\exp\left(-\frac{\kappa_\nu}{\bar{\kappa}}\,\tau\,\sec\vartheta\right) d\left(\frac{\kappa_\nu}{\bar{\kappa}}\,\tau\,\sec\vartheta\right), \tag{2}$$

where $B_\nu(T_\tau)$ is the Planck intensity in the frequency ν and at the temperature T_τ prevailing at τ. Under the same conditions the emergent flux $F_\nu(0)$ in the frequency ν will be given by

$$F_\nu\,(0) = 2\int_0^\infty B_\nu\,(T_\tau)\,E_2\left(\frac{\kappa_\nu}{\bar{\kappa}}\,\tau\right) d\left(\frac{\kappa_\nu}{\bar{\kappa}}\,\tau\right), \tag{3}$$

where

$$E_2\,(x) = \int_1^\infty \frac{e^{-xw}}{w^2}\,dw. \tag{4}$$

It is convenient to re-write equations (2) and (3) in the forms

$$I_\nu\,(\vartheta) = B_\nu\,(T_0)\int_0^\infty b_\nu\,(\tau)\,\exp\left(-\frac{\kappa_\nu}{\bar{\kappa}}\,\tau\,\sec\vartheta\right) d\left(\frac{\kappa_\nu}{\bar{\kappa}}\,\tau\,\sec\vartheta\right) \tag{5}$$

and

$$F_\nu\,(0) = 2B_\nu\,(T_0)\int_0^\infty b_\nu\,(\tau)\,E_2\left(\frac{\kappa_\nu}{\bar{\kappa}}\,\tau\right) d\left(\frac{\kappa_\nu}{\bar{\kappa}}\,\tau\right), \tag{6}$$

where

$$b_\nu\,(\tau) = \frac{B_\nu\,(T_\tau)}{B_\nu\,(T_0)} = \frac{e^{h\nu/kT_0} - 1}{e^{h\nu/kT_\tau} - 1} \tag{7}$$

and $B_\nu(T_0)$ is the Planck function for the boundary temperature, T_0.

[1] *Ap. J.*, **101**, 328, 1945.

Since the dependence on frequency and on the effective temperature of the emergent intensity and flux is determined only by the value of $h\nu/kT_e$, we shall write

$$\alpha = \frac{h\nu}{kT_e} \tag{8}$$

and express $I_\nu(\vartheta)$ and $F_\nu(0)$ in terms of the two integrals

$$\Im(\alpha; \beta) = \int_0^\infty e^{-\beta\tau} b_\alpha(\tau)\, d(\beta\tau) \tag{9}$$

and

$$\Im(\alpha; \beta) = 2\int_0^\infty E_2(\beta\tau)\, b_\alpha(\tau)\, d(\beta\tau). \tag{10}$$

Thus

$$I_\nu(\vartheta) = B_\nu(T_0)\, \Im\left(\frac{h\nu}{kT_e}; \frac{\kappa_\nu}{\bar{\kappa}} \sec\vartheta\right), \tag{11}$$

and

$$F_\nu(0) = B_\nu(T_0)\, \Im\left(\frac{h\nu}{kT_e}; \frac{\kappa_\nu}{\bar{\kappa}}\right). \tag{12}$$

For the temperature distribution given by formula (1),

$$b_\alpha(\tau) = \frac{\exp\left\{\left(\frac{4}{\sqrt{3}}\right)^{1/4}\alpha\right\} - 1}{\exp\left\{\alpha\left[\tfrac{3}{4}(\tau+q)\right]^{-1/4}\right\} - 1}, \tag{13}$$

and

$$B_\nu(T_0) = B_\alpha(0) = \frac{15}{\pi^4}\frac{\alpha^3}{\exp\left\{\left(\frac{4}{\sqrt{3}}\right)^{1/4}\alpha\right\} - 1} F. \tag{14}$$

From the expressions for $I_\nu(\vartheta)$ and $F_\nu(0)$ in terms of the two-parametric integrals, $\Im(\alpha; \beta)$ and $\Im(\alpha; \beta)$, it is apparent that, both for deriving the theoretical consequences of a known source of continuous absorption and for inferring the variation of the continuous absorption coefficient with wave length required by the results of spectrophotometry, it is necessary to have adequate tables of the basic integrals.

Now integrals equivalent to our $\Im(\alpha; \beta)$ and $\Im(\alpha; \beta)$ have been evaluated for certain ranges of values of α and β by Milne,[2] Lindblad and Burkhardt.[3] But none of these tables is extensive enough to cover satisfactorily all the situations which arise in practice. Indeed, the large number of uncertain entries in current calculations[4] of theoretical color temperatures and Balmer and Paschen discontinuities arises largely from this source. For this reason it has seemed to us worth while (even at this late date!) to provide tables of the integrals $\Im(\alpha; \beta)$ and $\Im(\alpha; \beta)$ which will prove adequate for all practical purposes.

2. *Tables of the integrals* $\Im(\alpha; \beta)$ *and* $\Im(\alpha; \beta)$.—One of the principal reasons why the existing tables of $\Im(\alpha; \beta)$ and $\Im(\alpha; \beta)$, or their equivalents, is so inadequate, is the labor that is required for evaluating the integrals by a straightforward numerical process over the ranges of α and β which are of interest. However, on the basis of actual numerical tests which we have made, it has appeared that the required integrals can be

[2] *Phil. Trans. R. Soc.*, A, **223**, 201, 1922.

[3] *Zs. f. Ap.*, **13**, 56, 1936.

[4] See, e.g., S. Chandrasekhar and G. Münch, *Ap. J.*, **104**, 446, 1946; also G. Münch, *Ap. J.*, **102**, 385, 1945.

evaluated with sufficient precision, very simply, by a five-point quadrature formula based on the zeros of the Laguerre polynomials.

It is known that the formula[5]

$$\int_0^\infty e^{-x}\Phi(x)\,dx \simeq \sum_{i=1}^{n} q_i \Phi(x_i) \tag{15}$$

where the x_i's are the zeros of the Laguerre polynomial,

$$L_n(x) = e^x \frac{d^n}{dx^n}(x^n e^{-x}) \tag{16}$$

of order n, and where

$$q_i = \frac{[n!]^2}{x_i [L_n'(x_i)]^2} \tag{17}$$

evaluates the integral on the left-hand side of equation (15) *exactly* for any arbitrary polynomial of degree $2n - 1$. With a five-point formula, we are, therefore, essentially approximating the function under the integral sign by a polynomial of degree 9. And this would seem sufficient for most purposes. The integrals (9) and (10) were, accordingly, approximated by the sums

$$\mathfrak{Z}(\alpha; \beta) = \sum_{i=1}^{5} q_i b_\alpha\left(\frac{x_i}{\beta}\right) \tag{18}$$

and

$$\mathfrak{F}(\alpha; \beta) = 2\sum_{i=1}^{5} Q_i b_\alpha\left(\frac{x_i}{\beta}\right), \tag{19}$$

where

$$Q_i = q_i e^{x_i} E_2(x_i) \qquad (i = 1, \ldots, 5). \tag{20}$$

In Table 1 we have collected the values of x_i, q_i, and Q_i which were used in the calculations.

TABLE 1

THE CONSTANTS x_i, q_i, AND Q_i

i	x_i	q_i	Q_i
1	0.2635603	0.5217556	0.342162
2	1.413403	.3986668	.134927
3	3.596426	.0759424	.0143132
4	7.085810	.0036118	.00040598
5	12.640801	0.0000234	0.00000161

The evaluation of the integrals according to formulae (18) and (19) is a relatively simple matter, since for each value of β we need $b_\alpha(\tau)$ only for five values of the argument. We may add that we have verified by direct numerical integrations the fact that the precision reached in evaluating the integrals $\mathfrak{Z}(\alpha; \beta)$ and $\mathfrak{F}(\alpha; \beta)$ by the five-point Laguerre formula justifies the number of significant figures which have been retained in the tables of these integrals (Tables 2–9).

[5] A. Reiz, *Ark. f. Math., Astr. och Fys.*, Vol. 29, Part IV, 1943.

TABLE 2

$\Im(\alpha;\beta)$

$(0 \leqslant \alpha \leqslant 12;\ 0.2 \leqslant \beta \leqslant 2)$

β	$\alpha=0$	$\alpha=1$	$\alpha=2$	$\alpha=3$	$\alpha=4$	$\alpha=6$	$\alpha=8$	$\alpha=10$	$\alpha=12$
0.2	1.668	2.228	3.225	4.994	8.143	24.07	77.93	267.5	957.2
0.3	1.542	1.990	2.764	4.087	6.340	16.87	49.03	151.2	487.4
0.4	1.463	1.843	2.485	3.551	5.309	13.05	34.96	99.41	296.0
0.5	1.408	1.741	2.294	3.192	4.633	10.688	26.81	71.41	199.3
0.6	1.367	1.665	2.153	2.930	4.152	9.085	21.56	54.35	143.7
0.7	1.335	1.606	2.043	2.730	3.789	7.926	17.95	43.12	108.8
0.8	1.309	1.557	1.955	2.571	3.505	7.052	15.32	35.30	85.40
0.9	1.288	1.518	1.883	2.442	3.278	6.370	13.34	29.60	69.02
1.0	1.269	1.484	1.822	2.334	3.090	5.823	11.80	25.32	57.07
1.1	1.253	1.455	1.770	2.243	2.932	5.376	10.575	22.01	48.10
1.2	1.240	1.430	1.725	2.164	2.798	5.004	9.580	19.39	41.19
1.3	1.227	1.407	1.686	2.095	2.682	4.688	8.755	17.27	35.75
1.4	1.217	1.388	1.651	2.035	2.581	4.419	8.067	15.54	31.39
1.5	1.207	1.370	1.620	1.982	2.492	4.186	7.482	14.10	27.85
1.6	1.198	1.354	1.592	1.935	2.414	3.982	6.981	12.88	24.92
1.7	1.190	1.340	1.567	1.892	2.343	3.802	6.545	11.85	22.47
1.8	1.183	1.327	1.544	1.853	2.280	3.643	6.165	10.964	20.41
1.9	1.176	1.315	1.523	1.818	2.222	3.501	5.831	10.201	18.64
2.0	1.170	1.304	1.503	1.786	2.170	3.373	5.536	9.524	17.13

TABLE 3

$\Im(\alpha;\beta)$

$(0 \leqslant \alpha \leqslant 12;\ 0 \leqslant \beta^{-1} \leqslant 0.5)$

$1/\beta$	$\alpha=0$	$\alpha=1$	$\alpha=2$	$\alpha=3$	$\alpha=4$	$\alpha=6$	$\alpha=8$	$\alpha=10$	$\alpha=12$
0	1.000	1.000	1.000	1.000	1.000	1.000	1.000	1.000	1.000
0.05	1.027	1.048	1.076	1.109	1.147	1.233	1.331	1.444	1.575
.10	1.050	1.088	1.140	1.205	1.281	1.466	1.699	1.993	2.367
.15	1.070	1.123	1.197	1.292	1.407	1.701	2.097	2.637	3.380
.20	1.087	1.154	1.249	1.373	1.527	1.936	2.523	3.372	4.627
.25	1.103	1.183	1.297	1.449	1.642	2.173	2.972	4.196	6.112
.30	1.119	1.210	1.343	1.522	1.753	2.411	3.445	5.102	7.837
.40	1.146	1.259	1.427	1.658	1.967	2.890	4.452	7.158	11.99
0.50	1.170	1.304	1.503	1.786	2.170	3.373	5.536	9.524	17.13

TABLE 4

LOG $\Im(\alpha;\beta)$
$(0 \leqslant \alpha \leqslant 12;\ 0.2 \leqslant \beta \leqslant 2)$

β	$\alpha=0$	$\alpha=1$	$\alpha=2$	$\alpha=3$	$\alpha=4$	$\alpha=6$	$\alpha=8$	$\alpha=10$	$\alpha=12$
0.2	0.2223	0.3480	0.5085	0.6984	0.9108	1.3815	1.8917	2.4273	2.9810
0.3	.1880	.2988	.4416	.6114	.8021	1.2270	1.6905	2.1796	2.6879
0.4	.1653	.2655	.3954	.5504	.7250	1.1156	1.5435	1.9974	2.4712
0.5	.1487	.2408	.3606	.5040	.6659	1.0289	1.4283	1.8537	2.2996
0.6	.1359	.2214	.3330	.4669	.6182	0.9583	1.3337	1.7352	2.1574
0.7	.1256	.2056	.3104	.4361	.5785	0.8991	1.2540	1.6347	2.0365
0.8	.1170	.1924	.2912	.4101	.5447	0.8483	1.1853	1.5478	1.9315
0.9	.1097	.1811	.2749	.3877	.5156	0.8042	1.1252	1.4712	1.8389
1.0	.1035	.1713	.2606	.3681	.4899	0.7652	1.0719	1.4035	1.7564
1.1	.0981	.1628	.2480	.3507	.4672	0.7305	1.0243	1.3426	1.6821
1.2	.0933	.1552	.2368	.3352	.4469	0.6993	0.9813	1.2876	1.6148
1.3	.0890	.1484	.2268	.3213	.4285	0.6710	0.9423	1.2373	1.5532
1.4	.0852	.1423	.2177	.3086	.4118	0.6453	0.9067	1.1914	1.4968
1.5	.0817	.1368	.2095	.2971	.3966	0.6218	0.8740	1.1492	1.4447
1.6	.0785	.1317	.2019	.2866	.3827	0.6001	0.8439	1.1101	1.3965
1.7	.0757	.1270	.1950	.2769	.3698	0.5800	0.8159	1.0737	1.3516
1.8	.0730	.1228	.1885	.2679	.3579	0.5615	0.7899	1.0400	1.3097
1.9	.0706	.1188	.1826	.2595	.3468	0.5442	0.7657	1.0086	1.2704
2.0	0.0683	0.1152	0.1771	0.2518	0.3365	0.5280	0.7432	0.9788	1.2338

TABLE 5

LOG $\Im(\alpha;\beta)$
$(0 \leqslant \alpha \leqslant 2;\ 0 \leqslant \beta^{-1} \leqslant 0.5)$

$1/\beta$	$\alpha=0$	$\alpha=1$	$\alpha=2$	$\alpha=3$	$\alpha=4$	$\alpha=6$	$\alpha=8$	$\alpha=10$	$\alpha=12$
0	0.0000	0.0000	0.0000	0.0000	0.0000	0.0000	0.0000	0.0000	0.0000
0.05	.0118	.0204	.0317	.0449	.0595	.0908	.1242	.1595	0.1974
.10	.0212	.0366	.0569	.0809	.1076	.1662	.2302	.2994	0.3741
.15	.0293	.0503	.0781	.1113	.1483	.2306	.3217	.4211	0.5290
.20	.0364	.0623	.0966	.1377	.1838	.2870	.4018	.5279	0.6653
.25	.0428	.0731	.1131	.1612	.2154	.3371	.4731	.6228	0.7862
.30	.0487	.0828	.1281	.1824	.2439	.3821	.5372	.7078	0.8941
.40	.0591	.1001	.1543	.2197	.2937	.4609	.6486	.8548	1.0788
0.50	0.0683	0.1152	0.1771	0.2518	0.3365	0.5280	0.7432	0.9788	1.2338

TABLE 6

$\mathfrak{F}(\alpha; \beta)$
$(0 \leqslant \alpha \leqslant 12;\ 0.2 \leqslant \beta \leqslant 2)$

β	$\alpha=0$	$\alpha=1$	$\alpha=2$	$\alpha=3$	$\alpha=4$	$\alpha=6$	$\alpha=8$	$\alpha=10$	$\alpha=12$
0.2	1.52	1.97	2.74	4.05	6.28	16.8	49.3	156.0	520.0
0.3	1.42	1.77	2.36	3.32	4.90	11.7	30.8	87.1	260.0
0.4	1.35	1.65	2.13	2.90	4.12	9.08	21.9	57.0	157.0
0.5	1.30	1.56	1.98	2.62	3.61	7.47	16.9	40.9	105.0
0.6	1.27	1.50	1.86	2.42	3.25	6.38	13.6	31.2	75.7
0.7	1.24	1.45	1.78	2.26	2.99	5.60	11.4	24.8	57.4
0.8	1.22	1.41	1.71	2.14	2.78	5.02	9.80	20.4	45.2
0.9	1.20	1.38	1.65	2.04	2.61	4.56	8.59	17.2	36.7
1.0	1.19	1.35	1.60	1.96	2.47	4.20	7.64	14.8	30.5
1.1	1.18	1.33	1.56	1.89	2.36	3.90	6.90	13.0	25.8
1.2	1.17	1.31	1.52	1.83	2.26	3.65	6.29	11.5	22.3
1.3	1.16	1.29	1.49	1.78	2.18	3.44	5.79	10.32	19.4
1.4	1.15	1.28	1.47	1.74	2.10	3.26	5.37	9.35	17.2
1.5	1.14	1.26	1.44	1.70	2.04	3.11	5.01	8.54	15.3
1.6	1.13	1.25	1.42	1.66	1.98	2.97	4.71	7.86	13.8
1.7	1.13	1.24	1.40	1.63	1.93	2.85	4.44	7.28	12.5
1.8	1.12	1.23	1.38	1.60	1.89	2.74	4.21	6.78	11.5
1.9	1.12	1.22	1.37	1.57	1.85	2.65	4.00	6.35	10.56
2.0	1.11	1.21	1.35	1.55	1.81	2.57	3.82	5.97	9.77

TABLE 7

$\mathfrak{F}(\alpha; \beta)$
$(0 \leqslant \alpha \leqslant 12;\ 0 \leqslant \beta^{-1} \leqslant 0.5)$

$1/\beta$	$\alpha=0$	$\alpha=1$	$\alpha=2$	$\alpha=3$	$\alpha=4$	$\alpha=6$	$\alpha=8$	$\alpha=10$	$\alpha=12$
0	1.00	1.00	1.00	1.00	1.00	1.00	1.00	1.00	1.00
0.05	1.00	1.02	1.04	1.06	1.08	1.14	1.20	1.27	1.35
.10	1.02	1.05	1.08	1.13	1.18	1.30	1.44	1.61	1.82
.15	1.03	1.07	1.12	1.19	1.26	1.45	1.69	2.00	2.41
.20	1.05	1.09	1.16	1.25	1.35	1.61	1.96	2.44	3.11
.25	1.06	1.12	1.20	1.30	1.43	1.77	2.24	2.92	3.93
.30	1.07	1.14	1.23	1.35	1.51	1.93	2.54	3.45	4.86
.40	1.09	1.17	1.29	1.46	1.66	2.24	3.16	4.63	7.07
0.50	1.11	1.21	1.35	1.55	1.81	2.57	3.82	5.97	9.77

TABLE 8

LOG $\mathfrak{F}(\alpha; \beta)$
$(0 \leqslant \alpha \leqslant 12;\ 0.2 \leqslant \beta \leqslant 2)$

β	$\alpha=0$	$\alpha=1$	$\alpha=2$	$\alpha=3$	$\alpha=4$	$\alpha=6$	$\alpha=8$	$\alpha=10$	$\alpha=12$
0.2	0.183	0.294	0.438	0.607	0.798	1.224	1.693	2.193	2.716
0.3	.151	.247	.373	.522	.690	1.069	1.489	1.940	2.415
0.4	.130	.216	.328	.463	.615	0.958	1.341	1.756	2.195
0.5	.115	.194	.296	.419	.558	0.873	1.227	1.612	2.021
0.6	.104	.176	.270	.384	.512	0.805	1.135	1.495	1.879
0.7	.095	.162	.249	.355	.475	0.749	1.057	1.395	1.759
0.8	.087	.150	.232	.331	.444	0.701	0.991	1.311	1.655
0.9	.081	.140	.217	.311	.417	0.659	0.934	1.237	1.564
1.0	.075	.131	.204	.293	.393	0.623	0.883	1.171	1.484
1.1	.071	.124	.193	.277	.373	0.591	0.839	1.113	1.412
1.2	.067	.117	.183	.263	.354	0.562	0.799	1.061	1.347
1.3	.063	.111	.174	.251	.338	0.537	0.763	1.014	1.289
1.4	.060	.106	.166	.240	.323	0.513	0.730	0.971	1.235
1.5	.057	.101	.159	.230	.310	0.492	0.700	0.932	1.186
1.6	.054	.097	.153	.220	.297	0.473	0.673	0.896	1.141
1.7	.052	.093	.147	.212	.286	0.455	0.647	0.862	1.099
1.8	.050	.089	.141	.204	.276	0.439	0.624	0.831	1.060
1.9	.047	.086	.136	.197	.266	0.423	0.603	0.803	1.024
2.0	0.046	0.082	0.131	0.190	0.257	0.409	0.582	0.776	0.990

TABLE 9

LOG $\mathfrak{F}(\alpha; \beta)$
$(0 \leqslant \alpha \leqslant 12;\ 0 \leqslant \beta^{-1} \leqslant 0.5)$

$1/\beta$	$\alpha=0$	$\alpha=1$	$\alpha=2$	$\alpha=3$	$\alpha=4$	$\alpha=6$	$\alpha=8$	$\alpha=10$	$\alpha=12$
0	0	0	0	0	0	0	0	0	0
0.05	0.001	0.007	0.015	0.025	0.035	0.057	0.080	0.104	0.130
.10	.008	.019	.034	.051	.071	.113	.159	.208	.261
.15	.014	.030	.050	.075	.102	.162	.229	.302	.382
.20	.020	.039	.065	.096	.130	.207	.293	.388	.493
.25	.025	.048	.078	.114	.155	.247	.351	.466	.594
.30	.030	.056	.090	.132	.179	.285	.404	.538	.687
.40	.038	.070	.112	.163	.221	.351	.500	.666	.849
0.50	0.046	0.082	0.131	0.190	0.257	0.409	0.582	0.776	0.990

Finally, for convenience, we have provided in Table 10 a short list of values of $B_a(0)/F$.

3. *The solution for the temperature distribution in the (2, 2) approximation.*—If we wish to avoid the approximations leading to the simple solution discussed in the preceding sections, then we must use solutions of the transfer problem in higher approximations, which lead to expressions for the temperature distribution that are considerably

TABLE 10

$B_a(0)/F$

a	$B_a(0)/F$	a	$B_a(0)/F$	a	$B_a(0)/F$
0	0	3	0.105602	8	0.00411062
1	0.063357	4	.071678	10	.00068218
2	0.114401	6	0.0204198	12	0.000100166

more complicated. Thus, in the (2, 2) approximation of Paper VII, the temperature distribution is given by (cf. Paper VII, eqs. [109]–[118])

$$\left.\begin{aligned} B(\tau) = \frac{\sigma}{\pi}T^4 = \tfrac{3}{4}F(\tau + 0.6940 - 0.1167\,e^{-k_1\tau}) + \tfrac{1}{2}\bar{\delta}_1 \\ - 0.1664\,(2 + 0.2301\,e^{-k_1\tau})\int_0^\infty e^{-k_1\tau}(\bar{\delta}_3 - \tfrac{1}{3}\bar{\delta}_1 + k_1\bar{\delta}_4)\,d(k_1\tau) \\ + \tfrac{3}{4}\,e^{-k_1\tau}\int_0^\tau e^{+k_1\tau}(\bar{\delta}_3 - \tfrac{1}{3}\bar{\delta}_1 - k_1\bar{\delta}_4)\,d(k_1\tau) \\ + \tfrac{3}{4}\,e^{+k_1\tau}\int_\tau^\infty e^{-k_1\tau}(\bar{\delta}_3 - \tfrac{1}{3}\bar{\delta}_1 + k_1\bar{\delta}_4)\,d(k_1\tau), \end{aligned}\right\} \quad (21)$$

where

$$k_1 = 1.972$$

and (cf. Paper VII, eq. [49])

$$\bar{\delta}_m = \int_0^\infty \left(\frac{\kappa_\nu}{\bar{\kappa}} - 1\right)\sum a_j\mu_j^m \frac{dI_{\nu,j}^{(1)}}{d\tau}\,d\nu, \quad (22)$$

the superscript to $I_{\nu,j}$ indicating that the intensity in a gray atmosphere is implied.

For the foregoing solution in the (2, 2) approximation to be useful, it is necessary that we have tables of the weight functions,

$$W_{1,\nu}(\tau) = \frac{1}{2}\frac{dF_\nu^{(1)}}{d\tau} = \int_{-1}^{+1}\frac{dI_\nu^{(1)}}{d\tau}\,\mu\,d\mu, \quad (23)$$

$$W_{3,\nu}(\tau) = \sum a_j\frac{dI_{\nu,j}^{(1)}}{d\tau}\,\mu_j^3 \simeq \int_{-1}^{+1}\frac{dI_\nu^{(1)}}{d\tau}\,\mu^3\,d\mu, \quad (24)$$

and

$$W_{4,\nu}(\tau) = \sum a_j\frac{dI_{\nu,j}^{(1)}}{d\tau}\,\mu_j^4 \simeq \int_{-1}^{+1}\frac{dI_\nu^{(1)}}{d\tau}\,\mu^4\,d\mu, \quad (25)$$

which are needed in the evaluation of $\bar{\delta}_1$, $\bar{\delta}_3$, and $\bar{\delta}_4$ which occur in the solution.

Now, since $I_\nu^{(1)}$ in equations (23)–(25) refer to the monochromatic intensities in a gray atmosphere (in which κ_ν is independent of ν and equal to $\bar{\kappa}$), it follows that

$$W_{3,\nu}(\tau) = 2\left[K_\nu^{(1)}(\tau) - \tfrac{1}{3}B_\nu^{(1)}(\tau)\right] \tag{26}$$ [6]

and

$$W_{4,\nu}(\tau) = \int_0^\tau W_{3,\nu}(\tau)\, d\tau + 2L_\nu^{(1)}(0), \tag{27}$$

where

$$K_\nu^{(1)}(\tau) = \frac{1}{4}\int_0^\tau F_\nu^{(1)}(\tau)\, d\tau + K_\nu^{(1)}(0) \tag{28}$$

and (cf. Paper VII, eq. [25])

$$\left.\begin{aligned} K_\nu^{(1)}(0) &= \frac{1}{2}\int_0^\infty B_\nu^{(1)}(T_\tau)\, E_3(\tau)\, d\tau, \\ L_\nu^{(1)}(0) &= \frac{1}{2}\int_0^\infty B_\nu^{(1)}(T_\tau)\, E_4(\tau)\, d\tau. \end{aligned}\right\} \tag{29}$$

The derivatives $dF_\nu^{(1)}/d\tau$ of the monochromatic fluxes in a gray atmosphere have already been tabulated in Paper VII (Table 3). We now provide a similar tabulation of the functions $W_{3,a}(\tau)$ and $W_{4,a}(\tau)$ (Table 11).

[6] In Paper VII, eq. (121), there is a slight error; it should read

$$\frac{dK_\nu^{(1)}}{d\tau} = \tfrac{1}{4}F_\nu^{(1)}; \qquad M_\nu^{(1)}(\tau) = K_\nu^{(1)}(\tau) - \tfrac{1}{3}B_\nu^{(1)}(\tau).$$

TABLE 11

THE WEIGHT FUNCTIONS $W_{3,\alpha}(\tau)$ AND $W_{4,\alpha}(\tau)$

α	$\alpha=1$		$\alpha=2$		$\alpha=3$		$\alpha=4$		$\alpha=6$		$\alpha=8$		$\alpha=10$		$\alpha=12$	
	$W_3(\tau)$	$W_4(\tau)$	$W_3(\tau)$	$W_4(\tau)$	$W_3(\tau)$	$W_4(\tau)$	$W_3(\tau)$	$W_4(\tau)$	$W_3(\tau)$	$W_4(\tau)$	$W_3(\tau)$	$W_4(\tau)$	$W_3(\tau)$	$W_4(\tau)$	$W_3(\tau)$	$W_4(\tau)$
0....	−0.0127	0.0224	−0.0126	0.0487	+0.00244	0.0561	+0.0153	0.0490	0.0177	0.0247	0.00906	0.00947	0.00344	0.00317	0.00113	0.000535
0.1....	.0127	.0212	.0152	.0473	−0.00259	.0561	+ .0102	.0503	.0158	.0264	.00889	.0104	.00357	.00352	.00122	.000652
0.2....	.0121	.0199	.0162	.0457	− .00573	.0557	+ .00657	.0511	.0141	.0279	.00866	.0112	.00367	.00359	.00130	.000778
0.3....	.0114	.0187	.0165	.0441	− .00771	.0550	+ .00387	.0516	.0127	.0292	.00841	.0121	.00374	.00426	.00137	.000911
0.4....	.0107	.0176	.0162	.0425	− .00892	.0542	+ .00186	.0519	.0114	.0304	.00815	.0129	.00379	.00463	00143	.00105
0.5....	.00986	.0166	.0157	.0409	− .00962	.0532	+0.000351	.0520	.0103	.0315	.00789	.0137	.00383	.00501	.00149	.00120
0.6....	.00910	.0157	.0150	.0393	− .00998	.0522	−0.00080	.0520	.00932	.0325	.00764	.0145	.00385	.00540	.00154	.00135
0.7....	.00838	.0148	.0143	.0379	− .01015	.0512	− .00172	.0519	.00843	.0334	.00737	.0153	.00386	.00578	.00159	.00151
0.8....	.00771	.0140	.0135	.0365	− .01016	.0502	− .00243	.0516	.00763	.0342	.00711	.0160	.00386	.00617	.00164	.00167
0.9....	.00709	.0133	.0128	.0351	− .01008	.0492	− .00301	.0514	.00690	.0349	.00685	.0167	.00385	.00656	.00167	.00183
1.0....	.00653	.0126	.0121	.0339	− .00991	.0482	− .00346	.0511	.00623	.0356	.00659	.0174	.00382	.00694	.00171	.00200
1.2....	.00554	.0114	.0107	.0316	− .00948	.0463	− .00412	.0503	.00503	.0367	.00607	.0186	.00375	.00770	.00176	.00235
1.4....	.00470	.0103	.00945	.0296	− .00889	.0444	− .00446	.0494	.00406	.0376	.00559	.0198	.00367	.00844	.00180	.00270
1.6....	.00400	.00960	.00837	.0278	− .00831	.0427	− .00467	.0485	.00321	.0383	.00511	.0209	.00356	.00916	.00182	.00307
1.8....	.00343	.00897	.00742	.0263	− .00774	.0411	− .00476	.0476	.00248	.0389	.00466	.0218	.00343	.00986	.00182	.00343
2.0....	−0.00294	0.00833	−0.00657	0.0249	−0.00716	0.0396	−0.00474	0.0466	0.00187	0.0393	0.00424	0.0227	0.00330	0.01054	0.00182	0.00380

ZODIACAL LIGHT IN THE SOLAR CORONA

H. C. VAN DE HULST
Yerkes Observatory
Received March 20, 1947

ABSTRACT

The observations of Grotrian and Öhman show that the continuous light of the corona consists of two components: a component K, strongly polarized and showing no Fraunhofer lines, and a component F, unpolarized and having unbroadened Fraunhofer lines. The former component is believed to arise from electron scattering; the latter is the subject of this paper.

An analysis of the photometric data on the corona and on the zodiacal light indicates that the F-component dominates in the outer corona and suggests strongly that this component is just the extension of the zodiacal light. Other suggested explanations seem to be insufficient.

A theory of the scattering in interplanetary space is given. The scattering by a solid particle consists of diffraction and reflection; the first and the most important part has been neglected in earlier discussion. Curves of the surface brightness as a function of the elongation are obtained for particles of various sizes on the assumption of a constant space density. The assumption that there are no particles within 0.1 A.U. from the sun changes the results only slightly.

Theory and observations are then combined to give the distribution function of the radii, a. It has the form

$$n(a) = 3.5 \times 10^{-20} a^{-2.6}.$$

Particles with radii larger than 0.035 cm are less abundant. In addition, the calculation shows that the color of the F-corona should be slightly redder than the sun. Comparison with the brightness of the zodiacal light at 90° elongation shows either that the albedo of the particles is about 1 per cent or that the space density increases a little toward the sun.

The mean free path in the interplanetary medium is 10^6 A.U. The mean space density is 5×10^{-21} gm/cm^3. The largest particles found in this analysis are of the same size as telescopic meteors but about ten thousand times more abundant. The difference is probably real and indicates the existence of a quiescent cloud besides the rapidly moving meteors.

Some methods by which the theory outlined in this paper may be confirmed and by which further data on the real corona may be obtained are suggested. The F-component is eliminated from Baumbach's table of electron densities, and a revised table is given.

In 1934 W. Grotrian[1] discovered that the Fraunhofer lines in the corona are weaker, but not broader, than the corresponding lines in the solar spectrum. The light of the corona is therefore thought to consist of two superposed components, denoted by F and K. The K-component is characterized by the fact that it has no Fraunhofer lines; they are blurred out by Doppler effect. This component can be explained on the usual assumption that the light is scattered by an atmosphere of free electrons around the sun. On the other hand, the F-component has Fraunhofer lines which have the ordinary depth and width. Near the limb it has only a small fraction of the intensity of the K-component, but it decreases more slowly than does the K-component with increasing distance from the limb and exceeds the K-component at distances larger than 1 solar radius. Presumably, the F-component contributes most of the light of the outer corona.

The explanation suggested by Grotrian is that the F-component arises from scattering by solid particles, possibly related to the particles that cause the zodiacal light. It appears improbable, however, that such particles could exist in the hot region near the sun. But the observations themselves appear reliable. Spectrographic observations by J. H. Moore[2] have given similar results. Furthermore, the way in which the polarization of the corona changes with the distance from the limb strongly indicates the existence of an unpolarized component that dominates in the outer corona. This component may be

[1] *Zs. f. Ap.*, **8**, 124, 1934.

[2] *Pub. A.S.P.*, **46**, 298, 1934.

identified with the *F*-component. Recently, polarigraphic observations of the eclipse in 1945 by Y. Öhman[3] have established beyond doubt the existence of these two components. In particular, Öhman has obtained some spectrograms for the different directions of polarization which demonstrate that the polarization is due wholly to the *K*-component. The characteristics of the two components, as summarized by Öhman, are shown in Table 1.

The last difference in Table 1 is particularly significant. It shows that the *F*-component at the 1945 eclipse had no relation to the equatorial streamers[4] that mark the form of the corona at a minimum in solar activity. Further, it has also been noticed[5] that the isophotes at very large distances from the center are nearly circular. It is therefore quite likely that the *F*-component has a perfect circular symmetry both in its inner and in its outer parts. Consequently, it is possible that this component has no direct connection with the sun at all and is caused by a diffusing medium somewhere between the sun and the earth. This suggestion implies that—as far as *solar* physics is concerned—the corona outside one or two solar radii from the limb is, for the greater part, a spurious corona. In view of the present widespread interest in the physical state of the corona, a clarification of this problem would be useful.

TABLE 1

CHARACTERISTICS OF THE TWO COMPONENTS OF THE CORONA

K-Component	*F*-Component
No spectral lines	Fraunhofer lines
Steep decrease of intensity outward	Slow decrease of intensity outward
High degree of polarization	Low polarization, or none
Same color as the sun	Same color as the sun
Much stronger near the sun's equator than near the sun's pole	Equally bright in polar and equatorial regions

PHOTOMETRIC DATA

Let ρ denote the angular distance from the center of the sun, measured in solar radii. Then, according to S. Baumbach,[6] the surface brightness of the corona in the range $1.02 < \rho < 5$ can be represented by the formula

$$H(\rho) = \frac{0.053}{\rho^{2.5}} + \frac{1.425}{\rho^{7}} + \frac{2.565}{\rho^{17}},$$

where $H(\rho)$ is expressed in the unit which is 10^{-6} times the surface brightness at the center of the disk; we shall denote this unit by "unit$_B$."

Grotrian[1] expresses the results of his measurements in an arbitrary unit, "unit$_G$." By plotting the curves on a logarithmic scale, it was found that Grotrian's curve for the *F*- and *K*-components combined coincides approximately with Baumbach's curve if

$$\log \text{unit}_G - \log \text{unit}_B = -2.20 .$$

Figure 1 shows the resulting position of these curves and also the curves for the separate *F*- and *K*-components. Since the steep decrease of the *K*-component continues beyond $\rho = 2$, we may assume that the light beyond $\rho = 3$ is almost entirely due to the *F*-component. Thus we have fairly good curves for the *F*-component in the ranges $1.2 < \rho < 2$ (Grotrian) and $3 < \rho < 5$ (Baumbach). These curves are shown also by the heavy lines in the upper left corner of Figure 2, in which the ρ-scale is logarithmic. They can be con-

[3] *Pop. astr. Tidskr.*, **27**, 133, 1946.

[4] Photographs in this *Journal*, **102**, 135, 1945.

[5] Cf. D. K. Bailey, *Ap. J.*, **87**, 74, 1938.

[6] *A.N.*, **263**, 121, 1937.

nected by a smooth curve with an initial slope of -5 and a final slope of -2.5. We can accordingly represent this curve by the approximate expression,

$$H_F(\rho) = \frac{0.053}{\rho^{2.5}} + \frac{0.20}{\rho^5}.$$

We can now estimate the total light. For the solar disk we may assume a limb-darkening coefficient of 0.8. Integrating the surface brightness of the various components over the entire surface, we find

$$I_{\text{disk}} = 0.8 \times 10^6,$$

$$I_{\text{corona}} = 1.12,$$

$$I_{F\text{-corona}} = 0.34.$$

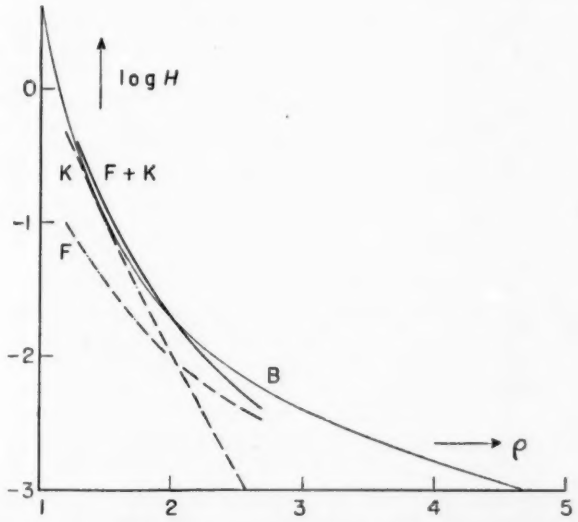

FIG. 1.—Surface brightness of the corona against distance from the center of the sun. *B*, Baumbach's curve; $F + K$, F, K, Grotrian's curves for the total light and the separate components.

Consequently, the F-component contributes 30 per cent of the total light of the corona. It should be noted, however, that the ratio of the two components is not constant. It varies considerably with the position angle and may also vary from eclipse to eclipse. Photometry is mostly made in the region of the coronal streamers. Since these streamers consist of electrons, they belong to the K-corona. It is possible, therefore, that an unbiased estimate of the light of the F-component would amount to even more than 30 per cent of the total light. On the whole, the accurate photometric separation of the F- and K-components deserves further attention.

Nothing reliable is known about the surface brightness between elongations 1°20′ ($\rho = 5$) and 30° from the sun. Observations in this region, both during an eclipse and after sunset, are hindered by scattered light in the earth's atmosphere. For greater elongations, however, we have measurements of the zodiacal light. During a solar eclipse it cannot be observed, but it is certainly present. Therefore, apart from the different circumstances of observation, there is no obvious distinction between the outer corona and the inner zodiacal light.

Accurate photoelectric photometry of the zodiacal light has been made by C. T. Elvey and F. E. Roach.[7] From their isophotal maps the intensities along the ecliptic were read. They show a seasonal variation of some 20 per cent around the average, but the mean curve is well defined in the entire range, $40^\circ < \epsilon < 180^\circ$ (ϵ = elongation). The unit of surface brightness, unit$_{ER}$, corresponds to 1 star of the tenth magnitude per square degree. The sun has the photovisual magnitude[8] of -26.8, an area of 0.22 square degrees, and a mean surface brightness of 0.73×10^6 Baumbach units. Combining these data, we find

$$\log \text{unit}_B = \log \text{unit}_{ER} + 9.50 .$$

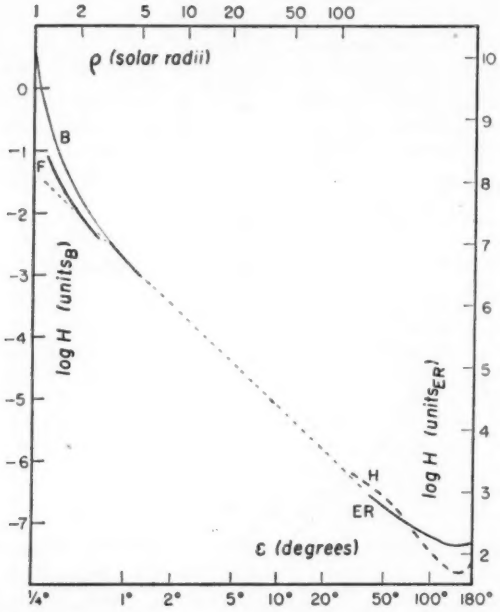

FIG. 2.—Surface brightness of the corona and of the zodiacal light on corresponding scales. Curves *F* and *B* are taken from Fig. 1; *ER*, Elvey and Roach; *H*, Hoffmeister. The two parts are tentatively connected by the dotted line, slope -2.4.

Further, there is an extensive set of visual observations by C. Hoffmeister[9] in the range $30^\circ < \epsilon < 180^\circ$. The results are given in a unit which corresponds to one star of magnitude 2.22 per square degree. A simple reduction gives

$$\log \text{unit}_H = \log \text{unit}_{ER} + 3.11 .$$

We can now plot the surface brightness of the zodiacal light in the same graph in which the surface brightness of the corona was plotted. The new curves are shown in the lower right corner of Figure 2. Though there is a wide gap between the elongations 1°.3 and 30°, a smooth connection between both curves is strongly suggested by the slopes of the curves at either end of the gap. Tentatively connecting both ends by a straight line (the dotted line in Fig. 2), we find that the surface brightness decreases with the inverse 2.4th power of the elongation.

[7] *Ap. J.*, **85**, 231, 1937.

[8] G. P. Kuiper, *Ap. J.*, **88**, 429, 1938.

[9] *Veröff. Berlin-Babelsberg*, Vol. **8**, No. 2, 1930, and Vol. **10**, No. 1, 1932.

SOME INSUFFICIENT EXPLANATIONS

We may first mention some suggested explanations of the *F*-component that would seem inadmissible.

a) First, there is scattering—atmospheric and instrumental—of the coronal light itself. Various effects of this type have been discussed by Baumbach[10] and by Y. Hagihara.[11] However, they cannot explain the presence of the Fraunhofer lines in the *F*-component. We must therefore look for some other mechanism by which *photospheric* light can be received without the aid of the free electrons.

b) Direct scattering in the atmosphere of the earth may be excluded for geometrical reasons. Let the observing station be in the center of the shadow cone. The line of sight directed to some point of the corona then passes into sunlit regions of space at several thousands of kilometers above the surface of the earth. At such altitudes there is no atmosphere that would cause any appreciable scattering.

c) Baumbach has also made calculation on multiple scattering in the atmosphere. This effect involves at least two scatterings under fairly large angles. It probably determines the general brightness of the sky during an eclipse.[12] However, the light thus scattered also covers the dark surface of the moon, and there is no reason why it should show any increase of intensity near the sun's limb. Moreover, it may be partially polarized. For all these reasons it cannot explain the *F*-component.

d) An apparently new suggestion is that we might observe photospheric light that is diffracted around the edge of the moon. Such light is certainly present; only by a quantitative computation can we show that its effect is negligible. If the sun were a point source and the moon were a screen with a straight edge, the intensity at the surface of the earth would have the regular Fresnel-type distribution, $F(v)$. Here v is the distance outward from the geometric edge of the shadow limit, divided by $(b\lambda/2)^{1/2}$, where b is the distance from the moon to the earth. Substituting $\lambda = 5000$ A and $b = 380{,}000$ km, we find that this unit is 10 meters. More than 100 meters outside the edge of the shadow ($v > 10$) we have $F(v) = 1$, i.e., normal illumination. Near the edge of the shadow we have the typical fluctuations of the Fresnel distribution that can be observed during occultations of bright stars.[13] More than 100 meters inside the shadow edge ($v < -10$) we have

$$F(v) = (2\pi^2 v^2)^{-1} = \frac{0.05}{v^2}.$$

It follows that at the center of a band of totality, of width 34 km, the illumination by a point on the solar limb is 2×10^{-8} times the normal and the illumination by a point near the center of the disk is 2×10^{-12} times the normal. Integration gives the illumination by light from the whole solar disk in that case to be 4×10^{-10} times the normal illumination. This means that the "lunar corona" has a total intensity 0.0003 times that of the observed corona, i.e., 0.001 times that of the *F*-component.

Though this effect is now ruled out as a possible explanation of the *F*-component, we may ask whether it would still be observable. The diffracted light should be observed as coming from a brilliant line along the edge of the moon. The theory[14] has not been worked out in sufficient detail to predict the intensity distribution across this brilliant line. In order for its surface brightness to exceed the surface brightness of the inner corona, it should extend over only 0".04. Since this distance cannot be resolved, the effect is unobservable.[15]

[10] *A.N.*, **267**, 273, 1939.

[11] *Ann. Tokyo Astr. Obs.*, Vol. **1**, Nos. 3 and 4, 1939.

[12] J. Q. Stewart and C. D. MacCracken, *Ap. J.*, **91**, 51, 1940.

[13] A. E. Whitford, *Ap. J.*, **89**, 472, 1939; *A. J.*, **52**, 131, 1947.

[14] A. Sommerfeld, *Frank und Von Mises, Diff. Gl. der Physik.* (New York, 1943), **2**, 845 ff.

[15] The effect might be stronger near the beginning and the end of totality. However, even the brightness gradient at the edge of the solar disk, measured by B. Lindblad and calculated by R. Wildt (*Ap. J.*, **105**, 82, 1947), is not very steep. The corrections for diffraction may amount to 1 per cent at most.

SCATTERING IN INTERPLANETARY SPACE

The only explanation left is Grotrian's original hypothesis that the F-component is due to scattering by solid particles. For convenience we assume that the particles are spherical. We define[16] the scattering function $I(\theta)$ of a spherical particle as the amount of radiation scattered per unit solid angle in a direction inclined at an angle θ with the direction of incidence, divided by the incident radiation that hits the geometrical cross-section of the particle.

Let J denote the intensity of the solar radiation at a distance $R = 1$ A.U. from the sun.

Consider a column of height $d\Delta$ and cross-section σ, seen at an elongation ϵ from the sun (see Fig. 3). Let its distance from the sun be r and its distance from the earth be Δ.

Let the column $(\sigma, d\Delta)$ contain n particles per cubic centimeter with radii a. These particles receive the flux of solar radiation,

$$J \cdot (r/R)^{-2} \cdot \sigma d\Delta n \cdot \pi a^2 ,$$

of which the fraction $I(\theta)\Delta^{-2}$ is scattered to 1 cm^2 of the surface of the earth. This flux is seen coming from a solid angle $\sigma\Delta^{-2}$, so that the surface brightness of the column is

$$H_{\text{col}} = JR^2 r^{-2} n\pi a^2 I(\theta)\, d\Delta .$$

The total surface brightness at elongation ϵ from the sun is found by integrating H_{col} over the entire line of sight EQ. Substituting

$$r = R\frac{\sin\epsilon}{\sin\theta} \qquad \text{and} \qquad d\Delta = R\frac{\sin\epsilon}{\sin^2\theta}\, d\theta$$

and assuming, further, that there are $n(a)da$ particles per cubic centimeter that have radii in the interval da, we find for the surface brightness at elongation ϵ:

$$H(\epsilon) = JR(\sin\epsilon)^{-1}\int_0^\infty \pi a^2 da \int_\epsilon^\pi n(a)\, I(\theta)\, d\theta . \tag{1}$$

All earlier theories of the zodiacal light emphasize Seeliger's statement that the curve of $H(\epsilon)$ for $\epsilon < 90°$ does not depend very much on the exact form of $I(\theta)$. The main cause of the increasing brightness toward the sun must then be an increase of the "optical space density,"

$$f(r) = \int_0^\infty n(a)\, a^2 da ,$$

with decreasing r. In particular, the observed law, $H(\epsilon) \sim \epsilon^{-2.4}$, would require $f(r) \sim r^{-1.4}$, and near the sun the optical density would have to be very high.

The error in this reasoning is that it *neglects the diffracted light*. The light diffracted by a large particle shows a rapid decrease of intensity with increasing θ. Taking this fact into consideration, the importance of the two effects is completely reversed. The high gradient of the surface brightness is entirely due to the form of the scattering function, $I(\theta)$, and we need not assume an increase of the optical space density. This will become apparent from the following analysis.

The intensity of diffracted light may be calculated by means of the usual Fraunhofer diffraction theory. It can also be derived from G. Mie's[17] electromagnetic theory of the scattering by spheres of arbitrary size and refractive index. In a recent study[16] of this

[16] H. C. van de Hulst, "Optics of Spherical Particles" (Thesis, Utrecht, 1946); also published in *Rech. astr. de l'Obs. d'Utrecht*, Vol. **11**, Part I, 1946.

[17] *Ann. d. phys.*, **25**, 377, 1908.

theory and its asymptotic cases it was shown that ordinary diffraction, reflection, and refraction together constitute the scattering by a sphere whose radius is much larger than the wave length. Setting $2\pi/\lambda = k$ and $x = ka$, we can write the scattering function for $x \gg 1$ in the form

$$I(\theta) = I_r(\theta) + I_d(\theta).$$

The first part, due to reflection and refraction, depends on the material of the sphere but not on x. For instance, smooth, totally reflecting spheres give

$$I_r(\theta) = \frac{1}{4\pi}.$$

The second part, due to diffraction, depends on x but not on the material. It is expressed by the formula[18]

$$I_d(\theta) = \frac{1}{4\pi} x^2 \Phi(x\theta),$$

where

$$\Phi(z) = \{2z^{-1}J_1(z)\}^2.$$

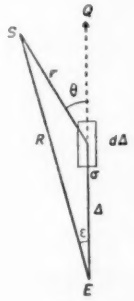

FIG. 3

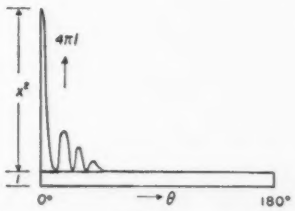

FIG. 4

FIG. 3.—Position of scattering element in space; S = sun, E = earth

FIG. 4.—Schematic representation of the scattering function of a totally reflecting sphere

Figure 4 gives a schematic representation of the scattering function. The importance of the diffracted radiation is further illustrated by the fact that its total amount, found by integrating $I_d(\theta)$ over all directions, is 1, i.e., just equal to the total amount of reflected and refracted radiation. For absorbing particles the latter amount is even less.

The separation of $I(\theta)$ into the parts $I_d(\theta)$ and $I_r(\theta)$ is not possible when x is small. For transparent particles, e.g., water drops, the limit of correctness of the ordinary diffraction theory is at about $x = 20$ (Van de Hulst, *op. cit.*, chaps. vii and viii). For totally reflecting particles it is at about $x = 3$ (*ibid.*, chap. vi), and for metallic particles we may put the limit near $x = 5$ (*ibid.*, chap. ix). We may assume that also for particles with a rough surface the ordinary diffraction theory is valid if $x > 5$. In this case we may choose for $I_r(\theta)$ one of the classical phase functions.[19] On account of the present definition of $I(\theta)$, we have to multiply the usual expressions for these phase functions by γ/π, where γ is the albedo, and to replace the scattering angle by its supplement. For a sphere with Lambert's phase function we then have

$$I_r(\theta) = \frac{2\gamma}{3\pi^2}(\sin\theta - \theta\cos\theta).$$

[18] In textbooks one may find this formula with the argument $x \sin\theta$ and with an additional factor $\cos^4\theta/2$. It would seem that the difference has no meaning: for small θ it vanishes and for large θ the presence of the reflected and refracted light renders the distinction inessential (Van de Hulst, *op. cit.*, chap. v).

[19] E. Schoenberg, *Handb. d. Ap.*, **2**, Part I, 159, 1929.

In our further analysis we assume that $n(a)$ is *the same function throughout the plane of the earth's orbit*. Equation (1) may then be written in the form

$$H(\epsilon) = \tfrac{1}{4} J R \epsilon^{-1} \int_0^\infty n(a)\, a^2 F(\epsilon)\, da\,, \tag{2}$$

where

$$F(\epsilon) = \frac{\epsilon}{\sin \epsilon} \int_\epsilon^\pi 4\pi I(\theta)\, d\theta\,. \tag{3}$$

Apart from the factor ϵ^{-1}, the function $F(\epsilon)$ is proportional to the surface brightness due to particles of a given size. Our next step is therefore to calculate the functions $F(\epsilon)$ for particles of various sizes and surface conditions. Again we may separate $F(\epsilon)$ into the parts $F_d(\epsilon)$ and $F_r(\epsilon)$.

TABLE 2

FUNCTIONS CONNECTED WITH THE DIFFRACTED LIGHT

z	$\Phi(z)$	$\Psi(z)$	z	$\Phi(z)$	$\Psi(z)$
0	1.0000	1.698	5	0.0172	0.0301
1	0.7746	0.779	6	0.0085	0.0156
2	0.3336	0.225	7	0.0000	0.0127
3	0.0511	0.055	8	0.0035	0.0112
4	0.0011	0.040	9	0.0030	0.0074
			10	0.0001	0.0061

The function $F_d(\epsilon)$ depends on x. Substituting for $I_d(\theta)$, we obtain

$$F_d(\epsilon) = x\Psi(x\epsilon)\,,$$

with

$$\Psi(z) = \int_z^\infty \Phi(z')\, dz'\,.$$

Since the diffraction theory is accurate only for small values of θ, we have omitted the factor $\epsilon/\sin\epsilon$ and extended the range of integration to ∞. The functions $\Phi(z)$ and $\Psi(z)$ are tabulated in Table 2; the values of the latter function have been obtained by numerical integration. It may be mentioned[20] that $\Psi(0) = 16/3\pi$ and that for large values of z the function $\Phi(z)$ fluctuates around the values $4/\pi z^3 = 1.27z^{-3}$, while $\Psi(z)$ fluctuates around $2/\pi z^2 = 0.64z^{-2}$. The surface brightness of the light diffracted by large particles is therefore proportional to ϵ^{-3}, which is more than sufficient to allow for the observed intensity gradient of the corona and the zodiacal light.

The function $F_r(\epsilon)$ depends on the composition and the surface condition of the spheres. For polished spheres we have

$$F_r(\epsilon) = \frac{\epsilon(\pi - \epsilon)}{\sin \epsilon}\,;$$

this is approximately constant, varying between 2.45 at $\epsilon = \pi/2$ and 3.14 at $\epsilon = 0$ or π. If the spheres reflect the light according to Lambert's phase function, we obtain

$$F_r(\epsilon) = \gamma \frac{\epsilon}{\sin \epsilon} \frac{8}{3\pi} (2 + 2\cos\epsilon + \epsilon \sin\epsilon)\,.$$

[20] Cf. G. N. Watson, *Bessel Functions* (Cambridge, England: Cambridge University Press, 1944), p. 389.

Table 3 shows the values of this function, together with the values of $I_r(\theta)$; the tabulated values are for $\gamma = 1$. Again we see that $F_r(\epsilon)$ does not change its order of magnitude in the entire range of directions. Therefore, the surface brightness of the reflected light is approximately proportional to ϵ^{-1}.

The values of $F(\epsilon)$ thus calculated are shown together as the solid curves in Figure 5. The curve for polished totally reflecting spheres has only theoretical interest. For the

TABLE 3

FUNCTIONS CONNECTED WITH LAMBERT'S PHASE FUNCTION

θ	$I_r(\theta)$	$F_r(\theta)$	θ	$I_r(\theta)$	$F_r(\theta)$
0	0.0000	3.40	105	0.097	5.25
15	.0004	3.44	120	.129	5.77
30	.0032	3.54	135	.160	6.35
45	.0102	3.74			
60	.0231	4.00	150	.187	7.00
			165	.205	7.71
75	.0424	4.36	180	0.212	8.39
90	0.0674	4.76			

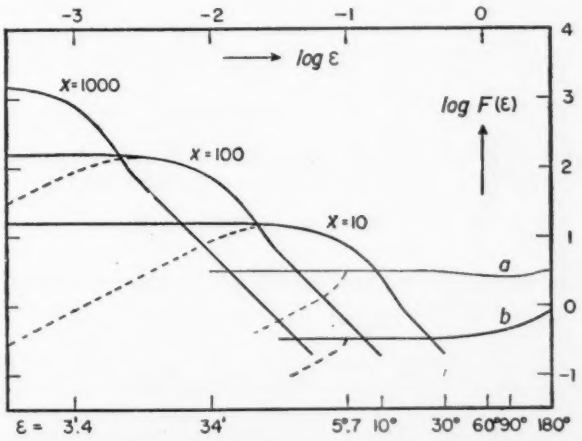

FIG. 5.—Theoretical scattering curves for particles of various sizes. Both scales are logarithmic; $F(\epsilon)$ is proportional to ϵ, the surface brightness. The solid curves are derived on the assumption of a homogeneous density throughout space, the dashed curves on the assumption that there are no particles within 0.1 A.U. from the sun. *Left*, the diffraction part for various values of x; *right*, the reflection part for polished spheres (a) and for Lambert spheres with albedo 0.1 (b).

actual particles we assume that Lambert's phase function is valid and that the albedo is 0.10; this value of γ may be a suitable estimate for metallic or stony particles. The complete curve of $F(\epsilon)$ for particles of a given size consists now of three distinct parts. For $\epsilon < \epsilon_1$, $F(\epsilon)$ has the constant value $1.70\,x$; for $\epsilon_1 < \epsilon < \epsilon_2$ it decreases proportionally to ϵ^{-2}; and, finally, for $\epsilon > \epsilon_2$ reflection is the main source of scattered light and $F(\epsilon)$ is again approximately constant, having a value between 0.4 and 0.8. The surface brightness in these three regions is proportional to ϵ^{-1}, ϵ^{-3}, and ϵ^{-1}, respectively. Table 4 shows the values of ϵ_1 and ϵ_2; they have been computed on the assumption that $\lambda = 4400$ A, $k = 1.4 \times 10^{-5}$ cm^{-1}.

One serious objection may be raised against the foregoing calculations. The factor $(\sin \epsilon)^{-1}$ in formula (1) arises from the fact that the particles are more strongly illuminated, the nearer they are to the sun. Obviously, this relation must break down for very small values of ϵ, because solid particles cannot exist in the regions close to the sun. By fairly complex calculations[21] one can estimate the distances in which particles of various sizes and thermal properties can approach the sun. However, we shall make here the simple assumption that there is a region of radius 0.1 A.U. around the sun which is void of particles and that outside this region the density is uniform as before. A black body at 0.1 A.U. from the sun would have a temperature of 870° K.

The effect on $F(\epsilon)$ is easily calculated; we denote the revised values by $F'(\epsilon)$. For $\epsilon > 5\overset{\circ}{.}7$ we have $F'(\epsilon) = F(\epsilon)$, because the line of sight does not pass through the empty region. For $\epsilon < 5\overset{\circ}{.}7$ the range of integration in formula (3) has to be changed. It now consists of two parts, one extending from ϵ to θ_1, and the other extending from θ_2 to π. Here θ_1 and θ_2 are the sharp and obtuse angle, respectively, defined by

$$\sin \theta_1 = \sin \theta_2 = 10 \sin \epsilon .$$

TABLE 4

ANGLES BETWEEN WHICH THE SURFACE BRIGHTNESS CHANGES PROPORTIONALLY TO ϵ^{-3}

a	x	ϵ_1	ϵ_2	a	x	ϵ_1	ϵ_2
7×10^{-5} cm	10	$3\overset{\circ}{.}5$	25°	7×10^{-3} cm	1,000	$2\overset{'}{.}1$	$2\overset{\circ}{.}5$
7×10^{-4}	100	$21'$	8°	7×10^{-2}	10,000	$0\overset{'}{.}2$	$47'$

Obviously, the correction is largest if ϵ is very small. In that case we have $\theta_1 = 10\epsilon$ and $\theta_2 = \pi - 10\epsilon$. The revised expression for the diffracted light is then

$$F'_d(\epsilon) = x\{\Psi(x\epsilon) - \Psi(10x\epsilon)\}.$$

Only for $x\epsilon < 0.1$ the second term has a serious effect; the expression then reduces to

$$F'_d(\epsilon) = 9x^2\epsilon .$$

For moderate values of $x\epsilon$ the correction can be derived from Table 2. For large values of $x\epsilon$ the second term is just 1 per cent of the first one, so that the correction is negligible.

This result reveals an interesting fact: As long as we deal with the outer portions of the diffraction pattern, *the brightness observed at small elongations from the sun is due to particles that are* not *relatively close to the sun.* The explanation is apparent from equation (2). The effect that the particles near the sun are more strongly illuminated is overcompensated by the effect that the particles closer to the earth diffract the light more effectively because of the smaller angle.

Conversely, the reflected light is contributed mostly by that part of the line of sight that is nearest to the sun. The exclusion of the empty region has therefore a serious effect on $F_r(\epsilon)$. It is sufficient to write down the revised formulae for the case where ϵ *and* θ_1 are small. These formulae are

$$\text{Polished spheres} : F'_r(\epsilon) = \pi - \theta_2 + \theta_1 - \epsilon = 19\epsilon ,$$

$$\text{Lambert spheres} : F'_r(\epsilon) = \tfrac{8}{3}\gamma(\pi - \theta_2) = 26.7\gamma\epsilon .$$

[21] H. N. Russell, *Ap. J.*, **69**, 49, 1929.

The values of $F'(\epsilon)$ are shown by the dashed curves in Figure 5. It is seen that for very small angles the $F'(\epsilon)$ of each component is proportional to ϵ, so that the corresponding surface brightness is a constant. For the reflected light this occurs as soon as $\epsilon < 5°.7$ but for the diffracted light it occurs only when $\epsilon < \epsilon_1/4$. The surprising result emerges that those parts of the curves which are most effective in determining the scattering by a mixture of particles of various sizes are just the parts that are not affected by the absence of particles in the hot region around the sun.

THE DISTRIBUTION FUNCTION OF THE RADII

We shall now investigate what information about the interplanetary particles can be gained from a comparison of the photometric data and the theoretical scattering curves. First, we assume that the photometric data are exactly represented by the straight line in Figure 2. The equation of this line is

$$H(\epsilon) = 1.2 \times 10^{-7} \epsilon^{-2.4}, \tag{4}$$

where H is expressed in units$_B$ and ϵ in radians. We may anticipate that the distribution function of the radii has the form

$$n(a)\, da = C a^{-p} da \qquad (a_1 < a < a_2). \tag{5}$$

We confine ourselves to elongations $< 30°$, for which the reflected light may be neglected. Equation (2) then becomes

$$H(\epsilon) = \tfrac{1}{4} JR\epsilon^{-1} \int_{a_1}^{a_2} C a^{-p+2} k a \Psi(k a \epsilon)\, da .$$

After replacing the limits of integration by 0 and ∞, we obtain

$$H(\epsilon) = \tfrac{1}{4} JRCC_p k^{p-3} \epsilon^{p-5}, \tag{6}$$

where

$$C_p = \int_0^\infty z^{-p+3} \Psi(z)\, dz .$$

Comparison of equations (4) and (6) gives $p = 2.6$. By numerical integration it was found that $C_{2.6} = 2.1$. If Ψ is replaced by Ψ' (empty region around the sun), the value is only 4 per cent less.

The intensity J may be expressed in the present units by writing it as the product of the mean surface brightness of the sun and the solid angle subtended by the solar disk. These factors are 0.8×10^6 units$_B$ and 0.64×10^{-4} steradians, respectively, so that $J = 51$. By substituting further the values $R = 1.5 \times 10^{13}$ and $k = 1.4 \times 10^5$ ($\lambda = 4400$ A), equation (6) is reduced to

$$H(\epsilon) = 3.5 \times 10^{12} C \epsilon^{-2.4},$$

so that equation (4) is satisfied by $C = 3.5 \times 10^{-20}$

The factor k ($= 2\pi/\lambda$) appears in equation (6) with the exponent -0.4. This means that the F-corona and the zodiacal light at small elongations should be a little redder than the sun. This result may seem surprising at first sight. It should be noted, however, that the total light diffracted by a large particle is independent of wave length (and equal to the light falling on its cross-section[22]). The outer parts of the diffraction pattern are relatively red, while the inner part is relatively blue; the intermediate parts are the most effective parts in the present solution.

The predicted color difference between the corona and the sun is even smaller than the difference between the center and the limb of the sun. Therefore, it may easily have

[22] Van de Hulst, *op. cit.*, chaps. ii and v.

escaped detection. Accurate photometry at two widely different wave lengths would seem desirable for a check. Radiometric observations by V. B. Nikonov[23] have indeed indicated an infrared excess of the corona; however, the observation is very uncertain.

We shall next discuss the surface brightness in the immediate neighborhood of the sun. The curve marked F in Figure 2 shows an increase over the dotted line, which represents the exponential relation (4). An obvious explanation for such an increase is given by the sun's size. In order to confirm this explanation quantitatively, we may formulate the following problem: Given the surface brightness of diffuse light at an angular distance ρ from a point source of intensity 1 equal to ρ^{-q}, what will be the surface brightness at the angular distance ρ from the center of a luminous disk with radius 1 and total intensity 1? The answer to this problem is expressed by the integral

$$f(\rho) = \frac{1}{\pi} \int_0^{2\pi} d\varphi \int_0^1 (\rho^2 + r^2 - 2r\rho \cos\varphi)^{-q/2} r \, dr .$$

It should be noted that we are allowed to consider the sun as a luminous disk instead of a luminous sphere because it was stated earlier that the effect of particles close to the sun is negligible. For the case $q = 2$, analytical integration gives

$$f(\rho) = -\ln(1 - \rho^{-2}) .$$

TABLE 5

INCREASE OF LOG $H(\rho)$ DUE TO THE SUN'S SIZE

ρ	Calc. $q=2$	Calc. $q=2.5$	Obs. $q=2.4$	ρ	Calc. $q=2$	Calc. $q=2.5$	Obs. $q=2.4$
1.2.....	0.23	0.32	0.41	1.6.....	0.10	0.18	0.18
1.4.....	0.14	0.23	0.27	2.0.....	0.06	0.10	0.01

Further, a graphical integration for the case $q = 2.5$ was made. The disk was divided into about six parts, separated by concentric circles around a point at a distance ρ from its center; the areas of these part were measured and multiplied by the appropriate factor $\rho'^{-2.5}$, and the products were added. Table 5 gives the resulting values of $\log f(\rho) - \log(\rho^{-q})$, i.e., the increase of $\log H(\epsilon)$ over the exponential relation. The corresponding increase shown by the photometric data is given in the last column. The observed increase seems a little steeper than the calculated ones, and this difference would be enhanced if the limb darkening were taken into account. Yet the measurements of the F-component near the sun are not accurate enough to consider the differences as real.

We may conclude that the exponential relation (5) holds, down to the smallest angle for which observations were made. This angle—now measured from the limb—is about 0.2 solar radii, i.e., 0.001 radian. The definite integral $C_{2.6}$ decreases by 20 per cent if the upper limit of integration is taken as 5 instead of as ∞. If 20 per cent is taken for the observational tolerance, this means that the approximation which we made is correct if $ka_2\epsilon > 5$. It is correct down to $\epsilon = 0.001$ if $ka_2 > 5000$, i.e., $a_2 > 0.035$ cm.

The surface brightness at large angles requires a quite different discussion. For $\epsilon > 30°$ the diffracted light comes mainly from very small particles, for which the diffraction formula is not accurately valid. Further, the reflection comes in as an additional cause of scattering. However, we may assume that for $\epsilon > 60°$, reflection is the only effect to

[23] *Bull. Abastumani Obs.*, **7**, 33, 1943.

be taken into account. Substituting the value $F_r(\epsilon) = 4.4$, valid for Lambert spheres and ϵ near 75°, and assuming again the distribution function of the radii given by equation (5), we find from equation (2) that

$$H(\epsilon) = \tfrac{1}{4} JR\epsilon^{-1} 4.4\gamma C \frac{(a_2^{3-p} - a_1^{3-p})}{(3-p)}.$$

Since $3 - p = 0.4$, we may replace a_1 by 0. The photometric curve in the range $60° < \epsilon < 90°$ is approximately represented by the equation

$$H(\epsilon) = 1.0 \times 10^{-7} \epsilon^{-1}.$$

Equating these expressions and using the values of the constants derived earlier, we find

$$\gamma = 0.0013 a_2^{-0.4},$$

which, in combination with the lower limit of a_2, gives

$$\gamma < 0.005.$$

This result is a little lower than we had expected. Since meteorites and meteoric dust are often black,[24] however, a fairly low albedo appears not impossible. In addition, there are several possibilities to widen the margin. First, the phase function of the moon would make the reflected light about three times weaker than it would be on account of Lambert's phase function. Furthermore, we may expect that an irregular form of the particles would enhance the diffracted light without causing a proportional increase of the reflected light. Finally, almost any change in the surface brightness may be effected by assuming that the density varies through the plane of the ecliptic.

For example, we may consider as an extreme case the one in which the distribution of the radii has the form (4) within 0.5 A.U. from the sun, and space is empty outside this region. The surface brightness for $\epsilon > 30°$ is then zero. For $\epsilon < 30°$ it is found by adding a factor $2^{p-4} = 0.38$ to the right-hand member of equation (5). The resulting value of C is then 2.6 times the previous value. This model would therefore explain the surface brightness of the corona without leading to too high a value for the surface brightness of the zodiacal light.

Summarizing the results, we may say that the photometric data are well represented by theory if we assume: (*a*) that the albedo is about 0.1; (*b*) that the distribution of radii has the form

$$n(a) = Ca^{-2.6} \qquad (5a)$$

but that particles with dimensions >1 mm are less abundant than would follow from this formula; and (*c*) that C is about 10^{-20} near the orbit of the earth, 5×10^{-20} at 0.5 A.U. from the sun and 0 within 0.1 A.U. from the sun.

A few words may be added about the zodiacal light at elongations >90°. Part of the variation of brightness in this region may be due to real density variations. This explanation is likely, since there are also seasonal variations in the position of the axis and of the Gegenschein[25] that seem to have some relation with the orbit of Jupiter.[26] In addition, the scattering angles are different from the angles that are effective in the region of small and medium elongations. Consequently, the zodiacal light at large elongations offers a problem which has only little relation to the problem treated above.

[24] I found no values of the albedo mentioned.

[25] C. T. Elvey, *Ap. J.*, **77**, 56, 1933.

[26] Hoffmeister, *op. cit.*

DENSITY OF THE INTERPLANETARY MEDIUM AND RELATION TO METEORS

We return to the original solution, in which the density was supposed to be homogeneous. Using the values $p = 2.6$, $C = 3.5 \times 10^{-20}$, and $a_2 = 0.035$ cm, we find that the mean free path among the interplanetary particles is

$$\left(\frac{\pi C a_2^{0.4}}{0.4}\right)^{-1} = 10^6 \text{A.U.}$$

Roughly the same value follows directly from the ratio of the total intensity of the corona to the total intensity of the sun. It shows that the interplanetary dust cloud is extremely transparent and justifies our assumption that interaction between the scattering particles may be neglected.

The space density is

$$\frac{\frac{4}{3}\pi s C a_2^{1.4}}{1.4} = 5 \times 10^{-21} \text{ gm/cm}^3,$$

where s, the density of the particles, is taken to be 5. P. van Rhyn[27] estimated a density of 5×10^{-18} gm/cm^3 near the earth. The difference of a factor of 1,000 is mainly due to the fact that Van Rhyn assumes arbitrarily that the zodiacal light is caused by rocks with radii of about 50 cm, which is more than 1000 times larger than the radii following from the present investigation.

The thickness of the dust cloud perpendicular to the plane of the ecliptic may be about 0.1 A.U. The total mass of the particles within the orbit of the earth then is 5×10^{18} gm, i.e., 10^{-9} times the mass of the earth. This mass is far too small to produce observable effects on the motion of the planets.

Perhaps the most interesting problem is the relation of these particles to the meteors. The following discussion is based on F. Watson's[28] analysis of meteor frequencies. Watson's formula (1′) gives the relation between mass, velocity, and magnitude of the meteor, based on calculations by E. Öpik.[29] If M = mass in grams, m_z = magnitude reduced to the zenith, and the geocentric velocity is 56 km/sec, this relation becomes

$$\log M = -1.1 - 0.4 m_z . \tag{7}$$

For instance, a second-magnitude meteor has a mass of 0.012 gm. Assuming a density of 5, we have, further,

$$\log M = 1.3 + 3 \log a ,$$

so that

$$\log a = -0.8 - 0.133 m_z .$$

It follows that the naked-eye meteors ($-1.5 < m_z < 5$) are caused by particles with radii in the range $0.25 > a > 0.03$, while the range for telescopic meteors ($5 < m_z < 9$) is $0.03 > a > 0.01$. The particles that cause the F-component of the corona, according to the preceding analysis, have radii up to 0.03 cm. The largest particles among them correspond, therefore, to the telescopic meteors.

Let N be the number of particles per cubic centimeter and let the number in a given interval of mass, radius, or magnitude be denoted by dN. Watson's Figure 2 gives the number of meteors of a given magnitude that daily enter the entire atmosphere of the earth. Assuming again a geocentric velocity of 56 km/sec, we find that this number is

[27] *Pub. Astr. Lab., Groningen*, Vol. **31**, 1921.

[28] *Harvard Ann.*, **105**, 623, 1937.

[29] *Tartu Pub.*, Vol. **29**, No. 5, 1937.

$10^{29.8}$ times the number per cubic centimeter. The straight line in this figure is therefore represented by

$$10^{29.8}\frac{dN}{dm_z} = 10^{4.4+0.60m_z}.$$

Since $dm_z = 10^{0.5}\, a^{-1}\, da$, this relation can be reduced to

$$\frac{dN}{da} = 10^{-28.5}a^{-5.5}. \tag{8a}$$

A similar result is found from Watson's Figure 4: the total number per cubic parsec in a given interval of log M is

$$10^{55.5}\frac{dN}{d(\log M)} = 10^{29.0-1.40\log M},$$

which is reduced by means of $d(\log M) = 10^{0.1}a^{-1}da$ to

$$\frac{dN}{da} = 10^{-28.2}a^{-5.2}. \tag{8b}$$

TABLE 6

NUMBER OF PARTICLES IN INTERPLANETARY SPACE

a (Cm)	m_z	log dN/da			Difference (5)−(8)
		(5)	(8a)	(8b)	
0.10	1.5	<−16.9	−23.0	−23.0	<6.1
.03	5.2	−15.6	−20.3	−20.4	4.8
0.01	9.0	−14.3	−17.5	−17.8	3.4

These results may be compared with the result of the present paper:

$$\frac{dN}{da} = 10^{-19.5}a^{-2.6}. \tag{5}$$

Table 6 shows the values of log dN/da for some values of a in the region where both determinations are valid. The differences shown in the last column are considerable: *the number of particles with sizes between 1 mm and 0.1 mm in interplanetary space is about 10,000 times larger than can be inferred from the number of telescopic meteors.*

Before drawing further conclusions we shall estimate just how reliable this result is. The constants in equation (5) do not depend on any arbitrary estimates; the resultant numbers may be accurate within a factor two. As we have seen earlier, it is also very unlikely that the F-corona can be explained in any different way. The meteor data are more flexible; in particular, the question of the meteor velocities is still a matter for controversy. Fortunately, it does not matter for the present estimate whether the particles come from interstellar space or belong to the solar system: in either case they must be present in interplanetary space. Therefore, even drastic corrections of the velocities cannot change the order of magnitude of the estimated density. Further, Watson's counts refer to sporadic meteors; the number of shower meteors should still be added. However, there are fewer shower meteors than there are sporadic meteors, for the telescopic magnitudes in particular. Therefore, no appreciable change results from this

correction. Independent counts cited by Watson and a later paper by J. D. Williams[30] confirm the general order of magnitude. The total uncertainty would amount to about a factor of 10. The only way to change appreciably the estimates derived from equation (8) is to assume that the physical theory of meteors[29] leads to masses which are much too small. At present this possibility seems unlikely.

Taking, then, the italicized result as significant, we may inquire into its meaning. An obvious explanation is that only a very small fraction of the interplanetary particles have velocities high enough to cause visible meteors. The majority of the particles might move in approximately circular orbits in the same way that the planets and the asteroids do. The dynamical relation of this system to the meteor streams and to the sporadic meteors is not clear. We may, however, mention that a particle moving in some cometary orbit would hit a particle of the quiescent cloud once in 10^6 or 10^7 years. One may therefore conclude from the existing motions that there is some supply from outside the solar system, even if the direct evidence for interstellar meteors is considered doubtful. Furthermore, the existence of such an interplanetary medium may have implications for the motion of comets and for the cosmogony of the solar system.

THE REAL CORONA: SOME SUGGESTIONS

After this discussion of the "spurious" corona, we may ask how the best information about the "real" corona can be obtained. First, we shall have to make quite certain that the *F*-component has indeed no direct connection with the sun. This might be confirmed by observations that would narrow the gap shown by Figure 2. Measurements of the zodiacal light might be extended to 10° from the sun if proper precautions were taken to eliminate twilight. The brightness of the corona, on the other hand, may be measured to considerably larger distances from the sun than has been done so far. The most serious disturbance is the light scattered from outside the eclipse cone. From the measurements by J. Stebbins and A. E. Whitford[31] with a potassium cell, it would follow that the surface brightness of the sky during an eclipse is about one four-hundredth that of the full moon, i.e., $10^{-2.4}$ units$_B$. Since the skylight has the regular blue color, it might be reduced by a factor 25 by observing in the infrared about 1μ; a further factor of 2 or more may be gained by observing from an aircraft. The sky brightness would then come down to $10^{-4.1}$ units$_B$, so that, according to Figure 2, it would equal the brightness of the corona at 4° from the sun.

One unexplained observation should be mentioned. On two occasions Moore[32] found that the Fraunhofer lines in the spectrum of the corona showed a red shift of about 20 km/sec. This observation conflicts with the present explanation of the *F*-component. Even if the diffracting particles had large radial motions, the Doppler effect would not influence the diffracted light. However, the free electrons probably are ejected from the sun with a speed[33] of the order of 1 A.U. per 4 days, i.e., 400 km/sec. Consequently, the Fraunhofer lines of the *K*-corona should have a red shift of this amount. These lines are broadened into very shallow, nearly invisible depressions. Grotrian[34] finds that their broadening between 1′ and 5′ from the limb corresponds to a mean random velocity of 4000 km/sec. At the levels of 10′ and 20′ from the limb, where Moore's observations were made, the broadening might be considerably less, though still large enough to make the lines very shallow. Superposition of the displaced shallow lines over the undisplaced narrow lines of the *F*-corona might then cause an apparent shift of the latter, especially if the dispersion is low.

[30] *Ap. J.*, **92**, 424, 1940.

[31] *Ap. J.*, **87**, 225, 1938.

[32] *Pub. A.S.P.*, **35**, 333, 1923, and **45**, 147, 1933.

[33] K. O. Kiepenheuer, *Ap. J.*, **105**, 408, 1947.

[34] *Zs. f. Ap.*, **3**, 199, 1931, and **8**, 124, 1934.

In several papers on the physical state of the corona, reference is made to the electron densities derived by Baumbach.[6] They have been computed on the assumption that the entire brightness of the corona is due to electron scattering. However, on our present ideas the *F*-component should be excluded. We may obtain the corrected values for the electron density in the following way.

With little change in the numerical values we can write the brightness of the *F*-component in the form

$$H_F(\rho) = \frac{0.053}{\rho^{2.5}} + \frac{0.30}{\rho^{7}}.$$

This formula contains the same powers of ρ as Baumbach's formula for the total brightness, viz., $\rho^{-2.5}$, ρ^{-7}, and ρ^{-17}; the coefficients are the fractions 1.00, 0.21, and 0.00 of the coefficients for the total light. The corrected formula is therefore obtained by multiplying these coefficients by the factors 0.00, 0.79, and 1.00, respectively. Baumbach's analysis

TABLE 7

CORRECTED ELECTRON DENSITIES

r	f	$10^{-6} N(r)$		r	f	$10^{-6} N(r)$	
		Old	New			Old	New
1.00	0.94	458	430	2.2	0.47	2.50	1.2
1.03	.92	311	290	2.4	.39	1.79	0.7
1.06	.90	229	210	2.6	.31	1.35	0.42
1.10	.88	156	137	2.8	.26	1.10	0.29
1.2	.83	70.4	58	3.0	.21	0.91	0.19
1.3	.79	38.4	30	3.5	(.11)	0.63	(0.08)
1.4	.74	23.8	18	4.0	(.07)	0.51	(0.04)
1.6	.67	11.1	7.5	5.0	(0.03)	0.38	(0.01)
1.8	.61	6.1	3.8	6.0	.....	0.25	.....
2.0	0.54	3.7	2.0	8.0	.....	0.16	.....

shows that the same factors should be applied to the formula for the source function, $F(r)$ (Baumbach's formula [6]). The new values of $F(r)$ are computed and found to be a fraction, f, of the original values. Since the geometrical conditions are not changed, f is also the correction factor for the electron densities, $N(r)$. Table 7 shows the results. Near the limb the correction is small; beyond $r = 3$ the correction is so large that the electron density becomes very uncertain.

The *F*-component is only roughly eliminated in this way. The resulting picture of an electron density which is constant in spherical shells around the sun is certainly much too simple. One of the reasons why the data compiled by Baumbach fit so nicely to a single curve is undoubtedly just the presence of the constant *F*-component. The *K*-corona alone probably shows much stronger fluctuations. We may also expect that the coronal streamers, especially their outer parts, actually show more distinct features than are seen on the usual photographs. Taking one calibration spectrum (e.g., along the polar axis) and assuming that the *F*-component has circular symmetry, one might correct the isophotes of the total light so as to obtain the isophotes of the *K*-component. A more reliable method would be the use of various calibration spectra along different lines. It would be still better to exclude the *F*-component directly from the observations. This might be effected by observing the corona, or a part of it, through a filter transmitting a wave-length interval of about 5 A around the center of the H- or K-line. The

F-corona would then be cut down by a factor of 6, while the K-corona would show in approximately full strength.

Addendum, March 31.—In a paper just received, C. W. Allen[35] gives the same explanation of the F-corona as that proposed in the present paper. Allen's paper is particularly important, since it gives new data, obtained at the eclipse of October 1, 1940. A few further points that lend support to the present explanation may now be noted: (*a*) The F-corona seems slightly reddish according to Allen's measurements, in agreement with our formula (6); (*b*) the discrepancy suggested by our Table 5 vanishes when Allen's data are used instead of Grotrian's; and (*c*) Allen finds no confirmation of the unexplained red shift.

The ratio of the F-component to the total intensity found by Allen is smaller than the ratio found by Grotrian at the same distance from the limb. We may suggest that the difference is due to the K-component; this component may have been weak in 1923 (minimum of solar activity) and strong in 1940 (3 years after maximum). Future eclipse expeditions should consider the separation of the two components as a major point of their photometric program.

[35] *M.N.*, **106**, 137, 1947.

RADIAL VELOCITIES AND ABSOLUTE MAGNITUDES OF Be STARS*

BURKE SMITH
Yerkes and McDonald Observatories
Received February 22, 1947

ABSTRACT

The radial velocities of 111 stars listed in the Mount Wilson catalogue of Be stars were measured from spectrograms taken with the McDonald 82-inch telescope. The average measured difference between absorption and emission velocities was -4.3 ± 4.9 km/sec. Comparing the measured absorption velocities with published velocities of B-type stars, the author concludes that, for the magnitude groups which were studied, the mean absolute magnitudes of Be stars agree with those of B-type stars to the same order of magnitude.

Spectrograms of 111 stars with bright-line spectra, obtained in 1942–1943 with the Cassegrain spectrograph of the 82-inch McDonald telescope, have been measured for radial velocity. These spectrograms were taken originally for another purpose, and the radial-velocity measurements are in the nature of a by-product. They were taken on glass plates with quartz prisms and a 500-mm ultraviolet-glass camera, giving a dispersion of 55 A/mm at $H\gamma$. The list includes two Ae and two Oe stars, the remainder being of type Be. In most cases, only one spectrogram per star was available, but for 28 stars there were two or more spectrograms. The apparent magnitudes range from 4.2 to 12.5, with the greater number of stars between the fifth and the ninth magnitudes. All stars are listed in the Mount Wilson catalogue,[1] or supplement,[2] of A and B stars whose spectra have bright hydrogen lines. The line $H\alpha$ is not visible on these plates, which accounts for the fact that emission lines were measured on only about half the plates. For the 65 stars having measurable emission lines, the average measured difference—absorption velocity *minus* emission velocity—was found to be

$$A - E = -4.3 \pm 4.9 \text{ km/sec.}$$

It is concluded that the average velocity derived from emission lines is substantially the same as that derived from absorption lines. In the discussion which follows, only velocities derived from absorption lines will be used.[3]

Of the 111 stars which were measured, there are 32 which also appear in the Victoria catalogue of O- and B-type stars.[4] A comparison of the average measured velocity of these 32 stars with the average velocity of the same stars as published in the Victoria catalogue gives

$$\text{Victoria } \textit{minus} \text{ McDonald} = +0.04 \pm 2.8 \text{ km/sec.}$$

There has been some question as to the luminosity of Be stars compared to that of the average main-sequence B-type stars. By taking account of the galactic-rotation effect and determining the average distance factor, $\bar{r}$, for various groups of stars selected according to apparent magnitude, it should be possible to compare the absolute magni-

* *Contributions from the McDonald Observatory, University of Texas*, No. 133.

[1] *Ap. J.*, **78**, 87, 1933.

[2] *Ap. J.*, **98**, 153, 1943.

[3] Because of lack of space, the measured velocities of individual stars are not given here but are preserved in the files of the Yerkes Observatory.

[4] *Pub. Dom. Ap. Obs., Victoria*, Vol. **5**, No. 2, 1935.

tude of Be stars with that of ordinary B-type stars for each magnitude group. The Victoria catalogue and the results of studies of faint B-type stars by Seyfert and Popper[5] were used to supplement the list of Be stars which were measured by the author. From the Victoria catalogue a total of 97 Be stars was chosen, including the 32 stars mentioned above. Only stars which are listed in the Mount Wilson catalogue were chosen, and stars marked "variable velocity" or which are known to be peculiar or to be spectroscopic binaries were omitted. Eighteen Be stars were selected from the list of faint B-type stars published by Seyfert and Popper. The velocities of these 18 stars are based on measurements of two spectrograms per star. Six stars from the list of 111 measured by the author were omitted, including the 2 A-type stars and others having extreme or peculiar velocities. With these omissions, we have a total of 188 Be stars, which are fairly well distributed in galactic longitude. Table 1 shows the distribution in magnitude.

The effect of galactic rotation was computed by means of the well-known formula,

$$\rho = A\,\bar{r}\,\sin 2\,(l - l_0)\cos^2 b + K\,,$$

where ρ is the observed velocity, corrected for the sun's motion through space and l, b and l_0 are, respectively, the galactic longitude and latitude of the star and the longitude

TABLE 1

DISTRIBUTION OF Be STARS IN MAGNITUDE

Source	Magnitude Groups								Total Stars
	2.0–4.0	4.1–5.0	5.1–6.0	6.1–7.0	7.1–8.0	8.1–9.0	9.1–10.0	10.1–12.5	
Victoria catalogue	8	15	18	15	9	.....	.....	.....	65
McDonald stars	.....	8	13	21	28	26	6	3	105
Seyfert and Popper	.....	.....	.....	.....	.....	3	11	4	18
Total	8	23	31	36	37	29	17	7	188

of the center of rotation. The mean distance of the stars in any magnitude group is found from $A\bar{r}$ when A is known. According to R. E. Wilson,[6] the mean value of A for the type of stars here considered is 17.5 km/sec/kpc.

In their studies of galactic rotation, Plaskett and Pearce[7] determined $A\bar{r}$ and K for each of five magnitude groups of B-type stars, and Seyfert and Popper[5] obtained a solution by the same method for the group of faint B-type stars studied by them. Four magnitude groups were chosen from the 188 stars, and solutions were obtained for $A\bar{r}$ and K which are directly comparable to the solutions for the B-type stars. The value of l_0 was taken as 331°.7, to agree with the value used by Plaskett and Pearce. The corrections for solar motion were obtained from the chart by Pearce and Hill.[8] In obtaining a solution for each magnitude group the velocities were arranged in normal places at intervals of galactic longitude of about 15°, combining velocities for stars 180° apart in longitude. The velocities of the 32 Be stars that are common to the Victoria catalogue and the McDonald list were averaged by weighting according to the number of plates. The normal points were weighted according to the square root of the number of stars included in each longitude group. Least-squares solutions for $A\bar{r}$ and K were then obtained for the stellar lines. In addition, in the case of two magnitude groups (5.6–8.6 and 7.0–10.0), solutions were obtained for the interstellar clouds. For the latter solutions, only stars of spectral type B5 or earlier were used.

[5] *Ap. J.*, **93**, 461, 1941; **100**, 94, 1944.

[6] *Ap. J.*, **92**, 170, 1940.

[7] *Pub. Dom. Ap. Obs., Victoria*, **5**, No. 3, 179, 1935.

[8] *Pub. Dom. Ap. Obs., Victoria*, Vol. **6**, No. 4, 1938.

Table 2 summarizes the results, and in Figure 1 the values for $A\bar{r}$ are plotted against mean magnitude, including both Be and B-type stars. It will be noted that in the case of interstellar lines the Be stars follow closely the trend shown by the ordinary B-type stars. For the stellar lines the agreement is not so good but is within the limits of the probable errors.

TABLE 2

Be STARS—GALACTIC ROTATION FOR MAGNITUDE GROUPS

MAG. LIMITS	MEAN MAG.	STARS	$A\bar{r}$		K	
			Stars	Clouds	Stars	Clouds
0– 5.9	4.89	58	+10.3 ±3.1	.....	+9.17±2.1	.....
4.5– 6.5	5.49	67	+11.17±3.1	.....	+5.0 ±2.1	.....
5.6– 8.6	7.15	103	+14.28±4.1	.....	+0.5 ±2.8	.....
	7.24	68	.....	+10.24±3.7	.....	+0.16±2.8
7.0–10.0	8.12	93	+16.3 ±4.7	.....	−0.5 ±3.3	.....
	8.15	70	.....	+12.74±3.2	.....	+5.5 ±2.3

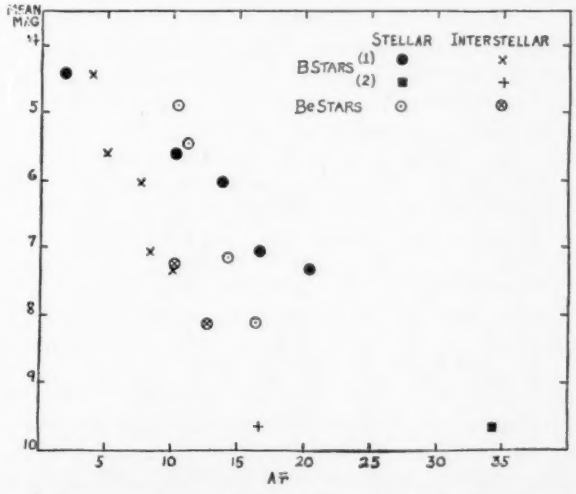

FIG. 1.—Relation between mean magnitude and $A\bar{r}$. Results for B stars (*1*) are from Plaskett and Pearce; for B stars (*2*), from Seyfert and Popper.

Considering the character of the material and the possibility of errors, it is hardly safe to draw any very general conclusions as to the luminosity of the Be stars. However, with due allowance for unknown factors, it seems fair to conclude that, for the magnitude groups which were studied, the mean absolute magnitudes of the Be stars agree with those of the B-type stars to the same order of magnitude.[9]

I am greatly indebted to Dr. Struve for the use of the spectrograms, most of which were obtained by him and Dr. P. Swings in the course of their observations of peculiar stars, and for his kind advice and encouragement.

[9] This is in general agreement with some results obtained by R. E. Wilson (*Ap. J.*, **94**, 20, 1941), who compared a small group (16) of cBe stars with a larger group of cB stars. He concluded that the cBe stars have essentially the same mean luminosity as the cB stars.

THE M-TYPE SUPERGIANT MEMBERS OF THE DOUBLE CLUSTER IN PERSEUS*

W. P. BIDELMAN
Yerkes and McDonald Observatories
Received March 22, 1947

ABSTRACT

Thirteen supergiants of type M are attributed to the galactic cluster h and χ Persei on the basis of spectroscopic absolute magnitude, apparent position, and radial velocity. Most of these stars have been previously suggested as probable cluster members. As this cluster is already known to contain a large number of early-type supergiants, its great abundance of very luminous stars makes it practically unique among investigated galactic clusters.

On the assumption of a true distance modulus of 11.4 for the double cluster, the visual absolute magnitude of early M stars of luminosity class I*a*–I*b* on the system of the Yerkes *Atlas of Stellar Spectra* may be estimated as approximately −5.0. The star of the group which appears to be the most luminous, at least at some times, is S Persei, the light-curve of which shows a rough periodicity of about 835 days but remarkable changes in amplitude.

I. SPECTRAL CLASSIFICATION AND ABSOLUTE MAGNITUDES

That seven of the very red stars situated near the double cluster in Perseus should be considered to be cluster members was pointed out by Adams, Joy, and Humason as early as 1926.[1] Later, Keenan demonstrated, in a study of the spectra of M-type irregular variables of small range, that a clustering of five of the most luminous of these stars exists at the position of the double cluster, and he showed that their spectroscopic absolute magnitudes are consistent with cluster membership.[2] Three of these five stars had been included in the paper of Adams, Joy, and Humason. The extent of the area defined by the late-type supergiants is considerably larger than that usually accepted for h and χ Persei; it was shown subsequently that most of the many early-type supergiants in this region are also associated with the double cluster and that the large cluster comprising these stars extends over an area with a diameter of about 5 degrees.[3]

To investigate further the membership of this extraordinary galactic cluster, spectra of all the late-type stars which have heretofore been suggested as cluster members, together with a few additional stars, were obtained with the $f/1$ Schmidt spectrograph camera attached to the 82-inch telescope of the McDonald Observatory. This combination gives a dispersion of 150 A/mm at Hγ. Spectral types and luminosity classes were estimated following the criteria given in the Yerkes *Atlas of Stellar Spectra*.[4] The spectroscopic luminosity classes and apparent positions of the stars listed in Table 1 are such that association with h and χ Persei appears to be quite certain.

The positions of these red supergiants with respect to the double cluster are illustrated in Figure 1, which is a reproduction of a Tikhov exposure taken in the manner described by Münch and Terrazas.[5] By examining the relative intensity of the two concentric rings of the stellar images, the approximate colors of the stars may be quickly estimated. Three of the stars included in Table 1 are slightly outside the field shown in Figure 1, two being slightly above and the other slightly to the left. All the stars listed in Table 1

* *Contribution from the McDonald Observatory, University of Texas*, No. 134.

[1] *Ap. J.*, **64**, 225, 1926. [2] *Ap. J.*, **95**, 461, 1942. [3] *Ap. J.*, **98**, 61, 1943.

[4] Morgan, Keenan, and Kellman, "Astrophysical Monographs" (1943).

[5] *Ap. J.*, **103**, 371, 1946.

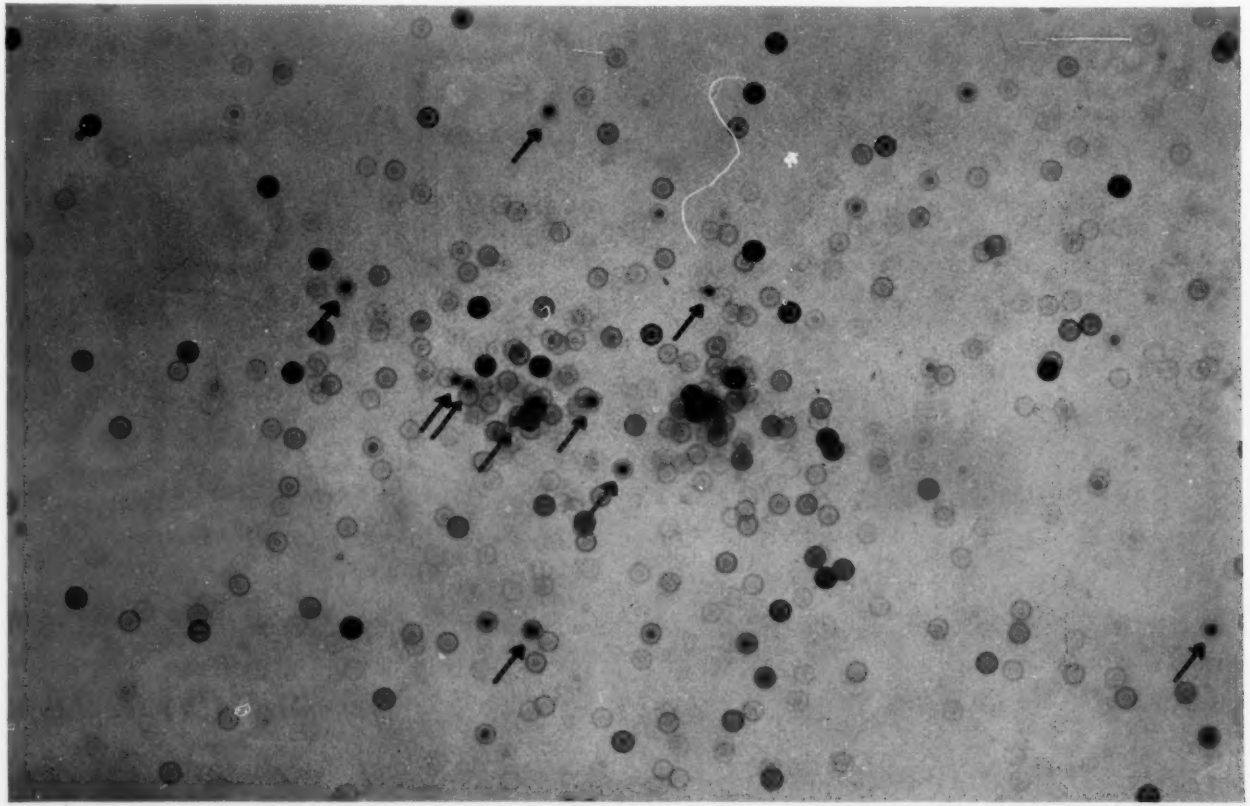

FIG. 1.—Tikhov exposure of the double cluster in Perseus. Ten of the M-type supergiant members of the cluster are indicated, the other three stars being slightly outside the region shown. The colors of the stars may be estimated by comparing the intensities of the inner and outer concentric rings of the star images. The outer rings are due to blue light; the inner, to red. Plate taken with 10-inch Bruce telescope with a 6-inch central stopover lens. Eastman 103a-E plate. The exposure was made on September 27, 1946. North is toward binding; east is at bottom of page.

are within $2\frac{1}{2}°$ of the center of the double cluster, but the close association of four of the M-type supergiants with the cluster χ Persei is especially noteworthy.

Published radial velocities are available for but three of the supergiants; these are given in the notes to Table 1, and they agree well with the radial velocities of the B- and A-type supergiant members of the cluster. To determine whether the radial velocities of the other stars are consistent with cluster membership, one low-dispersion plate (150 A/mm) of each star was measured. It was found that no star differed in velocity from the mean of the thirteen by more than 8 km/sec.

TABLE 1

HD or BD Number	Variable Designation	Spectral Type and Luminosity Class	JD of Observation	Probable m_v at Date of Observation	M_v, Assuming Cluster Membership	Remarks
			2432000+			
13136		M2 *Ib*	139	8^m0	-4^m7	4
+56°512	HV 10644	M4 *Ib*	139	9.0	4.1	5
14142	T Persei	M2 *Ia–Ib*	139	8.5	5.7:	2
14270	AD Persei	M3 *Ia–Ib*	141	8.1	5.0	1, 2, 6
14330		M1 *Ia–Ib*	141	8.1	5.0	1, 9
14404		M2 *Ib*	141	8.6	4.9	1
14469	SU Persei	M3 *Ia–Ib*	141	8.0	4.8	1, 2, 7
14488	RS Persei	M4 *Ia–Ib*	141	8.7	4.4	1, 2, 8
14528	S Persei	M3e *Ia*	139	8.6	5.6:	
+56°595		M0 *Ia–Ib*	142	8.6	4.7	1
14580		M0 *Ia–Ib*	142	8.6	4.7	1, 10
14826		M2 *Ia–Ib*	152	8.5	5.2	1, 3
236979	YZ Persei	M3 *Ia–Ib*	141	8.0	−5.8:	2

NOTES TO TABLE 1

1. Spectroscopic parallaxes are available for these stars from the work of the Mount Wilson investigators (*Ap. J.*, **64**, 225, 1926, and **81**, 187, 1935).
2. Attributed to the cluster by Keenan (*Ap. J.*, **95**, 461, 1942).
3. Attributed to the cluster by Keenan (*Ap. J.*, **104**, 458, 1946).
4. Probable cluster membership suggested by Keenan in private communication.
5. Light-curve in *Harvard Bull.*, **915**, 25, 1941.
6. Radial velocity −43 km/sec (Joy, *Ap. J.*, **96**, 344, 1942).
7. Radial velocity −39 km/sec (*ibid.*).
8. Radial velocity −38 km/sec (*ibid.*).
9. Possibly variable (see Z. Kopal and V. Vand, *A.N.*, **252**, 125, 1934).
10. Possibly variable. This star is Zinner No. 124, in *Astr. Abh.*, Vol. **8**, No. 1, 1931.

Consequently, it appears that cluster membership for these stars is quite well established, and, assuming this, it is then possible to compute their individual absolute magnitudes from the known distance modulus of h and χ Persei. This procedure is difficult to carry out accurately, however, because of the considerable variation with apparent position in the amount of interstellar absorption affecting the light of these stars.[6] It is thus not permissible to assume the same *apparent* distance modulus for all the stars. Instead, the total visual absorption has been estimated for each star from a positional plot of the photoelectric color excesses shown by the early-type cluster members. The colors of Stebbins, Huffer, and Whitford[7] were used; it was assumed that multiplication of the color excesses by 7 would give the total visual interstellar absorptions. The visual absolute magnitudes were then computed with a value of 11.4 for the true distance

[6] *Ap. J.*, **98**, 61, 1943.

[7] *Ap. J.*, **91**, 20, 1940.

modulus of h and χ Persei. I am indebted to Dr. W. W. Morgan for this value, as well as for the use of slightly different normal photoelectric colors of early-type stars than were adopted by Stebbins, Huffer, and Whitford.

The visual absolute magnitudes computed on the assumption of cluster membership are given in Table 1, which also shows the visual apparent magnitudes adopted. For most of the variable stars the magnitude given is the mean of the maximum and minimum of the light-curve. For S Persei the apparent magnitude is taken from A.A.V.S.O. observations, communicated through the courtesy of Mr. Leon Campbell.

There are several sources of error intrinsic to this method of deriving the absolute magnitudes of these M-type supergiants:

a) The visual apparent magnitudes at the date of observation may be in error by several tenths of a magnitude.

b) The corrections for interstellar absorption may have been estimated incorrectly. Since the total visual absorptions adopted range from 1.3 mag. for HD 13136 to 2.8 mag. for S and T Persei, this error can be fairly serious. The cases involving extrapolation of the color excesses are indicated by colons following the absolute magnitudes; these are probably the most uncertain.

c) The basic assumption has been made that the total visual interstellar absorption of the light of a star is independent of its normal color, over the range of color from a B-type to an M-type supergiant.

Because of the accidental errors discussed in paragraphs *a* and *b* above, the small discrepancies shown in Table 1 between the computed absolute magnitudes and the spectroscopic luminosity classes should not be given any weight. On the basis of the data available, the visual absolute magnitude of early M stars of luminosity class I*a*–I*b* may be estimated as about -5.0.

II. THE RUSSELL-HERTZSPRUNG DIAGRAM FOR THE KNOWN HIGH-LUMINOSITY MEMBERS OF THE DOUBLE CLUSTER

In Figure 2 is plotted the Russell-Hertzsprung diagram for h and χ Persei, including only those stars whose visual absolute magnitudes exceed -4.0. All the absolute magnitudes used were computed on the assumption of a true distance modulus of 11.4, with the correction for interstellar absorption being estimated separately for each star. Some unpublished data obtained by Dr. W. W. Morgan have been incorporated in the diagram. For the late-type stars the absolute magnitudes given in Table 1 have been used, and it should be remembered that these are not the maximum absolute magnitudes for these stars. The maximum absolute magnitudes would be at least half a magnitude brighter, on the average, than the values plotted in the figure.

The most striking feature of the Russell-Hertzsprung diagram is the absence of stars of spectral types F, G, or K. Since there has been no thorough investigation of stars of these types in the region of the cluster, however, it should not be concluded that high-luminosity stars of these types are absent.

III. THE REMARKABLE STAR S PERSEI

The late-type supergiant associated with the double cluster for which the highest luminosity is indicated from the appearance of its spectrum is S Persei, which has been considered to be an irregular variable with an over-all visual range of from 7.2 to 12.2 mag.[8] L. Campbell's light-curve covering the years from 1880 to 1938,[9] however, shows clearly that its light-variation is decidedly different from that of a typical irregular variable. In fact, a rough periodicity of about 835 days was maintained throughout the time covered by Campbell's light-curve, but the amplitude of the variation showed strik-

[8] Payne-Gaposchkin and Gaposchkin, *Variable Stars* (1938), p. 222.

[9] *Pop. Astr.*, **47**, 277, 1939.

ing differences at different times. For example, from 1919 to 1927 the star varied over almost 4 mag., while for the next 11 years it varied only between the limits of 8.9 and 10.3. Subsequent to 1938,[10] the range began to increase; in April, 1946, the star was 11.2, 3 mag. fainter than it had been in December, 1944. The McDonald spectrogram was taken in November, 1946, when the star was approaching the maximum of its current cycle.

As might be expected from the abnormal light-curve of S Persei, its spectrum is also peculiar. The appearance of the spectrum is that of a star of very high luminosity, showing somewhat stronger *TiO* bands but otherwise an absorption spectrum generally similar to that of μ Cephei, which is classified as M2 I*a*. The distinct peculiarity, however, is

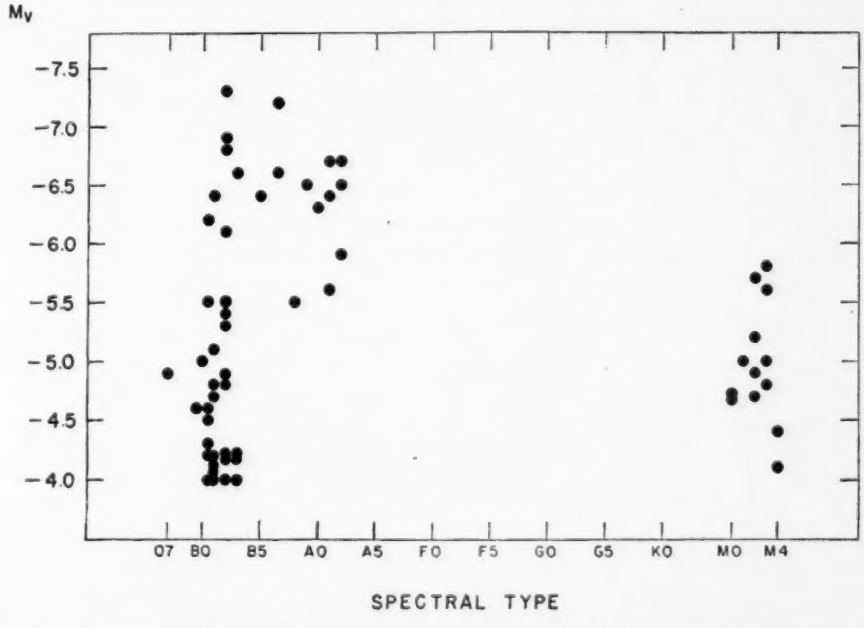

FIG. 2.—The Russell-Hertzsprung diagram for the known high-luminosity members of h and χ Persei. All absolute magnitudes are computed, assuming a true distance modulus of 11.4 for the cluster, the correction for interstellar absorption being made separately for each star.

the presence of strong emission lines at $H\gamma$ and $H\delta$, with $H\delta$ probably a little stronger than $H\gamma$. Since both the light-curve and the spectrum of S Persei showed a similarity to that of a long-period variable at the time that the spectrogram was obtained, it appears possible that the star is quite analogous to a typical long-period variable during the time its light-curve shows large amplitude variations. However, it is almost certainly of considerably higher luminosity than most long-period variables. In fact, at its brightest recorded maximum, the data in Table 1 would indicate that its visual absolute magnitude was of the order of −7.0.

The only previously published spectroscopic observation of S Persei is that contained in the *Henry Draper Catalogue*, in which it is stated that $H\delta$ is in emission on one plate. The apparent visual magnitude of the star was then about 9.4, and the amplitude of its light-variation was quite small. Further spectroscopic study of this star would be very desirable.

[10] For this information I am indebted to Mr. Leon Campbell.

From a mathematical standpoint, the complex light-curve of S Persei may be represented for some time by assuming that there exist simultaneously in the star two sinusoidal light-variations, with similar amplitudes and only slightly different periods. The changes in amplitude of the observed light-curve are then produced by interference of the two fundamental variations.[11] Since the *amplitude changes* are not strictly periodic, this representation is valid for only a few cycles. In connection with the high luminosity of the star, it is probably significant that, among those stars whose light-curves show evidence of multiple periods,[11] S Persei possesses the longest fundamental period.

[11] Frida Palmér, *Lund Medd.*, Ser. II, No. 103, 1939.

NOTES

A NEW SPECTROSCOPIC TRIPLE STAR, HD 157978–9

Recently, several composite stellar spectra have been examined at the Michigan Observatory, in the hope of finding interesting binaries. The second plate of HD 157978–9[1] showed the K line as a sharp double, while the remainder of the lines (due to the G-type component) were single. Radial velocities from all plates of the past season are given in Table 1. Except as noted, the dispersion was 40 A/mm at $H\gamma$.

The two components of the K line are so nearly equal that an ambiguity remains in the period. It has been narrowed down to either 1.327 or 3.946 days. The latter is considered the more probable. Corresponding periods slightly longer than 1.33 and 4.0 days

TABLE 1

RADIAL VELOCITIES OF HD 157978–9

DATE, U.T.	VELOCITIES			
	G-Type	K Line		
		Violet	Single	Red
July 18.137	− 4.6	.....	−16	.....
August 9.224	− 2.7	− 86	.....	+ 54
14.092	+ 0.3	−115	.....	+ 82
15.097	− 6.0	.....	−22	.....
18.069*	−12	−109	.....	+134
18.099*	.....	−119	.....	+138
October 3.081*	.....	.....	−34	.....
4.065	+ 5.0	−133	.....	+ 84

* Two-prism and 6-inch camera, dispersion 80 A/mm at $H\gamma$.

are definitely ruled out. A still shorter period, near 0.8 day, is considered very unlikely because of the sharpness of the K lines.

The mean velocities of the G-type spectrum and the K line (omitting the low-dispersion plates) are −2 and −19 km/sec, respectively. The difference is considered as evidence of relative motion of the G-type star and the early-type pair. The fact that these two velocities changed in opposite senses between August and October is favorable to such an interpretation. The system should prove to be another interesting one similar to 59d Serpentis.[2]

DEAN B. MCLAUGHLIN

OBSERVATORY OF THE
UNIVERSITY OF MICHIGAN
December 26, 1946

[1] 1900: $\alpha = 17^h21^m.5$; $\delta = +7°41'$; mag. 5.98; spec. A0G.

[2] McLaughlin, *Ap. J.*, **88**, 356, 1938; E. C. Tilley, *Ap. J.*, **98**, 347, 1943.

THE ECLIPSING SYSTEM RY PERSEI

Recently, W. A. Hiltner[1] has discussed spectrographic observations of RY Persei, while the author has presented a photometric study.[2] The present note combines the results of the two.

A mass ratio of between 1 and 2 is indicated by the luminosities of the components. Because of the small mass function, either of these assumptions indicates an abnormally small mass for the B star. On the other hand, for a mass ratio greater than 5, the system appears dynamically unstable. Probably the limiting cases are represented by $m_b/m_f = 2$ and $m_b/m_f = 4$. Absolute dimensions for the two cases are as shown in Table 1. These dimensions are computed by use of the photometric elements given by the author and Hiltner's spectrographic elements. For the latter, the elements derived from the velocity-curve of the *He* I lines are used. These are chosen in preference to those derived from the hydrogen lines because of Hiltner's conclusion that "it is probable that hydrogen forms a slowly rotating envelope about the reversing layer of the star."

TABLE 1

m_b/m_f	2	4
r_b	2.0 ⊙	3.3 ⊙
r_f	4.1 ⊙	6.9 ⊙
m_b	0.61 ⊙	3.4 ⊙
m_f	0.30 ⊙	0.84 ⊙
ρ_b	0.11 ⊙	0.13 ⊙
ρ_f	0.0060 ⊙	0.0036 ⊙

The spectrographic value of the eccentricity is $e = 0.21$. With an ω of 14° (found spectrographically), $e \cos \omega = 0.20$. This requires a large displacement of secondary minimum on the photometric curve. If the spectrographic work is correct, the secondary is displaced by $0^d.90$, and its center lies at $4^d.33$. The photometric curve contains no observations in this region. The observations between 3.0 and 4.0 days do not definitely demand a centrally located secondary and do give some indication of a displacement in the direction indicated by the spectrographic work. The photometric evidence on this point is as yet inconclusive.

Hiltner computed his phases by use of Nijland's light-elements. The improved period[2] of $6^d.8635654$ requires that $0^d.011$ be added to these phases. Also, the first four phases on October 16, 1945, cited by Hiltner, appear to represent a slight miscalculation; the phases in days (from Nijland's elements) should be 0.009, 0.054, 0.088, and 0.120, respectively.

FRANK BRADSHAW WOOD*

STEWARD OBSERVATORY
UNIVERSITY OF ARIZONA
January 1947

[1] *Ap. J.*, **104**, 396, 1946.

[2] *Princeton Contr.*, No. 21, p. 54, 1947.

* National Research Fellow.

NOTE ON THE ECLIPSING SYSTEM RX GEMINORUM

While my paper, "The Eclipsing System RX Geminorum," was in press,[1] I received the Victoria radial velocities of Dr. R. M. Petrie for this star. Since these additional and independent velocities contribute greatly to the observational material of the star, they are given here. All data are from Dr. R. M. Petrie's letters except those under the column "Phase," which are computed by me.

DR. R. M. PETRIE'S RADIAI VELOCITIES FOR RX GEMINORUM (VICTORIA)

JD	Rad. Vel. (Km/Sec)	No. of Lines	Phase*	Remarks
2428232^d.741	+15.3	6	0^p.514	Weak
500.875	31.0	10, 6	.476	Weak, two measures
504.910	45.6	12	.807	Good
813.015	6.8	9	.043	Good
816.021	19.4	6, 4	.230	Weak, two measures
817.022	18.6	7	.372	Good
29621.889	+13.7	5	0.297	Good

* Computed with the formula $\varphi = 0.081908936\ (JD - 2400000)$, the number 0.081908936 being the reciprocal of $P = 12^d.20868$.

SERGEI GAPOSCHKIN

HARVARD COLLEGE OBSERVATORY
February 1947

THE TRUMPLER STARS

In some recent discussions of these stars the impression has been given that they form a group apart from the main sequence of the normal O-type stars. Trumpler's original article[2] does not bear out this view: he considers the class-O members of galactic clusters as typical stars of their respective spectral subdivisions. But, since the red-shifts observed by him could be measured only with reference to other cluster stars, there remains the possibility that the O-stars in clusters differ systematically from O-stars which are not members of clusters.

Several years ago a red-shift of appreciable amount (about +15 km/sec) was found among the stars of the Trapezium in Orion, where the nebula serves as a reference.[3] There is a strong suspicion that this phenomenon is related to that discovered by Trumpler. Two of the Orion stars are of class O. These have the largest red-shifts. The other stars are of class B0 and B2 and have smaller—but still appreciable—red-shifts. An examination of the spectra of the Orion stars shows no difference from the spectra of normal stars of similar spectral types. The irregular variables of the Orion nebula, of Spectral types A–K, seem to share the velocity of the Trapezium stars of types O–B.[4]

Among the Trumpler stars the most reliable determination of the red-shift was obtained for 15 S Monocerotis, in the cluster NGC 2264.[5] I have secured several excellent spectrograms of S Mon with the quartz spectrograph of the McDonald Observatory, some on Eastman Process emulsion. The spectrum appears entirely normal for its class,

[1] *Ap. J.*, **104**, 376, 1946.

[2] *Pub. A.S.P.*, **47**, 249, 1935.

[3] *Ap. J.*, **99**, 84, 1944.

[4] *Pub. A.S.P.*, **58**, 367, 1946.

[5] See footnote to Table 34*c*, p. 490, in S. Chandrasekhar, *Introduction to the Study of Stellar Structure*.

O7. The last Balmer line is H 15, which agrees perfectly with the trend of other main-sequence stars in the diagram by Unsöld and the writer, where the quantum number of the upper state of the last visible H line is plotted against spectral type.[6] There are no spectroscopic features in the photographic region which would justify us in setting off S Mon from the rest of the normal O stars.

The question might be asked why some statistical studies of the radial velocities of O-type stars have given small values for the K-term,[7] while others have given values of the order of +6 km/sec.[8] Perhaps this is due to the uneven distribution of these stars in galactic longitude and to the difficulty of separating supergiants from members of the main sequence.

O. STRUVE

McDONALD OBSERVATORY
February 16, 1947

CHANGES IN THE INFRARED SPECTRUM OF VV CEPHEI

On our first infrared spectrograms of VV Cephei, taken in October and November, 1944, and described in a previous note,[1] the most noteworthy features were the blended absorption lines of *O* I at λ 7773 and λ 8446 A. The star was again photographed on July 21, 1945, and at this time the oxygen lines were much weaker (exposure 2 on Fig. 1). By August 19, when the next succeeding spectrogram was taken, λ 8446 had disappeared, and λ 7773 had become so weak that it could barely be distinguished from the background of blended metallic lines of the M2 spectrum. No further marked changes were observed up to the beginning of December, 1946. In the meantime we have found an earlier spectrogram, taken, also with the Perkins reflector, by A. G. Mowbray on September 8, 1943. The lines of *O* I are not recognizable on this plate; and, although the quality of the image is not very good, it is certain that the oxygen lines were much weaker in 1943 than in the autumn of 1944. The record of the observations is given in Table 1.

It is evident that the presence of strong *O* I lines in the spectrum was a transient phenomenon. From the rapidity of the fading of these lines in 1945, in contrast to the consistency of their strength on the spectrograms of October and November of the preceding year, it appears likely that the 1944 plates were taken near the time of their maximum strength. At that time the total absorption of λ 7773 was 2.1 A, which is close to the greatest strength observed for this line in any supergiant of luminosity class I*b*. Since in the sequence of supergiants the *O* I lines have a broad, flat maximum, extending approximately from A0 to F5, the excitation of λ 7773 in VV Cep was equivalent to that in a normal supergiant lying somewhere within this range of types.

The series of spectrograms now available reveals that variations in the intensity of several other lines have also occurred. Lines of the Paschen series of hydrogen are difficult to observe because of bad blending with the *Ca* II infrared triplet and other metallic lines; but two of them—P 12 at 8750.5 A and P 14 at 8598.4 A—are free enough from blends to be visible on our spectrograms (scale 47 A/mm) of M-type stars of high luminosity. These two lines were strengthened, slightly but definitely, in the spectrum of VV Cep during the period of the *O* I maximum. Note this effect in λ 8598 in Figure 1, *b*.

Ionized iron has only one strong line—λ 7711.7 ($b^4D - z^4D^o$, e.p. 3.89 volts)—to the red of λ 7600 and is not usually observed in a spectrum of the type of VV Cep (M2, I*b*) on our plates. At the time of the *O*I maximum, however, λ 7712 was present. It can be seen in the top exposure of Figure 1, where it appears partly blended with λ 7714 of *Ni* I, which is a normal feature of an M-type spectrum and remains essentially unchanged on all our exposures.

[6] *Ap. J.*, **91**, 365, 1940.

[7] See, e.g., R. E. Wilson, *Ap. J.*, **94**, 15, 1941.

[8] J. S. Plaskett, *M.N.*, **90**, 630, 1930.

[1] *Ap. J.*, **101**, 270, 1945.

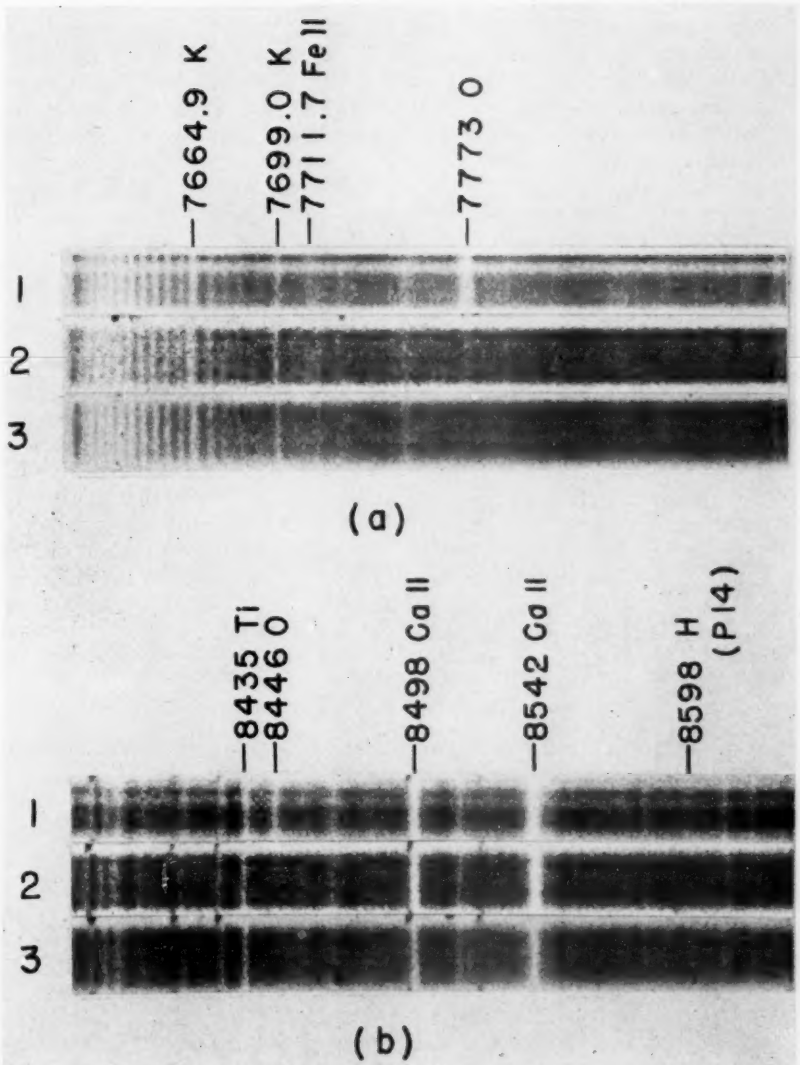

FIG. 1.—The infrared spectrum of VV Cephei. *1*, 1944 Oct. 7; *2*, 1945 July 21; *3*, 1946 Dec. 3

The simultaneous enhancement of the lines of *O* I (e.p. 9.1 volts), *H* (e.p. 12.0 volts), and *Fe* II (total e.p. 11.8 volts) indicates that in 1944 the atmosphere of the red supergiant was subjected to superexcitation. This superexcitation could result from an excess of radiation in the ultraviolet region around 1000–1300 A. It was suggested in our earlier note that the high-temperature radiation of the B-type companion might produce just this effect in the atmosphere of the M-type star, and an approximate calculation showed that the intensity of the dilute radiation from the companion should be of the right order of magnitude. The later vanishing of the high-excitation lines, however, shows that this simple picture must be modified. Although the distance separating the two stars was increasing during the period of observation, the radius vector varied only from 0.83 a.u. to 0.88 a.u. between October, 1944, and August, 1945 (on the basis of Goedicke's spectroscopic orbit[2]). Thus the radiation reaching the red component from the hot component when the oxygen lines had almost vanished was 86 per cent as much as at the time of their maximum, and the small difference seems inadequate to explain the great change in excitation.

TABLE 1

SPECTROGRAMS OF VV CEP IN THE INFRARED REGION

Plate No.	Date	Observers	*O* I Lines
930	Sept. 8, 1943	Mowbray	Imperceptible
1169	Oct. 7, 1944	Hynek	Strong
1189	Nov. 25, 1944	Bobrovnikoff	Strong
1339	July 21, 1945	Hynek	Rather weak
1363	Aug. 19, 1945	Hynek	Imperceptible
1377	Oct. 13, 1945	Hynek, Bobrovnikoff	Imperceptible
1458	May 23, 1946	Hynek, Keenan	Imperceptible
1556	July 16, 1946	Keenan	Imperceptible
1651	Sept. 5, 1946	Keenan	Imperceptible
1734	Oct. 2, 1946	Keenan	Imperceptible
1965	Dec. 3, 1946	Keenan	Imperceptible

Two alternative explanations can be advanced. Either fluctuations in the ultraviolet radiation from the B-type star control the excitation in the atmosphere of the red supergiant, or the high-excitation lines were produced in an extended atmosphere surrounding the B-type star and projected against the disk of the red star. The latter possibility is suggested by the fact that the *O* I lines were strong near the predicted time of secondary minimum; but this hypothesis would require radical revision in our ideas of the relative dimensions of the two components.

Further discussion of these points will be worth while only when a more extended series of observations becomes available. The main purpose of this note is to call attention to the great importance of securing spectrograms nearly simultaneously in the blue and infrared spectral regions at all phases of the orbital motion of this system.

One other recent change in the infrared spectrum should be mentioned. It can be noticed in Figure 1 that on the last exposure the *Ca* II lines appear to have weakened greatly. Microphotometer tracings show that on this plate (G_β 1965) the lines are flat-bottomed with central absorptions 10–15 per cent less than on the earlier plates. The diminution in intensity appears to have begun earlier in the fall of 1946. The spectrogram of December 3 was the last which could be taken at the Perkins Observatory before the star became too far west for further observation this season.

P. C. KEENAN
J. A. HYNEK

PERKINS OBSERVATORY
February 1947

[2] *Pub. Michigan Obs.*, Vol. 8, No. 1, 1939.

RECENT CHANGES IN THE SPECTRUM OF β MONOCEROTIS A

The star β Monocerotis A, the brightest component of a visual triple, is a well-known emission star of type B2nne. Its spectrum is characterized by very wide rotationally broadened absorption lines of *He* I, bright lines of *Fe* II, and hydrogen lines of varying complexity. As observed at Yerkes in 1918, 1920, 1924, and 1931, the hydrogen lines in the photographic region showed sharp absorption cores, flanked by wide emission components, which were superposed upon still wider absorption wings. In later years the hydrogen absorption cores became much less pronounced.[1]

In the course of a low-dispersion investigation of the spectra of rapidly rotating stars undertaken recently at the Yerkes Observatory, it was found that the strong absorption cores of the hydrogen lines have reappeared in the spectrum of β Monocerotis A, being present on a plate taken on December 12, 1946. The changes in the spectrum of this star over an interval of four years are shown in Figure 1, *a* and *b*. These spectrograms were taken on March 17, 1943, and February 4, 1947, respectively. The changes in the structure of the hydrogen absorption lines are conspicuous, while the intensity of $H\beta$ and the *Fe* II emission lines appears to be unchanged. In addition to the great strengthening of the central absorptions in $H\gamma$, $H\delta$, and $H\epsilon$, the broad wings of these lines, which are due to the underlying star, appear to have become considerably weaker, and a slight weakening of the *He* I spectrum is also apparent.

In Figure 1, *c*, is reproduced a spectrogram obtained on February 4, 1947, with a dispersion twice that of the spectrograms shown in *a* and *b*. From a consideration of the widths of the helium lines λ 4009 and λ 4026, the rotational velocity of the star is estimated as about 400 km/sec. An interesting phenomenon shown by this spectrogram is the asymmetry of the line λ 4026. This may be caused by the superposition of a violet-displaced shell line over the broad line from the underlying star. Since the *He* I line λ 3965, which arises from a metastable level, is very weak or absent on these low-dispersion spectrograms, the dilution of radiation in the shell is presumably fairly small. If the asymmetry of the line λ 4026 is due to a rapid expansion of the shell, however, the dilution would be expected gradually to increase.

ARNE SLETTEBAK

YERKES OBSERVATORY
February 1947

THE SPECTRAL TYPE AND LUMINOSITY OF β CANIS MAJORIS

The quality of the lines in β Canis Majoris is known to vary with a period of 0.2513015 day, and changes in depth and equivalent width of the lines were found on high-dispersion plates.[2] In order to see if there is any change in spectral type or luminosity during the period, a series of spectra covering the 6-hour period was taken on December 29, 1946, with the one-prism spectrograph used at the Yerkes Observatory for spectral classification. The 12-inch camera was used, giving a dispersion of about 65 A/mm at $H\gamma$.

The series of spectra were found to be remarkably consistent, the star appearing to be slightly earlier than B1 at all times, though not quite B0.5. The spectral variation, if any, is not so much as half a tenth of a class. Likewise, the luminosity criteria are consistent with the classification II–III throughout the cycle. There is a suspicion that the

[1] O. Struve, *Pop. Astr.*, **53**, 261, 1945.

[2] *Ap. J.*, **104**, 388, 1946.

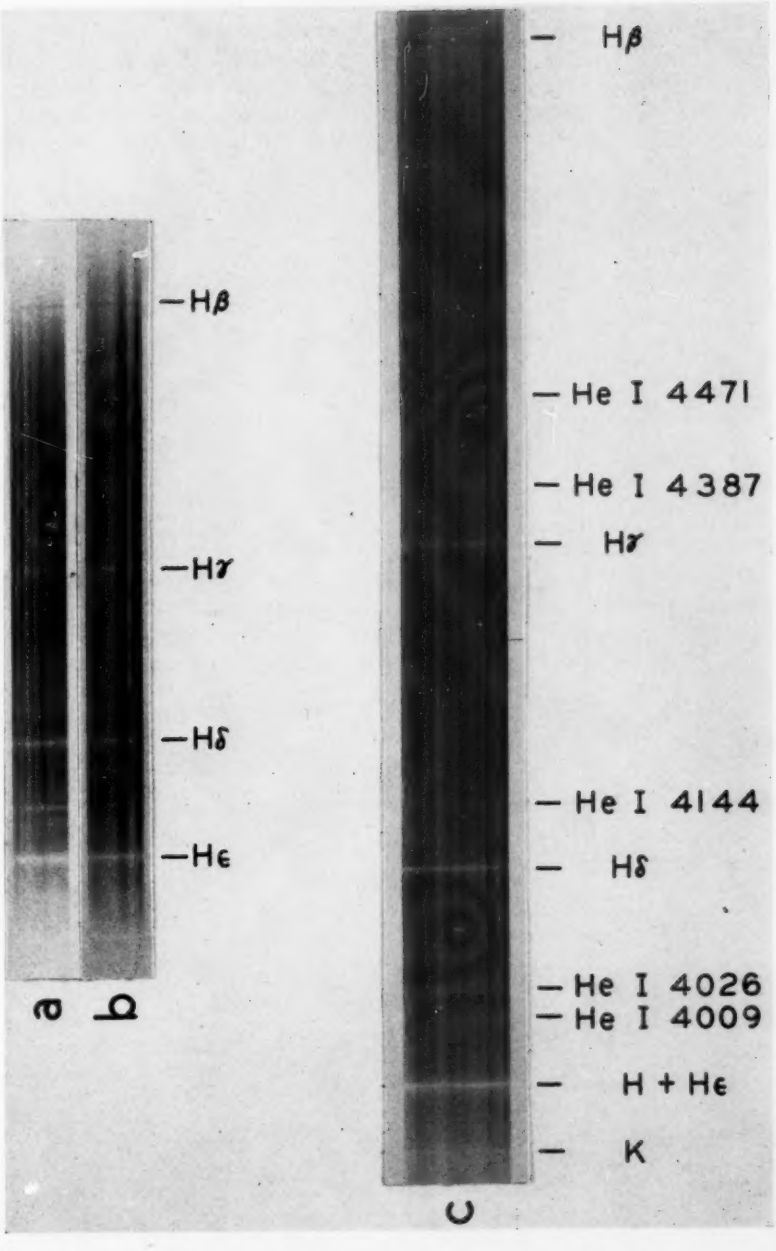

FIG. 1.—Spectrograms of β Monocerotis A. Reproductions *a* and *b* were made from plates taken March 17, 1943, and February 4, 1947, respectively, with a dispersion of 125 A/mm. Reproduction *c* is that of a plate obtained on February 4, 1947, with a dispersion of 60 A/mm.

luminosity may be slightly lower when the lines are diffuse than when they are sharp, but the variation, if any, is not so much as a luminosity class, which is in accord with the smallness of the observed variation in light.

The stars shown in the accompanying tabulation were used as standards of spectral class and luminosity. Their types and luminosity classes were furnished by W. W. Morgan; they are on the system of the Yerkes spectral atlas.

Star	Type	α (1950)	δ (1950)
ϵ Per	B0.5 IV–V	3^h54^m	$+39°\,52'$
γ Ori	B2 III	5 22	+ 6 18
139 Tau	B0.5 IV	5 55	+25 57
15 CMa	B1 III	6 51	−20 9
ϵ CMa	B2 II	6 57	−28 54

ANNE B. UNDERHILL

YERKES OBSERVATORY
March 13, 1947

THE PERIOD OF THE SPECTRUM VARIABLE 56 ARIETIS

Variation of certain absorption lines in the spectrum of the A0p star, 56 Arietis, has already been announced, and a description of the spectrum has been given.[1] From 12 spectrograms obtained at the Yerkes Observatory and 14 obtained at the Perkins Observatory, the elements of variation have now been found. These are

$$He\,\text{I maximum} = \text{JD } 2432227.55 + 2.563\,\text{E}\,.$$

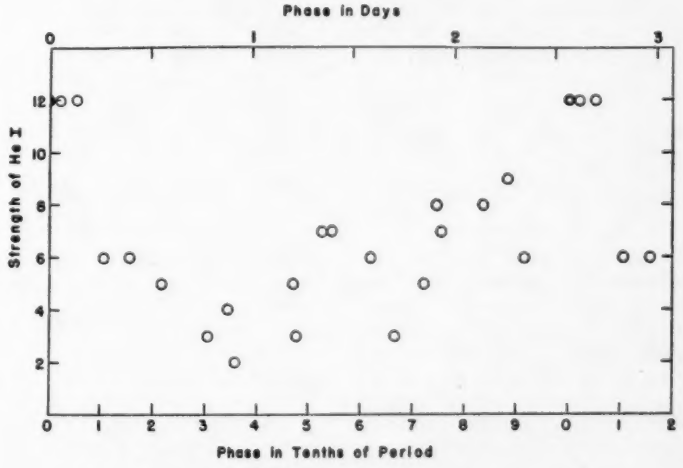

FIG 1.—Intensities of *He* I lines in 56 Arietis

The estimates of line intensity on which these elements are based are given in Table 1. The strengths of *He* I 4026 and *He* I 4471 have been estimated twice on each plate, the scale running from 0 for invisibility of the lines to 3 for maximum strength. In Figure 1

[1] Deutsch, *Ap. J.*, **105**, in press.

the sum of the four estimates on each plate is plotted against phase. The decline of the helium lines appears to be more rapid than their rise.

The period of 56 Ari differs from that of BD+33°1008 by only 0.1 day, or 4 per cent. The latter star shows the same spectroscopic peculiarities as the former but has much sharper lines. Were it not for the rotational broadening of the lines in 56 Ari, the two spectra would be nearly identical. The curves giving the variation of the helium lines are also very similar.

TABLE 1

OBSERVATIONS OF 56 ARIETIS

PLATE	JD 2430000+	PHASE*	STRENGTH OF *He* I	
			λ 4026	λ 4471
α39	1758.89	0P157	2 3	0 1:
α42	1761.92	343	2 2	0 0
β28	1863.61	020	3 3	3 3
β33	1869.91	359	1 0	0 1
β77	2003.88	745	2 3	2 1
β80	2005.88	526	1 2	2 2
β81	2006.88	916	1 3	1 1
β83	2007.87	304	0 1:	1 1
β90	2021.84	754	1 1	3 2
β93	2023.86	543	1 2	2 2
β97	2027.87	105	3 3	0 0
β99	2029.86	881	3 2	2 2
Pβ1921	2144.78	721	0 0	3: 2:
Pβ1933	2145.84	215	2 2	0 1
Pβ1964	2156.76	480	1: 2:	1: 1
Pβ1999, Pβ2000	2173.69	000	3 3	3 3
Pβ2043	2205.66	476	0 1	1 1
Pβ2054, Pβ2055	2221.53	667	0 1:	1 1
Pβ2056, Pβ2057	2222.51	051	3 3	3 3
Pβ2058	2224.52	835	1: 1	3 3
Pβ2063	2226.54	620	1: 1:	2: 2:
Pβ2064, Pβ2065	2227.51	0.000	3 3	3 3

* Phase = 0 at JD 2432227.55 + 2.563 E.

ARMIN J. DEUTSCH

PERKINS OBSERVATORY

REVIEWS

Science since 1500: A Short History of Mathematics, Physics, Chemistry, Biology. By H. T. PLEDGE. New York: Philosophical Library, 1947. Pp. 357. $5.00.

The author, who is librarian at the Science Museum of London, has presented "a short co-ordinating survey" of the history of science "down . . . . to the last year or so to avoid an arbitrary end-point." The book presents a study of the development of fundamental ideas in science rather than a mere account of factual material. It should be of help to research workers in drawing their attention to the historical processes which have culminated in present-day ideas and attitudes. Because of the enormous amount of specialization in science during the past century, no single person, however erudite, can successfully co-ordinate so many different fields of study. Pledge has wisely accepted the "criticism and other help" of a number of distinguished specialists. Astronomy forms an important part of the book, even though it is not listed in the title. But in several places the astronomically trained reader will see evidence of the truth of the author's remark in the Introduction that he "is keenly aware that his account of recent years can be but a reflection of his personal interests." For example, the amount of space devoted to cosmology and cosmogony is perhaps unnecessarily large, while other problems—no less significant from a philosophical point of view—for example, the physics of planets and meteors, have been omitted, presumably because of lack of space. There are other indications that the book was not written by an astronomer. An example of this appears on page 291, where a diagram, originally prepared by H. Mineur and now reprinted without change by the author, purports to show the gradual increase in precision of astronomical star positions. The various points of the diagram mark significant advances. Thus Hipparchus is credited with a precision of only 20′, while Auwers obtained a precision of 0″.1. But astronomical readers will be surprised to find that Tycho Brahe's "most accurate observations" are given as 4′. In reality, his best precision was more nearly 25″.[1] It may also appear misleading to a nonastronomical reader that the highest precision, 0″.003, is attributed to van Maanen. Schlesinger's name is not mentioned.

Such small drawbacks are unavoidable in a book of this sort, and the author must be congratulated upon having undertaken the arduous task of co-ordinating and digesting an enormous amount of highly specialized information.

O. STRUVE

McDonald Observatory

The Soochow Astronomical Chart. By W. CARL RUFUS and HSING-CHIH TIEN. Ann Arbor: University of Michigan Press. Pp. 24+v. $2.50, postpaid in U.S.A.

The Soochow star map was engraved in stone in A.D. 1247. Because of its completeness and because of additional astronomical and astrological text, this document is frequently referred to in discussions of Chinese astronomy. The publication of a complete English translation with notes and commentary is therefore to be welcomed. The grouping in constellations follows the Far Eastern pattern, totally different from the asterisms familiar to us. The editors wisely refrained from an attempt at establishing correspondences for all stars mentioned. Also, the astrological part is totally different from Western astrology, even in its earlier appearance as "judicial" astrology in Mesopotamia. The latter is closely related to the general idea of omina, whereas the Chinese form represents a much more general correspondence between cosmos and state, though the future-predicting element is not totally absent. The astronomical doctrine represented by our text is rather crude and elementary. The strangely high value of 1½° for the apparent diameter of sun and moon defies explanation, though the even higher value of 2° was used by Aristarchas (not 2½° as stated in note 19).

O. NEUGEBAUER

Brown University

[1] See, e.g., H. Spencer Jones, *Nature*, **158**, 858, 1946.

Tables of Spherical Bessel Functions, Vol. **1**. Prepared by the MATHEMATICAL TABLES PROJECT, NATIONAL BUREAU OF STANDARDS. New York: Columbia University Press, 1947. Pp. xxviii+375.

This volume lists the functions $\sqrt{\pi/2x}J_{n+1/2}(x)$, known in the literature as "spherical Bessel functions" or "Stokes functions." The main table contains the functions of orders $\pm(n+1/2)$, where $n = 0\ (1)\ 13$ and $x = 0\ (0.01)\ 10\ (0.1)\ 25$. The majority of the entries are given to eight significant figures for $x < 10$ and to seven significant figures for $x > 10$, except near the zeros of the functions. In some regions a few additional places are given for the sake of uniformity in format.

Astronomy. By FREEMAN D. MILLER. ("Vocational and Professional Monographs," No. 72.) Boston: Bellman Pub. Co., Inc., 1947. Pp. 30. $0.75.

This pamphlet is intended as a guide for students interested in astronomy as a profession. It contains a short outline of astronomy and lists opportunities for study and employment in the astronomical institutions of the United States.

INDEX TO VOLUME 105

INDEX TO SUBJECTS

INDEX TO AUTHORS

350
489
505
499
92
235
502
393
471
36
498
85